Advances in Underactuated Spacecraft Control

by

Christopher Petersen

A dissertation submitted in partial fulfillment
of the requirements for the degree of
Doctor of Philosophy
(Aerospace Engineering)
in the University of Michigan
2016

Doctoral Committee:

Professor Ilya V. Kolmanovsky, Chair
Professor Anthony Bloch
Professor Anouck Girard
Frederick Leve, Air Force Office of Scientific Research

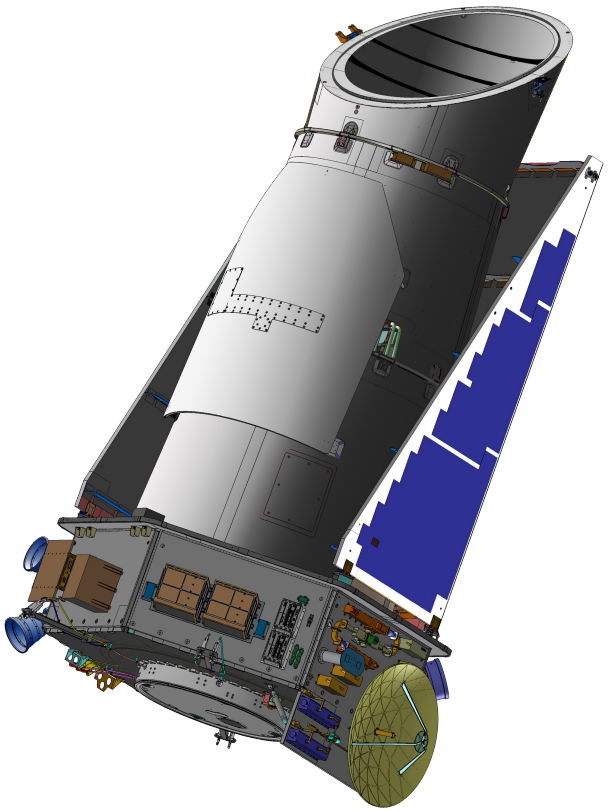

2016

To my family: from Petersen, to Bourassa, to Schooley,
to everyone else in between.

Firstly, and most importantly, I would like to thank my advisor Professor Ilya Kolmanovsky. He has always been, and will continue to be, an example to follow as I continue my career. The time and effort spent, guiding me with a smile, is something I won't forget. As an advisor, your support has been invaluable, pushing me past my limits, allowing me to research avenues that I really only dreamed of. Words cannot express how truly grateful I am for the time spent as your student.

Secondly I would like to thank the GN&C group at AFRL at Kirtland Air Force Base. By having the opportunity to perform research with the group, I was able to explore and further my passion in spacecraft navigation and control. Specifically I would like to thank Frederick Leve, who has been an excellent mentor, colleague, and friend. His support and guidance is invaluable, and his enthusiasm towards learning is an inspiration to me. In addition, I would like to thank Morgan Baldwin and Scott Erwin, who have made my time at the base unforgettable.

Thirdly I would like to thank the rest of my committee. For Professor Bloch, you have helped me explore connections between math and engineering that continue to excite me. For Professor Girard, your advice with humor is always a breath of fresh air.

Now to others at Michigan. For Professor Cutler, your excitement towards space research is always welcoming and I've always enjoyed our numerous conversations. For Professor Atkins, thanks for putting up with my struggling with c-code and reinforcing the importance of real-time application. As for students (past and present), I would like to thank Ray, Mortiz, Dave, Alex, Dae Young, Pedro, Uros, Kevin, and Avi. You have truly helped shape my time at Michigan. In particular, I would also like to thank Will, Greg, Dominic, Robert, and Richard in the lab group for good times. I know I'll be leaving the lab in great hands.

Finally I would like to thank my family and friends other than those at Michigan for their full support in this entire process. Specifically Seth and my fiancée Alicia. For Seth, your comments on mathematics is always stimulating my research forward. For Alicia, simply thank you for everything.

TABLE OF CONTENTS

LIST OF FIGURES

LIST OF TABLES

LIST OF APPENDICES

LIST OF ABBREVIATIONS

RW Reaction Wheel

MPC Model Predictive Control

CMG Control Moment Gyro

SRP Solar Radiation Pressure

COM Center-of-Mass

STLC Small-time Local Controllability

LQ Linear Quadratic

RAE Reduced Attitude Equations of Motion

HCW Hill-Clohessy-Wiltshire

ISS International Space Station

PBH The Popov-Belevitch-Hautus

ABSTRACT

Advances in Underactuated Spacecraft Control

by

Christopher Petersen

Chair: Ilya V. Kolmanovksy

This dissertation addresses the control of a spacecraft which either becomes underactuated as a consequence of onboard failures or is made underactuated by design. Successfully controlling an underactuated spacecraft can extend spacecraft operational life in orbit and improve the robustness of space missions. The novel contributions of the dissertation include the following.

Firstly, switching feedback controllers are developed for the attitude control of an underactuated spacecraft equipped with two pairs of thrusters, or two reaction wheels (RWs), or two control moment gyros (CMGs). The problem is challenging; e.g., even in the zero total angular momentum case, no smooth or even continuous time-invariant feedback law for stabilizing a desired orientation exists. The overall method exploits the separation of the system states into inner-loop base variables and outer-loop fiber variables. The base variables track periodic reference trajectories, the amplitude of which is governed by parameters that are adjusted to induce an appropriate change in the fiber variables towards the desired pointing configuration.

Secondly, nonlinear Model Predictive Control (MPC) is applied to the attitude dynamics of an underactuated spacecraft with two RWs and zero angular momentum. Though such a system cannot be stabilized by any smooth or continuous time-invariant feedback law, MPC has the remarkable ability, which is exploited in this research, to generate control laws that are discontinuous in the state. By utilizing nonlinear MPC, the obstruction to stabilizability is overcome and attitude maneuvers can be performed while enforcing constraints.

Thirdly, an unconventional pathway is discussed for recovering the linear controllability of an underactuated spacecraft with two RWs by accounting for the effects of solar radiation pressure (SRP) in the spacecraft attitude model. A comprehensive analysis of the addition of SRP torques into the attitude model is given, including necessary and sufficient conditions for recovering linear controllability. With linear controllability restored, conventional controllers can be designed for underactuated spacecraft.

Lastly, a set of coupled translational and rotational equations of motion for a spacecraft in a central gravity field are derived. The spacecraft is assumed to have only internal attitude actuators and the equations of motion are such that they are relative with respect to an equilibrium orbit. These equations are then approximated, and for certain orbits, yield dynamics very similar to Hill-Clohessy-Wiltshire (HCW) dynamics. Under reasonable assumptions on the spacecraft configuration and equilibrium orbit, it is proven that the coupled dynamics are small-time locally controllable (STLC), which opens a path to utilizing conventional control techniques to move translationally in space by employing attitude control only.

CHAPTER 1

Introduction

1.1 Underactuated Spacecraft

If the number of degrees-of-freedom is greater than the number of degrees-of-actuation, a system may be viewed as *underactuated* [2]. This is a large concern for spacecraft systems in particular, as being underactuated can shorten its operational life and reduce its capabilities while on orbit.

There are two ways in which a spacecraft becomes underactuated. Firstly, a spacecraft can be underactuated by design. This is typically the case for small spacecraft, such as cubesats, which have stringent constraints on volume, power, and weight that may not allow for full actuation. Secondly, and more detrimental to the mission of the spacecraft, is the failure of an actuator. The general rule of thumb for larger spacecraft is to equip the bus with redundant actuators so that in case of failure the other actuators can compensate. However, in some cases multiple actuator failures can occur. For example, the satellite FUSE had three out of its four reaction wheels (RWs) fail within their expected lifetime and consequently had to perform attitude maneuvers using magnetic actuators and one RW [3]. The Kepler telescope lost two out of its four RWs before its extended mission was complete. While its gas thruster can also be used to perform attitude maneuvers, this type of actuation expends fuel and was not designed to provide the precise orientation needed [4]. The Japanese

Hayabusa spacecraft, which was involved in an asteroid sample return mission, also lost two out its four RWs. Its mission profile had to be modified to conserve fuel in order to have enough propellant to return to Earth after performing the necessary attitude maneuvers with gas thrusters [5].

The general problem can be stated as follows: "What methods can be developed to control an underactuated spacecraft?" This dissertation specifically addresses this question for two different spacecraft situations:

- The control of the attitude (orientation) of a spacecraft when equipped with either two pairs of thrusters, two RWs, or two control moment gyros (CMGs).
- The orbit and attitude control of a spacecraft when equipped with only RWs or CMGs.

1.2 Attitude Control of Underactuated Spacecraft

1.2.1 Background

Underactuated attitude control with thruster pairs and RWs was first discussed in the 1980's by P. Crouch [6]. For the case of thruster pair actuation, it was proven that asymmetric spacecraft systems (and some symmetric systems) were globally controllable on the attitude and angular velocity space $SO(3) \times \mathbb{R}^3$ if actuation was provided by two pairs of thrusters generating two independent torques or with one pair of thrusters generating a torque about a non-principal axis of the spacecraft. Furthermore, a spacecraft with two pairs of thrusters was proven small-time locally controllable (STLC) from all equilibria if and only if it was globally controllable. For the case of RW actuation, however, [6] showed that the spacecraft dynamics were inaccessible with less than two RWs due to angular momentum conservation. A decade later, Krishnan et al. [7] proved that if the total spacecraft system had two

reaction wheels and zero total angular momentum, then a reduced set of attitude dynamics were STLC from all at-rest attitudes.

Results on controllability properties of an underactuated spacecraft with CMGs began to appear in the late 2000s. Since CMGs are internal momentum devices like RWs, they suffer the same obstruction to controllability due to angular momentum conservation. Using a reduced set of equations of motion defined by constant angular momentum, a spacecraft system can be globally controllable with only one CMG [8]. STLC for at-rest equilibria, on the other-hand, is more difficult to achieve, as the property depends heavily on the arrangement and momentum of the individual CMGs [9–11].

The difficulty of the underactuated attitude control problem arises from the fact that even if the system is STLC from any at-rest equilibria by either thrusters, RWs, or some configurations of CMGs, the dynamics cannot be stabilized by any smooth or continuous time-invariant feedback law [7, 9, 12–14] because the equations of motion violate Brockett's necessary condition [15,16]. Stabilization is still possible with time-periodic feedback laws, but exponential convergence rates cannot be achieved if the feedback law is smooth [17].

Despite this obstruction to stabilizability, there is a great deal of literature on techniques for underactuated attitude control. For thruster actuation and RW actuation where the spacecraft system has total zero angular momentum, the control laws fall into several different categories:

- Open-loop methods that induce a sequence of rotations [7, 13, 18, 19];
- Nonlinear, Lyapunov-based, feedback control using local representations of attitude [10, 20–23];
- Diffeomorphic transformations of the equations of motion to a simpler form for control design [7, 13, 24];

- Time-varying/parameter varying feedback techniques [25–28];
- Nonholonomic approaches based on averaging [29–32];
- Geometric phase exploitation [13, 18, 32].

There are fewer results for CMG actuation where the spacecraft system has zero total angular momentum, in part because the issue of singularity prevents most feedback techniques from being used. However, there are open-loop maneuvers [33] and nonlinear, Lyapunov-based techniques [34–36] that can be used to stabilize the attitude with two CMGs.

The total zero angular momentum assumption for a spacecraft with two RWs or CMGs may be limiting in practical applications as it is difficult to achieve it in a space environment. It is undesirable for spacecraft with less than four RWs to have total zero angular momentum since the wheels must be spinned down during inertial pointing and operated in the zero crossing region, where their accuracy is decreased, the friction coefficient is increased and their operational life is reduced. In the case of CMGs, the total zero angular momentum can result in the CMGs entering a singular configuration at equilibrium.

The case of nonzero total angular momentum for internal momentum actuation is less studied. For RWs, [37] defines a subspace of feasible attitudes defined by the law of angular momentum conservation and gives a procedure for constructing an open-loop control. A spin-axis stabilization is performed about the uncontrollable axis of a spacecraft with nonzero total angular momentum and two RWs in [38], but the topic of inertial pointing is not discussed. Reference [39] discusses the topic of control of an underactuated spacecraft with two RWs and initial nonzero angular momentum, but the control law proposed can send the spacecraft into an uncontrolled rotation for some initial conditions. The inclusion of constant angular momentum for underactuated attitude control with CMGs is more easily found in the literature, but

the control laws are limited to being either Lyapunov-based, feedback techniques [14] or parameter-varying techniques [40].

1.2.2 Contributions & Outline

The contributions of this disseration to the underactuated attitude control problem are as follows:

1. The development of geometric switching schemes for attitude stabilization of an underactuated spacecraft with two thrusters, two RWs, or two CMGs. For RWs, the constant nonzero angular momentum case is treated.

2. The analysis and demonstration that nonlinear model predictive control (MPC) can be used to generate a discontinuous control law for the stabilization of an underactuated spacecraft with two RWs and zero angular momentum.

3. The derivation of sufficient and necessary conditions to recover linear controllability of the attitude of a spacecraft with two RWs and Solar Radiation Pressure (SRP). This result enables the application of conventional linear control design techniques to control the underactuated spacecraft with two RWs and SRP.

These contributions are reflected in Chapters 2-5.

To begin the dissertation, the attitude equations of motion for thruster pair, RW, and CMG actuation are derived in Chapter 2 with all assumptions outlined. These equations will be basis for all control analysis and design in subsequent chapters.

Chapter 3 discusses the first contribution of the dissertation. The general approach utilizes switching feedback stabilization techniques which exploit the decomposition of the system variables into base variables and fiber variables. The base variables are stabilized to periodic motions with feedback, and the parameters of these periodic motions are adjusted at discrete time instants to induce a change in the fiber variables

towards the desired values. The method is applied to spacecraft with thruster pairs, RWs, and CMGs.

Chapter 4 discusses the second contribution. While MPC has been used for attitude control when the spacecraft is fully actuated by either thrusters and RWs, it has not been previously utilized in the underactuated case. It is known, however, that MPC has the remarkable ability to construct control laws that are discontinuous in terms of state [41, 42]. In this chapter, it is proven that MPC can generate a stabilizing control law for a set of approximate, discrete attitude dynamics which cannot be stabilized by smooth feedback. Furthermore, numerical simulations demonstrate that the control law is discontinuous in terms of state, and can be used to stabilize the actual nonlinear, underactuated attitude dynamics.

Chapter 5 discusses the third contribution and demonstrates a framework for restoring linear control by including the effects of SRP torques, modeled following [43], into the spacecraft model. The analysis shows that under appropriate assumptions, linear controllability is regained and hence spacecraft stabilization can be achieved with conventional control schemes. In particular, a Linear Quadratic (LQ) approach is first applied. The LQ approach is chosen due to its robustness, its optimal control properties and its familiarity to aerospace engineers. A pole placement scheme will also be used to improve convergence time. By taking advantage of the change in the dynamics induced by SRP torques, two RWs are able to slowly correct the attitude errors over time.

1.3 Rotational and Translational Underactuated Control in a Gravity Field

1.3.1 Background

For satellite orbits about a large central body, the ratio between a spacecraft's largest dimension and the radius of its orbit is small. Thus in the orbit and attitude equations of motion, terms higher than first-order in this "dimension ratio" are typically neglected, resulting in decoupled translational and rotational dynamics. In the 1960's, the equations of motion of a rigid spacecraft under the influence of spherical and oblate gravitational fields were developed [44–46], revealing that if second-order and higher terms in the dimension ratio are included, then a spacecraft's translational motion is affected by its attitude and vice versa. In particular for very large spacecraft, terms up to third and fourth-order in the dimension ratio must be included for accurate orbital motion analysis and simulation [47].

The primary use of these coupled rotational and translational dynamics has been to determine conditions for the existence of free (unforced) motions in a central gravity field [48–51] as well as their stability when they exist [50, 52–54]. Some literature relaxes the assumption of a central gravity field and analyzes the existence and stability of free motion of satellites when the central body is oblate [55] and non-spherical (produced by asteroids and small bodies) [56, 57]. While the stability analysis is extensive, there exists limited literature on the controllability of these coupled dynamics [58–61].

In Chapter 6, we consider the question of controllability of the coupled rotational and translational dynamics if the spacecraft is only equipped with internal attitude actuation. The only controllability analysis of a spacecraft in a central gravity field with attitude actuation was performed by Lian et al. [58]. It was proven that under certain assumptions on spacecraft configurations, a spacecraft was globally control-

lable in terms of translation and orientation as long as the spacecraft could generate three independent torques via either thruster pairs or RWs. However, because the translational dynamics are expressed in inertial space, the topic of local controllability about an equilibrium orbit has not been explored. In addition, even though controllability has been proven, no control law has been developed that can take advantage of this gravity-induced coupling between translational and attitude dynamics.

1.3.2 Contributions & Outline

The contributions of the dissertation towards underactuated spacecraft control are as follows:

1 The derivation of exact and approximate, coupled translational and rotational equations of motion that are relative with respect to an unforced trajectory and which evolve on a manifold defined by constant angular momentum.

2. The small-time local controllability proof for specific spacecraft assemblies equipped with three RWs.

3. The proof that the approximate coupled translational and rotational equations of motion are linearly controllable for certain spacecraft assemblies with great circle equilibrium orbits, facilitating the construction of linear controllers for stabilization.

One of the interesting consequences of this analysis is that the relative dynamics are similar to that of Hill-Clohessy-Wiltshire (HCW) relative spacecraft dynamics [62]. The local controllability analysis is of particular interest, as to the author's knowledge, it has never been explored in the literature. These developments are contained in Chapter 6 of the dissertation.

1.4 Relevant Publications

Below is a list of relevant publications pertaining to the subject matter of this dissertation:

Underactuated Attitude Control

- Petersen, C., Leve, F., and Kolmanovsky, I., "Model Predictive Control of an Underactuated Spacecraft with Two Reaction Wheels." *Journal of Guidance, Control, and Dynamics,* (to appear), AIAA, 2016.

- Petersen, C., Leve, F., and Kolmanovsky, I., "Underactuated Spacecraft Switching Law for Two Reaction Wheels and Constant Angular Momentum." *Journal of Guidance, Control, and Dynamics*, (to appear), AIAA, 2016.

- Petersen, C., Leve, F., Flynn, M., and Kolmanovsky, I., "Recovering Linear Controllability of an Underactuated Spacecraft by Exploiting Solar Radiation Pressure." *Journal of Guidance, Control, and Dynamics*, Vol. 39, No. 4, 2016, pp. 826–837.

- Petersen, C., Leve, F., and Kolmanovsky, I., "On Controllability of an Underactuated Spacecraft with Two Wheels and Constant Nonzero Angular Momentum." *Journal of Guidance, Control, and Dynamics*, (in preparation), AIAA, 2016.

- Petersen, C., Leve, F., and Bloch, A., Kolmanovsky, I., Using Geometric Phase for Attitude Control of a Spacecraft with Two Control Moment Gyros." *Journal of Guidance, Control, and Dynamics*, (in preparation), AIAA, 2016

- Petersen, C., Leve, F., and Kolmanovsky, I., "Hybrid Switching Attitude Control of Underactuated Spacecraft Subject to Solar Radiation Pressure," *Space*

Flight Mechanics, Proceedings of the AIAA/AAS Meeting on, Paper 15-327, AIAA/AAS, Williamsburg, VA, 2015.

- M. Flynn, F. Leve, C. Petersen, and I. Kolmanovsky, Linear Control of Underactuated Spacecraft with Two Reaction Wheels Made Feasible by Solar Radiation Pressure, *American Control, Proceedings of the IEEE Conference on*, IEEE, Chicago, IL, 2015, pp. 3193-3198.

Underactuated Rotational and Translational Control

- Petersen, C., Leve, F., Bloch, A., and Kolmanovsky, I., "Local Controllability of a Spacecraft in a Central Gravity Field with only Attitude Actuation." *Journal of Guidance, Control, and Dynamics*, (in preparation), AIAA, 2016.

1.5 Notation

Throughout this dissertation the following notation is used.

- Frames are denoted by script font, $\mathcal{S}$.
- Bodies (i.e., collections of mass particles) are given by Fraktur font, $\mathfrak{S}$.
- The mass of a body $\mathfrak{S}$ is given by $m_{\mathfrak{S}}$.
- General physical vectors are designated by an overscript arrow $\vec{*}$.
- The physical position vector of A with respect to point B is given by $\vec{r}_{A/B}$.
- The physical angular velocity vector of $\mathcal{S}$ with respect to $\mathcal{T}$ is given by $\vec{\omega}_{\mathcal{S}/\mathcal{T}}$.
- The physical linear angular momentum of A with respect to point B in frame $\mathcal{S}$ is given by $\vec{p}_{A/B/\mathcal{S}}$.
- The physical angular momentum of A with respect to point B in frame $\mathcal{S}$ is given by $\vec{H}_{A/B/\mathcal{S}}$.

- Physical unit vectors are expressed with an overscript hat, $\hat{*}$.

- The physical inertia matrix of body $\mathfrak{S}$ with respect to B is denoted by $\vec{J}_{\mathfrak{S}/B}$. Note that the physical inertia matrix is coordinate-independent and operates by dyadic product on a physical vector to produce a physical vector, see [63].

- The time derivative of a physical vector or matrix $\vec{*}$ with respect to a given frame $\mathcal{S}$ is $\overset{\mathcal{S}\cdot}{\vec{*}}$.

- The notation for a mathematical vector obtained by resolving a physical vector $\vec{r}$ in a given frame $\mathcal{S}$ is $\vec{r}|_{\mathcal{S}}$.

- All orientation matrices are denoted by bold font, $\mathbf{B}$.

- All mathematical vectors/matrices are designated by overbars, $\bar{*}$.

- All mathematical unit vectors are given by overscript checks, $\check{*}$.

- An $n \times n$ identity matrix is denoted as I_n.

- The trace of a mathematical matrix $\bar{J}$ is denoted by $\mathrm{tr}\left[\bar{J}\right]$.

- The determinant of a mathematical matrix $\bar{J}$ is denoted by $\det\left[\bar{J}\right]$.

- The skew-symmetric operator is given by $[*]^{\times}$. This operator is related to the cross product between physical vectors or mathematical vectors, i.e., $\vec{r}_{A/B} \times \vec{r}_{C/B} = \left[\vec{r}_{A/B}\right]^{\times} \vec{r}_{C/B}$ and $\bar{a} \times \bar{b} = [\bar{a}]^{\times} \bar{b}$. In particular, for mathematical vectors of the general form $\bar{a} = [\ a_1 \ \ a_2 \ \ a_3\ ]^{\mathrm{T}}$,

$$[\bar{a}]^{\times} = \begin{bmatrix} 0 & -a_3 & a_2 \\ a_3 & 0 & -a_1 \\ -a_2 & a_1 & 0 \end{bmatrix}. \tag{1.1}$$

- The double cross operator is given by $[*]^{2\times} = \left([*]^{\times}\right)^2$.

CHAPTER 2

Attitude Equations of Motion

The following chapter derives equations of motion which are subsequently used in Chapters 3, 4, and 5. Step-by step derivations are given, with a summary of the equations, variables, and assumptions provided afterwards. Please refer to Section 1.5 for clarifications on the notation. While the equations of motion are derived in other references (e.g. see [1, 63, 64]), in this chapter we provide relevant derivations and assumptions in one place, utilizing common notation. In addition, there are derivations which include the general treatment of reduced attitude equations which are novel.

2.1 Spacecraft Configuration

For the underactuated attitude control problem, we will consider a rigid spacecraft bus equipped with one of three types of actuators,

- External moment actuation via pairs of gas thrusters or of cold gas jets;
- RW actuation;
- CMG actuation.

Each type of actuation has its advantages and disadvantages, which are discussed below.

2.1.1 External Moment Actuation

External moment actuation using thrusters or jets is a simple way to perform attitude maneuvers, and is advantageous in that it is not restricted by the law of angular momentum conservation. The disadvantage is that thrusters are typically on-off, and thus any intermediary values of thrust must be obtained through pulse-width modulation (PWM), resulting in coarse attitude maneuvers. The most limiting factor to thruster-based actuation is that fuel must be expended. Thus thrusters are used sparingly for attitude maneuvers and desaturation of RWs [65, 66].

2.1.2 Reaction Wheel Actuation

RWs are flywheels with spin axes fixed relative to the spacecraft bus and with the wheel speeds controlled using electric motors. By spinning up and down the wheel, momentum is exchanged to and from the spacecraft bus, resulting in a torque that causes the spacecraft to rotate. There are two large incentives to using RWs. Firstly, because RWs only require electric power, no fuel is expended while performing maneuvers. Secondly, since the spinning of the wheel can be commanded accurately, RWs can be used for precise-pointing missions. However, RWs are internal moment devices and must obey the law of angular momentum conservation. In addition, operating the wheels in the so called "zero crossing" region (near zero speed), where friction and stiction are high, can increase power consumption and degrade the operational life of the actuator. RWs also cannot exert constant torques for long periods of time. Since constant torque corresponds to constant wheel acceleration, the RWs may reach their saturation limits, preventing the further transfer of momentum necessary for a desired attitude maneuver. To desaturate the wheels, momentum dumping maneuvers can be performed with actuators that provide an external torque and are not constrained by angular momentum conservation, such as external thrusters [65, 66], magnetorquers [67–69], or both [70].

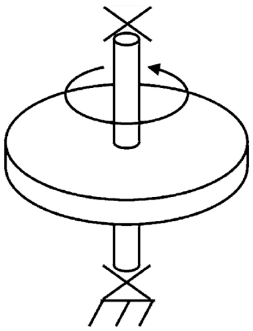

Figure 2.1: Simplified RW [1].

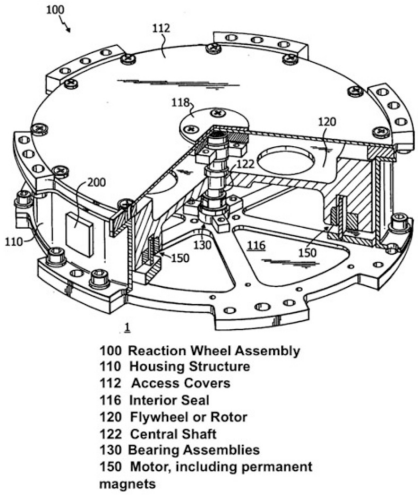

Figure 2.2: RW major parts [1].

2.1.3 Control Moment Gyro Actuation

CMGs are also momentum exchanging devices and can be thought of as extensions of RWs [1], in that the spin axes are free to rotate within the spacecraft bus. Though torques can be generated by accelerating the wheel as in the RW case, larger torques can be produced by rotating the spin axis of the wheel. CMG actuators are advantageous in that they can be used for precise pointing, do not expend fuel, and can generate a larger magnitude of torque. However, because these actuators are internal moment devices, they are, similarly to RWs, constrained by the law of angular momentum conservation. Furthermore, because the main contribution to the total

torque is produced by rotating the spin axis, there are configurations in which all of the CMG torque axes lie in a plane. This is known as CMG singularity, and while such configurations can be avoided using some steering laws [71], the problem in dealing with such singularities is still being actively researched. In this thesis, we will consider the most common type of CMG, a single gimbaled control moment gyro in which the spin axis spans a plane and whose wheel is spinning at a constant rate.

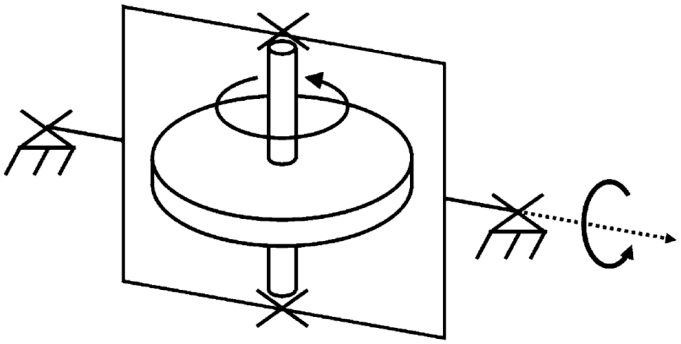

Figure 2.3: Simplified CMG [1].

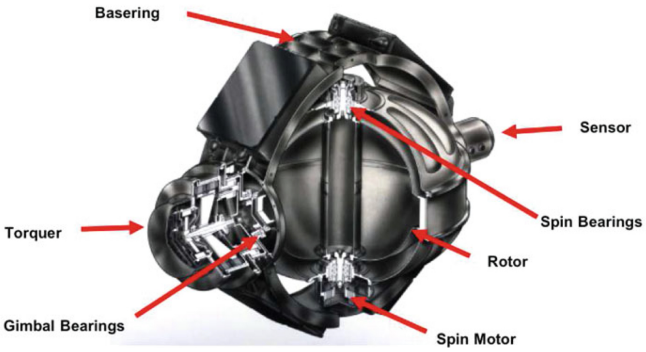

Figure 2.4: CMG major parts [1].

2.2 Frames

The rotational equations of motion are derived with the help of several frames:

- An inertial frame $\mathcal{I}$;

- A frame $\mathcal{B}$ with an orthonormal coordinate system defined by $\hat{b}_x, \hat{b}_y, \hat{b}_z$ which is attached to the spacecraft bus;

- Frames $\mathcal{W}_i$ with orthonormal coordinate systems defined by $\hat{w}_{ix}, \hat{w}_{iy}, \hat{w}_{iz}$ which are attached to the principal frames for each ith RW;

- Frames $\mathcal{G}_j$ with orthonormal coordinate systems defined by $\hat{g}_{jx}, \hat{g}_{jy}, \hat{g}_{jz}$ which are attached to the principal frames for each jth gimbal. The coordinate systems are also assumed to align with the principal axes of the jth rotor;

- Frames $\mathcal{R}_j$ attached to the jth rotor.

Without loss of generality, we assume that frame $\mathcal{I}$ is aligned to coincide with the desired inertial pointing attitude, the unit vectors $\hat{w}_{ix}$ and $\hat{g}_{jx}$ are aligned with the spin axes of the RW and rotor, respectively, and the unit vector $\hat{g}_{jy}$ is aligned with the gimbal spin axis. The objective in Chapters 3, 4, and 5 is to align $\mathcal{B}$ with $\mathcal{I}$. Note as well that at this point, we do not assume that any frame's origin coincides with the center-of-mass (COM) of the spacecraft bus.

2.3 Attitude Representations & Kinematics

In this dissertation we will use two different types of attitude representations to describe the orientation of $\mathcal{B}$ relative to $\mathcal{I}$; orientation matrices and 3-2-1 Euler angles.

Orientation matrices, also known as direction cosine matrices (DCMs), are the most direct way of describing attitude. All orientation matrices belong to the matrix representation of the mathematical group $SO(3)$ (which stands for the special orthogonal group of 3×3 matrices with determinant equal to 1). If $\mathbf{B}$ is the orientation matrix of $\mathcal{B}$ relative to $\mathcal{I}$ and $\bar{\omega} = [\ \omega_1 \ \ \omega_2 \ \ \omega_3\ ]^{\mathrm{T}}$ is the angular velocity of $\mathcal{B}$ relative to $\mathcal{I}$ expressed in $\mathcal{B}$ (i.e., $\bar{\omega} = \vec{\omega}_{\mathcal{B}/\mathcal{I}}\big|_{\mathcal{B}}$), then the orientation kinematics, given by [64],

are

$$\dot{\mathbf{B}} = -\left[\bar{\omega}\right]^{\times} \mathbf{B}. \tag{2.1}$$

Equation (2.1) is simple and linear, but since orientation matrices are constrained to have a determinant of 1, the nine matrix entries are constrained by six algebraic equations.

The second type of attitude parameterization used is a sequence of 3-2-1 Euler angles ψ (yaw), θ (pitch), and ϕ (roll). With this representation, the matrix $\mathbf{B}$ can be constructed as

$$\mathbf{B} = \begin{bmatrix} \theta_c\psi_c & \theta_c\psi_s & -\theta_s \\ \phi_s\theta_s\psi_c - \phi_c\psi_s & \phi_s\theta_s\psi_s + \phi_c\psi_c & \phi_s\theta_c \\ \phi_c\theta_s\psi_c + \phi_s\psi_s & \phi_c\theta_s\psi_s - \phi_s\psi_c & \phi_c\theta_c \end{bmatrix}, \tag{2.2}$$

where $\sin(*) = *_s$ and $\cos(*) = *_c$. The kinematic equations using Euler angles, given in [64], are

$$\dot{\bar{\Theta}} = \bar{M}(\bar{\Theta})\bar{\omega}, \tag{2.3}$$

where $\bar{\Theta} = [\ \phi \ \ \theta \ \ \psi\ ]^{\mathrm{T}}$ and

$$\bar{M}(\Theta) = \frac{1}{\cos(\theta)} \begin{bmatrix} \cos(\theta) & \sin(\phi)\sin(\theta) & \cos(\phi)\sin(\theta) \\ 0 & \cos(\phi)\cos(\theta) & -\sin(\phi)\cos(\theta) \\ 0 & \sin(\phi) & \cos(\phi) \end{bmatrix}. \tag{2.4}$$

Note that (2.3) is undefined at $\theta = 90°$. This is due to that fact that there is no unique mapping from an orientation matrix to an Euler sequence with $\theta = 90°$. This phenomenon is called gimbal lock, and it is a natural consequence of any three parameter representation of orientation. Thus 3-2-1 Euler angles are primarily used when small attitude maneuvers are considered.

2.4 Angular Momentum

The total angular momentum of the spacecraft system $\mathfrak{T}$ about a point O (which we will take to be fixed in the spacecraft bus) in the inertial frame $\mathcal{I}$ can be given as the sum of individual terms,

$$\vec{H}_{_{\mathfrak{T}/O/\mathcal{I}}} = \vec{H}_{_{\mathfrak{B}/O/\mathcal{I}}} + \sum_{i=1}^{N_{RW}} \vec{H}_{_{\mathfrak{W}_i/O/\mathcal{I}}} + \sum_{j=1}^{N_{CMG}} \vec{H}_{_{\mathfrak{CMG}_j/O/\mathcal{I}}}, \tag{2.5}$$

where $\vec{H}_{_{\mathfrak{B}/O/\mathcal{I}}}$ is the angular momentum of the spacecraft bus about O, $\vec{H}_{_{\mathfrak{W}_i/O/\mathcal{I}}}$ is the angular momentum of the ith RW about O, and $\vec{H}_{_{\mathfrak{CMG}_j/O/\mathcal{I}}}$ is the angular momentum of the jth CMG about O. Note that the individual momentum components in (2.5) are with respect to the inertial frame $\mathcal{I}$. Each of the individual momentum components are characterized in the subsections that follow.

2.4.1 Spacecraft Bus Angular Momentum

The angular momentum of the spacecraft bus about point O is given by

$$\vec{H}_{_{\mathfrak{B}/O/\mathcal{I}}} = \int_{\mathfrak{B}} \left(\vec{r}_{_{B_c/O}} + \vec{r}_{_{\rho/B_c}}\right) \times \left(\overset{\mathcal{I}}{\vec{r}}_{_{B_c/O}} + \overset{\mathcal{I}}{\vec{r}}_{_{\rho/B_c}}\right) dm, \tag{2.6}$$

where point B_c is a point at the bus' COM and ρ designates an infinitesimal point mass in the bus. Using the transport theorem on (2.6) yields

$$\vec{H}_{_{\mathfrak{B}/O/\mathcal{I}}} = \int_{\mathfrak{B}} \left(\vec{r}_{_{B_c/O}} + \vec{r}_{_{\rho/B_c}}\right) \times \left(\overset{\mathcal{B}}{\vec{r}}_{_{B_c/O}} + \overset{\mathcal{B}}{\vec{r}}_{_{\rho/B_c}} + \vec{\omega}_{_{\mathcal{B}/\mathcal{I}}} \times \left(\vec{r}_{_{B_c/O}} + \vec{r}_{_{\rho/B_c}}\right)\right) dm. \tag{2.7}$$

We now make the following assumption:

Assumption 2.1 The spacecraft bus is a rigid body.

By Assumption 2.1, $\overset{\mathcal{B}\cdot}{\vec{r}}_{\rho/O} = 0$ and $\overset{\mathcal{B}\cdot}{\vec{r}}_{B_c/O} = 0$. Since $\int_{\mathfrak{B}} \vec{r}_{\rho/B_c} dm = 0$, (2.7) simplifies to

$$\vec{H}_{\mathfrak{B}/O/\mathcal{I}} = -\int_{\mathfrak{B}} \left(\left[\vec{r}_{\rho/B_c}\right]^{2\times} + \left[\vec{r}_{\rho/B_c}\right]^{2\times} \right) \vec{\omega}_{\mathcal{B}/\mathcal{I}} dm. \tag{2.8}$$

Integrating over the entire body in (2.8) gives the final inertial angular momentum expression

$$\begin{aligned} \vec{H}_{\mathfrak{B}/O/\mathcal{I}} &= \left(-m_{\mathfrak{B}} \left[\vec{r}_{B_c/O}\right]^{2\times} + \vec{J}_{\mathfrak{B}/B_c} \right) \vec{\omega}_{\mathcal{B}/\mathcal{I}} \\ &= \vec{J}_{\mathfrak{B}/O} \vec{\omega}_{\mathcal{B}/\mathcal{I}}. \end{aligned} \tag{2.9}$$

2.4.2 Reaction Wheel Angular Momentum

Consider an ith RW wheel in the spacecraft bus with the following assumptions:

Assumption 2.2 The RW rotors are rigid with constant density.

Assumption 2.3 The RWs are symmetric about their spin axes.

Let the location of the ith RW's COM be denoted by point W_{ic}. Then the angular momentum of the ith RW about point O is

$$\vec{H}_{\mathfrak{W}_i/O/\mathcal{I}} = \int_{\mathfrak{W}_i} \left(\vec{r}_{W_{ic}/O} + \vec{r}_{\rho/W_{ic}} \right) \times \left(\overset{\mathcal{I}\cdot}{\vec{r}}_{W_{ic}/O} + \overset{\mathcal{I}\cdot}{\vec{r}}_{\rho/W_{ic}} \right) dm, \tag{2.10}$$

where ρ designates an infinitesimal point mass within the ith RW. Recalling that the RW is spinning and using the transport theorem in (2.10) gives

$$\begin{aligned} \vec{H}_{\mathfrak{W}_i/O/\mathcal{I}} &= \int_{\mathfrak{W}_i} \vec{r}_{W_{ic}/O} \times \left(\overset{\mathcal{B}\cdot}{\vec{r}}_{W_{ic}/O} + \vec{\omega}_{\mathcal{B}/\mathcal{I}} \times \vec{r}_{W_{ic}/O} + \overset{\mathcal{W}_i\cdot}{\vec{r}}_{\rho/W_{ic}} + \vec{\omega}_{\mathcal{W}_i/\mathcal{I}} \times \vec{r}_{\rho/W_{ic}} \right) dm \\ &\quad + \int_{\mathfrak{W}_i} \vec{r}_{\rho/W_{ic}} \times \left(\overset{\mathcal{B}\cdot}{\vec{r}}_{W_{ic}/O} + \vec{\omega}_{\mathcal{B}/\mathcal{I}} \times \vec{r}_{W_{ic}/O} + \overset{\mathcal{W}_i\cdot}{\vec{r}}_{\rho/W_{ic}} + \vec{\omega}_{\mathcal{W}_i/\mathcal{I}} \times \vec{r}_{\rho/W_{ic}} \right) dm. \end{aligned} \tag{2.11}$$

Assumption 2.2 implies that $\overset{\mathcal{W}_i\cdot}{\vec{r}}_{\rho/W_{ic}} = 0$. Assumption 2.3 implies that the COM of the RW lies along its spin axis. Combined with Assumption 2.2, this gives that the COM of the RW remains fixed in $\mathcal{B}$, (i.e., $\overset{\mathcal{B}\cdot}{\vec{r}}_{W_{ic}/O} = 0$). Then (2.11) simplifies to

$$\vec{H}_{\mathfrak{W}_i/O/\mathcal{I}} = -\int_{\mathfrak{W}_i} \left(\left(\left[\vec{r}_{W_{ic}/O}\right]^{2\times} + \left[\vec{r}_{\rho/W_{ic}}\right]^{2\times} \right) \vec{\omega}_{\mathcal{B}/\mathcal{I}} + \left[\vec{r}_{\rho/W_{ic}}\right]^{2\times} \vec{\omega}_{\mathcal{W}_i/\mathcal{B}} \right) dm. \quad (2.12)$$

Integrating (2.12) yields the final angular momentum of the ith RW,

$$\begin{aligned} \vec{H}_{\mathfrak{W}_i/O/\mathcal{I}} &= \left(-m_{\mathfrak{W}_i} \left[\vec{r}_{W_{ic}/O}\right]^{2\times} + \vec{J}_{\mathfrak{W}_i/W_{ic}} \right) \vec{\omega}_{\mathcal{B}/\mathcal{I}} + \vec{J}_{\mathfrak{W}_i/W_{ic}} \vec{\omega}_{\mathcal{W}_i/\mathcal{B}} \\ &= \vec{J}_{\mathfrak{W}_i/O} \vec{\omega}_{\mathcal{B}/\mathcal{I}} + \vec{J}_{\mathfrak{W}_i/W_{ic}} \vec{\omega}_{\mathcal{W}_i/\mathcal{B}}. \end{aligned} \quad (2.13)$$

2.4.3 Angular Momentum of the Control Moment Gyro

For the jth CMG, we make the following assumptions:

Assumption 2.4 Both the gimbal and the rotor of each CMG are two separate rigid bodies of constant density.

Assumption 2.5 Both the gimbal and rotor of each CMG are symmetric about their spin axes.

Assumption 2.4 and Assumption 2.5 will play similar roles as they did in the RW case. Since the CMG is a configuration of two rigid bodies, the total angular momentum contribution of the jth CMG is the sum of its parts. Thus,

$$\vec{H}_{\mathfrak{CMG}_j/O/\mathcal{I}} = \vec{H}_{\mathfrak{R}_j/O/\mathcal{I}} + \vec{H}_{\mathfrak{G}_j/O/\mathcal{I}}. \quad (2.14)$$

The derivation of the gimbal's angular momentum is the same as for the RW case. Denote by G_{jc} the location of the jth gimbal's COM. As in the RW case, Assumption

2.4 and Assumption 2.5 imply that the COM of the gimbal alone is along its spin axis and is fixed in frame $\mathcal{B}$. Thus its angular momentum about O is

$$\vec{H}_{\mathfrak{G}_j/O/\mathcal{I}} = \vec{J}_{\mathfrak{G}_j/O}\vec{\omega}_{\mathcal{B}/\mathcal{I}} + \vec{J}_{\mathfrak{G}_j/G_{jc}}\vec{\omega}_{\mathcal{G}_j/\mathcal{B}}. \tag{2.15}$$

Now consider the rotor of the jth CMG. Denoting its COM by R_{jc}, the rotor angular momentum contribution about O is

$$\vec{H}_{\mathfrak{R}_j/O/\mathcal{I}} = \int_{\mathfrak{R}_j} \left(\vec{r}_{R_{jc}/O} + \vec{r}_{\rho/R_{jc}}\right) \times \left(\overset{\mathcal{I}\cdot}{\vec{r}}_{R_{jc}/O} + \overset{\mathcal{I}\cdot}{\vec{r}}_{\rho/R_{jc}}\right) dm. \tag{2.16}$$

In a similar fashion as when deriving the dynamics for the spacecraft bus, RW, and CMG gimbal, we use the transport theorem in (2.16) and obtain

$$\begin{aligned}\vec{H}_{\mathfrak{W}_i/O/\mathcal{I}} &= \int_{\mathfrak{R}_j} \vec{r}_{R_{jc}/O} \times \left(\overset{\mathcal{B}\cdot}{\vec{r}}_{R_{jc}/O} + \vec{\omega}_{\mathcal{B}/\mathcal{I}} \times \vec{r}_{R_{jc}/O} + \overset{\mathcal{R}_j\cdot}{\vec{r}}_{\rho/R_{jc}} + \vec{\omega}_{\mathcal{R}_j/\mathcal{I}} \times \vec{r}_{\rho/R_{jc}}\right) dm \\ &\quad + \int_{\mathfrak{R}_j} \vec{r}_{\rho/R_{jc}} \times \left(\overset{\mathcal{B}\cdot}{\vec{r}}_{R_{jc}/O} + \vec{\omega}_{\mathcal{B}/\mathcal{I}} \times \vec{r}_{R_{jc}/O} + \overset{\mathcal{R}_j\cdot}{\vec{r}}_{\rho/R_{jc}} + \vec{\omega}_{\mathcal{R}_j/\mathcal{I}} \times \vec{r}_{\rho/R_{jc}}\right) dm.\end{aligned} \tag{2.17}$$

Under Assumption 2.4 and 2.5, the location of the rotor's COM is along its rotation axis, but due to the rotation of the gimbal, it could be changing with time in $\mathcal{B}$ (i.e., $\overset{\mathcal{B}\cdot}{\vec{r}}_{R_{jc}/O} \neq 0$ in contrast to the gimbal and the RW case). Thus the following assumption is now made:

> **Assumption 2.6** The COM of each rotor is located at the intersection of the rotor spin axis and the gimbal spin axis.

Assumption 2.6 is valid as manufacturers of CMGs will balance the gimbals and rotors in such a fashion. With Assumption 2.6, the rotor's COM remains fixed in $\mathcal{B}$, and its

angular momentum becomes

$$\vec{H}_{\mathfrak{R}_j/O/\mathcal{I}} = -\int_{\mathfrak{R}_j} \left(\left(\left[\vec{r}_{R_{jc}/O} \right]^{2\times} + \left[\vec{r}_{\rho/R_{jc}} \right]^{2\times} \right) \vec{\omega}_{\mathcal{B}/\mathcal{I}} + \left[\vec{r}_{\rho/R_{jc}} \right]^{2\times} \vec{\omega}_{\mathcal{R}_j/\mathcal{B}} \right) dm. \quad (2.18)$$

Integrating (2.18) over the entire rotor gives

$$\begin{aligned} \vec{H}_{\mathfrak{R}_j/O/\mathcal{I}} &= (-m_{\mathfrak{R}_j} \left[\vec{r}_{R_{jc}/O} \right]^{2\times} + \vec{J}_{\mathfrak{R}_j/R_{jc}}) \vec{\omega}_{\mathcal{B}/\mathcal{I}} + \vec{J}_{\mathfrak{R}_j/R_{ic}} \vec{\omega}_{\mathcal{R}_j/\mathcal{B}} \\ &= \vec{J}_{\mathfrak{R}_j/O} \vec{\omega}_{\mathcal{B}/\mathcal{I}} + \vec{J}_{\mathfrak{R}_j/R_{ic}} \vec{\omega}_{\mathcal{G}_j/\mathcal{B}} + \vec{J}_{\mathfrak{R}_j/R_{ic}} \vec{\omega}_{\mathcal{R}_j/\mathcal{G}_j}. \end{aligned} \quad (2.19)$$

The total angular momentum due to the jth CMG is then

$$\vec{H}_{\mathfrak{CMG}_j/O/\mathcal{I}} = \left(\vec{J}_{\mathfrak{G}_j/O} + \vec{J}_{\mathfrak{R}_j/O} \right) \vec{\omega}_{\mathcal{B}/\mathcal{I}} + \left(\vec{J}_{\mathfrak{G}_j/G_{jc}} + \vec{J}_{\mathfrak{R}_j/R_{jc}} \right) \vec{\omega}_{\mathcal{G}_j/\mathcal{B}} + \vec{J}_{\mathfrak{R}_j/R_{jc}} \vec{\omega}_{\mathcal{R}_j/\mathcal{G}_j}. \quad (2.20)$$

2.4.4 Total Angular Momentum

The total angular momentum of the spacecraft using (2.9), (2.13) and (2.20) is

$$\begin{aligned} \vec{H}_{\mathfrak{T}/O/\mathcal{I}} &= \vec{J}_{\mathfrak{T}/O} \vec{\omega}_{\mathcal{B}/\mathcal{I}} + \sum_{i=1}^{N_{RW}} \vec{J}_{\mathfrak{W}_i/W_{ic}} \vec{\omega}_{\mathcal{W}_i/\mathcal{B}} \\ &\quad + \sum_{j=1}^{N_{CMG}} \left(\vec{J}_{\mathfrak{G}_j/G_{jc}} + \vec{J}_{\mathfrak{R}_j/R_{jc}} \right) \vec{\omega}_{\mathcal{G}_j/\mathcal{B}} + \vec{J}_{\mathfrak{R}/R_{jc}} \vec{\omega}_{\mathcal{R}_j/\mathcal{G}_j}, \end{aligned} \quad (2.21)$$

where

$$\vec{J}_{\mathfrak{T}/O} = \vec{J}_{\mathcal{B}/O} + \sum_{i=1}^{N_{RW}} \vec{J}_{\mathfrak{W}_i/O} + \sum_{j=1}^{N_{CMG}} \vec{J}_{\mathfrak{G}_j/O} + \vec{J}_{\mathfrak{R}_j/O}. \quad (2.22)$$

Note that since frames $\mathcal{W}_i$ and $\mathcal{G}_j$ by construction coincide with the principal frames of the RWs and the CMG gimbals/rotors, respectively, the actuator physical

inertia matrices can be expressed as

$$\begin{aligned}
\vec{J}_{\mathfrak{W}_{i/W_{ic}}} &= J_{w_{s}i}\hat{w}_{ix}\hat{w}'_{ix} + J_{w_{t}i}\hat{w}_{iy}\hat{w}'_{iy} + J_{w_{t}i}\hat{w}_{iz}\hat{w}'_{iz}, \\
\vec{J}_{\mathfrak{G}_{j/G_{jc}}} &= J_{g_{s}j}\hat{g}_{jx}\hat{g}'_{jx} + J_{g_{g}j}\hat{g}_{jy}\hat{g}'_{jy} + J_{g_{t}j}\hat{g}_{jz}\hat{g}'_{jz}, \\
\vec{R}_{\mathfrak{R}_{j/R_{jc}}} &= J_{r_{s}j}\hat{g}_{jx}\hat{g}'_{jx} + J_{r_{t}j}\hat{g}_{jy}\hat{g}'_{jy} + J_{r_{t}j}\hat{g}_{jz}\hat{g}'_{jz},
\end{aligned} \tag{2.23}$$

where $*'$ is the dual of a physical vector $*$ [63]. Note that the constant density and symmetry assumptions about the spin axes are reflected in these expressions. We can also express the rotations of the RW, gimbal, and rotor by the following expressions:

$$\begin{aligned}
\vec{\omega}_{\mathcal{W}_{i}/\mathcal{B}} &= \nu_{i}\hat{w}_{ix}, \\
\vec{\omega}_{\mathcal{G}_{j}/\mathcal{B}} &= \dot{\delta}_{j}\hat{g}_{jy}, \\
\vec{\omega}_{\mathcal{R}_{j}/\mathcal{G}_{j}} &= \eta_{j}\hat{g}_{jx},
\end{aligned} \tag{2.24}$$

where ν_{i} is the speed of the ith RW, $\dot{\delta}_{j}$ is the gimbal rate of the jth CMG, and η_{j} is the rotor speed of the jth CMG. From (2.23) and (2.24), we note that

1 The vector $\vec{J}_{\mathfrak{W}_{i/W_{ic}}}\vec{\omega}_{\mathcal{W}_{i}/\mathcal{B}}$ is the angular momentum component about the RW spin axis;

2 The vector $\vec{J}_{\mathfrak{GR}_{j/G_{jc}}}\vec{\omega}_{\mathcal{G}_{j}/\mathcal{B}}$ is the angular momentum component of the rotor and the gimbal about the gimbal axis;

3 The vector $\vec{J}_{\mathfrak{R}_{j/R_{jc}}}\vec{\omega}_{\mathcal{R}_{j}/\mathcal{G}_{j}}$ is the angular momentum component of the rotor about the rotor axis.

Therefore, substituting in (2.23) and (2.24) into (2.21) gives the final angular mo-

mentum relation

$$\vec{H}_{\mathfrak{T}/O/\mathcal{I}} = \vec{J}_{\mathfrak{T}/O}\vec{\omega}_{\mathcal{B}/\mathcal{I}} + \sum_{i=1}^{N_{RW}} J_{w_s i}\nu_i\hat{w}_{ix} + \sum_{j=1}^{N_{CMG}} \left(J_{g_g j} + J_{r_t j}\right)\dot{\delta}_j\hat{g}_{jy} + J_{r_s i}\eta_j\hat{g}_{jx}. \tag{2.25}$$

2.5 Dynamics

From the angular momentum properties, it follows that

$$\overset{\mathcal{I}\cdot}{\vec{H}}_{\mathfrak{T}/O/\mathcal{I}} + m_{\mathfrak{T}}\vec{r}_{T_c/O} \times \overset{\mathcal{I}\cdot\cdot}{\vec{r}}_{O/A} = \vec{M}_{\mathfrak{T}/O}, \tag{2.26}$$

where $\vec{M}_{\mathfrak{T}/O}$ are the external moments acting on the spacecraft system about point O, A is a point fixed in $\mathcal{I}$, and T_c is a point coinciding with the COM of the entire spacecraft system $\mathfrak{T}$. At this point we make the following assumption:

> **Assumption 2.7** The COM of the spacecraft system that includes the spacecraft bus, RWs, and CMGs coincides with O,

which eliminates the second term on the left in (2.26). In order to calculate the time derivative of the total angular momentum with respect to the inertial frame, we will separate the problem into parts and use various transport theorems.

Firstly, we analyze the time derivative of the first term of (2.25), yielding

$$\begin{aligned} \overbrace{\vec{J}_{\mathfrak{T}/O}\vec{\omega}_{\mathcal{B}/\mathcal{I}}}^{\mathcal{I}\cdot} &= \overbrace{\vec{J}_{\mathfrak{T}/O}\vec{\omega}_{\mathcal{B}/\mathcal{I}}}^{\mathcal{B}\cdot} + \vec{\omega}_{\mathcal{B}/\mathcal{I}} \times \vec{J}_{\mathfrak{T}/O}\vec{\omega}_{\mathcal{B}/\mathcal{I}}, \\ &= \overset{\mathcal{B}\cdot}{\vec{J}}_{\mathfrak{T}/O}\vec{\omega}_{\mathcal{B}/\mathcal{I}} + \vec{J}_{\mathfrak{T}/O}\overset{\mathcal{B}\cdot}{\vec{\omega}}_{\mathcal{B}/\mathcal{I}} + +\vec{\omega}_{\mathcal{B}/\mathcal{I}} \times \vec{J}_{\mathfrak{T}/O}\vec{\omega}_{\mathcal{B}/\mathcal{I}}. \end{aligned} \tag{2.27}$$

Note that the spacecraft bus is a rigid body and thus its inertia matrix does not change with time in $\mathcal{B}$,

$$\overset{\mathcal{B}\cdot}{\vec{J}}_{\mathfrak{B}/O} = 0. \tag{2.28}$$

By Assumption 2.2 and Assumption 2.3, the RWs are symmetric and of constant density. Thus the inertia matrix does not change in time with respect to frame $\mathcal{B}$, regardless of whether the wheels accelerate,

$$\overset{\mathcal{B}\cdot}{\vec{J}}_{\mathfrak{W}_i/O} = 0. \tag{2.29}$$

The inertia of gimbal of the CMG can, however, change in $\mathcal{B}$, and thus

$$\begin{aligned} \overset{\mathcal{B}\cdot}{\vec{J}}_{\mathfrak{G}_j/O} &= \overset{\mathcal{B}\cdot}{\vec{J}}_{\mathfrak{G}_j/G_{jc}}, \\ &= \left[\vec{\omega}_{\mathcal{G}_j/\mathcal{B}}\right]^{\times} \vec{J}_{\mathfrak{G}_j/G_{jc}} - \vec{J}_{\mathfrak{G}_j/G_{jc}} \left[\vec{\omega}_{\mathcal{G}_j/\mathcal{B}}\right]^{\times}. \end{aligned} \tag{2.30}$$

The rotor's inertia does not change with time in $\mathcal{G}_j$, but it does change with time in $\mathcal{B}$, and therefore

$$\begin{aligned} \overset{\mathcal{B}\cdot}{\vec{J}}_{\mathfrak{R}_j/O} &= \overset{\mathcal{B}\cdot}{\vec{J}}_{\mathfrak{R}_j/R_{jc}}, \\ &= \left[\vec{\omega}_{\mathcal{G}_j/\mathcal{B}}\right]^{\times} \vec{J}_{\mathfrak{R}_j/R_{jc}} - \vec{J}_{\mathfrak{R}_j/R_{jc}} \left[\vec{\omega}_{\mathcal{G}_j/\mathcal{B}}\right]^{\times}. \end{aligned} \tag{2.31}$$

Substituting (2.28)-(2.31) into (2.27) gives

$$\begin{aligned} \overbrace{\vec{J}_{\mathfrak{T}/O}\vec{\omega}_{\mathcal{B}/\mathcal{I}}}^{\mathcal{I}\cdot} &= \vec{J}_{\mathfrak{T}/O}\overset{\mathcal{B}\cdot}{\vec{\omega}}_{\mathcal{B}/\mathcal{I}} + \vec{\omega}_{\mathcal{B}/\mathcal{I}} \times \vec{J}_{\mathfrak{T}/O}\vec{\omega}_{\mathcal{B}/\mathcal{I}} + \left(\sum_{j=1}^{N_{CMG}} \left[\vec{\omega}_{\mathcal{G}_j/\mathcal{B}}\right]^{\times} (\vec{J}_{\mathfrak{G}_j/C_{jc}} + \vec{J}_{\mathfrak{R}_j/C_{jc}})\right)\vec{\omega}_{\mathcal{B}/\mathcal{I}} \\ &\quad - \left(\sum_{j=1}^{N_{CMG}} (\vec{J}_{\mathfrak{G}_j/C_{jc}} + \vec{J}_{\mathfrak{R}_j/C_{jc}}) \left[\vec{\omega}_{\mathcal{G}_j/\mathcal{B}}\right]^{\times}\right)\vec{\omega}_{\mathcal{B}/\mathcal{I}}. \end{aligned} \tag{2.32}$$

For the RWs, note that

$$\sum_{i=1}^{N_{RW}} \overbrace{J_{wsi}\nu_i\hat{w}_{ix}}^{\mathcal{I}\cdot} = \sum_{i=1}^{N_{RW}} J_{wsi}\left(\dot{\nu}_i\hat{w}_{ix} + \nu_i\left[\vec{\omega}_{\mathcal{B}/\mathcal{I}}\right]^{\times}\hat{w}_{ix}\right). \tag{2.33}$$

Similarly for the gimbals of the CMGs,

$$\sum_{j=1}^{N_{CMG}} \overbrace{\left(J_{g_{gj}} + J_{r_{tj}}\right)\dot{\delta}_j \hat{g}_{j_y}}^{\mathcal{I}\cdot} = \sum_{j=1}^{N_{CMG}} \left(J_{g_{gj}} + J_{r_{tj}}\right)\left(\ddot{\delta}_j \hat{g}_{j_y} + \dot{\delta}_j \left[\vec{\omega}_{\mathcal{B}/\mathcal{I}}\right]^{\times} \hat{g}_{j_y}\right). \tag{2.34}$$

The rotors of the CMGs are a little different, as the spin axis of the rotor changes in $\mathcal{B}$, therefore

$$\begin{aligned}
\sum_{j=1}^{N_{CMG}} \overbrace{J_{r_{si}}\eta_j \hat{g}_{j_x}}^{\mathcal{I}\cdot} &= \sum_{j=1}^{N_{CMG}} J_{r_{si}}\left(\dot{\eta}_j \hat{g}_{j_x} + \eta_j \left[\vec{\omega}_{\mathcal{G}_j/I}\right]^{\times} \hat{g}_{j_x}\right) \\
&= \sum_{j=1}^{N_{CMG}} J_{r_{si}}\left(\dot{\eta}_j \hat{g}_{j_x} + \eta_j \left[\dot{\delta}_j \hat{g}_{j_y} + \vec{\omega}_{\mathcal{B}/I}\right]^{\times} \hat{g}_{j_x}\right) \\
&= \sum_{j=1}^{N_{CMG}} J_{r_{si}}\left(\dot{\eta}_j \hat{g}_{j_x} + \eta_j \dot{\delta}_j \hat{g}_{z_j} + \left[\vec{\omega}_{\mathcal{B}/I}\right]^{\times} \hat{g}_{j_x}\right).
\end{aligned} \tag{2.35}$$

The full dynamics, substituting in (2.32), (2.33), (2.34), and (2.35) into (2.26) is given by

$$\begin{aligned}
\vec{J}_{\mathfrak{T}/O} \overset{\mathcal{B}\cdot}{\vec{\omega}}_{\mathcal{B}/\mathcal{I}} &= -\left[\vec{\omega}_{\mathcal{B}/\mathcal{I}}\right]^{\times} \vec{H}_{\mathfrak{T}/O/\mathcal{I}} + \vec{M}_{ext/O} - \sum_{i=1}^{N_{RW}} J_{w_{si}} \dot{\nu}_i \hat{w}_{i_x} - \sum_{j=1}^{N_{CMG}} \left(J_{g_{gj}} + J_{r_{tj}}\right)\ddot{\delta}_j \hat{g}_{j_y} \\
&\quad - \sum_{j=1}^{N_{CMG}} J_{r_{si}}\left(\dot{\eta}_j \hat{g}_{j_x} + \eta_j \dot{\delta}_j \hat{g}_{z_j}\right) + \left(\sum_{j=1}^{N_{CMG}} \left[\vec{\omega}_{\mathcal{G}_j/\mathcal{B}}\right]^{\times} (\vec{J}_{\mathfrak{G}_{j/C_{jc}}}\right)\vec{\omega}_{\mathcal{B}/\mathcal{I}} \\
&\quad - \left(\sum_{j=1}^{N_{CMG}} (\vec{J}_{\mathfrak{G}_{j/C_{jc}}} + \vec{J}_{\mathfrak{R}_{j/C_{jc}}})\left[\vec{\omega}_{\mathcal{G}_j/\mathcal{B}}\right]^{\times}\right)\vec{\omega}_{\mathcal{B}/\mathcal{I}}.
\end{aligned} \tag{2.36}$$

2.6 Summary and Resolved Equations of Motion

The total angular momentum and dynamics of the spacecraft system, when physical vectors are resolved (notation is given after the equations), are described by the following equations:

Angular Momentum

$$\mathbf{B}\bar{H} = \bar{J}\bar{\omega} + \sum_{i=1}^{N_{RW}} J_{w_{s}i}\nu_{i}\check{w}_{i} + \sum_{j=1}^{N_{CMG}} \left(J_{g_{g}j} + J_{r_{t}j}\right)\dot{\delta}_{j}\check{g}_{j} + J_{r_{s}i}\eta_{j}\check{h}_{j}, \tag{2.37}$$

where

$$\bar{J} \;=\; \bar{J}_{\mathfrak{B}} + \sum_{i=1}^{N_{RW}} \bar{J}_{\mathfrak{W}_{j}} + \sum_{j=1}^{N_{CMG}} \mathbf{G}_{j}^{\mathrm{T}}\left(\bar{J}_{\mathfrak{G}_{j}} + \bar{J}_{\mathfrak{R}_{j}}\right)\mathbf{G}_{j} \;. \tag{2.38}$$

Dynamics

$$\begin{aligned}\bar{J}\dot{\bar{\omega}} \;=\; & [\bar{\omega}]^{\times}\mathbf{B}\bar{H} + \bar{M}_{ext} - \sum_{i=1}^{N_{RW}} J_{w_{s}i}\dot{\nu}_{i}\check{w}_{i} \\ & - \sum_{j=1}^{N_{CMG}} \left(J_{g_{g}j} + J_{r_{t}j}\right)\ddot{\delta}_{j}\check{g}_{j} - \sum_{j=1}^{N_{CMG}} J_{r_{s}i}\left(\dot{\eta}_{j}\check{h}_{j} + \eta_{j}\dot{\delta}_{j}\check{\tau}_{j}\right) \\ & - \sum_{j=1}^{N_{CMG}} \dot{\delta}_{j}\left(\left[\check{g}_{j}\right]^{\times}\mathbf{G}_{j}^{\mathrm{T}}(\bar{J}_{\mathfrak{G}_{j}} + \bar{J}_{\mathfrak{R}_{j}})\mathbf{G}_{j} - \mathbf{G}_{j}^{\mathrm{T}}(\bar{J}_{\mathfrak{G}_{j}} + \bar{J}_{\mathfrak{R}_{j}})\mathbf{G}_{j}\left[\check{g}_{j}\right]^{\times}\right)\bar{\omega}.\end{aligned} \tag{2.39}$$

The following notation corresponds to all related variables

Orientation Matrices

- $\mathbf{B}$: Orientation matrix of $\mathcal{B}$ relative to $\mathcal{I}$,
- $\mathbf{G}_{j}$: Orientation matrix of $\mathcal{G}_{j}$ relative to $\mathcal{B}$.

Rotational Vectors

- $\bar{\omega} = \vec{\omega}_{\mathcal{B}/\mathcal{I}}\big|_{\mathcal{B}}$: Angular velocity of $\mathcal{B}$ relative to $\mathcal{I}$ expressed in $\mathcal{B}$,
- $\bar{H} = \vec{H}_{\mathfrak{T}/O/\mathcal{I}}\big|_{\mathcal{I}}$: Total spacecraft system angular momentum about point O expressed in $\mathcal{I}$,
- $\bar{M}_{ext} = \vec{M}_{ext/O}\big|_{\mathcal{B}}$: External moments acting on the spacecraft system expressed in $\mathcal{B}$.

Resolved Inertia Matrices

- $\bar{J} = \vec{J}_{\mathfrak{T}/O}\big|_{\mathcal{B}}$: Locked inertia matrix expressed in $\mathcal{B}$ about point O,
- $\bar{J}_{\mathfrak{B}} = \vec{J}_{\mathfrak{B}/B_c}\big|_{\mathcal{G}}$: Bus inertia matrix expressed in $\mathcal{B}$ about point B_c,
- $\bar{J}_{\mathfrak{W}_i} = \vec{J}_{\mathfrak{W}_i/W_{ic}}\big|_{\mathcal{B}}$: ith RW inertia matrix expressed in $\mathcal{B}$ about point W_{ic},
- $\bar{J}_{\mathfrak{G}_j} = \vec{J}_{\mathfrak{G}_j/G_{jc}}\big|_{\mathcal{G}_j}$: jth gimbal inertia matrix expressed in $\mathcal{G}_j$ about point G_{jc},
- $\bar{J}_{\mathfrak{R}_j} = \vec{J}_{\mathfrak{R}_j/R_{jc}}\big|_{\mathcal{G}_j}$: jth rotor inertia matrix expressed in $\mathcal{G}_j$ about point R_{jc}.

Specific Inertias

- J_{ws_i} : ith RW inertia about its spin axis,
- J_{gs_j} : jth gimbal inertia about its spin axis,
- J_{rs_j} : jth rotor inertia about its spin axis,
- J_{rt_j} : jth rotor inertia about its transversal axis.

Actuator Unit Vectors

- $\check{w}_i = \hat{w}_{ix}\big|_{\mathcal{B}}$: Spin axis of ith RW expressed in $\mathcal{B}$,
- $\check{h}_j = \hat{g}_{jx}\big|_{\mathcal{B}}$: Spin axis of jth rotor expressed in $\mathcal{B}$,
- $\check{g}_j = \hat{g}_{jy}\big|_{\mathcal{B}}$: Spin axis of jth gimbal expressed in $\mathcal{B}$,
- $\check{\tau}_j = \hat{g}_{jz}\big|_{\mathcal{B}}$: Torque axis of jth gimbal expressed in $\mathcal{B}$.

Actuator Parameters

- ν_i : ith RW rate,
- δ_j : jth gimbal angle,
- η_j : jth rotor rate.

And recall that the following assumptions were made:

Assumption 2.1 The spacecraft bus is a rigid body.

Assumption 2.2 The RW rotors are rigid with constant density.

Assumption 2.3 The RWs are symmetric about their spin axes.

Assumption 2.4 Both the gimbal and the rotor of each CMG are two separate rigid bodies of constant density.

Assumption 2.5 Both the gimbal and rotor of each CMG are symmetric about their spin axes.

Assumption 2.6 The COM of the rotor is located at the intersection of the rotor spin axis and the gimbal spin axis.

Assumption 2.7 The COM of the spacecraft system that includes the spacecraft bus, RWs, and CMGs coincides with O.

2.6.1 External Moment Actuation Only

If only external moment actuation is considered, the dynamics of the spacecraft system simplify to

$$\bar{J}_{\mathfrak{B}}\dot{\bar{\omega}} = -[\bar{\omega}]^{\times}\bar{J}_{\mathfrak{B}}\bar{\omega} + \bar{u} + \bar{M}_{ext}. \tag{2.40}$$

In these dynamics, the following assumption is made:

Assumption 2.8 The expulsion of gas does not affect the spacecraft system's mass,

and therefore, for instance, the effects due to fuel slosh do not need to be accounted for. In general this assumption may be relaxed as there are control techniques that account for the effects of mass expulsion [72, 73].

2.6.2 Reaction Wheel Actuation Only

Considering only RW actuation, the dynamics of the spacecraft system become

$$\bar{J}\dot{\bar{\omega}} \;=\; -[\bar{\omega}]^{\times}\left(\bar{J}\bar{\omega}+\sum_{i=1}^{N_{RW}} J_{_{ws}i}\nu_{_i}\check{w}_{_i}\right)-\sum_{i=1}^{N_{RW}} J_{_{ws}i}\dot{\nu}_{_i}\check{w}_{_i}+\bar{M}_{_{ext}}, \tag{2.41}$$

where

$$\bar{J}=\bar{J}_{_{\mathfrak{B}}}+\sum_{i=1}^{N_{RW}}\bar{J}_{_{\mathfrak{W}_i}}. \tag{2.42}$$

The angular momentum of the system can be simply given as

$$\mathbf{B}\bar{H}=\bar{J}\bar{\omega}+\sum_{i=1}^{N_{RW}} J_{_{ws}i}\nu_{_i}\check{w}_{_i}. \tag{2.43}$$

The control inputs to the system are RW accelerations

$$u_{_i}=\dot{\nu}_{_i},\quad i=1\ldots N_{RW}. \tag{2.44}$$

2.6.3 Control Moment Gyro Actuation Only

For the control moment gyro actuation, the angular momentum is given by

$$\mathbf{B}\bar{H}=\bar{J}\bar{\omega}+\sum_{j=1}^{N_{CMG}}\left(J_{_{gg}j}+J_{_{rt}j}\right)\dot{\delta}_{_j}\check{g}_{_j}+J_{_{rs}i}\eta_{_j}\check{h}_{_j}+\bar{M}_{_{ext}} \tag{2.45}$$

where

$$\bar{J} \;=\; \bar{J}_{_{\mathfrak{B}}}+\sum_{j=1}^{N_{CMG}}\mathbf{G}_{_j}^{\mathrm{T}}\left(\bar{J}_{_{\mathfrak{G}_j}}+\bar{J}_{_{\mathfrak{R}_j}}\right)\mathbf{G}_{_j} \tag{2.46}$$

To simplify the treatment, we make the following assumptions

Assumption 2.9 The rotors spin at constant nonzero speeds.

Assumption 2.10 The torque on the spacecraft due to gimbal acceleration is neglectable.

Assumption 2.11 The time rate of change of $\bar{J}$ in $\mathcal{B}$ negligible.

These assumptions are reasonable and commonly made in the treatment of CMG actuation [1]. The dynamics of the spacecraft system with just CMG actuation then become

$$\bar{J}\dot{\bar{\omega}} = [\bar{\omega}]^{\times}\left(\bar{J}\bar{\omega} + \sum_{j=1}^{N_{CMG}}\left(J_{ggj} + J_{rtj}\right)\dot{\delta}_j\check{g}_j + J_{rsi}\eta_j\check{h}_j\right) - \sum_{j=1}^{N_{CMG}}\dot{\delta}_j J_{rsi}\check{\tau}_j + \bar{M}_{ext}. \tag{2.47}$$

The total angular momentum for the system reduces to

$$\mathbf{B}\bar{H} = \bar{J}\bar{\omega} + \sum_{j=1}^{N_{CMG}}\left(J_{ggj} + J_{rtj}\right)\dot{\delta}_j\check{g}_j + J_{rsi}\eta_j\check{h}_j. \tag{2.48}$$

Recall that the gimbal axis $\check{g}_j$ is fixed in the spacecraft bus and therefore, using the orientation matrix $\mathbf{G}_j$, can be explicitly given by

$$\check{g}_j = \mathbf{G}_j^{\mathrm{T}}\begin{bmatrix}0\\0\\1\end{bmatrix}, \tag{2.49}$$

whereas the angular momentum axis $\check{h}_j$ and the torque axis $\check{\tau}_j$ depend on the gimbal angle δ_j and are given by

$$\check{h}_j = \mathbf{G}_j^{\mathrm{T}}\begin{bmatrix}\cos(\delta_j)\\\sin(\delta_j)\\0\end{bmatrix}, \quad \check{\tau}_j = \mathbf{G}_j^{\mathrm{T}}\begin{bmatrix}\sin(\delta_j)\\-\cos(\delta_j)\\0\end{bmatrix}. \tag{2.50}$$

For CMGs, the control inputs are the gimbal rates

$$u_{_i} = \dot{\delta}_{_i}, \quad i = 1 \ldots N_{CMG}. \tag{2.51}$$

2.7 Reduced Attitude Equations of Motion

Consider now the special case in which there are no external moments acting on the spacecraft system (i.e., $\bar{M}_{_{ext}} = 0$). When attitude control is provided by RWs or CMGs, angular momentum is conserved and the spacecraft's motion is constrained. However, this conservation relation can also be exploited to derive a reduced set of attitude equations of motion, denoted as RAE's. In this dissertation, we use two sets of reduced dynamics, one for RWs and one for CMGs.

For RWs, the angular momentum (2.43) can be rewritten as

$$\bar{\omega} = \bar{J}^{-1} \left(\mathbf{B}\bar{H} - \sum_{i=1}^{N_{RW}} J_{_{ws}i} \nu_{_i} \check{w}_{_i} \right). \tag{2.52}$$

We will choose Euler angles to parameterize the attitude in the case of RW actuation. Substituting (2.52) into (2.3), and noting that the control inputs are the RW accelerations, the RAE's for RWs are

$$\begin{aligned} \dot{\bar{\Theta}} &= \bar{M}(\bar{\Theta})\bar{J}^{-1} \left(\mathbf{B}\bar{H} - \sum_{i=1}^{N_{RW}} J_{_{ws}i} \nu_{_i} \check{w}_{_i} \right), \\ \dot{\nu}_{_i} &= u_{_i}, \quad i = 1 \ldots N_{RW}. \end{aligned} \tag{2.53}$$

For CMGs, the angular momentum (2.48) can be similarly rewritten as

$$\bar{\omega} = \bar{J}^{-1} \left(\mathbf{B}\bar{H} - \sum_{j=1}^{N_{CMG}} \left(J_{_{gg}j} + J_{_{rt}j} \right) \dot{\delta}_{_j} \check{g}_{_j} - J_{_{rs}i} \eta_{_j} \check{h}_{_j} \right). \tag{2.54}$$

For attitude parametrization, $SO(3)$ is used. Substituting (2.54) into (2.1), and noting that the control is given by (2.51), the RAE's for CMGs are

$$\begin{aligned} \dot{\mathbf{B}} &= \left[\bar{J}^{-1}\left(\mathbf{B}\bar{H} - \sum_{j=1}^{N_{CMG}}\left(J_{g_{gj}} + J_{r_{tj}}\right)\dot{\delta}_j\check{g}_j - J_{r_{si}}\eta_j\check{h}_j\right)\right]^{\times} B, \\ \dot{\delta}_i &= u_i, \quad i = 1\ldots N_{CMG}. \end{aligned} \tag{2.55}$$

Note that (2.53) and (2.55) are two systems that evolve in time on the kinematic level, defined by some constant inertial angular momentum $\bar{H}$.

CHAPTER 3

Underactuated Attitude Control Using Geometric Switching Feedback Control

3.1 Introduction

This chapter describes new attitude control schemes for an underactuated spacecraft equipped with two external thrusters, or two RWs, or two CMGs. The general approach pursued in this section utilizes the switching feedback stabilization techniques of [74, 75] that exploit the decomposition of the system variables into base variables and fiber variables. The base variables are stabilized to periodic motions with feedback, and the parameters of these periodic motions are adjusted at discrete time instants to induce a change in the fiber variables towards the desired equilibrium. For a spacecraft actuated with either two thrusters or two RWs, the Euler angles and the angular velocities corresponding to the two actuated axes are treated as base variables while the Euler angle and angular velocity corresponding to the uncontrolled axis are treated as the fiber variables. When the spacecraft is actuated by two CMGs, the base variables are chosen as the gimbal angles while the fiber variable is taken as the orientation matrix in $SO(3)$. There are several advantages to these control schemes. Firstly, exponential convergence rates can be achieved. Secondly, these methods are analytic and can be run rapidly onboard in real-time. Thirdly, for the RW case, the method is not restricted to the zero angular momentum assumption.

Finally, for the CMG case, stabilization is possible even though the uncontrollable axis varies with time with respect to a spacecraft bus fixed frame.

3.2 External Moment Actuation

3.2.1 Spacecraft Configuration & Equations of Motion

In this section, we consider a spacecraft system consisting of a bus equipped with two pairs of external thrusters. Recall that without loss of generality we assume frame $\mathcal{I}$ is aligned to coincide with the desired inertial pointing attitude. We also make the following assumptions:

Assumption 3.2.1 The axes $\hat{b}_x$, $\hat{b}_y$, $\hat{b}_z$ of the spacecraft bus fixed frame $\mathcal{B}$ coincide with the spacecraft bus' principal axes.

Assumption 3.2.2 The two pairs of thrusters exert torques about $\hat{b}_x$ and $\hat{b}_y$.

Assumption 3.2.3 There are no other external moments acting on the spacecraft system.

Assumption 3.2.4 The maneuvers being performed involve relatively small attitude adjustments near the desired pointing orientation.

Under the above assumptions, and choosing Euler angles to represent the attitude, the equations of motion (2.3), (2.40) become

$$\begin{aligned} \dot{\bar{\Theta}} &= \bar{M}(\bar{\Theta})\bar{\omega}, \\ \dot{\omega}_1 &= \tfrac{1}{J_1}\left(u_1 + (J_2 - J_3)\omega_2\omega_3\right), \\ \dot{\omega}_2 &= \tfrac{1}{J_2}\left(u_2 + (J_3 - J_1)\omega_1\omega_3\right), \\ \dot{\omega}_3 &= \tfrac{J_1 - J_2}{J_3}\omega_1\omega_2, \end{aligned} \tag{3.1}$$

where J_1, J_2, and J_3 are the principal moments of inertia of the spacecraft bus. Note that since attitude maneuvers are small by Assumption 3.2.4, (3.1) will never reach the Euler angle singularity.

3.2.2 Hybrid Controller

In the following switching scheme, the 6-dimensional state vector, consisting of Euler angles and angular velocities, is divided into base variables and fiber variables. For the spacecraft with two external moments, we choose the base variables as ϕ, θ, ω_1, and ω_2, and the fiber variables as ψ and ω_3.

3.2.2.1 Base Variables

Consider a small angle assumption for the kinematics of ϕ and θ in (3.1)

$$\begin{aligned} \dot{\phi} &= \omega_1, \\ \dot{\theta} &= \omega_2. \end{aligned} \tag{3.2}$$

Let the external moments be governed by the feedback law

$$\begin{aligned} u_1 &= J_1 \left(-\tfrac{J_2 - J_3}{J_1} \omega_2 \omega_3 - k_{11}\phi - k_{12}\omega_1 + v_1 \right), \\ u_2 &= J_2 \left(-\tfrac{J_3 - J_1}{J_2} \omega_3 \omega_1 - k_{21}\theta - k_{22}\omega_2 + v_2 \right), \end{aligned} \tag{3.3}$$

where k_{11}, k_{12}, k_{21} and k_{22} are constants. Under the control law (3.3) and defining $\bar{x} = [\ \phi \ \ \omega_1 \ \ \theta \ \ \omega_2\ ]^{\mathrm{T}}$ and $\bar{v} = [\ v_1 \ \ v_2\ ]^{\mathrm{T}}$, the base dynamics can be written as a linear system,

$$\dot{\bar{x}} = \bar{A}\bar{x} + \bar{B}\bar{v}, \tag{3.4}$$

where

$$\bar{A} = \begin{bmatrix} 0 & 1 & 0 & 0 \\ -k_{11} & -k_{12} & 0 & 0 \\ 0 & 0 & 0 & 1 \\ 0 & 0 & -k_{21} & -k_{22} \end{bmatrix}, \qquad \bar{B} = \begin{bmatrix} 0 & 0 \\ 1 & 0 \\ 0 & 0 \\ 0 & 1 \end{bmatrix}. \tag{3.5}$$

The constants k_{11}, k_{12}, k_{21} and k_{22} are chosen to make $\bar{A}$ Hurwitz.

Now let the base variables be excited by the $T = \frac{2\pi}{n}$ periodic inputs,

$$\begin{aligned} v_1 &= \alpha_1 (nt + \sigma_1)_c, \\ v_2 &= \alpha_2 (nt + \sigma_2)_c, \end{aligned} \tag{3.6}$$

where n is the excitation frequency, α_1, α_2, σ_1 and σ_2 are parameters, and $(*)_c = \cos(*)$. Since the base dynamics are exponentially stable, the steady-state trajectories of (3.4) induced by the inputs in (3.6) will be periodic and at the excitation frequency n, determined by

$$\bar{x}^{ss}(t) = Re \left\{ (njI_{4\times 4} - \bar{A})^{-1} \bar{B} \begin{bmatrix} \alpha_1 \exp(j\sigma_1) \\ \alpha_2 \exp(j\sigma_2) \end{bmatrix} \exp(jnt) \right\}, \tag{3.7}$$

where $Re\{*\}$ denotes the real part. More specifically, these steady-state trajectories have the following form,

$$\bar{x}^{ss}(t) = \begin{bmatrix} \phi^{ss}(t) \\ \omega_1^{ss}(t) \\ \theta^{ss}(t) \\ \omega_2^{ss}(t) \end{bmatrix} = \begin{bmatrix} \alpha_1\beta_1(nt+\sigma_1+\gamma_1)_c \\ \alpha_1\beta_2(nt+\sigma_1+\gamma_2)_c \\ \alpha_2\beta_3(nt+\sigma_2+\gamma_3)_c \\ \alpha_2\beta_4(nt+\sigma_2+\gamma_4)_c \end{bmatrix}, \tag{3.8}$$

where

$$\begin{aligned} \beta_1 &= |k_{11}^2 - 2k_{11}n^2 + k_{12}^2n^2 + n^4|^{-\frac{1}{2}}, \\ \beta_2 &= n|k_{11}^2 - 2k_{11}n^2 + k_{12}^2n^2 + n^4|^{-\frac{1}{2}}, \\ \beta_3 &= |k_{21}^2 - 2k_{21}n^2 + k_{22}^2n^2 + n^4|^{-\frac{1}{2}}, \\ \beta_4 &= n|k_{21}^2 - 2k_{21}n^2 + k_{22}^2n^2 + n^4|^{-\frac{1}{2}}, \end{aligned} \tag{3.9}$$

$$\begin{aligned} \gamma_1 &= \tan^{-1}\left(\tfrac{-nk_{12}}{k_{11}-n^2}\right), \\ \gamma_2 &= \tan^{-1}\left(\tfrac{-n^2+k_{11}}{nk_{12}}\right), \\ \gamma_3 &= \tan^{-1}\left(\tfrac{-nk_{22}}{k_{21}-n^2}\right), \\ \gamma_4 &= \tan^{-1}\left(\tfrac{-n^2+k_{21}}{nk_{22}}\right). \end{aligned} \tag{3.10}$$

In the sequel, σ_1 and σ_2 are constants chosen by the designer while α_1 and α_2 are treated as new control parameters that are adjusted at every periodic cycle.

3.2.2.2 Fiber Variables

Consider now the change in fiber variables induced by one cycle of steady-state motion of the base variables. The change in ω_3, based on (3.1), is computed as

$$\omega_3((k+1)T) - \omega_3(kT) = \int_{kT}^{(k+1)T} \frac{J_1 - J_2}{J_3}\omega_1^{ss}\omega_2^{ss}dt, \tag{3.11}$$

where $T = \frac{2\pi}{n}$. Substituting expressions from (3.8) into (3.11) and integrating gives

$$\omega_3((k+1)T) - \omega_3(kT) = \frac{\pi\beta_2\beta_4(J_1 - J_2)}{nJ_3}\cos\left(\sigma_1 + \gamma_2 - (\sigma_2 + \gamma_4)\right)\alpha_1\alpha_2. \tag{3.12}$$

Likewise the change in the fiber variable ψ can be computed as,

$$\psi((k+1)T) - \psi(kT) = \frac{\pi^2\beta_2\beta_4(J_1 - J_2)}{n^2J_3}\cos\left(\sigma_1 + \gamma_2 - (\sigma_2 + \gamma_4)\right)\alpha_1\alpha_2. \tag{3.13}$$

Let $\bar{y}(kT) = [\psi(kT)\ \ \omega_3(kT)]^{\mathrm{T}}$ be the vector of fiber variables. Then discrete dynamics of the fiber variables over one period T are

$$\begin{gathered}\bar{y}((k+1)T) = \bar{A}_y\bar{y}(kT) + \bar{B}_y\left(\alpha_1(kT)\alpha_2(kT)\right), \\ \bar{A}_y = \begin{bmatrix} 1 & \frac{2\pi}{n} \\ 0 & 1 \end{bmatrix}, \qquad \bar{B}_y = \begin{bmatrix} \frac{\pi^2\beta_2\beta_4(J_1-J_2)}{n^2J_3}\cos(\sigma_1 + \gamma_2 - \sigma_2 - \gamma_4) \\ \frac{\pi\beta_2\beta_4(J_1-J_2)}{nJ_3}\cos(\sigma_1 + \gamma_2 - \sigma_2 - \gamma_4) \end{bmatrix}.\end{gathered} \tag{3.14}$$

3.2.3 Switching LQ Control

At this point, we make the following assumption on the spacecraft's dynamics:

> **Assumption 3.2.5** The spacecraft principal moments of inertia J_1 and J_2 are not equal.

Under Assumption 3.2.5 and suitable choices of σ_1 and σ_2, the system (3.14) is linear and controllable because the controllability gramian is full rank [76]. We can thus use a discrete-time LQ controller to stabilize $\bar{y}(kT)$ to zero.

The discrete-time LQ controller prescribes the linear time-invariant feedback law

$$\left(\alpha_1(kT)\alpha_2(kT)\right) = \bar{K}_y\bar{y}(kT), \tag{3.15}$$

where $\bar{K}_y$ is the controller gain. Rewriting (3.15) yields the required amplitudes

$$\begin{aligned} \alpha_1(kT) &= c\sqrt{\left|\bar{K}_y\bar{y}(kT)\right|}, \\ \alpha_2(kT) &= \tfrac{1}{c}\sqrt{\left|\bar{K}_y\bar{y}(kT)\right|}\text{sign}(\bar{K}_y\bar{y}(kT)). \end{aligned} \tag{3.16}$$

for some real constant $c \neq 0$.

The underlying idea behind the controller is straightforward. Assuming that the base dynamics are sufficiently fast, the base variables achieve their steady-states quickly, inducing the change in fiber variables predicted by the steady-state relationship in (3.14) towards the equilibrium. This, in turn, leads to progressively smaller base variables. See Reference [75] for convergence results for systems in cascade form similar to the one considered in this section.

Remark 3.2.1: If J_1 and J_2 are equal, the pair $(\bar{A}_y, \bar{B}_y)$ becomes uncontrollable. However, under the assumption that $J_1 = J_2$, (3.1) can be simplified to

$$\begin{aligned} \dot{\phi} &= \omega_1 + \omega_2 \sin(\phi)\tan(\theta) + \omega_3 \cos(\phi)\tan(\theta), \\ \dot{\theta} &= \omega_2 \cos(\phi) - \omega_3 \sin(\phi), \\ \dot{\psi} &= \omega_2 \sin(\phi)\sec(\theta) + \omega_3 \cos(\phi)\sec(\theta), \\ \dot{\omega}_1 &= \tfrac{J_2 - J_3}{J_1}\omega_2\omega_3 + u_2, \\ \dot{\omega}_2 &= \tfrac{J_3 - J_1}{J_2}\omega_2\omega_3 + u_1, \\ \dot{\omega}_3 &= 0. \end{aligned} \tag{3.17}$$

If the maneuver is rest-to-rest, then $\omega_3 = 0$ and

$$\begin{aligned} \dot{\phi} &= \omega_1 + \omega_2 \sin(\phi) \tan(\theta) \\ \dot{\theta} &= \omega_2 \cos(\phi) \\ \dot{\psi} &= \omega_2 \sin(\phi) \sec(\theta) \\ \dot{\omega}_1 &= u_1, \\ \dot{\omega}_2 &= u_2. \end{aligned} \tag{3.18}$$

The simplified equations of motion in (3.18) are similar to the equations of motion in the next section for RWs. Using a controller scheme similar to the one outlined in Section 3.3, (3.18) can be stabilized to $\phi = \theta = \psi = \omega_1 = \omega_2 = 0$ even if $J_1 = J_2$. The controllability properties of (3.18) can be shown similarly to that of the RW RAE's, given in Appendix A.

3.2.4 Simulation Results

To validate this control law, we consider a spacecraft bus with the principal moments of inertia of 430, 1210, and 1300 kg m^2. For the feedback law (3.3), the constants that yield the linear base dynamics in (3.4) and (3.5) are $k_{11} = k_{21} = 0.1$ and $k_{12} = k_{22} = 1$. The sinusoidal excitation is applied at a frequency of $n = 0.03$ sec^{-1} with phase angles $\sigma_1 = \sigma_2 = \frac{\pi}{2}$. For the fiber dynamics, the discrete LQ controller was created using a state weight matrix of identity and a control weight matrix of $R = 1{\times}10^6$, with $c = 1$ in (3.16). The large control weight is used to induce the time scale separation between the closed-loop fiber variable response and base variable closed-loop response.

Two simulations are performed and presented in Figures 3.1 and 3.2. For Figure 3.1, the initial conditions are $\phi(0) = 0$ rad, $\theta(0) = 0$ rad, $\psi(0) = 0.1$ rad, $\bar{\omega}(0) = 0$ while for Figure 3.2, $\phi(0) = -0.05$ rad, $\theta(0) = 0.1$ rad, $\psi(0) = -0.2$ rad, $\bar{\omega}(0) = 0$. In both simulations, the controller is able to guide the Euler angles and angular velocities to zero.

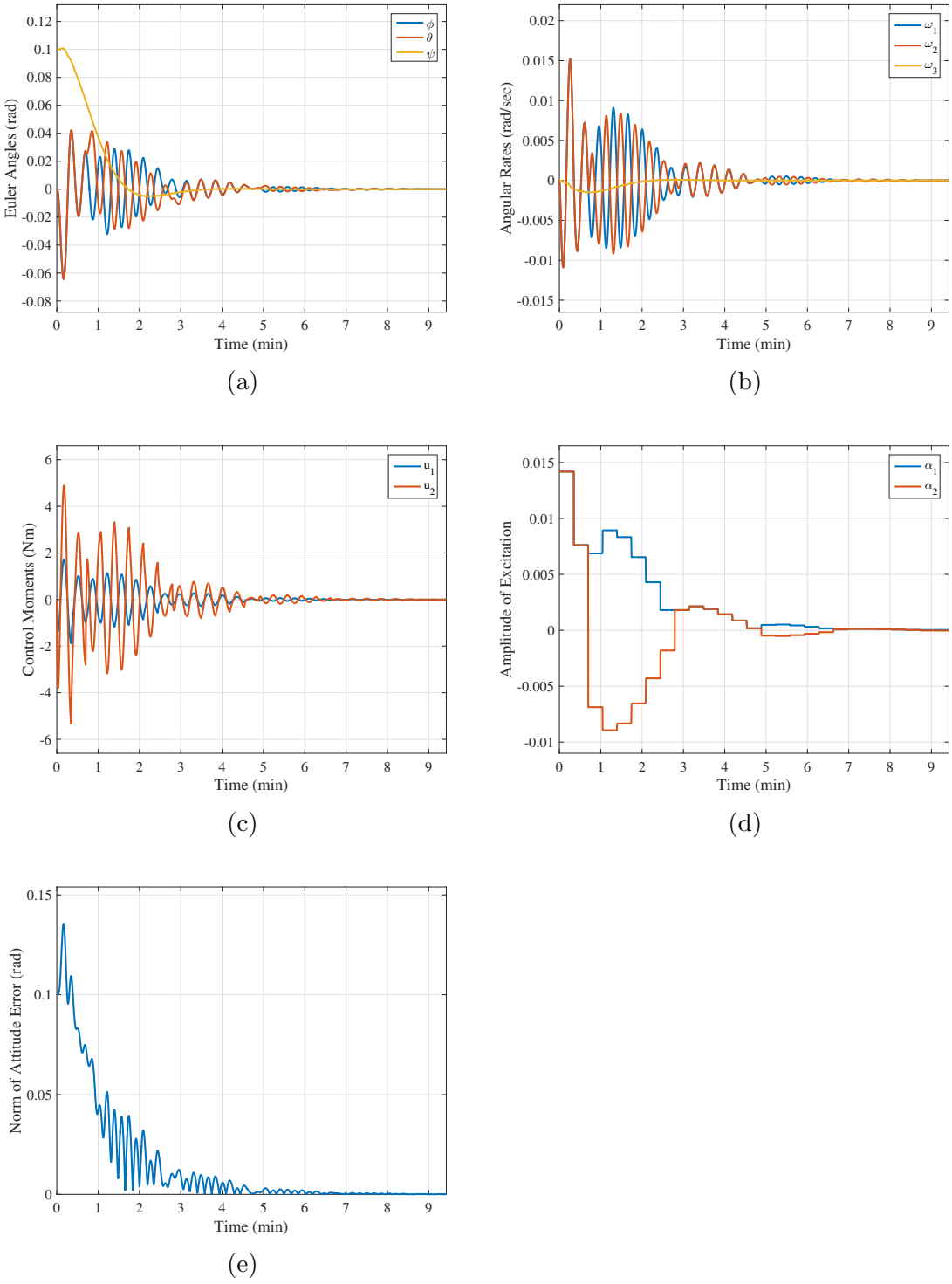

Figure 3.1: First simulation for an underactuated spacecraft with two gas thrusters (a) Euler angles, (b) angular velocities, (c) control moments, (d) excitation parameters, (e) 2-norm of attitude error.

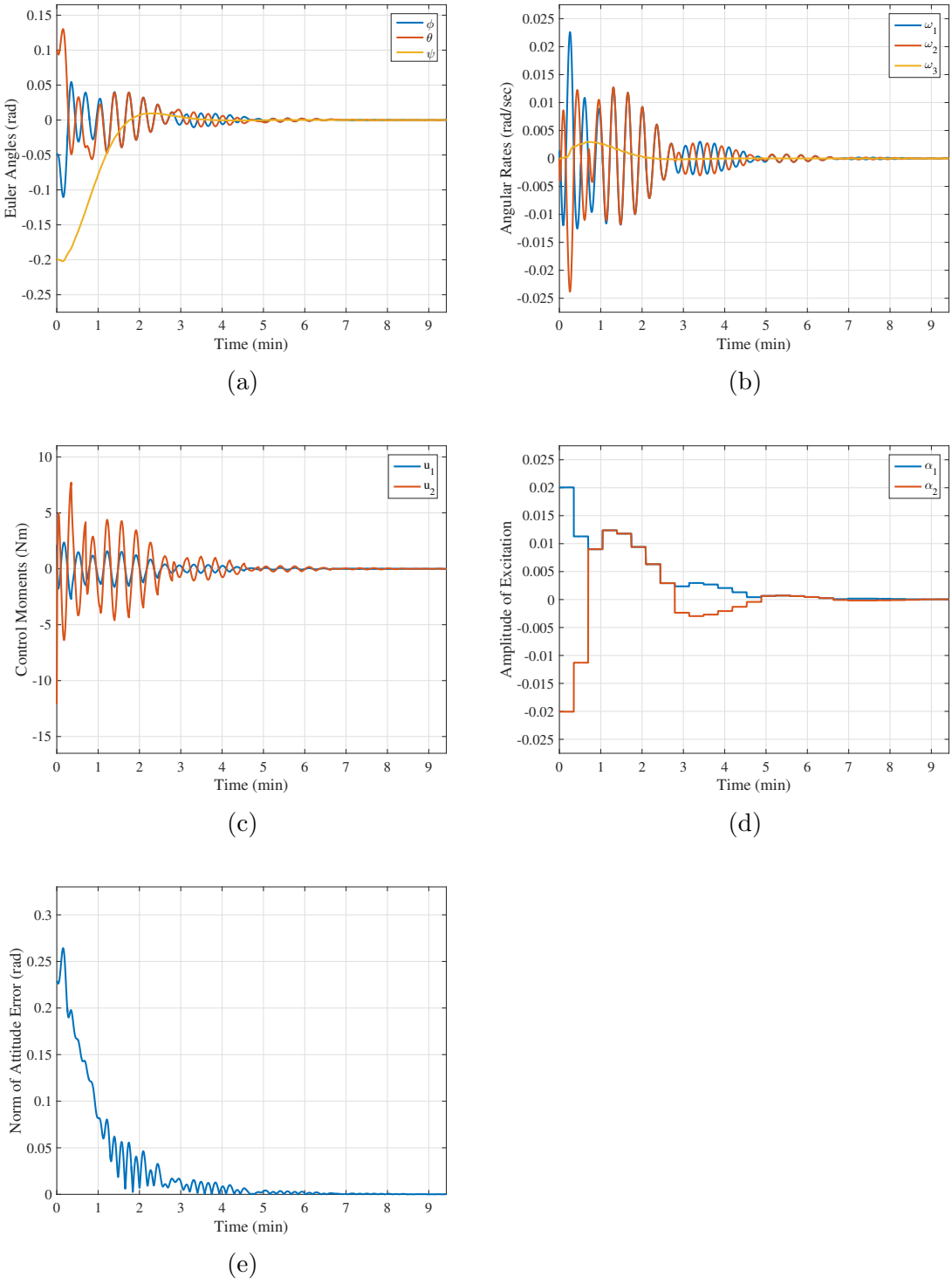

Figure 3.2: Second simulation for an underactuated spacecraft with two gas thrusters (a) Euler angles, (b) angular velocities, (c) control moments, (d) excitation parameters, (e) 2-norm of attitude error.

3.3 Reaction Wheel Actuation

3.3.1 Spacecraft Configuration & Equations of Motion

In this section, we consider a spacecraft system consisting of a bus equipped with two RWs. The assumptions on the spacecraft system are the following:

Assumption 3.3.1 The RW spin axes are non-parallel and lie in the plane defined by $\hat{b}_x$ and $\hat{b}_y$, i.e., unit vectors along the x and y direction of the spacecraft bus fixed frame $\mathcal{B}$.

Assumption 3.3.2 There are no external moments acting on the spacecraft system.

Assumption 3.3.3 The maneuvers being performed involve relatively small attitude adjustments near the desired pointing orientation.

Note that we do not assume $\mathcal{B}$ is a principal frame as we did for the external thruster actuation case. Thus we treat the attitude control problem for an underactuated spacecraft in a more general setting. The plane spanned by $\hat{b}_x$ and $\hat{b}_y$ may be thought of as a plane of controllability where all body-fixed torques induced by RWs must lie. The unit vector $\hat{b}_z$ is orthogonal to this plane and corresponds to the underactuated axis.

Under the above assumptions and choosing Euler angles as the attitude parameterization, the equations of motion (2.3), (2.41) become

$$\begin{aligned} \dot{\bar{\Theta}} &= M(\bar{\Theta})\bar{\omega}, \\ \bar{J}\dot{\bar{\omega}} &= -[\bar{\omega}]^{\times}\left(\bar{J}\bar{\omega} + \bar{W}\bar{\nu}\right) - \bar{W}\bar{u}, \end{aligned} \tag{3.19}$$

where

$$\begin{aligned} \bar{W} &= [\ J_{ws1}\check{w}_1 \quad J_{ws2}\check{w}_2\ ], \\ \bar{\nu} &= [\ \nu_1 \quad \nu_2\ ]^{\mathrm{T}}, \\ \bar{u} &= [\ u_1 \quad u_2\ ]^{\mathrm{T}} = [\ \dot{\nu}_1 \quad \dot{\nu}_2\ ]^{\mathrm{T}}. \end{aligned} \tag{3.20}$$

The total angular momentum of the spacecraft system, using the above notation, is given as

$$\mathbf{B}\bar{H} = \bar{J}\bar{\omega} + \bar{W}\bar{\nu}. \tag{3.21}$$

Let the locked inertia matrix $\bar{J}$ have the following form,

$$\bar{J} = \begin{bmatrix} j_{11} & j_{12} & j_{13} \\ j_{12} & j_{22} & j_{23} \\ j_{13} & j_{23} & j_{33} \end{bmatrix}. \tag{3.22}$$

3.3.1.1 Angular Momentum Conservation Law

Proposition 3.3.1 presents a requirement for $\bar{\Theta} = \bar{\omega} = 0$ to be an equilibrium when there are no external moments acting on the spacecraft. This corresponds to maintaining inertial pointing at the desired attitude.

Proposition 3.3.1: Let $\bar{H} = [\ h_1 \quad h_2 \quad h_3\ ]^{\mathrm{T}}$ and assume that $\bar{M}_{ext} = 0$ for an underactuated spacecraft satisfying the above assumptions. Then $\bar{\Theta} = \bar{\omega} = 0$ is an equilibrium if and only if $h_3 = 0$.

Proof: If $\bar{\Theta}(t) = \bar{\omega}(t) = 0$ for all t, then (3.21) reduces to

$$\bar{H} = \bar{W}\bar{\nu}. \tag{3.23}$$

From the assumptions on the spacecraft configuration, $[\ 0 \quad 0 \quad 1\ ]\bar{W}\nu = 0$. Premulti-

plying (3.23) by [0 0 1] yields

$$h_3 = 0. \tag{3.24}$$

□

Note that throughout this chapter we assume that the total angular momentum is conserved by Assumption 3.3.2, but we do not require that $H = 0$.

The angular velocity component ω_3 can also be found from the angular momentum expression in (3.21). Define $\bar{\zeta}_1 = [\ \omega_1 \ \ \omega_2 \ \ 0\ ]^{\mathrm{T}}$ and $\bar{\zeta}_2 = [\ \nu^{\mathrm{T}} \ \ \omega_3\ ]^{\mathrm{T}}$. Then (3.21) can be written as

$$\mathbf{B}\bar{H} - \bar{J}\bar{Z}_1\bar{\zeta}_1 = (\bar{J}\bar{Z}_2 + \bar{W}\bar{Z}_3)\bar{\zeta}_2, \tag{3.25}$$

where

$$\begin{aligned} \bar{Z}_1 &= \begin{bmatrix} I_{2\times 2} \\ 0_{1\times 2} \end{bmatrix}, \\ \bar{Z}_2 &= \mathrm{diag}(0,0,1), \\ \bar{Z}_3 &= \begin{bmatrix} I_{2\times 2} & 0_{2\times 1} \end{bmatrix}. \end{aligned} \tag{3.26}$$

Solving for $\bar{\zeta}_2$ and extracting ω_3 gives

$$\omega_3 = -\frac{j_{13}}{j_{33}}\omega_1 - \frac{j_{23}}{j_{33}}\omega_2 + \frac{h_1}{j_{33}}(\phi_c\theta_s\psi_c + \phi_s\psi_s) + \frac{h_2}{j_{33}}(\phi_c\theta_s\psi_s - \phi_s\psi_c) + \frac{h_3}{j_{33}}\phi_c\theta_c, \tag{3.27}$$

where again $\sin(*) = *_s$ and $\cos(*) = *_c$.

3.3.2 Base and Fiber Variables

In the following switching scheme, the 6-dimensional state vector, consisting of Euler angles and angular velocities, is divided into base variables and fiber variables. The base variables are chosen to be the controllable variables $\phi,\ \theta,\ \omega_1,\ \omega_2$. The uncon-

trolled angle ψ is treated as a fiber variable. The reason why ω_3 is not included in either the base or fiber variables is mentioned in Subsection 3.3.2.2.

3.3.2.1 Base Variables

The description of the base variable set-up is very similar to that in Section 3.2.2.1. First we consider a small angle assumption in the kinematics of ϕ and θ in (5.1). This results in $\dot{\phi} = \omega_1$, $\dot{\theta} = \omega_2$. Then let the RW accelerations be determined by the feedback law

$$\bar{u} = \left(\bar{Z}_3 \bar{J}^{-1} \bar{W}\right)^{-1} \left(\bar{Z}_3 \bar{J}^{-1} (-\bar{\omega} \times (\bar{J}\bar{\omega} + \bar{W}\bar{\nu})) + (\bar{v}_{fb} - \bar{v})\right), \tag{3.28}$$

where

$$\bar{v}_{fb} = \begin{bmatrix} k_{11}\phi + k_{12}\omega_1 \\ k_{21}\theta + k_{22}\omega_2 \end{bmatrix}, \qquad \bar{v} = \begin{bmatrix} v_1 \\ v_2 \end{bmatrix}, \tag{3.29}$$

$\bar{Z}_3$ is from (3.26), and k_{11}, k_{12}, k_{21}, k_{22} are constants. Under the above control law and by defining $x = [\ \phi \ \ \omega_1 \ \ \theta \ \ \omega_2\ ]^{\mathrm{T}}$, the base dynamics can again be written as the linear system

$$\dot{\bar{x}} = \bar{A}\bar{x} + \bar{B}\bar{v}, \tag{3.30}$$

where $\bar{A}$ and $\bar{B}$ are the same as in (3.5). Now if the base variables are excited by the $T = \frac{2\pi}{n}$ periodic inputs,

$$\begin{aligned} v_1 &= \alpha_1 (nt + \sigma_1)_c, \\ v_2 &= \alpha_2 (nt + \sigma_2)_c, \end{aligned} \tag{3.31}$$

where n is the excitation frequency and α_1, α_2, σ_1 and σ_2 are parameters, the steady-state trajectories of (3.4) induced by the inputs in (3.31) will be periodic and at the

excitation. These trajectories are given in (3.8) and repeated below

$$\bar{x}^{ss}(t) = \begin{bmatrix} \phi^{ss}(t) \\ \omega_1^{ss}(t) \\ \theta^{ss}(t) \\ \omega_2^{ss}(t) \end{bmatrix} = \begin{bmatrix} \alpha_1\beta_1(nt+\sigma_1+\gamma_1)_c \\ \alpha_1\beta_2(nt+\sigma_1+\gamma_2)_c \\ \alpha_2\beta_3(nt+\sigma_2+\gamma_3)_c \\ \alpha_2\beta_4(nt+\sigma_2+\gamma_4)_c \end{bmatrix}. \tag{3.32}$$

3.3.2.2 Fiber Variables

We treat ψ as the only fiber variable in our switching scheme. Note that ω_3 is determined by (3.27) (i.e., conservation of angular momentum) and hence we choose not to consider it as a fiber variable explicitly. To control ψ, its change over one period of excitation induced by steady-state base variable motions needs to be characterized. If the base variables are in steady-state, ψ evolves in time according to

$$\begin{aligned} \dot{\psi} = {} & \omega_2^{ss}\phi_s^{ss}\theta_{se}^{ss} + \left(-\tfrac{j_{13}}{j_{33}}\omega_1^{ss} - \tfrac{j_{23}}{j_{33}}\omega_2^{ss}\right)\phi_c^{ss}\theta_{se}^{ss} \\ & + \left(\tfrac{h_1}{j_{33}}(\phi_c^{ss}\theta_s^{ss}\psi_c + \phi_s^{ss}\psi_s) + \tfrac{h_2}{j_{33}}(\phi_c^{ss}\theta_s^{ss}\psi_s - \phi_s^{ss}\psi_c) + \tfrac{h_3}{j_{33}}\phi_c^{ss}\theta_c^{ss}\right)\phi_c^{ss}\theta_{se}^{ss}, \end{aligned} \tag{3.33}$$

where ϕ^{ss}, θ^{ss}, ω_1^{ss}, ω_2^{ss} are the steady-state trajectories from (3.32) and $\sec(*) = *_{se}$. Assuming small angles simplifies (3.33) to

$$\dot{\psi} = \left(\frac{h_1}{j_{33}}\phi^{ss} + \frac{h_2}{j_{33}}\theta^{ss}\right)\psi + \omega_2^{ss}\phi^{ss} + \frac{h_1}{j_{33}}\theta^{ss} - \frac{h_2}{j_{33}}\phi^{ss} - \frac{j_{13}}{j_{33}}\omega_1^{ss} - \frac{j_{23}}{j_{33}}\omega_2^{ss} + \frac{h_3}{j_{33}}. \tag{3.34}$$

Using (3.32), (3.34) becomes

$$\begin{aligned}\dot{\psi} = &\left(\tfrac{h_1\alpha\beta_1}{j_{33}}(nt+\delta_1+\gamma_1)_c + \tfrac{h_2\alpha_2\beta_3}{j_{33}}(nt+\delta_2+\gamma_3)_c\right)\psi \\ &+\alpha_1\alpha_2\beta_1\beta_4(nt+\delta_1+\gamma_1)_c(nt+\delta_2+\gamma_4)_c \\ &+\tfrac{h_1\alpha_2\beta_3}{j_{33}}(nt+\delta_2+\gamma_3)_c - \tfrac{h_2\alpha_1\beta_1}{j_{33}}(nt+\delta_1+\gamma_1)_c \\ &-\tfrac{\alpha_1\beta_2 j_{13}}{j_{33}}(nt+\delta_1+\gamma_2)_c - \tfrac{j_{23}\alpha_2\beta_4}{j_{33}}(nt+\delta_2+\gamma_4)_c + \tfrac{h_3}{j_{33}}.\end{aligned} \tag{3.35}$$

We note that while the approximations (3.34) and (3.35) are used as a basis for the subsequent control law design, the simulation results in Subsection 3.3.5 are performed on the original nonlinear model, given by (3.19).

3.3.3 Switching Feedback Law

We now develop a switching feedback law that adjusts parameters of periodic excitation amplitude of the base dynamics (α_1 and α_2), in order to induce a change in the fiber variable (ψ) towards the desired pointing equilibrium. The switching feedback law construction is based on [74] and relies on the characterization of the change in ψ induced by one cycle of periodic, steady-state base variable motion.

Let the exact change in ψ, determined by the integration of (3.33), be denoted as $\Delta\psi$. Note that equation (3.33) cannot be analytically integrated. Thus an approximation of $\Delta\psi$, denoted as $\Delta_a\psi$ and based on the integration of (3.35), is used for analysis.

Two cases are considered when analyzing $\Delta_a\psi$. First studied is the zero total angular momentum case, i.e., $h_1 = h_2 = h_3 = 0$, which yields an exact integration of (3.35). Then the nonzero total angular momentum with $h_3 = 0$ (consistent with Proposition 3.3.1) is studied using a second order Taylor-series expansion. In both

cases, it is required that the mapping $G_a : (\alpha_1, \alpha_2) \to \Delta_a\psi$ be open at $(\alpha_1, \alpha_2) = (0, 0)$, i.e., an image of an open neighborhood of $(\alpha_1, \alpha_2) = (0, 0)$ is an open interval, and hence the change of ψ over one period of steady-state base variable motion can be made in any direction, regardless of how small the magnitude of α_1 and α_2 is. This can be seen as a controllability-like property of the fiber variables by periodic base variable motions. It is shown that if G_a is open at $(\alpha_1, \alpha_2) = (0, 0)$, then the map for the actual change in ψ, defined as $G : (\alpha_1, \alpha_2) \to \Delta\psi$, is also open at $(\alpha_1, \alpha_2) = (0, 0)$.

3.3.3.1 Zero Inertial Angular Momentum

If $h_1 = h_2 = h_3 = 0$, (3.35) reduces to

$$\begin{aligned}\dot{\psi} = \alpha_1\alpha_2\beta_1\beta_4(nt + \sigma_1 + \gamma_1)_c(nt + \sigma_2 + \gamma_4)_c \\ -\tfrac{\alpha_1\beta_2 j_{13}}{j_{33}}(nt + \sigma_1 + \gamma_2)_c - \tfrac{j_{23}\alpha_2\beta_4}{j_{33}}(nt + \sigma_2 + \gamma_4)_c.\end{aligned} \tag{3.36}$$

The right hand side of (3.36) is not a function of ψ. The change in ψ induced by one period of steady-state base variable motion is then approximated as

$$\Delta_a\psi = \alpha_1\alpha_2\Gamma, \tag{3.37}$$

where

$$\Gamma = \frac{\pi\beta_1\beta_4}{n}(\sigma_1 - \sigma_2 + \gamma_1 - \gamma_4)_c. \tag{3.38}$$

Note that (3.36) defines a function of α_1 and α_2, with all other parameters considered fixed. Assuming that $\Gamma \neq 0$, which can be assured by choosing suitable values for k_{11}, k_{12}, k_{21}, k_{22}, σ_1 and σ_2, it follows that the map G_a is open at $(\alpha_1, \alpha_2) = (0, 0)$.

We note that the derivation of (3.37) relies on the assumption of small angles that was made in obtaining (3.34) and (3.35). The predicted change $\Delta_a\psi$ is very close to $\Delta\psi$ provided that α_1 and α_2 are sufficiently small. Figure 3.3 demonstrates this by

showing the change predicted by (3.37) along with a numerical integration of (3.33) using the spacecraft parameters outlined in Subsection 3.3.5.1 and the controller parameters listed in Table 3.1 in Subsection 3.3.5.

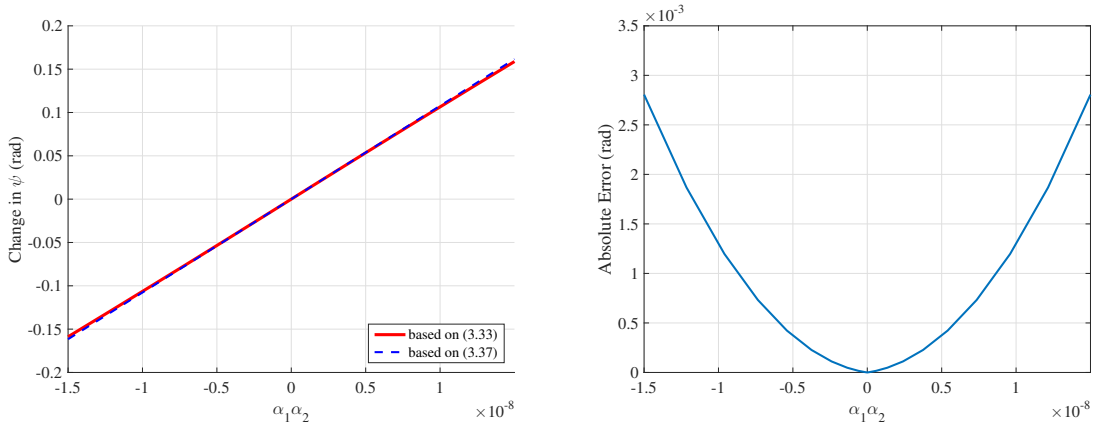

(a) (b)

Figure 3.3: Change in ψ due to periodic base dynamic excitation for the zero angular momentum case (**a**) exact change based on (3.33) (solid) versus approximation based on (3.37) (dashed), (**b**) error magnitude.

3.3.3.2 Nonzero Inertial Angular Momentum with $h_3 = 0$

Suppose now h_1 and/or h_2 are nonzero while $h_3 = 0$, which is the case consistent with Proposition 1. Note that (3.35) is linear with respect to ψ. As (3.35) is also a scalar differential equation, its state transition matrix is computed as

$$\bar{\Phi}(t, t_0) = \exp\left(\frac{h_1\alpha_1\beta_1}{nj_{33}}(nt + \sigma_1 + \gamma_1)_s + \frac{h_2\alpha_2\beta_3}{nj_{33}}(nt + \sigma_2 + \gamma_3)_s\right) \tag{3.39}$$

$$* \exp\left(-\frac{h_1\alpha_1\beta_1}{nj_{33}}(nt_0 + \sigma_1 + \gamma_1)_s - \frac{h_2\alpha_2\beta_3}{nj_{33}}(nt_0 + \sigma_2 + \gamma_3)_s\right).$$

Note that the state transition matrix is T periodic. Thus the change in ψ over one period does not depend on the initial state at the beginning of the period. Then

$$\Delta_a\psi = \int_0^T \bar{\Phi}(t,\tau)b(\tau)d\tau, \tag{3.40}$$

where

$$\begin{aligned} b(\tau) = {} & \alpha_1\alpha_2\beta_1\beta_4(n\tau+\sigma_1+\gamma_1)_c(n\tau+\sigma_2+\gamma_4)_c \\ & + \tfrac{h_1\alpha_2\beta_3}{j_{33}}(n\tau+\sigma_2+\gamma_3)_c - \tfrac{h_2\alpha_1\beta_1}{j_{33}}(n\tau+\sigma_1+\gamma_1)_c \\ & - \tfrac{\alpha_1\beta_2 j_{13}}{j_{33}}(nt+\sigma_1+\gamma_2)_c - \tfrac{j_{23}\alpha_2\beta_4}{j_{33}}(nt+\sigma_2+\gamma_4)_c. \end{aligned} \tag{3.41}$$

While $\Delta_a\psi$ can be constructed by fitting numerical values, it turns out that accurate analytical approximations can also be developed. For sufficiently small α_1 and α_2, a second order Taylor-series expansion about $\alpha_1 = \alpha_2 = 0$ can approximate (3.40),

$$\Delta_a\psi = \alpha^{\mathrm{T}}\bar{\Xi}\alpha, \tag{3.42}$$

where

$$\alpha = [\alpha_1 \quad \alpha_2]^{\mathrm{T}},$$

$$\bar{\Xi} = \begin{bmatrix} \Gamma_1 & \frac{1}{2}\Gamma_3 \\ \frac{1}{2}\Gamma_3 & \Gamma_2 \end{bmatrix},$$

$$\begin{aligned} \Gamma_1 &= \tfrac{\pi j_{13}\beta_1\beta_2 h_1}{j_{33}^2 n^2}(\gamma_1 - \gamma_2)_s, \\ \Gamma_2 &= \tfrac{\pi j_{23}\beta_3\beta_4 h_2}{j_{33}^2 n^2}(\gamma_3 - \gamma_4)_s, \end{aligned} \tag{3.43}$$

$$\Gamma_3 = \tfrac{\pi\beta_1\beta_4}{n}(\sigma_1 - \sigma_2 + \gamma_1 - \gamma_4)_c - \tfrac{\pi\beta_1\beta_3}{j_{33}^2 n^2}(h_1^2 + h_2^2)(\sigma_1 - \sigma_2 + \gamma_1 - \gamma_3)_s,$$

$$-\tfrac{\pi j_{13}\beta_2\beta_3 h_2}{j_{33}^2 n^2}(\sigma_1 - \sigma_2 + \gamma_2 - \gamma_3)_s + \tfrac{\pi j_{23}\beta_1\beta_4 h_1}{j_{33}^2 n^2}(\sigma_1 - \sigma_2 + \gamma_1 - \gamma_4)_s.$$

Note that the map G_a given by (3.42) is open at $(\alpha_1, \alpha_2) = (0, 0)$ if the symmetric matrix Ξ is indefinite, i.e., has a positive and a negative eigenvalue. Under this condition, which can be satisfied by choosing suitable values for k_{11}, k_{12}, k_{21}, k_{22}, σ_1 and σ_2, the exact map G can also be shown to be open at $(\alpha_1, \alpha_2) = (0, 0)$. Note that (3.37) is recovered from (3.42) if $h_1 = h_2 = 0$.

Figure 3.4 shows, based on the spacecraft parameters in Subsection 3.3.5.1 and control parameters in Table 4.1, that when $h_1 = h_2 = 1$ kg m^2 sec^{-1} and $h_3 = 0$ the approximation $\Delta_a\psi$ from (3.42) is a fairly accurate approximation to the actual change $\Delta\psi$ and that the mapping is open at $(\alpha_1, \alpha_2) = (0, 0)$.

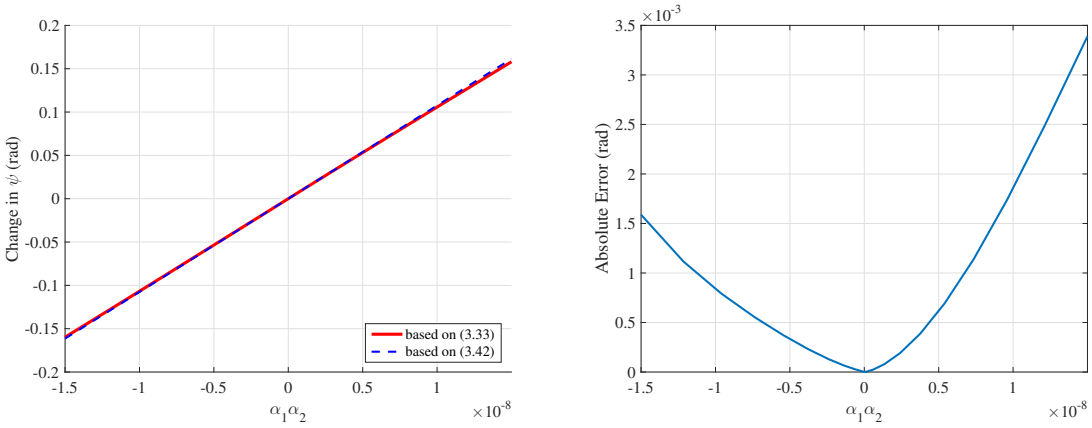

(a) (b)

Figure 3.4: Change in ψ for the nonzero angular momentum using the switching scheme (**a**) exact change based on (3.33) (solid) versus approximation based on (3.42) (dashed), (**b**) error magnitude.

3.3.3.3 Hybrid Controller Scheme

A switching scheme, based on [74], that stabilizes the fiber and base variables is now implemented for the case when $h_3 = 0$. This is consistent with Proposition 3.3.1 and hence stabilization to the desired pointing equilibrium is possible. The parameters that this algorithm concerns itself with are α_2 and ϵ, with $\alpha_1 = \epsilon\alpha_2$. Each of these parameters are adjusted at the beginning of each cycle of duration T and are kept constant throughout the cycle,

$$\begin{aligned} \alpha_2(t) &= \alpha_2(kT) = \alpha_2^k, \ kT \leq t < (k+1)T, \\ \epsilon(t) &= \epsilon(kT) = \epsilon^k, \ kT \leq t < (k+1)T. \end{aligned} \tag{3.44}$$

Note that as an abuse of notation, α_2^k and ϵ^k represent the values of $\alpha_2(t)$ and $\epsilon(t)$ at time kT (not $\alpha_2(t)$ and $\epsilon(t)$ raised to the kth power). Let $k \geq 0$ represent the cycle number, $\psi^k = \psi(kT)$, and choose $\mu_1 \in (0,1)$, ξ_1 to be sufficiently small, and ξ_2 to be such that $\xi_1\xi_2$ is sufficiently small. The switching scheme is then outlined by

Algorithm 1. Note that the computation involved for α_1, α_2, v_1, v_2 and the control law in (3.28) rely on closed-form, algebraic manipulations that do not require much processing power to execute.

Algorithm 1: Control Computation for RWs when $h_3 = 0$

Given:

$k \geq 0$, $\mu_1 \in (0,1)$, ξ_1 sufficiently small, and ξ_2 such that $\xi_1\xi_2$ is sufficiently small

if $k = 0$ **then**
  if $\psi^k = 0$ **then**
    $\alpha_2^k = 0,\ \epsilon^k = 0$
  else
    $\alpha_2^k = \xi_1,\ \epsilon^k = -\xi_2 \text{sign}(\Gamma_3 \psi^0)$
  end if
else $\{k > 0\}$
  Compute $G_a(\epsilon^{k-1}\alpha_2^{k-1}, \alpha_2^{k-1})\psi^k$ using (3.42)
  if $\psi^k = 0$ **or** $G_a(\epsilon^{k-1}\alpha_2^{k-1}, \alpha_2^{k-1})\psi^k < 0$ **then**
    $\alpha^k = \alpha_2^{k-1},\ \epsilon^k = \epsilon^{k-1}$
  else $\{G_a(\epsilon^{k-1}\alpha_2^{k-1}, \alpha_2^{k-1})\psi^k \geq 0\}$
    $\alpha^k = \mu_1 \alpha_2^{k-1},\ \epsilon^k = -\epsilon^{k-1},$
  end if
end if
Control During Cycle k:

$v_1(t) = \alpha_2^k \epsilon^k (nt + \sigma_1)_c, \quad v_2(t) = \alpha_2^k (nt + \sigma_2)_c, \quad v(t) = [\ v_1(t) \quad v_2(t)\ ]^{\mathrm{T}}$, for $t \in [kT, (k+1)T)$

Compute $u(t)$ from the feedback law in (3.28)

The methodology of Algorithm 1 is as follows. The sign of ϵ dictates the direction of $\Delta_a\psi$ (which can be seen from Figures 3.3 and 3.4). Furthermore, the magnitude of $\Delta_a\psi$ is dictated by α_2. If the direction of $\Delta_a\psi$ is to be reversed, the sign of ϵ is changed and the magnitude of α_2 is reduced by a factor of μ_1. As α_2 approaches zero, so does ψ, which in turn causes the base variables to converge to zero. The initial values for α_2 and ϵ, i.e., α_2^0 and ϵ^0, are governed by ξ_1 and ξ_2, which are chosen to not cause large transients in ψ.

3.3.3.4 Convergence Properties

In [74], global asymptotic convergence was proven for a cascade connection of a linear time-invariant subsystem, representing the base dynamics, and a subsystem of nonlinear integrators, representing the fiber dynamics. Related local stabilization results have been obtained in [75] for the more general case of fiber dynamics with drift. For the zero angular momentum case, $h_1 = h_2 = h_3 = 0$, the results in [74] can be applied directly to demonstrate exponential convergence. In the case when h_1 and/or h_2 are nonzero while $h_3 = 0$, the rationale for our switching feedback law is very similar; however, existing theoretical guarantees appear to be insufficient, in particular, due to the form of the fiber dynamics in (3.35) not being explicitly treated in prior publications. For the proofs in [74] to carry over to our present case, it is necessary to guarantee (a) that G_a does not depend on the initial conditions of the fiber variable and (b) the boundedness of the error between the fiber variable trajectory, ψ, induced by exponentially convergent base variable motions to a periodic steady-steady state and the fiber variable trajectory, ψ^{ss}, induced by the base variable motion in the periodic steady-state. Equation (3.39) shows that the state transition matrix is T periodic, and therefore G_a is independent of the initial condition of ψ. Lemma 3.3.1 proves the boundedness of the error between ψ and ψ^{ss} if the dynamics of the fiber variable are given by (3.34).

Lemma 3.3.1: Let the fiber variable dynamics for ψ be given by (3.34) with $h_3 = 0$. Then the error between ψ and ψ^{ss} remains bounded over time.

Proof: Define $e_\psi = \psi - \psi^{ss}$. Then

$$\dot{e}_\psi = \dot{\psi} - \dot{\psi^{ss}}. \tag{3.45}$$

Using (3.34) with $h_3 = 0$, (3.45) can be rewritten as

$$\dot{e}_\psi = \left(\frac{h_1}{j_{33}}\phi + \frac{h_2}{j_{33}}\theta\right)\psi + d(\phi,\theta,\omega_1,\omega_2) - \left(\frac{h_1}{j_{33}}\phi^{ss} + \frac{h_2}{j_{33}}\theta^{ss}\right)\psi^{ss} - d(\phi^{ss},\theta^{ss},{\omega_1}^{ss},\omega_2^{ss}), \tag{3.46}$$

where

$$d(\phi,\theta,\omega_1,\omega_2) = \omega_2\phi + \frac{h_1}{j_{33}}\theta - \frac{h_2}{j_{33}}\phi - \frac{j_{13}}{j_{33}}\omega_1 - \frac{j_{23}}{j_{33}}\omega_2. \tag{3.47}$$

Adding and subtracting $\left(\frac{h_1}{j_{33}}\phi^{ss} + \frac{h_2}{j_{33}}\theta^{ss}\right)\psi$ from (3.46), and simplifying yields,

$$\dot{e}_\psi = \left(\frac{h_1}{j_{33}}\phi^{ss} + \frac{h_2}{j_{33}}\theta^{ss}\right)e_\psi + \left(\frac{h_1}{j_{33}}e_\phi + \frac{h_2}{j_{33}}e_\theta\right)\psi + (d(\phi,\theta,\omega_1,\omega_2) - d(\phi^{ss},\theta^{ss},\omega_1^{ss},\omega_2^{ss})), \tag{3.48}$$

where $e_\phi = \phi - \phi^{ss}$ and $e_\theta = \theta - \theta^{ss}$. Equation (3.48) is linear with respect to e_ψ and its solution at time t can be written as

$$e_\psi(t) = \bar{\Phi}(t,0)e_\psi(0) + \int_0^t \bar{\Phi}(t,\tau)f(\tau)d\tau, \tag{3.49}$$

where $e_\psi(0)$ is the initial error, $\bar{\Phi}(t,0)$ is the state transition matrix from (3.39) and

$$f(t) = \left(\frac{h_1}{j_{33}}e_\phi + \frac{h_2}{j_{33}}e_\theta\right)\psi + (d(\phi,\theta,\omega_1,\omega_2) - d(\phi^{ss},\theta^{ss},\omega_1^{ss},\omega_2^{ss})). \tag{3.50}$$

The base variables converge exponentially to the steady-state periodic motions (i.e., $\phi(t) \to \phi^{ss}(t)$, $\theta(t) \to \theta^{ss}(t)$, $\omega_1(t) \to \omega_1^{ss}(t)$, $\omega_2(t) \to \omega_2^{ss}(t)$ as $t \to \infty$), and $\psi(0)$ is initially known and bounded. The function $f(t)$ given by (3.50) hence converges to zero exponentially. This implies that there exists a constant $c_1 > 0$ such that

$$|e_\psi(t)| \leq |\bar{\Phi}(t,0)e_\psi(0)| + \int_0^t |\bar{\Phi}(\tau,0)||f(\tau)|d\tau \leq |\bar{\Phi}(t,0)e_\psi(0)| + c_1. \tag{3.51}$$

The state transition matrix $\bar{\Phi}(t,0)$ in (3.39) is bounded, and therefore the error e_ψ is

bounded. □

We summarize the theoretical convergence guarantees as follows:

Theorem 3.3.1: Consider the fiber dynamics (3.34) with $h_3 = 0$ and base dynamics (3.30) with the switching controller given in Algorithm 1 and (3.6). Under the above assumptions, $\alpha_1^k,\ \alpha_2^k \to 0$ as $k \to \infty$, and $\phi(t),\ \theta(t),\ \psi(t) \to 0$ as $t \to \infty$. □

Remark 3.3.1: The development and analysis of convergence for the above controller have relied on small angle approximations to simplify the representation for the base variable kinematics and fiber variable dynamics. Our subsequent simulations are performed on a model that does not use these approximations, thereby validating these desirable convergence properties. Note also the theoretical results in [74] allow for inexact knowledge of G in maintaining convergence properties.

3.3.3.5 Switching Scheme when $h_3 \neq 0$

Now consider the case when $h_3 \neq 0$. Stabilization at $\bar{\Theta} = \bar{\omega} = 0$ is not possible by Proposition 3.3.1 (i.e., it violates the law of angular momentum conservation). If $\alpha_1 = \alpha_2 = 0$ at $\bar{\Theta} = \bar{\omega} = 0$, (3.33) becomes

$$\dot{\psi} = \frac{h_3}{j_{33}}, \tag{3.52}$$

which can be integrated over one steady-state cycle to give

$$\Delta\psi = \frac{2\pi h_3}{n j_{33}}. \tag{3.53}$$

Equation (3.53) shows that G is not open at $(\alpha_1, \alpha_2) = (0, 0)$ and thus Algorithm 1 cannot be used. By modifying the algorithm, however, controlled oscillations of Euler angles in a neighborhood of $\bar{\Theta} = 0$ can be achieved.

Remark 3.3.2: The fact that G is not open in the case of $h_3 \neq 0$ gives insight

into the system's controllability. In this case, if α_1 and α_2 are made arbitrarily small, then the drift in ψ can only be induced in one direction. This is in contrast to the case of $h_3 = 0$, when a controlled drift in ψ can be made in both directions regardless of how small α_1 and α_2 are.

Let the approximation of the change in ψ induced by one steady-state cycle of base variable motions when $h_3 \neq 0$ be denoted by $\Delta_{a,h_3}\psi$ and define the map $G_{a,h_3} : (\alpha_1, \alpha_2) \rightarrow \Delta_{a,h_3}\psi$. This approximation is based on (3.35) and the small angles assumption. Note that even if $h_3 \neq 0$, the state transition matrix for (3.35) remains the same as in (3.39). Then

$$\Delta_{a,h_3}\psi = \int_0^T \bar{\Phi}(T,\tau)\left(b(\tau) + \frac{h_{33}}{j_{33}}\right) d\tau, \tag{3.54}$$

where $b(t)$ is defined in (3.41). Performing a second order Taylor-series expansion of (3.54) about $(\alpha_1, \alpha_2) = (0, 0)$, $\Delta\psi$ for sufficiently small α_1 and α_2 can be approximated by

$$\Delta_{a,h_3}\psi = \tilde{\Gamma}_0 + \tilde{\Gamma}_{1,1}\alpha_1 + \tilde{\Gamma}_{1,2}\alpha_2 + (\Gamma_1 + \tilde{\Gamma}_{2,1})\alpha_1^2 + (\Gamma_2 + \tilde{\Gamma}_{2,2})\alpha_2^2 + (\Gamma_3 + \tilde{\Gamma}_{2,3})\alpha_1\alpha_2, \tag{3.55}$$

where Γ_1, Γ_2, and Γ_3 are given in (3.43) and

$$\begin{aligned}
\tilde{\Gamma}_0 &= \tfrac{2\pi h_3}{j_{33} n}, \\
\tilde{\Gamma}_{1,1} &= \tfrac{2\pi \beta_1 h_1 h_3}{j_{33}^2 n^2} (\sigma_1 + \gamma_1)_s, \\
\tilde{\Gamma}_{1,2} &= \tfrac{2\pi \beta_3 h_2 h_3}{j_{33}^2 n^2} (\sigma_2 + \gamma_3)_s, \\
\tilde{\Gamma}_{2,1} &= \tfrac{\pi \beta_1^2 h_1^2 h_3}{2 j_{33}^3 n^3} (1 + 2(\sigma_1 + \gamma_1)_s^2), \\
\tilde{\Gamma}_{2,2} &= \tfrac{\pi \beta_3^2 h_2^2 h_3}{2 j_{33}^3 n^3} (1 + 2(\sigma_2 + \gamma_3)_s^2), \\
\tilde{\Gamma}_{2,3} &= -\tfrac{\pi \beta_1 \beta_3 h_1 h_2 h_3}{j_{33}^3 n^3} ((\sigma_1 + \sigma_2 + \gamma_1 + \gamma_3)_c - 2(\sigma_1 - \sigma_2 + \gamma_1 - \gamma_3)_c).
\end{aligned} \tag{3.56}$$

Let $\alpha_1 = \epsilon \alpha_2$. Then (3.55) implies

$$\Delta_{a,h_3} \psi = \Lambda_c + \Lambda_b \alpha_2 + \Lambda_a \alpha_2^2, \tag{3.57}$$

where

$$\begin{aligned}
\Lambda_a &= (\Gamma_1 + \tilde{\Gamma}_{2,1}) \epsilon^2 + (\Gamma_2 + \tilde{\Gamma}_{2,2}) + (\Gamma_3 + \tilde{\Gamma}_{2,3}) \epsilon, \\
\Lambda_b &= \tilde{\Gamma}_{1,1} \epsilon + \tilde{\Gamma}_{1,2}, \\
\Lambda_c &= \tilde{\Gamma}_0.
\end{aligned} \tag{3.58}$$

Since (3.57) is quadratic in α_2, the equation $\Delta_{a,h_3} \psi = 0$ can be solved if a specific constant ϵ_e is chosen for the quadratic equation (3.57). Denote $\alpha_{2,e}$ as a solution to $\Delta_{a,h_3} \psi = 0$ in (3.57) when $\epsilon = \epsilon_e$ in (3.58). By selecting k_{11}, k_{12}, k_{21}, k_{22}, σ_1, σ_2, and ϵ_e appropriately, the quadratic equation (3.57) will have a positive real solution. The significance of $\alpha_{2,e}$ is that it corresponds to the periodic excitation of the base dynamics, which on average counteracts the drift caused by $h_3 \neq 0$. Let

$\alpha_2 = \alpha_{2,e} + \delta\alpha_{2,e}$. Since $G_{a,h_3}(\epsilon_e\alpha_{2,e}, \alpha_{2,e}) = 0$, (3.57) can be rewritten as

$$\Delta_{a,h_3}\psi = \tilde{\Lambda}_1\delta\alpha_{2,e} + \tilde{\Lambda}_2\delta\alpha_{2,e}^2, \tag{3.59}$$

where

$$\begin{aligned}\tilde{\Lambda}_1 &= \tilde{\Gamma}_{1,1}\epsilon_e + \tilde{\Gamma}_{1,2} + 2\alpha_{2,e}\left((\Gamma_1 + \tilde{\Gamma}_{2,1})\epsilon_e{}^2 + (\Gamma_2 + \tilde{\Gamma}_{2,2}) + (\Gamma_3 + \tilde{\Gamma}_{2,3})\epsilon_e\right), \\ \tilde{\Lambda}_2 &= (\Gamma_1 + \tilde{\Gamma}_{2,1})\epsilon_e{}^2 + (\Gamma_2 + \tilde{\Gamma}_{2,2}) + (\Gamma_3 + \tilde{\Gamma}_{2,3})\epsilon_e.\end{aligned} \tag{3.60}$$

Define the map $G_{a,\delta\alpha_{2,e}} : \delta\alpha_{2,e} \to \Delta_{a,h_3}\psi$. If $\delta\alpha_{2,e}$ is sufficiently small, the linear term in (3.59) dominates the quadratic term. Therefore $G_{a,\delta\alpha_{2,e}}$ is open at $\delta\alpha_{2,e} = 0$ provided that $\tilde{\Lambda}_1 \neq 0$.

Now the modified switching scheme is described. Let $\delta\alpha_{2,e}$ be adjusted at the beginning of each time interval of length T and held constant,

$$\delta\alpha_{2,e}(t) = \delta\alpha_{2,e}(kT) = \delta\alpha_{2,e}^k,\ kT \leq t < (k+1)T. \tag{3.61}$$

Furthermore, let $\mu_1 \in (0,1)$, μ_2 be sufficiently small, and $\xi_3 > \mu_2$ be such that $|\tilde{\Lambda}_1\xi_3| > |\tilde{\Lambda}_2\xi_3^2|$. Then the control scheme for the case when $h_3 \neq 0$ is outlined by Algorithm 2.

The methodology of Algorithm 2 is as follows. It can be seen that $|\Delta_{a,h_3}\psi|$ is dictated by $|\delta\alpha_{2,e}|$ while the direction of $\Delta_{a,h_3}\psi$ is determined by the sign of $\delta\alpha_{2,e}$. The initial value of $|\delta\alpha_{2,e}^0|$ is determined by ξ_3 and it can be shown that $|\delta\alpha_{2,e}^k|$ is nonincreasing. Furthermore, as $k \to \infty$, $|\delta\alpha_{2,e}^k| \to \mu_2$, and in the limit α_2^k can assume either the value of $\alpha_{2,e} + \mu_2$ or $\alpha_{2,e} - \mu_2$. This steady-state "dither" in $\delta\alpha_{2,e}^k$ is introduced to compensate for the error/uncertainty in the approximation of $\Delta\psi$ by $\Delta_{a,h_3}\psi$. The value of μ_2 must be chosen as small as possible to minimize the "dither,"

Algorithm 2: Control Computation for RWs when $h_3 \neq 0$

Given:

$k \geq 0$, $\alpha_{2,e}$ and ϵ_e from (3.57)-(3.58), $\mu_1 \in (0,1)$, μ_2, sufficiently small, and $\xi_3 > \mu_2$ such that $|\bar{\Lambda}_1 \xi_3| > |\bar{\Lambda}_2 \xi_3^2|$

if $k = 0$ **then**
  if $\psi^k = 0$ **then**
    $\delta\alpha_{2,e}^0 = 0$
  else $\{\psi^k \neq 0\}$
    $\delta\alpha_{2,e}^0 = -\xi_3 \text{sign}(\bar{\Lambda}_1 \psi^0)$,
  end if
else $\{k > 0\}$
  Compute $G_{a,\delta\alpha_{2,e}}(\delta\alpha_{2,e}^{k-1})\psi^k$ using (3.59)
  if $\psi^k = 0$ **or** $G_{a,\delta\alpha_{2,e}}(\delta\alpha_{2,e}^{k-1})\psi^k < 0$ **then**
    $\delta\alpha_{2,e}^k = \delta\alpha_{2,e}^{k-1}$
  else $\{G_{a,\delta\alpha_{2,e}}(\delta\alpha_{2,e}^{k-1})\psi^k \geq 0\}$
    $\delta\alpha_{2,e}^k = -\min\{\mu_1 \delta\alpha_{2,e}^{k-1}, \mu_2\}$
  end if
end if
Control at Cycle k**:**

$\alpha_1^k = \epsilon_e(\alpha_{2,e} + \delta\alpha_{2,e}^k), \alpha_2^k = \alpha_{2,e} + \delta\alpha_{2,e}^k$

$v_1(t) = \alpha_1^k(nt + \sigma_1)_c$, $v_2(t) = \alpha_2^k(nt + \sigma_2)_c$, $v(t) = [\ v_1(t) \quad v_2(t)\ ]^{\text{T}}$, for $t \in [kT, (k+1)T)$

Compute $u(t)$ from the feedback law in (3.28)

while satisfying the following property,

$$G(\epsilon_e(\alpha_{2,e}+\mu_2),\alpha_e+\mu_2)G(\epsilon_e(\alpha_{2,e}-\mu_2),\alpha_{2,e}-\mu_2)<0, \tag{3.62}$$

for Algorithm 2 to be able to induce the changes in $\Delta\psi$ by the intended sign even in the presence of the approximation error.

Lemma 3.3.2 is a similar result to Lemma 3.3.1.

Lemma 3.3.2: Let the fiber variable dynamics for ψ be given in (3.34). The error between fiber variable trajectory, ψ, induced by base variable motions exponentially convergent to periodic steady-state (not necessarily zero) and fiber variable trajectory induced by base variable motion in periodic steady-state, ψ^{ss}, remains bounded.

Proof: If $h_3 \neq 0$, then (3.47) in the proof of Lemma 2.1 changes to

$$d_{h_3}(\phi,\theta,\omega_1,\omega_2)=\omega_2\phi+\frac{h_1}{j_{33}}\theta-\frac{h_2}{j_{33}}\phi-\frac{j_{13}}{j_{33}}\omega_1-\frac{j_{23}}{j_{33}}\omega_2+\frac{h_3}{j_{33}} \tag{3.63}$$

and (3.50) changes to

$$f_{h_3}(t)=\left(\frac{h_1}{j_{33}}e_\phi+\frac{h_2}{j_{33}}e_\theta\right)\psi+(d_{h_3}(\phi,\theta,\omega_1,\omega_2)-d_{h_3}(\phi^{ss},\theta^{ss},\omega_1^{ss},\omega_2^{ss})). \tag{3.64}$$

Since

$$d_{h_3}(\phi,\theta,\omega_1,\omega_2)-d_{h_3}(\phi^{ss},\theta^{ss},\bar{\omega_1},\bar{\omega_2})=d(\phi,\theta,\omega_1,\omega_2)-d(\phi^{ss},\theta^{ss},\bar{\omega_1},\bar{\omega_2}), \tag{3.65}$$

it follows that $f_{h_3}(t)=f(t)$ and $f_{h_3}(t)$ converges exponentially to zero. The rest of the proof proceeds similarly to the proof of Lemma 3.3.1 $\square$

While Lemma 3.3.2 is a similar result to Lemma 3.3.1, a convergence result similar to Theorem 3.3.1 does not hold if $h_3 \neq 0$, as steady-state oscillations in ψ, θ, and ϕ in a vicinity of zero will occur to accommodate nonzero h_3.

The amplitude of oscillations about $\bar{\Theta} = 0$ using this switching law can be uniformly upper bounded. Consider the situation when $\alpha_1 = \epsilon_e \alpha_{2,e}$, $\alpha_2 = \alpha_{2,e}$, the base variable motion is in steady-state, and $\psi(0) = 0$. If this is the case, then from (3.8),

$$\begin{aligned} |\phi(t)| &= |\epsilon_e \alpha_{2,e} \beta_1 (nt + \sigma_1 + \gamma_1)_c| \leq |\epsilon_e \alpha_{2,e} \beta_1| \quad \forall t \geq 0, \\ |\theta(t)| &= |\alpha_{2,e} \beta_3 (nt + \sigma_2 + \gamma_3)_c| \leq |\alpha_{2,e} \beta_3| \quad \forall t \geq 0. \end{aligned} \tag{3.66}$$

Furthermore, for $0 \leq t \leq T$,

$$\begin{aligned} |\psi(t)| &= \int_0^t \left| \bar{\Phi}(t,\tau) \left(b(\tau) + \tfrac{h_3}{j_{33}} \right) d\tau \right|, \\ &\leq \int_0^t |\bar{\Phi}(t,\tau)| \left| \left(b(\tau) + \tfrac{h_3}{j_{33}} \right) \right| d\tau, \\ &\leq \int_0^t |\bar{\Phi}(t,\tau)| \left(|(b(\tau)| + \tfrac{|h_3|}{j_{33}} \right) d\tau, \\ &\leq \int_0^T \tfrac{\exp(c_2)}{j_{33}} \left(|\alpha_{2,e}| c_3 + |h_3| \right) d\tau, \\ &\leq \tfrac{2\pi \exp(c_2)}{n j_{33}} \left(|\alpha_{2,e}| c_3 + |h_3| \right), \end{aligned} \tag{3.67}$$

where

$$\begin{aligned} c_2 &= \left| \tfrac{\alpha_{2,e}}{n j_{33}} \right| (|\epsilon_e h_1 \beta_1| + |h_2 \beta_3|), \\ c_3 &= |\alpha_{2,e} \epsilon_e \beta_1 \beta_4 j_{33}| + |h_1 \beta_3| + |\epsilon_e h_2 \beta_1| + |\epsilon_e \beta_2 j_{13}| + |\beta_4 j_{23}|. \end{aligned} \tag{3.68}$$

The value of $\alpha_{2,e}$ decreases with the value of h_3, and furthermore $\lim_{h_3 \to 0} \alpha_{2,e} = 0$. Therefore, the amplitude of the steady-state oscillation in ϕ, θ, and ψ around zero (and consequently the upper bound on Euler angle oscillation) will decrease as h_3 decreases.

3.3.4 Analysis of High Frequency Response

We now consider the case where the base variable excitation frequency n is large and analyze the motions of Euler angles ϕ, θ and ψ when the total angular momentum is zero and when there is a nonzero total angular momentum component about the uncontrollable axis.

3.3.4.1 Zero Angular Momentum Case

Let $h_1 = h_2 = h_3 = 0$ and assume that $\phi(0) = \theta(0) = \psi(0) = 0$. Consider the spacecraft excited by base variable motions (3.8) with constant α_1 and α_2, and let

$$\dot{\bar{\psi}} = \frac{\Delta_a \psi}{T}, \tag{3.69}$$

where $\Delta_a \psi$ is given by (3.37). Equation (3.69) defines an average rate of change of ψ over one steady-state cycle of period T. Substituting (3.37) and (3.38) into (3.69) gives

$$\dot{\bar{\psi}} = \frac{\alpha_1 \alpha_2 \beta_1 \beta_4}{2} (\sigma_1 - \sigma_2 + \gamma_1 - \gamma_4)_c. \tag{3.70}$$

If n is large, then it implies that (3.9) can be approximated by,

$$\begin{aligned} \beta_1 &\sim O\left(\tfrac{1}{n^2}\right), \\ \beta_2 &\sim O\left(\tfrac{1}{n^2}\right), \\ \beta_3 &\sim O\left(\tfrac{1}{n}\right), \\ \beta_4 &\sim O\left(\tfrac{1}{n}\right), \end{aligned} \tag{3.71}$$

and

$$\dot{\tilde{\psi}} \sim \frac{\alpha_1 \alpha_2}{n^3}(\sigma_1 - \sigma_2 + \gamma_1 - \gamma_4)_c, \tag{3.72}$$

where γ_1 and γ_4 also depend on n. Let α_1 and α_2 be nonzero and proportional to $n^{\frac{3}{2}}$, i.e.,

$$\begin{aligned} \alpha_1 &= n^{\frac{3}{2}}\rho_1, \\ \alpha_2 &= n^{\frac{3}{2}}\rho_2, \end{aligned} \tag{3.73}$$

where $\rho_1, \rho_2 \in \mathbb{R}\backslash\{0\}$. The steady-state values of ϕ and θ from (3.8) when n is large are approximated by

$$\begin{aligned} \phi^{ss}(t) &\sim \tfrac{\rho_1}{\sqrt{n}} \cos(nt + \sigma_1 + \gamma_1)_c, \\ \theta^{ss}(t) &\sim \tfrac{\rho_2}{\sqrt{n}} \cos(nt + \sigma_2 + \gamma_3)_c. \end{aligned} \tag{3.74}$$

As n approaches infinity, for any t, it is clear from (3.74) that

$$\begin{aligned} \lim_{n\to\infty} \phi^{ss}(t, n) &= 0, \\ \lim_{n\to\infty} \theta^{ss}(t, n) &= 0. \end{aligned} \tag{3.75}$$

Note that γ_1 and γ_4 have finite limits, $\tilde{\gamma}_1$ and $\tilde{\gamma}_4$, respectively, as n increases because $\tan^{-1}(*)$ is a continuous function that is bounded. Then,

$$\lim_{n\to\infty} \dot{\tilde{\psi}}(t, n) = \rho_1\rho_2(\sigma_1 - \sigma_2 + \tilde{\gamma}_1 - \tilde{\gamma}_4)_c. \tag{3.76}$$

Hence, as frequency increases, attitude trajectories of an underactuated spacecraft with zero total angular momentum can approach arbitrary close attitude trajectories of a spacecraft that has a nonzero total angular momentum component and rotates at a constant angular velocity about the uncontrollable axis. Note that as frequency n increases, the oscillation amplitudes in the spacecraft angular velocities ω_1, ω_2 and

RW speeds ν_1, ν_2 increases as $\sqrt{n}$.

3.3.4.2 Nonzero Angular Momentum Case

The same approach as in subsection 3.3.4.1 is used to analyze a spacecraft that has nonzero total angular momentum about its uncontrollable axis. Assume that $\phi(0) = \theta(0) = \psi(0) = 0$, $h_1, h_2 \in \mathbb{R}$, and $h_3 \neq 0$. Define

$$\dot{\tilde{\psi}}_{h_3} = \frac{\Delta\psi_{h_3}}{T} \tag{3.77}$$

where $\Delta_{a,h_3}\psi$ is given by (3.55). Let α_1 and α_2 be defined as in (3.73). If the frequency n is increased to infinity, then

$$\lim_{n\to\infty} \phi^{ss}(t,n) = 0,$$

$$\lim_{n\to\infty} \theta^{ss}(t,n) = 0, \tag{3.78}$$

$$\lim_{n\to\infty} \dot{\tilde{\psi}}(t,n) = \tfrac{h_3}{j_{33}} + \rho_1\rho_2(\sigma_1 - \sigma_2 + \tilde{\gamma}_1 - \tilde{\gamma}_4)_c,$$

where $\tilde{\gamma}_1$ and $\tilde{\gamma}_4$ denote finite limits of γ_1 and γ_4 as n increases. Choosing ρ_1 and ρ_2 so that

$$\rho_1\rho_2 = -\frac{h_3}{j_{33}(\sigma_1 - \sigma_2 + \tilde{\gamma}_1 - \tilde{\gamma}_4)_c}, \tag{3.79}$$

while assuming that the denominator is nonzero, results in

$$\lim_{n\to\infty} \dot{\tilde{\psi}}(t,n) = 0. \tag{3.80}$$

As n increases, attitude trajectories of the underactuated spacecraft with nonzero total angular momentum component about the uncontrollable axis can approach arbitrarily close to a fixed inertial pointing attitude. Similarly to the zero total angular

momentum case, as n increases, the amplitude of the spacecraft angular velocity and RW speed oscillation increase as $\sqrt{n}$.

Remark 3.3.3: The conclusions in this subsection may appear to be counter-intuitive at first glance given the angular momentum conservation. In [77], similar results were derived using averaging theory for a different system, a cylinder rotating about a fixed axis with three movable links.

3.3.5 Simulation Results

For the simulations, we consider a spacecraft bus with principal moments of inertia of 430, 1210, and 1300 kg m^2. The two reaction wheels are assumed symmetric, thin, and are mounted such that the COM of the spacecraft bus and total spacecraft system coincide. The inertias of the two functioning RWs about their spin axes are given by $J_{ws1} = J_{ws2} = 0.043$ kg m^2. The matrices $\bar{J}$ and $\bar{W}$ will be different between simulations as necessary to demonstrate that our approach can handle different spacecraft scenarios. In the first simulation, the spacecraft has zero total angular momentum. The second simulation involves a spacecraft with total angular momentum satisfying Proposition 3.3.1 (i.e., $h_3 = 0$). In the third simulation $h_3 \neq 0$. All simulations are performed on the full nonlinear model and demonstrate successful convergence to the desired pointing equilibrium in the case where $h_3 = 0$ and controlled oscillation about the desired pointing configuration when $h_3 \neq 0$. The parameters for the controller and switching schemes, outlined by Algorithms 1 and 2, are given in Table 3.1.

Parameter	Units	Value
n	sec^{-1}	0.03
k_{11}, k_{12}	-	$9 \times 10^{-4},\ 0.0180$
k_{21}, k_{22}	-	$9 \times 10^{-4},\ 0.0180$
σ_1, σ_2	-	$\frac{\pi}{4},\ -\frac{\pi}{4}$
ξ_1, ξ_2, ξ_3	-	1×10^{-4}, 1.5, 2.5×10^{-5}
μ_1, μ_2	-	0.5, 1×10^{-8}

Table 3.1: Parameters for RW switching controller.

3.3.5.1 Simulation 1

Consider the case when the two RWs are aligned with the first two principal axes of the spacecraft bus. Then

$$\bar{J} = \begin{bmatrix} 430.043 & 0 & 0 \\ 0 & 1210.043 & 0 \\ 0 & 0 & 1300 \end{bmatrix}, \quad \bar{W} = \begin{bmatrix} 0.043 & 0 \\ 0 & 0.043 \\ 0 & 0 \end{bmatrix}. \tag{3.81}$$

The initial conditions of the spacecraft are $\phi(0) = \theta(0) = 0$ rad, $\psi(0) = 0.1$ rad, $\omega_1(0) = \omega_2(0) = \omega_3(0) = 0$ rad/sec, and $\nu_1(0) = \nu_2(0) = 0$ rad/sec. The total angular momentum is hence zero, i.e., $\bar{H} = [\ 0\ \ 0\ \ 0\ ]^{\text{T}}$ kg m^2 sec^{-1}, and satisfies Proposition 3.3.1. The simulation shows that by using Algorithm 1, the spacecraft successfully converges to the desired pointing orientation. See Figure 3.5. Note from Figure 3.5 (a) and (e) that when α_1 changes sign (which is dictated by ϵ), the direction of $\Delta\psi$ also changes.

Remark 3.3.4: It should be noted that even though the convergence time is exponential, the convergence time for this simulation is over two hours. The convergence time can be improved by tuning the parameters in Table 3.1, specifically ξ_1 and

ξ_2, which govern the initial amplitude of the excitation, μ_1, which controls the decay of excitation, and n which defines when the control parameters are switched.

3.3.5.2 Simulation 2

Now consider the case where the RWs are not aligned with the first two principal axes of the spacecraft bus. After an appropriate coordinate transformation, the matrices $\bar{J}$ and $\bar{W}$ are

$$\bar{J} = \begin{bmatrix} 865 & 0 & -0.435 \\ 0 & 1210.043 & 0 \\ -0.435 & 0 & 865.043 \end{bmatrix}, \quad \bar{W} = \begin{bmatrix} 0.043 & 0 \\ 0 & 0.043 \\ 0 & 0 \end{bmatrix}. \tag{3.82}$$

The initial conditions for the spacecraft are the same as Simulation 1 with the exception that $\nu_1(0) = \nu_2(0) = 10$ rad/sec, yielding $\bar{H} = [\ 0.3849 \ \ 0.4708 \ \ 0\ ]^{\mathrm{T}}$ kg m^2 sec^{-1} which satisfies Proposition 3.3.1. The results are shown in Figure 3.6. As is demonstrated, even though the RWs are not aligned with the principal axes, Algorithm 1 is still able to guide the system to the pointing equilibrium. Note that the RW speeds are not zero in steady-state and absorb the nonzero total angular momentum of the spacecraft. The stabilization of this system takes a shorter amount of time in contrast to Simulation 1. In this case, the added angular momentum and the non-diagonal shape of $\bar{J}$ induce nonlinear terms that improve the convergence time, but this may not be always the case.

3.3.5.3 Simulation 3

Consider now the case where the RWs spin about the first two principal axes of the spacecraft bus. In this case, the matrices $\bar{J}$ and $\bar{W}$ are the same as in Simulation 1. Let $\phi(0) = 0.01$ rad, $\theta(0) = 0$ rad, $\psi(0) = 0.1$ rad, $\omega_1(0) = \omega_2(0) = \omega_3(0) = 0$ rad/sec, and $\nu_1(0) = \nu_2(0) = 10$ rad/sec. In this case, $\bar{H} = [\ 0.3849 \ \ 0.4708 \ \ 0.0043\ ]^{\mathrm{T}}$ kg m^2

$\sec^{-1}$, and does not satisfy Proposition 3.3.1. Figure 3.7 demonstrates the response of the spacecraft using Algorithm 2. Note that the attitude error in Figure 3.7 (f) reaches near zero, but then increases. This is due to the fact that simultaneous convergence of all three Euler angles to zero is impossible as the spacecraft is underactuated and has a nonzero total angular momentum component about the uncontrollable axis (Proposition 3.3.1). However, Figure 3.7 (a) demonstrates that by using Algorithm 2, controlled and bounded oscillations in a vicinity of $\bar{\Theta} = 0$ can be performed.

Remark 3.3.5: As mentioned in the introduction, the treatment of an underactuated spacecraft with nonzero total angular momentum has been limited in the previous literature. Even in the case where total angular momentum is taken into account, some proposed control schemes can send a spacecraft into an uncontrolled drift, see [39]. In [20, 23] it was shown that a Lyapunov-based controller designed for zero total angular momentum could perform oscillations about the desired pointing configuration when there was a nonzero component of total angular momentum about the uncontrollable axis. However, the Lyapunov functions used for controller synthesis in each method become undefined at certain orientations near the desired attitude, and thus singularity avoidance must be performed. The method described in this chapter in contrast does not have these singularity issues. Another benefit to the switching law presented is that the total angular momentum is taken into account when designing the controller, which could improve overall performance.

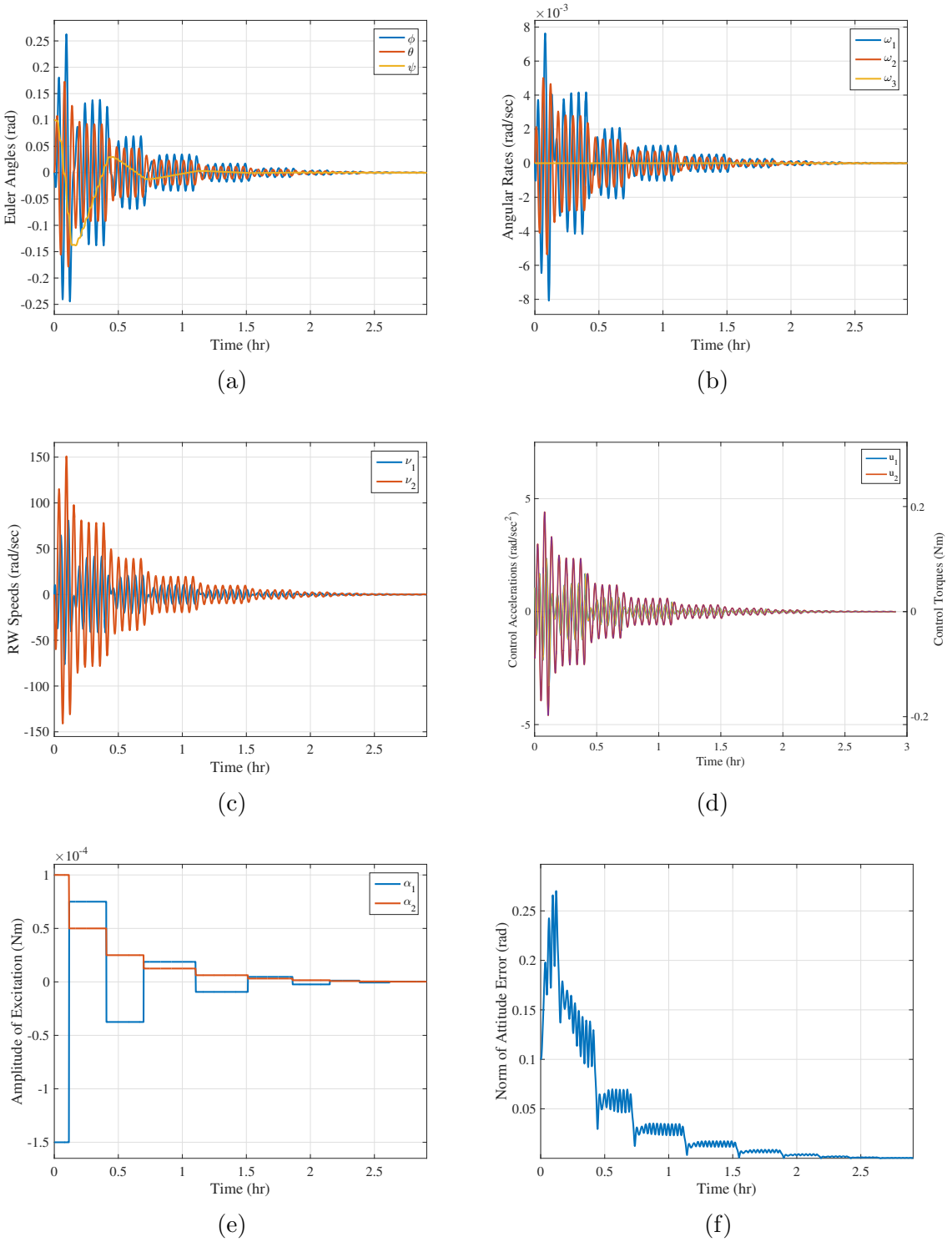

Figure 3.5: Response of a spacecraft using Algorithm 1 when the reaction wheels are aligned with the first two principal axes and $h_1 = h_2 = h_3 = 0$ (a) Euler angles, (b) angular velocities, (c) wheel speeds, (d) wheel accelerations, (e) excitation magnitude, (f) 2-norm of attitude error.

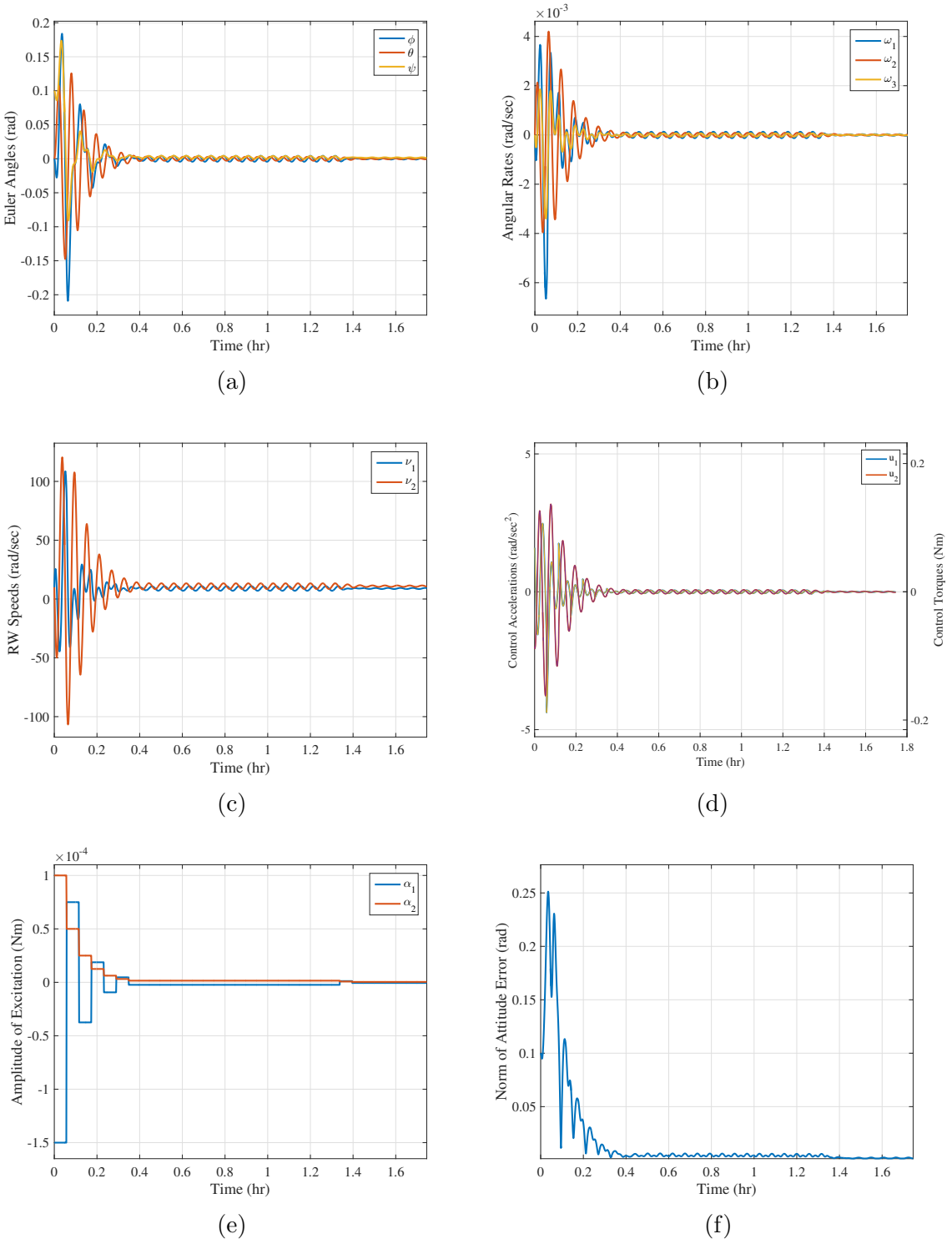

Figure 3.6: Response of a spacecraft using Algorithm 1 when the reaction wheels are not aligned with the first two principal axes and $h_3 = 0$ (a) Euler angles, (b) angular velocities, (c) wheel speeds, (d) wheel accelerations, (e) excitation magnitude, (f) 2-norm of attitude error.

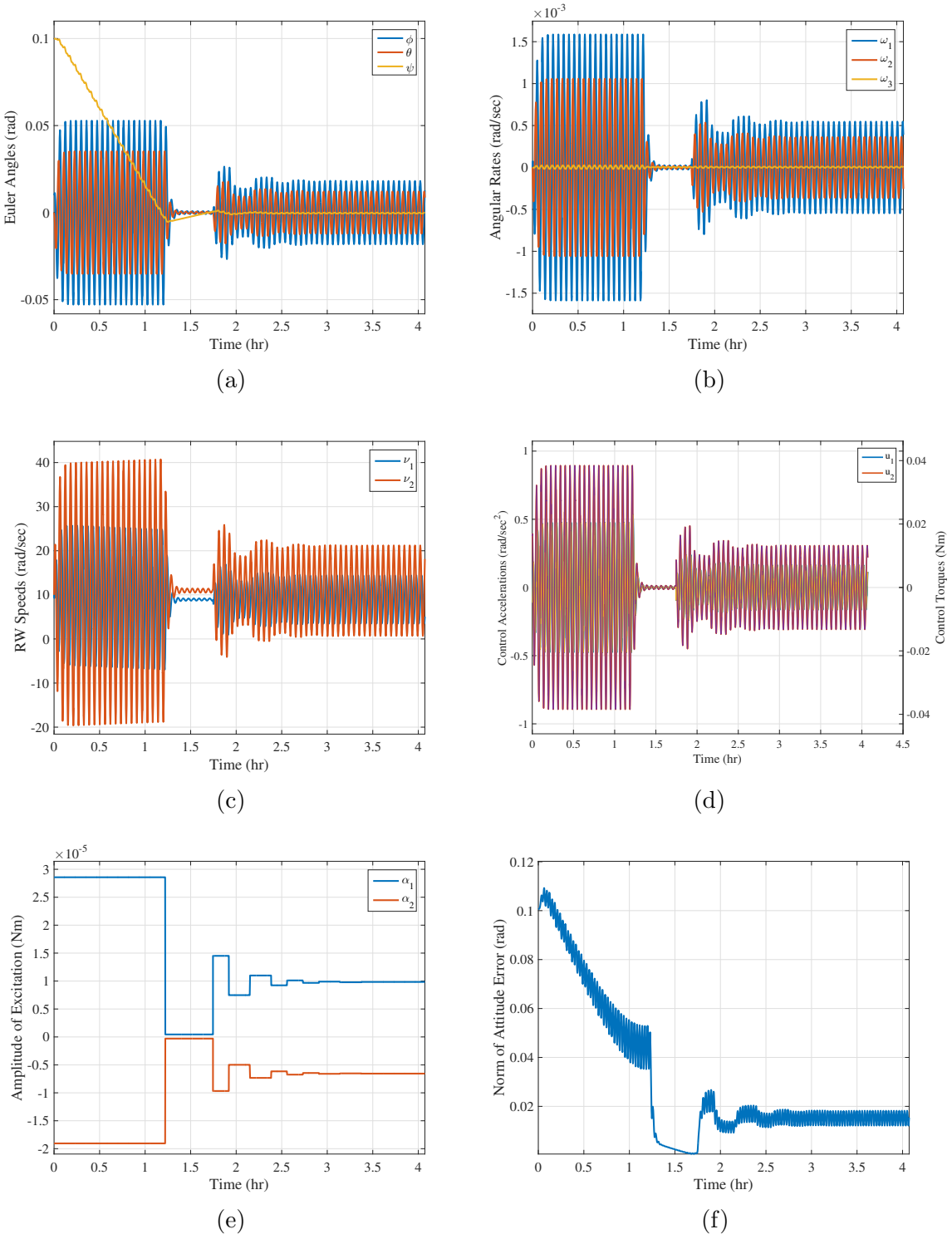

Figure 3.7: Response of a spacecraft using Algorithm 2 when the reaction wheels are aligned with the first two principal axes and $h_3 \neq 0$ (a) Euler angles, (b) angular velocities, (c) wheel speeds, (d) wheel accelerations, (e) excitation magnitude, (f) 2-norm of attitude error.

3.4 Control Moment Gyro Case

3.4.1 Spacecraft Configuration & Equations of Motion

In this section we consider a spacecraft system consisting of a bus equipped with two CMGs under the following assumption:

Assumption 3.4.1 There are no external moments acting on the total spacecraft system.

Since Assumption 3.4.1 holds, we can use the RAE's for CMGs in (2.55) to model the system dynamics:

$$\begin{aligned} \dot{\mathbf{B}} &= \left[\bar{J}^{-1}\left(\sum_{j=1}^{2}\left(J_{g_{gj}}+J_{r_{tj}}\right)\dot{\delta}_j\check{g}_j+J_{r_{sj}}\eta_j\check{h}_j-\mathbf{B}\bar{H}\right)\right]^{\times}\mathbf{B}, \\ \dot{\delta}_j &= u_j, \quad j=1,2, \end{aligned} \tag{3.83}$$

where

$$\bar{J} = \bar{J}_{\mathfrak{B}}+\sum_{j=1}^{2}\mathbf{G}_j^{\mathrm{T}}\left(\bar{J}_{\mathfrak{G}_j}+\bar{J}_{\mathfrak{R}_j}\right)\mathbf{G}_j. \tag{3.84}$$

Recall that the mathematical unit vector $\check{g}_j$ specifies the gimbal axis of the jth CMG, which remains fixed in $\mathcal{B}$ and is given by

$$\check{g}_j = \mathbf{G}_j^{\mathrm{T}}\begin{bmatrix}0\\0\\1\end{bmatrix}. \tag{3.85}$$

The mathematical unit vector $\check{h}_j$ is in the direction of the angular momentum of the jth CMG and depends on the gimbal angle δ_j,

$$\check{h}_j = \mathbf{G}_j^{\mathrm{T}} \begin{bmatrix} \cos(\delta_j) \\ \sin(\delta_j) \\ 0 \end{bmatrix}. \tag{3.86}$$

Note that for attitude representation, in the CMG case, an $SO(3)$-based description is chosen instead of Euler angles. The two switching schemes for thrusters and RWs relied on using Euler angles because, by construction, the uncontrollable axis is isolated in the third Euler angle ψ (yaw). This is not the case for CMGs, as the uncontrollable axis changes relative to the spacecraft bus, and may even become an uncontrollable plane if the CMGs reach singularity. The switching scheme presented in this section exploits the $SO(3)$-based attitude representation to avoid complications due to the time-varying uncontrollable axis.

We now make the following assumptions:

Assumption 3.4.2 The inertia of the spacecraft bus is much larger than that of the CMGs.

Assumption 3.4.3 The speed of the rotors is much larger than that of the gimbals.

Assumption 3.4.4 The total angular momentum of the system is zero.

Assumption 3.4.2 implies that the locked inertia $\bar{J}$ is approximately that of the spacecraft bus, i.e., $\bar{J} \approx \bar{J}_{\mathfrak{B}}$, which is reasonable since actuator inertias are relatively small when compared to the spacecraft bus inertia. Assumption 3.4.3 implies that the angular momentum contribution due to the gimbal rates can be neglected when compared to the rotor angular momentum. This is also reasonable, as the rotor spins at much higher speeds than the gimbal of the CMG. Assumption 3.4.4 simplifies the dynamics,

and though not practical, yields a starting point for the preliminary development of future control laws that have constant nonzero total angular momentum. Using all of the assumptions, (3.83) becomes

$$\begin{aligned} \dot{\mathbf{B}} &= \left[\bar{J}_{\mathfrak{B}}^{-1} \left(\sum_{j=1}^{2} \bar{h}_{j} \right) \right]^{\times} \mathbf{B}, \\ \dot{\delta}_{j} &= u_{j}, \quad j = 1, 2, \end{aligned} \tag{3.87}$$

where

$$\bar{h}_{j} = J_{rsj} \eta_{j} \check{h}_{j}. \tag{3.88}$$

Note that $\bar{h}_{j}$ depends on δ_{j} as per (3.86).

3.4.2 State Transition Approximation

In order to construct a switching controller for a spacecraft with two CMGs, we approximate the state transition matrix using the following method; let the kinematics of (3.87) be expanded using a Taylor-series about an at-rest configuration corresponding to nominal gimbal angles $\delta_{1,0} = 0$ and $\delta_{2,0} = 0$. Note that the case when the nominal gimbal angles are nonzero can be treated similarly. Then

$$\dot{\mathbf{B}} = \left[\bar{J}_{\mathfrak{B}}^{-1} \left(\sum_{j=1}^{2} \bar{h}_{j}(\delta_{j,0}) + \frac{\partial \bar{h}_{j}(\delta_{j,0})}{\partial \delta_{j}} \delta_{j} + \frac{1}{2} \frac{\partial^{2} \bar{h}_{j}(\delta_{j,0})}{\partial \delta_{j}^{2}} \delta_{j}^{2} + O(|\delta_{j}|^{3}) \right) \right]^{\times} \mathbf{B}, \tag{3.89}$$

where we explicitly show the dependency of $\bar{h}_{j}$ on the gimbal angle δ_{j}. Because the total angular momentum of the spacecraft is zero, it follows that at the nominal gimbal angle configuration,

$$\bar{h}_{1}(\delta_{1,0}) + \bar{h}_{2}(\delta_{2,0}) = 0. \tag{3.90}$$

From (2.50), we see that

$$\begin{aligned} \frac{\partial \bar{h}_j}{\partial \delta_j}(\delta_{j,0}) &= \bar{\tau}_j, \quad j = 1, 2, \\ \frac{\partial^2 \bar{h}_j}{\partial \delta_j^2}(\delta_{j,0}) &= -\bar{h}_j(\delta_{j,0}), \quad j = 1, 2, \end{aligned} \tag{3.91}$$

where $\bar{\tau}_j = J_{rsj}\eta_j\check{\tau}_j$ corresponds to the torque provided by the jth CMG. Then from (3.90) and (3.91), (3.89) becomes

$$\dot{\mathbf{B}} = \left[\bar{J}_{\mathfrak{B}}^{-1}\left(\bar{\tau}_1\delta_1 + \bar{\tau}_2\delta_2 - \frac{\bar{h}}{2}(\delta_1^2 - \delta_2^2) + \sum_{j=1}^{2} O(|\delta_j|^3)\right)\right]^{\times}\mathbf{B}, \tag{3.92}$$

where $\bar{h} = \bar{h}_1(\delta_{1,0}) = -\bar{h}_2(\delta_{2,0})$.

Now let the gimbal angles be in steady-state, denoted by $\delta_j = \delta_j^{ss}$, and let these trajectories be periodic with period T while satisfying

$$\int_0^T \delta_j^{ss}(\sigma)d\sigma = 0, \quad j = 1, 2. \tag{3.93}$$

Since (3.92) is linear with respect to $\mathbf{B}$ but time-varying, a Peano-Baker series [76] is used to approximate the state transition matrix over the time period T,

$$\bar{\Phi}(T, 0) = I + \int_0^T \bar{A}(\sigma)d\sigma + \int_0^T \bar{A}(\sigma)\int_0^\sigma \bar{A}(\sigma_1)d\sigma_1 d\sigma + \ldots, \tag{3.94}$$

where the matrix $\bar{A}(t)$ is given by

$$\bar{A}(t) = \left[\bar{J}_{\mathfrak{B}}^{-1}\left(\bar{\tau}_1\delta_1^{ss}(t) + \bar{\tau}_2\delta_2^{ss}(t) - \frac{\bar{h}}{2}\left(\left(\delta_1^{ss}(t)\right)^2 - \left(\delta_2^{ss}(t)\right)^2\right) + \sum_{j=1}^{2} O(|\delta_j^{ss}(t)|^3)\right)\right]^{\times}. \tag{3.95}$$

Thus the evolution of $\mathbf{B}$ over the time interval T is

$$\mathbf{B}(T) = \bar{\Phi}(T,0)\mathbf{B}(0). \tag{3.96}$$

Due to the periodicity of δ_j^{ss}, the first integral of the Peano-Baker series in (3.94),(3.95) is

$$\int_0^T \bar{A}(\sigma)d\sigma = \left[\bar{J}_{\mathfrak{B}}^{-1}\bar{h}\right]^{\times}\alpha_1 + \left[\int_0^T \sum_{j=1}^{2} O(|\delta_j^{ss}(\sigma)|^3)d\sigma\right]^{\times}, \tag{3.97}$$

where

$$\alpha_1 = -\frac{1}{2}\int_0^T \left\{(\delta_1^{ss}(\sigma))^2 - (\delta_2^{ss}(\sigma))^2\right\} d\sigma. \tag{3.98}$$

Likewise, the second integral term in the Peano-Baker series is

$$\begin{aligned}
\int_0^T \bar{A}(\sigma)\int_0^\sigma \bar{A}(\sigma_1)d\sigma_1 d\sigma \;=\; & \int_0^T\int_0^\sigma \Big(\left[\bar{J}_{\mathfrak{B}}^{-1}\bar{\tau}_1\right]^{2\times}\delta_1^{ss}(\sigma)\delta_1^{ss}(\sigma_1) + \left[\bar{J}_{\mathfrak{B}}^{-1}\bar{\tau}_2\right]^{2\times}\delta_2^{ss}(\sigma)\delta_2^{ss}(\sigma_1) \\
& + \tfrac{1}{4}\left[\bar{J}_{\mathfrak{B}}^{-1}\bar{h}\right]^{2\times}((\delta_1^{ss}(\sigma))^2 - (\delta_2^{ss}(\sigma))^2)((\delta_1^{ss}(\sigma_1))^2 - (\delta_2^{ss}(\sigma_1))^2) \\
& + \left[\bar{J}_{\mathfrak{B}}^{-1}\bar{\tau}_1\right]^{\times}\left[\bar{J}_{\mathfrak{B}}^{-1}\bar{\tau}_2\right]^{\times}\delta_1^{ss}(\sigma)\delta_2^{ss}(\sigma_1) \\
& + \left[\bar{J}_{\mathfrak{B}}^{-1}\bar{\tau}_2\right]^{\times}\left[\bar{J}_{\mathfrak{B}}^{-1}\bar{\tau}_1\right]^{\times}\delta_2^{ss}(\sigma)\delta_1^{ss}(\sigma_1) \\
& - \tfrac{1}{2}\left[\bar{J}_{\mathfrak{B}}^{-1}\bar{\tau}_1\right]^{\times}\left[\bar{J}_{\mathfrak{B}}^{-1}\bar{h}\right]^{\times}\delta_1^{ss}(\sigma)((\delta_1^{ss}(\sigma_1))^2 - (\delta_2^{ss}(\sigma_1))^2) \\
& - \tfrac{1}{2}\left[\bar{J}_{\mathfrak{B}}^{-1}\bar{h}\right]^{\times}\left[\bar{J}_{\mathfrak{B}}^{-1}\bar{\tau}_1\right]^{\times}((\delta_1^{ss}(\sigma))^2 - (\delta_2^{ss}(\sigma))^2)\delta_1^{ss}(\sigma_1) \\
& - \tfrac{1}{2}\left[\bar{J}_{\mathfrak{B}}^{-1}\bar{\tau}_2\right]^{\times}\left[\bar{J}_{\mathfrak{B}}^{-1}\bar{h}\right]^{\times}\delta_2^{ss}(\sigma)((\delta_1^{ss}(\sigma_1))^2 - (\delta_2^{ss}(\sigma_1))^2) \\
& - \tfrac{1}{2}\left[\bar{J}_{\mathfrak{B}}^{-1}\bar{h}\right]^{\times}\left[\bar{J}_{\mathfrak{B}}^{-1}\bar{\tau}_2\right]^{\times}((\delta_1^{ss}(\sigma))^2 - (\delta_2^{ss}(\sigma))^2)\delta_2^{ss}(\sigma_1) \\
& + \sum_{i=1}^{2}\sum_{j=1}^{2}\sum_{k=1}^{3} O(|\delta_i^{ss}(\sigma)|^3|\delta_j^{ss}(\sigma_1)|^k))d\sigma_1 d\sigma.
\end{aligned} \tag{3.99}$$

Note that (3.99) utilizes properties involving multiplication and integration of big "O" terms [78]. Using integration by parts and the skew symmetric matrix properties

(which may be found in [79]),

$$\begin{aligned}
[\bar{a}]^{\times}\left[\bar{b}\right]^{\times}-\left[\bar{b}\right]^{\times}[\bar{a}]^{\times}&=\left[\bar{a}\times\bar{b}\right]^{\times},\\
\left[\left(\bar{J}\bar{a}\right)\times\bar{J}\bar{b}\right]^{\times}&=\det\left[\bar{J}\right]\bar{J}^{-1}\left[\bar{a}\times\bar{b}\right]^{\times},
\end{aligned}\tag{3.100}$$

where $\bar{a}$ and $\bar{b}$ are arbitrary mathematical vectors, (3.99) reduces to

$$\begin{aligned}
\int_0^T\bar{A}(\sigma)\int_0^\sigma\bar{A}(\sigma_1)d\sigma_1d\sigma &= \left[\bar{J}_{\mathfrak{B}}(\bar{\tau}_1\times\bar{h})\right]^{\times}\alpha_2+\left[\bar{J}_{\mathfrak{B}}(\bar{\tau}_2\times\bar{h})\right]^{\times}\alpha_3+\left[\bar{J}_{\mathfrak{B}}(\bar{\tau}_1\times\bar{\tau}_2)\right]^{\times}\alpha_4\\
&\quad+\left[\int_0^T\int_0^\sigma\left(\sum_{i=1}^{2}\sum_{j=1}^{2}O(|\delta_i(\sigma)|^2|\delta_j(\sigma_1)|^2)\right)d\sigma_1d\sigma\right]^{\times}\\
&\quad+\left[\int_0^T\int_0^\sigma\left(\sum_{i=1}^{2}\sum_{j=1}^{2}\sum_{k=1}^{3}O(|\delta_i(\sigma)|^3|\delta_j(\sigma_1)|^k)\right)d\sigma_1d\sigma\right]^{\times},
\end{aligned}\tag{3.101}$$

where

$$\begin{aligned}
\alpha_2 &= \tfrac{\det\left[\bar{J}_{\mathfrak{B}}^{-1}\right]}{2}\int_0^T\int_0^\sigma\left\{((\delta_1^{ss}(\sigma))^2-(\delta_2^{ss}(\sigma))^2)\delta_1^{ss}(\sigma_1)\right\}d\sigma_1d\sigma,\\
\alpha_3 &= \tfrac{\det\left[\bar{J}_{\mathfrak{B}}^{-1}\right]}{2}\int_0^T\int_0^\sigma\left\{((\delta_1^{ss}(\sigma))^2-(\delta_2^{ss}(\sigma))^2)\delta_2^{ss}(\sigma_1)\right\}d\sigma_1d\sigma,\\
\alpha_4 &= \det\left[\bar{J}_{\mathfrak{B}}^{-1}\right]\int_0^T\int_0^\sigma\delta_1^{ss}(\sigma)\delta_2^{ss}(\sigma_1)d\sigma_1d\sigma.
\end{aligned}\tag{3.102}$$

Substituting (3.97) and (3.101) into (3.94), the state transition matrix for the underactuated spacecraft system with two CMGs over one periodic cycle is

$$\begin{aligned}
\bar{\Phi}(T,0) &= I_3+\left[\bar{J}_{\mathfrak{B}}^{-1}\bar{h}\right]^{\times}\alpha_1+[\bar{J}_{\mathfrak{B}}(\bar{\tau}_1\times\bar{h})]^{\times}\alpha_2+[\bar{J}_{\mathfrak{B}}(\bar{\tau}_2\times\bar{h})]^{\times}\alpha_3\\
&\quad+\left[\bar{J}_{\mathfrak{B}}(\bar{\tau}_1\times\bar{\tau}_2)\right]^{\times}\alpha_4+[E]^{\times}+...,
\end{aligned}\tag{3.103}$$

where

$$E = \int_0^T \sum_{j=1}^{2} O(|\delta_j^{ss}(\sigma)|^3)d\sigma + \int_0^T \int_0^\sigma \sum_{i=1}^{2}\sum_{j=1}^{2}\sum_{k=1}^{3} O(|\delta_i^{ss}(\sigma)|^3|\delta_j^{ss}(\sigma_1)|^k))d\sigma_1 d\sigma + \int_0^T \int_0^\sigma \sum_{i=1}^{2}\sum_{j=1}^{2} O(|\delta_{_i}(\sigma)|^2|\delta_{_j}(\sigma_1)|^2)d\sigma_1 d\sigma. \tag{3.104}$$

We now make the following assumption:

Assumption 3.4.5 The magnitude of the steady-state gimbal angles is small,

which can be guaranteed by an appropriate control input. Assumption 3.4.5 implies that $E \approx 0$. Furthermore, since the steady-state gimbal angles are small, integral terms of order three and higher in the Peano-Baker series can be neglected. Now recall that the matrix exponential for an arbitrary $m \times m$ matrix $\bar{D}$ is

$$\exp(\bar{D}) = I_m + \sum_{i=1}^{\infty} \frac{1}{i!}\bar{D}^i. \tag{3.105}$$

If second-order and higher order terms in $\bar{D}$ are small, the matrix exponential can be approximated by

$$\exp(\bar{D}) \approx I_m + \bar{D} \tag{3.106}$$

Thus, from Assumption 3.4.5, (3.96), (3.103), and (3.106), the orientation matrix $\mathbf{B}$ has the following approximate evolution over one periodic cycle T of gimbal angle movement,

$$\mathbf{B}(T) \approx \exp\left([\bar{w}_{_p}(T)]^\times\right)\mathbf{B}(0), \tag{3.107}$$

where

$$\bar{w}_{_p} = \bar{J}_{\mathfrak{B}}^{-1}\bar{h}\alpha_1 + \bar{J}_{\mathfrak{B}}(\bar{\tau}_{_1} \times \bar{h})\alpha_2 + \bar{J}_{\mathfrak{B}}(\bar{\tau}_{_2} \times \bar{h})\alpha_3 + \bar{J}_{\mathfrak{B}}(\bar{\tau}_{_1} \times \bar{\tau}_{_2})\alpha_4. \tag{3.108}$$

Note that we do not simply substitute (3.103) into (3.96). This is because if higher-

order terms are neglected, the multiplication of (3.103) by $\mathbf{B}(0)$ does not necessarily yield an orientation matrix. Therefore the matrix exponential is used to keep $\mathbf{B}(T)$ consistently on $SO(3)$.

Equation (3.107) represents an approximate eigenaxis maneuver, where the axis of rotation is given by $-\frac{\bar{w}_p}{||\bar{w}_p||}$ and the angle of rotation is given by $||\bar{w}_{_p}||$.

3.4.3 State Transition Matrix Under Sinusoidal Gimbal Angle Trajectories

Assume that the steady-state periodic trajectories $\delta_{_1}^{ss}$ and $\delta_{_2}^{ss}$ have the form

$$\begin{aligned} \delta_{_1}^{ss} &= a_1 \sin(nt) + b_1 \sin(2nt) + c_1 \sin(4nt), \\ \delta_{_2}^{ss} &= a_2 \sin(nt) + b_2 \sin(2nt) + c_2 \sin(4nt), \end{aligned} \tag{3.109}$$

where n is the frequency of excitation, i.e., $T = \frac{2\pi}{n}$, and $a_i, b_i, c_i,\ i = 1, 2$, are sinusoidal amplitudes (which will be chosen by the control law presented later in this section). Then the integrals (3.98) and (3.102) become

$$\int_0^T (\delta_{_1}^{ss}(\sigma))^2 - (\delta_{_2}^{ss}(\sigma))^2 d\sigma = \tfrac{\pi}{n}(a_1^2 + b_1^2 + c_1^2 - a_2^2 - b_2^2 - c_2^2), \tag{3.110}$$

$$\begin{aligned} \int_0^T \int_0^\sigma ((\delta_{_1}^{ss}(\sigma))^2 - (\delta_{_2}^{ss}(\sigma))^2)\delta_{_1}^{ss}(\sigma_1)\sigma_1 d\sigma = {} & \tfrac{\pi}{n^2}\left(a_1 + \tfrac{b_1}{2}\right)(a_1^2 + b_1^2 - a_2^2 - b_2^2) \\ & - \tfrac{3\pi}{4n^2} a_1^2 b_1 + \tfrac{\pi}{n^2} a_1 a_2 b_2 - \tfrac{\pi}{4n^2} a_2^2 b_1 \\ & - \tfrac{3\pi}{8n^2} b_1^2 c_1 + \tfrac{\pi}{2n^2} b_1 b_2 c_2 - \tfrac{\pi}{8n^2} b_2^2 c_1, \end{aligned} \tag{3.111}$$

$$\begin{aligned} \int_0^T \int_0^\sigma ((\delta_{_1}^{ss}(\sigma))^2 - (\delta_{_2}^{ss}(\sigma))^2)\delta_{_2}^{ss}(\sigma_1)\sigma_1 d\sigma = {} & \tfrac{\pi}{n^2}\left(a_2 + \tfrac{b_2}{2}\right)(a_1^2 + b_1^2 - a_2^2 - b_2^2) \\ & + \tfrac{3\pi}{4n^2} a_2^2 b_2 - \tfrac{\pi}{n^2} a_1 a_2 b_1 + \tfrac{\pi}{4n^2} a_1^2 b_2 \\ & + \tfrac{3\pi}{8n^2} b_2^2 c_2 - \tfrac{\pi}{2n^2} b_1 b_2 c_1 + \tfrac{\pi}{8n^2} b_1^2 c_2, \end{aligned} \tag{3.112}$$

$$\int_0^T \int_0^\sigma \delta_{_1}^{ss}(\sigma)\delta_{_2}^{ss}(\sigma_1)d\sigma_1 d\sigma = 0. \tag{3.113}$$

Let the following variables be defined

$$\begin{aligned}
\gamma_1 &= -\tfrac{\pi}{2n}, \\
\gamma_2 &= \tfrac{\pi \det\left[\bar{J}_{\mathfrak{B}}^{-1}\right]}{2n^2}, \\
\gamma_3 &= -\tfrac{\pi \det\left[\bar{J}_{\mathfrak{B}}^{-1}\right]}{2n^2}, \\
\beta_1 &= a_1^2 + b_1^2 - a_2^2 - b_2^2, \\
\beta_2 &= \left(a_1 + \tfrac{b_1}{2}\right)\left(a_1^2 + b_1^2 - a_2^2 - b_2^2\right) \\
&\quad -\tfrac{3}{4}a_1^2 b_1 + a_1 a_2 b_2 - \tfrac{1}{4}a_2^2 b_1 - \tfrac{3}{8}b_1^2 c_1 + \tfrac{1}{2}b_1 b_2 c_2 - \tfrac{1}{8}b_2^2 c_1, \\
\beta_3 &= \left(a_2 + \tfrac{b_2}{2}\right)\left(a_1^2 + b_1^2 - a_2^2 - b_2^2\right) \\
&\quad +\tfrac{3}{4}a_2^2 b_2 - a_1 a_2 b_1 + \tfrac{1}{4}a_1^2 b_2 + \tfrac{3}{8}b_2^2 c_2 - \tfrac{1}{2}b_1 b_2 c_1 + \tfrac{1}{8}b_1^2 c_2,
\end{aligned} \tag{3.114}$$

as well as the mathematical vectors

$$\begin{aligned}
\bar{g}_{_1} &= \bar{\tau}_{_1} \times \bar{h} = \left(J_{_{rs^1}}\eta_1\right)^2 \check{g}_{_1}, \\
\bar{g}_{_2} &= -\bar{\tau}_{_2} \times \bar{h} = -\left(J_{_{rs^2}}\eta_2\right)^2 \check{g}_{_2}.
\end{aligned} \tag{3.115}$$

Note that $\bar{g}_1$ and $\bar{g}_2$ lie along the first and second gimbal axes, respectively. Then using (3.110)-(3.115), (3.108) becomes

$$\bar{w}_p = \bar{N}[\ \beta_1 \quad \beta_2 \quad \beta_3\ ]^{\mathrm{T}}, \tag{3.116}$$

where $\bar{N} = [\ \gamma_1 \bar{J}_{\mathfrak{B}}^{-1}\bar{h} \quad \gamma_2 \bar{J}_{\mathfrak{B}}\bar{g}_1 \quad \gamma_3 \bar{J}_{\mathfrak{B}}\bar{g}_2\ ]$.

3.4.4 Control Law when CMG Gimbal Axes are Not Aligned

In designing a control law for an underactuated spacecraft with two CMGs, as in the thruster case and the RW case, we divide the system into base variables and fiber variables. In contrast to the thruster case or the RW actuation case, the base variables are chosen as the gimbal angles δ_1 and δ_2 whereas the fiber variable is chosen as the orientation matrix $\mathbf{B}$. If the gimbal angle trajectories are periodic with relatively small amplitude, then (3.107) implies that the attitude approximately evolves according to

$$\mathbf{B}((k+1)T) = \exp\left(\left[\bar{w}_p(T)\right]^{\times}\right)\mathbf{B}(kT), \tag{3.117}$$

where $\bar{w}_p$ is given by (3.116). To achieve the desired periodic gimbal angle movement, the following control law is used

$$\begin{aligned}
u_1(t) &= -k_1\delta_1(t) + a_1\sqrt{k_1^2+n^2}\sin(nt) + b_1\sqrt{k_1^2+4n^2}\sin(2nt) \\
&\quad + c_1\sqrt{k_1^2+16n^2}\sin(4nt), \\
u_2(t) &= -k_2\delta_2(t) + a_2\sqrt{k_2^2+n^2}\sin(nt) + b_2\sqrt{k_2^2+4n^2}\sin(2nt) \\
&\quad + c_2\sqrt{k_2^2+16n^2}\sin(4nt),
\end{aligned} \tag{3.118}$$

where $k_1, k_2 > 0$ are chosen such that the gimbal angles reach their steady-state trajectories sufficiently fast while keeping the transients small to satisfy Assumption 3.4.5. Then, if by using the proper choice of sinusoidal amplitudes we can obtain any $\bar{w}_{_p}$ in an open neighborhood of the origin, i.e., $0 \in \mathbb{R}^3$, a controlled drift can be induced that guides the attitude towards the desired pointing configuration $\mathbf{B} = I_3$.

At this point we make the following assumption on gimbal axes:

Assumption 3.4.6 The gimbal axes are not aligned,

which gives rise to the following Lemma:

Lemma 3.4.1: Let the gimbal axes $\check{g}_{_1}$ and $\check{g}_{_2}$ be non-parallel. Then the matrix $\bar{N}$ defined in (3.116) is nonsingular.

Proof: For the matrix $\bar{N}$ to be nonsingular, its columns must be nonzero and linearly independent. Already the columns are nonzero. The dot product of the first and second column of $\bar{N}$ gives

$$\begin{aligned} (\gamma_1 \bar{J}^{-1}\bar{h})^{\mathrm{T}}\gamma_2 \bar{J}_{\mathfrak{B}}\bar{g}_{_1} &= \gamma_1\gamma_2 \bar{h}^{\mathrm{T}}\bar{J}_{\mathfrak{B}}^{-1}\bar{J}_{\mathfrak{B}}\bar{g}_{_1}, \\ &= \gamma_1\gamma_2 \bar{h}^{\mathrm{T}}\bar{g}_{_1}. \end{aligned} \tag{3.119}$$

Recall that $\bar{h}$ is in the direction of the angular momentum vector while $\bar{g}_{_1}$ is in the direction of the 1st gimbal axis. By the construction of the CMG, these two vectors are orthogonal, and thus the first two columns are linearly independent. A similar procedure can be used to show that $\bar{h}$ and $\bar{g}_{_2}$ are linearly independent. Finally, if $\check{g}_{_1}$ and $\check{g}_{_2}$ are non-parallel, then $\bar{g}_{_1}$ and $\bar{g}_{_2}$ are non-parallel, and the second and third columns of $\bar{N}$ are linearly independent. Therefore, all three columns are independent from one another, and $\bar{N}$ is nonsingular. $\square$

With $\bar{N}$ being nonsingular, the only requirement to achieve any $\bar{w}_{_p}$ in a neighborhood of the origin is that the mapping from $a_i, b_i, c_i,\ i = 1, 2$, to $\beta_1, \beta_2, \beta_3$, must be open at $a_1 = a_2 = b_1 = b_2 = c_1 = c_2 = 0$. While no theorem is given in this chapter,

numerous tests via a numerical solver using a Levenberg-Marquardt method suggest that the map is indeed open. The in-depth analysis of this property for the CMG case is left to future work.

Remark 3.4.1: When the gimbal axes are aligned, $\bar{N}$ becomes singular and the switching scheme described in this section cannot be utilized. This configuration of CMGs is more difficult to handle when the spacecraft has zero angular momentum, as currently no claims can be made on STLC. A control law handling this situation is left to future work.

We now present a switching feedback law to stabilize a spacecraft equipped with only two skew CMGs (the explanation of the algorithm is given after):

Algorithm 3: Control Computation for CMGs

Given:

The current attitude $\mathbf{B}$, $d_{max} > 0$

for $k > 0$ **do**

1. Set $\mu = 1$.
2. Compute the rotation vector $\bar{w}_p$ such that $\exp\left(\left[\bar{w}_p\right]^{\times}\right) = \mathbf{B}^{\mathrm{T}}(kT)$.
3. Compute $a_1,\ a_2,\ b_1,\ b_2,\ c_1,\ c_2$ such that $[\ \beta_1\ \beta_2\ \beta_3\ ]^{\mathrm{T}} = \bar{N}^{-1}\bar{w}_p$.

if $\max\{|a_i|, |b_i|, |c_i|, i = 1, 2\} > d_{max}$ **then**

$\mu = \mu + 1$.

$\bar{w}_p = \frac{\bar{w}_p}{\mu}$ and go back to Step 3.

end if

end for

Control at Cycle k**:**

$$u_1(t) = -k_1\delta_1(t) + a_1\sqrt{k_1^2 + n^2}\sin(nt)$$

$$+b_1\sqrt{k_1^2 + 4n^2}\sin(2nt) + c_1\sqrt{k_1^2 + 16n^2}\sin(4nt) \text{ for } t \in [kT, (k+1)T)$$

$$u_2(t) = -k_2\delta_2(t) + a_2\sqrt{k_2^2 + n^2}\sin(nt)$$

$$+b_2\sqrt{k_2^2 + 4n^2}\sin(2nt) + c_2\sqrt{k_2^2 + 16n^2}\sin(4nt) \text{ for } t \in [kT, (k+1)T)$$

The intuition behind the algorithm is the following; at the beginning of each cycle, the amplitudes of the sinusoids $a_i, b_i, c_i,\ i = 1, 2$ are chosen to induce a change in the kinematics that will approximately guide the system towards $\mathbf{B} = I_3$, the desired orientation. If the magnitude of a_i, b_i, or c_i, for $i = 1, 2$, exceeds that of the constant value d_{max}, the rotation vector $\bar{w}_p$ is reduced by a factor of μ (which grows larger when

a solution cannot be found). The value d_{max} is chosen so the gimbal rates and gimbal angles are kept small, thus satisfying Assumption 3.4.5. In the simulation section below, $a_i, b_i, c_i,\ i = 1, 2$, are computed by a numerical solver using a Levenberg-Marquardt method since the mapping between $a_i, b_i, c_i,\ i = 1, 2$, and $\beta_1, \beta_2, \beta_3$ is highly nonlinear. No convergence proofs are given in this chapter for this switching controller, but numerical simulations on the full nonlinear model (3.87) demonstrate successful stabilization to the desired attitude.

3.4.5 Simulation Results

To validate the switching scheme, we consider a spacecraft bus with the principal moments of inertia of 100, 200, and 250 kg m^2. The gimbal axes are given by

$$\check{g}_1 = \begin{bmatrix} 0 \\ \cos\left(\frac{\pi}{6}\right) \\ \sin\left(\frac{\pi}{6}\right) \end{bmatrix}, \quad \check{g}_2 = \begin{bmatrix} 0 \\ -\cos\left(\frac{\pi}{6}\right) \\ \sin\left(\frac{\pi}{6}\right) \end{bmatrix}. \tag{3.120}$$

The angular momentum contribution due to each spinning rotor is $J_{r_{sj}}\eta_j = 15$ kg m^2 sec^{-1}, $\ j = 1, 2$. For the feedback law (3.118), the constants that yield the steady-state base dynamics in (3.109) are $k_1 = k_2 = 2$. The sinusoidal excitation is applied at a frequency of $n = 0.01$ sec^{-1}. The constant d_{max} is set to 0.5 in order to keep sinusoidal gimbal movement relatively small. All simulations are run on the nonlinear model (3.87).

In Figures 3.8 and 3.9, two at-rest, underactuated attitude maneuvers are performed (thus satisfying the assumption that total angular momentum of the system must be zero). Figure 3.8 shows a small angle maneuver corresponding to the initial 3-2-1 Euler angle sequence $\phi(0) = 0.0873$ rad (5 deg), $\theta(0) = -0.0873$ rad (-5 deg), $\psi(0) = -0.0524$ rad (-3 deg), with $\delta_1(0) = \delta_2(0) = 0$ rad. In the second simulation, the attitude maneuver is much larger, corresponding to an initial 3-2-1 Euler sequence

of $\phi(0) = -0.3491$ rad (20 deg), $\theta(0) = 0.7854$ rad (45 deg), $\psi(0) = -0.1745$ rad (-10 deg), with gimbal angles $\delta_1(0) = \delta_2(0) = 0$ rad. In both simulations, the attitude error goes to zero (shown in Figures 3.8 (a) and 3.9 (a)). It should be noted that though there are spikes in the attitude error, there is an overall decrease in the change over each sample period $T = \frac{2\pi}{n} = 0.17$ hours.

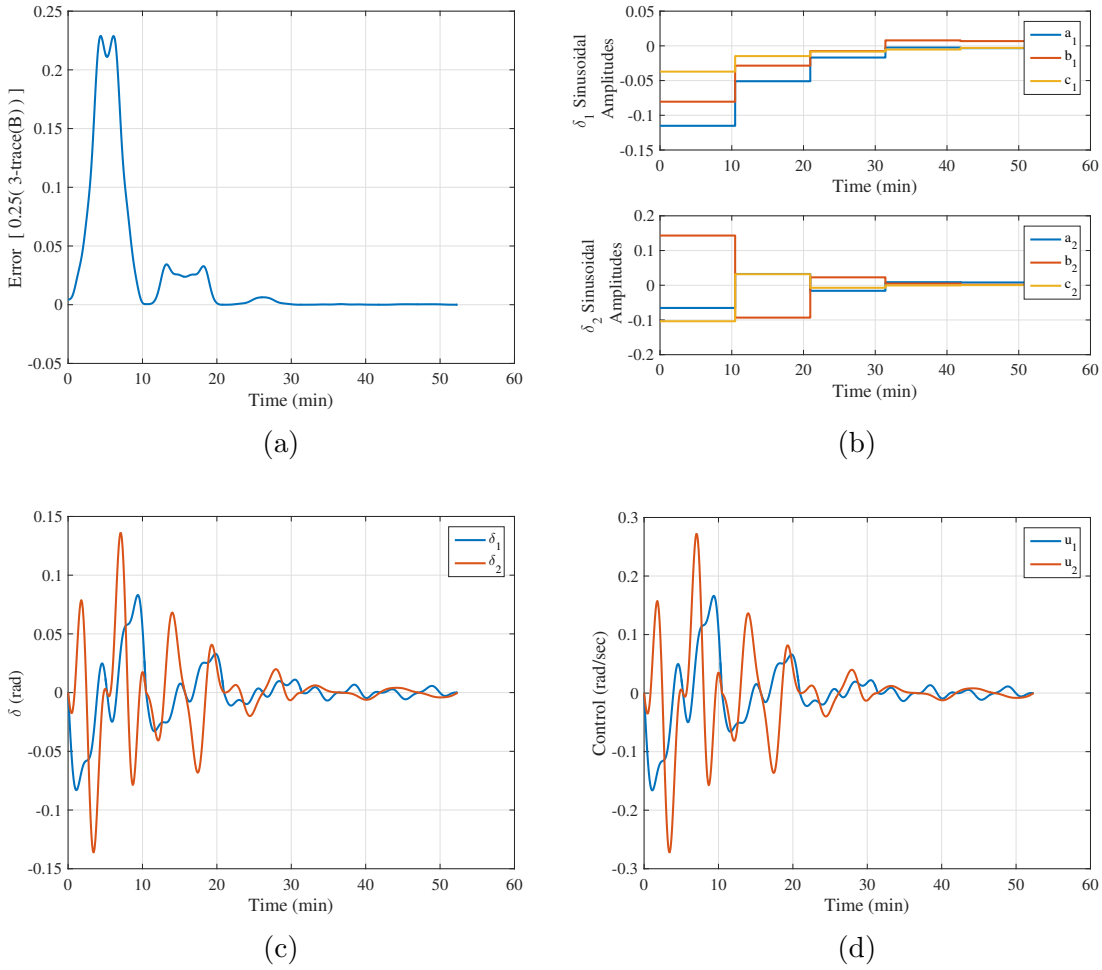

Figure 3.8: Small attitude maneuver for an underactuated spacecraft with two skew CMGs (a) $SO(3)$ error, (b) sinusoidal amplitudes, (c) gimbal angles, (d) gimbal rates.

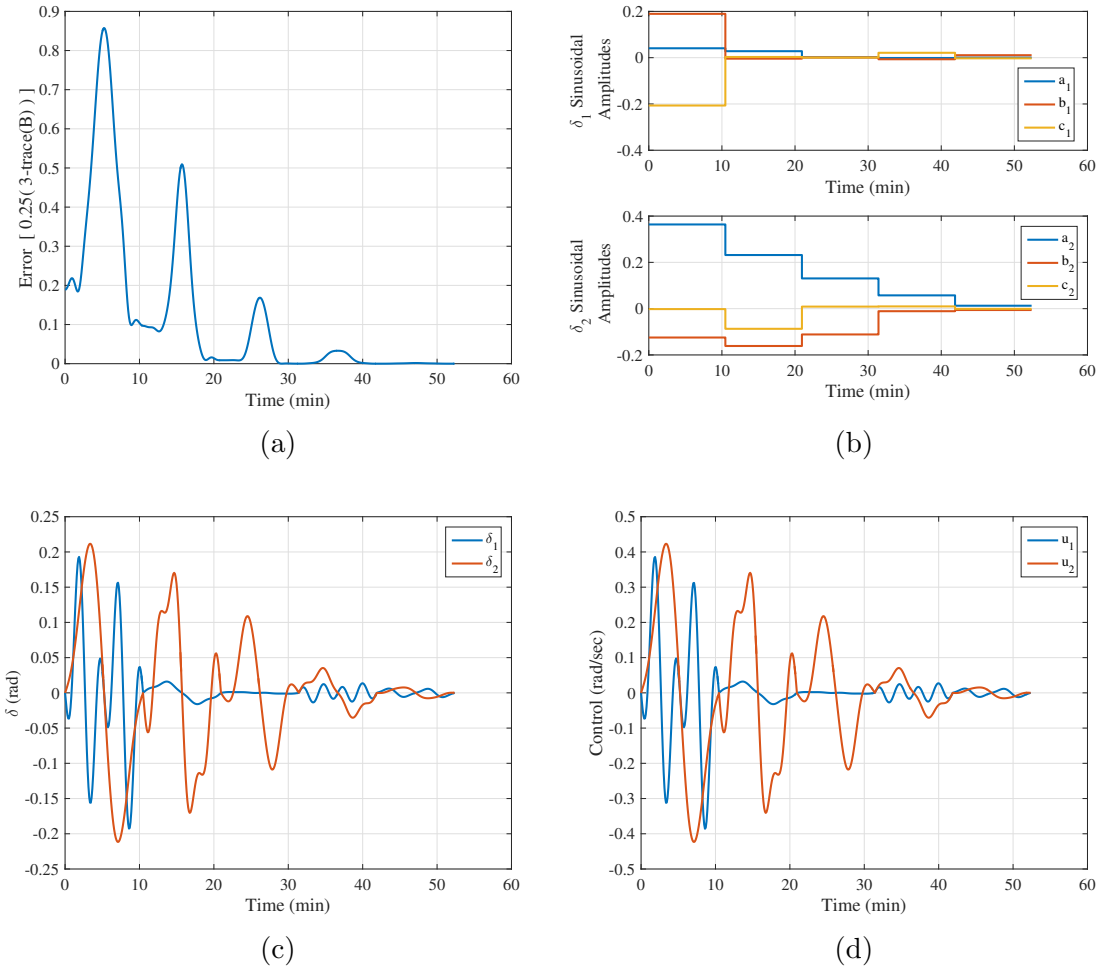

Figure 3.9: Large attitude maneuver for an underactuated spacecraft with two skew CMGs (a) $SO(3)$ error, (b) sinusoidal amplitudes, (c) gimbal angles, (d) gimbal rates.

CHAPTER 4

Underactuated Attitude Control Using Model Predictive Control

4.1 Introduction

MPC is a popular control technique due to its ability to generate feedback controllers that enforce specified constraints. Its application to the spacecraft attitude control problem began in the mid 1990's with [80] and [81]. In [80], attitude tracking was performed using a one-step ahead prediction of the states. On the other hand, [81] used a function-space MPC approach to track a reference attitude, and differs from standard MPC as it does not recompute the optimization solution at every discrete-time step. Since then, the topic of MPC for spacecraft attitude has been approached in numerous other publications. In [82], a spacecraft with multiple thrusters and one RW is controlled by using explicit MPC. Reference [83] develops an MPC controller that acts on the manifold $SO(3)$ in order to avoid mappings with singularities (such as Euler angles) and mappings that involve double covering (such as quaternions). Robust MPC for attitude control was discussed in [84, 85]. MPC laws developed specifically for the case of CMG and magnetic torque actuation are presented in [86] and [87,88], respectively. An MPC algorithm suitable for fixed-point implementation is applied to spacecraft attitude control with RWs in [89].

The existing references on applications of MPC have not, however, addressed the

case of a spacecraft that is underactuated by design or that becomes underactuated as a result of onboard failures. It was shown in [41, 42, 90] that MPC has the remarkable ability to generate a stabilizing feedback law that is discontinuous as a function of the state. Thus the obstruction to stabilization, which is a consequence of violating Brockett's condition, can be overcome. The use of MPC has several other advantages over other discontinuous feedback stabilization approaches in the literature: The design process is systematic, state and control constraints are handled, and a cost function reflecting performance objectives is optimized in a receding horizon sense.

This chapter addresses the following issues for an underactuated spacecraft problem with two RWs and zero angular momentum:

- The introduction and analysis of a nonlinear MPC controller for the underactuated spacecraft problem, including showing that the control law generated using the reduced, approximate dynamics is stabilizing. We also prove that the control law must be a nonsmooth function of the state and our numerical results indicate that the control law is actually a discontinuous function of the state.

- The implementation of the nonlinear MPC controller on the full nonlinear, underactuated spacecraft model, with discussion on real-time implementation of the controller.

The fact that MPC generates a feedback law that is discontinuous in the state is interesting because stabilizing, continuous, time-invariant feedback laws do not exist. Note that in other problems, the MPC feedback law is typically continuous in the state. For example, in LQ type MPC the control law is typically piecewise affine and continuous [91].

4.2 Spacecraft Configuration & Equations of Motion

In this chapter, we consider an underactuated spacecraft equipped with two RWs under the following assumptions:

Assumption 4.1 There are no external moments acting on the spacecraft system.

Assumption 4.2 The maneuvers being performed involve relatively small attitude adjustments near the desired pointing orientation.

Assumption 4.3 The total angular momentum of the system is zero.

By Assumption 4.1, inertial angular momentum is conserved, and by Assumption 4.2, singularity problems due to Euler angle representations are avoided. Therefore the RAE's in (2.53) can be used to model the spacecraft system. From Assumptions 4.1, 4.2, and 4.3, (2.53) becomes

$$\begin{aligned} \dot{\bar{\Theta}} &= -\bar{M}(\bar{\Theta})\bar{J}^{-1}\bar{W}\bar{\nu}, \\ \dot{\bar{\nu}} &= \bar{u}, \end{aligned} \tag{4.1}$$

where

$$\begin{aligned} \bar{W} &= [\ J_{ws1}\check{w}_1 \quad J_{ws2}\check{w}_2\ ], \\ \bar{\nu} &= [\ \nu_1 \quad \nu_2\ ]^{\mathrm{T}}, \\ \bar{u} &= [\ u_1 \quad u_2\ ]^{\mathrm{T}} = [\ \nu_1 \quad \nu_2\ ]^{\mathrm{T}}, \\ \bar{J} &= \bar{J}_{\mathfrak{B}} + \sum_{i=1}^{2} \bar{J}_{\mathfrak{W}_i}. \end{aligned} \tag{4.2}$$

We now make the additional assumption on the RW configuration:

Assumption 4.4 The RW spin axes are linearly independent and are orthogonal to $\hat{b}_z$, the unit axis aligned with the z direction in the spacecraft bus fixed frame $\mathcal{B}$.

Thus again, the uncontrollable axis is parallel to ω_3, isolating ψ as the uncontrollable angle. If $-\bar{J}^{-1}\bar{W} = \tilde{W}$, then $\tilde{W}$ can be written as

$$\tilde{W} = \begin{bmatrix} \alpha_1 & \alpha_2 \\ \beta_1 & \beta_2 \\ 0 & 0 \end{bmatrix}, \tag{4.3}$$

where $\alpha_1, \alpha_2, \beta_1, \beta_2 \in \mathbb{R}$. Substituting (4.3) into (4.1) yields

$$\begin{aligned} \dot{\phi} &= (\alpha_1\nu_1 + \alpha_2\nu_2) + (\beta_1\nu_1 + \beta_2\nu_2)\sin(\phi)\tan(\theta), \\ \dot{\theta} &= (\beta_1\nu_1 + \beta_2\nu_2)\cos(\phi), \\ \dot{\psi} &= (\beta_1\nu_1 + \beta_2\nu_2)\sin(\phi)\sec(\theta), \\ \dot{\nu}_1 &= u_1, \\ \dot{\nu}_2 &= u_2. \end{aligned} \tag{4.4}$$

We note that any equilibrium of (4.4) must be unforced, i.e., $u_1 = u_2 = 0$. Furthermore, since $\bar{M}(\bar{\Theta})$ is invertible, $\nu_1 = \nu_2 = 0$ at an equilibrium. Thus all attitudes with zero RW velocity are equilibria of (4.4).

4.2.1 Approximation of the Equations of Motion

To simplify controller design, the dynamics in (4.4) are approximated by a set of equations that do not contain any trigonometric functions. This is done by first expanding the trigonometric functions in (4.4) by a Taylor-series about $\phi = \theta = \psi = 0$, yielding

$$\dot{\phi} = (\alpha_1\nu_1 + \alpha_2\nu_2) + (\beta_1\nu_1 + \beta_2\nu_2)(\phi - \tfrac{1}{6}\phi^3 + \tfrac{1}{120}\phi^5 + ...)(\theta + \tfrac{1}{3}\theta^3 + \tfrac{2}{15}\theta^5 + ...),$$

$$\dot{\theta} = (\beta_1\nu_1 + \beta_2\nu_2)(1 - \tfrac{1}{2}\phi^2 + \tfrac{1}{24}\phi^4 + ...),$$

$$\dot{\psi} = (\beta_1\nu_1 + \beta_2\nu_2)(\phi - \tfrac{1}{6}\phi^3 + \tfrac{1}{120}\phi^5 + ...)(1 + \tfrac{1}{2}\theta^2 + \tfrac{5}{24}\theta^4 + ...),$$

$$\dot{\nu}_1 = u_1,$$

$$\dot{\nu}_2 = u_2. \tag{4.5}$$

The equations (4.5) can be compactly written as

$$\dot{\phi} = (\alpha_1\nu_1 + \alpha_2\nu_2) + O(||\bar{\Theta}(t)||^2),$$

$$\dot{\theta} = (\beta_1\nu_1 + \beta_2\nu_2) + O(||\bar{\Theta}(t)||^2),$$

$$\dot{\psi} = (\beta_1\nu_1 + \beta_2\nu_2)\phi + O(||\bar{\Theta}(t)||^2), \tag{4.6}$$

$$\dot{\nu}_1 = u_1,$$

$$\dot{\nu}_2 = u_2,$$

where $O(||\bar{\Theta}(t)||^2)$ denotes the remaining terms, which are higher order in Euler angles. Since the desired attitude maneuvers being performed are small, in a neighborhood of the desired pointing equilibrium $\bar{\Theta} = 0$, (4.4) can be approximated based on (4.6) by

$$\begin{aligned}
\dot{\phi} &= (\alpha_1\nu_1 + \alpha_2\nu_2), \\
\dot{\theta} &= (\beta_1\nu_1 + \beta_2\nu_2), \\
\dot{\psi} &= (\beta_1\nu_1 + \beta_2\nu_2)\phi, \\
\dot{\nu}_1 &= u_1, \\
\dot{\nu}_2 &= u_2.
\end{aligned} \tag{4.7}$$

Remark 4.1: When $\alpha_1 = \beta_2 = 1$ and $\alpha_2 = \beta_1 = 0$, the model (4.7) is essentially the same as the exact, transformed equations of motion of the underactuated spacecraft with zero angular momentum given in [7]. This implies that the MPC law presented in this paper can stabilize also the transformed dynamics of [7], and hence the actual spacecraft's attitude. The advantage to using the transformed dynamics is that errors due to approximations like small angles are nonexistent. In this chapter, the development of an MPC controller is based on (4.7), and the transformation is not used in order to preserve the physical meaning and intuitive sense of state and control variables, which, for instance, facilitates the imposition of constraints. The controller is validated in simulations using the exact model based on (2.3), (2.41), and (2.44).

Remark 4.2: The reduced, simplified, continuous dynamics in (4.7) are closely related to nonholonomic problems that have been studied in [92]. While this paper only considers and focuses on the application of nonlinear MPC to the underactuated

spacecraft problem, the results may be extended to stabilize other systems with similar characteristics. We leave such extensions to future work.

4.2.2 Discretization

In order to implement MPC, a discrete-time prediction model is needed. We assume that the control input is generated by a zero-order hold with a sampling period T, so that

$$\begin{aligned} u_1(t) &= u_{1,k}, \quad \forall t \in [kT, (k+1)T), \\ u_2(t) &= u_{2,k}, \quad \forall t \in [kT, (k+1)T), \end{aligned} \tag{4.8}$$

where k is a positive integer. In addition, we adopt the following notations,

$$\begin{aligned} &\phi_k = \phi(kT), \quad \theta_k = \theta(kT), \quad \psi_k = \psi(kT), \quad \nu_{1,k} = \nu_1(kT), \quad \nu_{2,k} = \nu_2(kT), \\ &x_k = [\ \phi_k \ \ \theta_k \ \ \psi_k \ \ \nu_{1,k} \ \ \nu_{2,k}\ ]^{\mathrm{T}}. \end{aligned} \tag{4.9}$$

The discrete-time dynamics for RW velocities are determined by integrating the last two equations of (4.6), yielding

$$\begin{aligned} \nu_{1,k+1} &= \nu_{1,k} + u_{1,k}T, \\ \nu_{2,k+1} &= \nu_{2,k} + u_{2,k}T. \end{aligned} \tag{4.10}$$

Based on (4.7), the approximate discrete dynamics for Euler angles ϕ and θ can be determined similarly as

$$\begin{aligned} \phi_{k+1} &= \phi_k + (\alpha_1\nu_{1,k} + \alpha_2\nu_{2,k})\,T + (\alpha_1 u_{1,k} + \alpha_2 u_{2,k})\,\tfrac{T^2}{2}, \\ \theta_{k+1} &= \theta_k + (\beta_1\nu_{1,k} + \beta_2\nu_{2,k})\,T + (\beta_1 u_{1,k} + \beta_2 u_{2,k})\,\tfrac{T^2}{2}. \end{aligned} \tag{4.11}$$

In order to determine the approximate discrete dynamics for ψ, the equation

$$\begin{aligned}\dot{\psi} = &(\phi_k + (\alpha_1\nu_{1,k} + \alpha_2\nu_{2,k})\,t + (\alpha_1 u_{1,k} + \alpha_2 u_{2,k})\,\tfrac{t^2}{2})(\beta_1(\nu_{1,k} + u_{1,k}t)) \\ &+(\phi_k + (\alpha_1\nu_{1,k} + \alpha_2\nu_{2,k})\,t + (\alpha_1 u_{1,k} + \alpha_2 u_{2,k})\,\tfrac{t^2}{2})(\beta_2(\nu_{2,k} + u_{2,k}t))\end{aligned} \tag{4.12}$$

must be integrated over the sampling period T, where (4.12) is obtained from substituting (4.10) and (4.11) into the kinematic equation for ψ in (4.7). Integrating (4.12) and collecting (4.10) and (4.11) gives the full set of approximate discrete dynamics

$$\begin{aligned}
\phi_{k+1} &= \phi_k + (\alpha_1\nu_{1,k} + \alpha_2\nu_{2,k})\,T + (\alpha_1 u_{1,k} + \alpha_2 u_{2,k})\,\tfrac{T^2}{2}, \\
\theta_{k+1} &= \theta_k + (\beta_1\nu_{1,k} + \beta_2\nu_{2,k})\,T + (\beta_1 u_{1,k} + \beta_2 u_{2,k})\,\tfrac{T^2}{2}, \\
\psi_{k+1} &= \psi_k + \phi_k(\beta_1\nu_{1,k} + \beta_2\nu_{2,k})T \\
&\quad +(\beta_1\phi_k u_{1,k} + \beta_2\phi_k u_{2,k} + \alpha_1\beta_1\nu_{1,k}^2 + \alpha_2\beta_2\nu_{2,k}^2 + \alpha_1\beta_2\nu_{1,k}\nu_{2,k} + \alpha_2\beta_1\nu_{1,k}\nu_{2,k})\tfrac{T^2}{2} \\
&\quad +(3\alpha_1\beta_1\nu_{1,k}u_{1,k} + 3\alpha_2\beta_2\nu_{2,k}u_{2,k} + 2\alpha_1\beta_2\nu_{1,k}u_{2,k} + 2\alpha_2\beta_1\nu_{2,k}u_{1,k})\tfrac{T^3}{6} \\
&\quad +(\alpha_1\beta_2\nu_{2,k}u_{1,k} + \alpha_2\beta_1\nu_{1,k}u_{2,k})\tfrac{T^3}{6} \\
&\quad +(\alpha_1\beta_1 u_{1,k}^2 + \alpha_2\beta_2 u_{2,k}^2 + \alpha_1\beta_2 u_{1,k}u_{2,k} + \alpha_2\beta_1 u_{1,k}u_{2,k})\tfrac{T^4}{8}, \\
\nu_{1,k+1} &= \nu_{1,k} + u_{1,k}T, \\
\nu_{2,k+1} &= \nu_{2,k} + u_{2,k}T.
\end{aligned} \tag{4.13}$$

Thus under the assumption that all attitude maneuvers are relatively small, the discrete dynamics in (4.13) approximate the actual discrete dynamics of the underactuated spacecraft system. We note that the approximate model (4.13) is nonlinear. The use of a nonlinear prediction model rather than linearized model is essential to be able to achieve discontinuous stabilization with MPC. This is due to the fact that the linearized model is not controllable and thus a linear controller cannot be designed for this problem. In contrast, the simplified nonlinear model is locally controllable and stabilizable, which is discussed in the next section.

4.3 Controllability and Stabilizability Analysis

In this section, controllability and stabilizability properties of the approximate dynamics, given by the continuous-time equations (4.7) and the discrete-time equations (4.13), are analyzed and compared with the properties of the actual nonlinear dynamics (4.4). This analysis indicates that (4.7) retains similar local controllability properties to (4.4) which are necessary to be able to use (4.7) as a basis for control design for an underactuated spacecraft. Controllability and stabilizability properties of the discrete-time system (4.13) will subsequently be needed to demonstrate closed-loop stability with MPC.

4.3.1 Controllability Analysis

The definition of STLC, as given by [2], is the following:

> **Definition 4.1 [2]:** A system $\dot{\bar{x}} = f(\bar{x}, \bar{u})$ is small-time locally controllable (STLC) from $\bar{x}_0$ if there exists a time $T > 0$ such that $\bar{x}_0$ for all time instants $t > 0$, $t \leq T$ is in the interior of the reachable set from x_0, $R(\bar{x}_0, t)$, at time instant t.

Intuitively if $\bar{x}_0$ is STLC, the reachable set from $\bar{x}_0$ will remain an open neighborhood

of $\bar{x}_0$ as time becomes infinitesimally small. In [7], the exact, reduced, underactuated attitude equations are proven STLC from any at-rest attitude. This property also holds for (4.4) (the proof of which is given in Appendix A). It is now demonstrated by Theorem 4.1 that the approximate, continuous-time dynamics in (4.7) remain STLC from any equilibrium. The proof of the theorem utilizes the concept of Lie brackets, which are reviewed in Appendix A.

Theorem 4.1: The approximate, underactuated spacecraft attitude equations (4.7) are STLC from all equilibria.

Proof: Let $\bar{x} = [\ \phi \ \ \theta \ \ \psi \ \ \nu_1 \ \ \nu_2\ ]^{\mathrm{T}}$. The drift vector field and the control vector fields of (4.7) are then given by

$$f_0 = [\ \alpha_1\nu_1 + \alpha_2\nu_2 \ \ \beta_1\nu_1 + \beta_2\nu_2 \ \ (\beta_1\nu_1 + \beta_2\nu_2)\phi \ \ 0 \ \ 0\ ]^{\mathrm{T}},$$

$$f_1 = [\ 0 \ \ 0 \ \ 0 \ \ 1 \ \ 0\ ]^{\mathrm{T}}, \tag{4.14}$$

$$f_2 = [\ 0 \ \ 0 \ \ 0 \ \ 0 \ \ 1\ ]^{\mathrm{T}}.$$

Using (A.2) from Appendix A, three Lie brackets are generated

$$B_1 = [\ f_1, \ \ f_0\ ] = [\ \alpha_1 \ \ \beta_1 \ \ \beta_1\phi \ \ 0 \ \ 0\ ]^{\mathrm{T}}, \tag{4.15}$$

$$B_2 = [\ f_2, \ \ f_0\ ] = [\ \alpha_2 \ \ \beta_2 \ \ \beta_2\phi \ \ 0 \ \ 0\ ]^{\mathrm{T}}, \tag{4.16}$$

$$B_3 = [\ B_1, \ \ B_2\ ] = [\ 0 \ \ 0 \ \ (\alpha_1\beta_2 - \alpha_2\beta_1) \ \ 0 \ \ 0\ ]^{\mathrm{T}}. \tag{4.17}$$

Note the following:

i. The top two entries of B_1 and B_2 are equivalent to the top two entries of the 1st and 2nd columns of $\tilde{W}$, respectively. Since the columns of $\tilde{W}$ are linearly independent (which consequently results in $\alpha_1 \neq \alpha_2$ and $\beta_1 \neq \beta_2$), B_1 and B_2

are linearly independent for all ϕ.

ii. The top three entries of B_3 are equivalent to the cross product of the columns of $\tilde{W}$. Since the columns of $\tilde{W}$ are linearly independent, B_3 is nonzero.

From the above, it can be seen that the vector fields f_1, f_2, B_1, B_2, B_3, when evaluated at any equilibrium (i.e., any orientation with zero RW velocity), span $\mathbb{R}^5$. By Theorem A1 in Appendix A, (4.7) is accessible from any equilibrium.

Now note that bracket B_3 has a 1-degree of 4, the largest out of this set of brackets. The only bad brackets that can be generated by f_0, f_1, f_2 with 1-degree less than 4 are $[\, f_1,\ \ B_1\,]$ and $[\, f_2,\ \ B_2\,]$, both of which have a 1-degree of 3 (other bad brackets of 1-degree of 3 can be written as linear combinations of these two due to the symmetric properties of the brackets themselves, see [93]). These brackets are zero and thus can be constructed trivially with good brackets of 1-degree of 1 or 2. From Theorem A2 in Appendix A, the system is STLC from all equilibria. □

The above analysis demonstrates that the approximate dynamics of (4.7) retain the STLC property of the actual nonlinear dynamics (4.4). Thus, even though the system is approximate, its nonlinear dynamics can be exploited by control designs that depend on local controllability properties.

Remark 4.3: Consider now the discrete-time system (4.13). We note that there are accessibility properties that can be obtained for discrete-time systems through the use of Lie brackets [94, 95], but currently there is no Lie bracket analysis that can demonstrate nonlinear, local controllability properties for discrete-time that are similar to that of STLC in continuous-time. Hence we present a direct construction of a control input which demonstrates the needed local controllability property in discrete-time in Appendix B. The open-loop control sequence that we construct brings any at-rest equilibrium of (4.13) to any state in six-steps, regardless of sample time. Thus the reachable set from any attitude equilibrium in six steps is an open neighborhood. Moreover the elements of the control sequence depend continuously on

the initial state, a property that will be used in the proof of the closed-loop stability of the MPC controller.

4.3.2 Stabilizability Analysis

As stated previously, the actual continuous-time attitude dynamics cannot be stabilized by any smooth or continuous, time-invariant feedback law due to Brockett's condition. This was proven in [7] and can be similarly shown for (4.4). To show that this obstruction to stabilization is still retained by (4.13) (the exact discretization of the reduced, approximate continuous-time dynamics in (4.7)) the following discrete-time variant of Brockett's condition from [96] is used.

Lemma 4.1: **[96]** Consider a discrete-time nonlinear control system governed by

$$\bar{x}_{k+1} = F_d(\bar{x}_k, \bar{u}_k), \tag{4.18}$$

with $F_d(0,0) = 0$ and F_d being smooth (i.e., C^∞) in a neighborhood of $(0,0)$. A necessary condition for the existence of a smooth state feedback control law $\bar{u}_k = \bar{u}(\bar{x}_k)$ which renders $(0,0)$ locally asymptotically stable is that the mapping $\bar{\Phi} : (\bar{x}, \bar{u}) \rightarrow \bar{x} - F_d(\bar{x}, \bar{u})$ be onto in an open neighborhood of the origin. $\square$

Lemma 4.1 is now used to prove the result of Theorem 4.2.

Theorem 4.2: There does not exist a smooth state feedback law that locally asymptotically stabilizes the discrete-time dynamics in (4.13) to the origin.

Proof: If the map $\bar{\Phi}$ is open, the equation

$$\bar{z} = \bar{x} - F_d(\bar{x}, \bar{u}), \tag{4.19}$$

is solvable for all $\bar{z}$ sufficiently small. Let F_d represent the discrete dynamics in (4.13) and $\bar{z} = [\ 0 \quad 0 \quad z \quad 0 \quad 0\ ]^{\mathrm{T}}$ for $z \in \mathbb{R}$. For (4.19) to be satisfied, u_1, u_2, ν_1, and ν_2 must be zero, which results in $\bar{x} - F_d(\bar{x}, \bar{u}) = 0$. Given that $\tilde{W}$ in (4.3) is rank 2,

(4.19) is not solvable for all $|z| > 0$ and implies that the mapping $\bar{\Phi}$ is not open. The conclusion of the theorem follows from Lemma 4.1. $\square$

Theorem 4.2 demonstrates that even though the dynamics are approximated and discretized, the obstruction to stabilizability present in (4.4) is retained by (4.13). However, since the approximate nonlinear system is locally controllable, a discontinuous feedback law to stabilize the system to the desired equilibrium can be generated using MPC techniques.

4.4 Model Predictive Control

Model Predictive Control optimizes a control sequence over a finite horizon into the future to minimize a specified cost function subject to constraints [97]. Then, the first element of the optimal sequence is applied over the first discrete time interval. The optimization horizon afterwards recedes by one step and the process is repeated starting with the current state as the initial condition.

Subsequently, we consider an MPC objective function for the underactuated spacecraft attitude control problem of the form

$$J_N(\bar{x}_0, u_{1,0}, ..., u_{1,N-1}, u_{2,0}, ..., u_{2,N-1}) = \sum_{i=0}^{N-1} L(\bar{x}_i, [u_{1,i}, u_{2,i}]^{\mathrm{T}}), \tag{4.20}$$

where N is the optimization horizon, $L(\bar{x}, [u_1, u_2]^{\mathrm{T}})$ is the incremental cost function given by

$$L(\bar{x}, [u_1, u_2]^{\mathrm{T}}) = \bar{x}^{\mathrm{T}} \bar{Q} \bar{x} + r_1 u_1^2 + r_2 u_2^2, \tag{4.21}$$

and where $\bar{Q} = \bar{Q}^{\mathrm{T}} > 0$ and $r_1, r_2 > 0$. The optimal control problem is given by

$$\min_{u_{i,j},\ i=1,2,\ j=0,1,...,N-1} J_N(\bar{x}_0, u_{1,0}, ..., u_{1,N-1}, u_{2,0}, ..., u_{2,N-1}), \tag{4.22}$$

subject to

$$\begin{gathered}\bar{x}_{k+1} = F_d(\bar{x}_k, [u_{1,k}, u_{2,k}]^{\mathrm{T}}), \quad \forall k = 0, 1, ..., N-1, \\ \bar{x}_0 = \bar{x}(t), \\ \max\{|u_{1,k}|, |u_{2,k}|\} \leq u_{max}, \quad k = 0, 1, ..., N-1, \\ \bar{x}_k \in \mathbb{X}_k, \quad k = 0, 1, ..., N-1, \\ \bar{x}_N = 0,\end{gathered} \tag{4.23}$$

where $\bar{x}(t)$ is the current state, u_{max} is the maximum bound on control, $\mathbb{X}_k$ is the state constraint set at a discrete time instant k assumed to be compact, and F_d are the approximate discrete dynamics (4.13). The value function of this optimization at $\bar{x}_0$ is defined as

$$V_N(\bar{x}_0) = \min_{u_{i,j},\ i=1,2,\ j=0,1,...N-1} J_N(\bar{x}_0, u_{1,0}, ..., u_{1,N-1}, u_{2,0}, ..., u_{2,N-1}). \tag{4.24}$$

4.4.1 Asymptotically Stabilizing Control Generated by MPC

To demonstrate that MPC generates an asymptotic stabilizing control law for the approximate discrete dynamics (4.13), the following theorem from [42] is used.

Theorem 4.3: [42] For a discrete-time MPC control problem with a terminal state condition $\bar{x}_N = 0$, if V_N is continuous at $\bar{x}_0 = 0$ and L satisfies the following:

R.4.1: $L(0, 0) = 0$,

R.4.2: There exists a non-decreasing function $\gamma : [0, \infty) \to [0, \infty]$ such that $\gamma(0) = 0$ and $0 < \gamma(||(\bar{x}, \bar{u})||) \leq L(\bar{x}, \bar{u})$ for all $(\bar{x}, \bar{u}) \neq 0$, where $||(*, *)||$ is a norm on the pair $(\bar{x}, \bar{u})$,

then the origin is an asymptotically stable equilibrium of the discrete-time system. □

Note that Theorem 4.3 only requires continuity of the value function at $\bar{x}_0 = 0$. Theorem 4.3 is now used to prove that the nonlinear MPC problem generates an

asymptotically stabilizing control law for when the input is unconstrained (Theorem 4.4) and constrained (Corollary 4.1).

Theorem 4.4: For the MPC problem (4.22)-(4.23), (4.13), let $\mathbb{X}_k = \mathbb{R}^5$ for $k = 0, 1, ...N-1$ and $u_{max} = \pm\infty$. Then the solution to the MPC optimization problem generates an asymptotically stabilizing control law to the origin when the horizon length satisfies $N \geq 6$.

Proof: Requirements **R.4.1** and **R.4.2** are satisfied from the construction of L in (4.21). It is now only necessary to show that V_N is continuous at $\bar{x}_0 = 0$ in order to apply Theorem 4.3. A sufficient condition for the continuity of V_N at $\bar{x}_0 = 0$ is that it is bounded from below and above by continuous functions that are zero at $\bar{x}_0 = 0$ [42]. The value function is bounded from below by a function $\bar{x}^{\mathrm{T}} Q \bar{x}$ due to (4.21), which is continuous and zero at $\bar{x}_0 = 0$. To show that V_N is bounded from above, it is sufficient to show that an open-loop trajectory exists, is feasible under control constraints, and has a maneuver cost that is continuous in the initial state $\bar{x}_0$ and is zero at $\bar{x}_0 = 0$.

Such an open-loop control sequence can be constructed as follows. Let the states $\phi,\ \theta,\ \nu_1,\ \nu_2$ be called base variables, as the linear system consisting of these states is completely controllable in 2 discrete-time steps. Define $\bar{x}_0 = [\ \phi_0\ \ \theta_0\ \ \psi_0\ \ \nu_{1,0}\ \ \nu_{2,0}\ ]^{\mathrm{T}}$ as the initial state vector, $\bar{y}_0 = [\ \phi_0\ \ \theta_0\ \ \nu_{1,0}\ \ \nu_{2,0}\ ]^{\mathrm{T}}$ as the initial base variable vector and $\bar{y}_c = [\ \tilde{\phi}\ \ \tilde{\theta}\ \ \tilde{\nu}_1\ \ \tilde{\nu}_2\ ]^{\mathrm{T}}$ as a chosen base variable vector (to be explicitly defined later in the proof). Then the control sequence $\{u_{i,j},\ i = 1, 2,\ j = 0, 1, ..., 5\}$, defined by

$$[\ u_{1,0}\ \ u_{2,0}\ \ u_{1,1}\ \ u_{2,1}\ ]^{\mathrm{T}} = -\left([\ \bar{A}\bar{B}\ \ \bar{B}\ ]\right)^{-1} \bar{A}^2 \bar{y}_0, \tag{4.25}$$

$$[\ u_{1,2}\ \ u_{2,2}\ \ u_{1,3}\ \ u_{2,3}\ ]^{\mathrm{T}} = \left([\ \bar{A}\bar{B}\ \ \bar{B}\ ]\right)^{-1} \bar{y}_c, \tag{4.26}$$

$$[\ u_{1,4}\ \ u_{2,4}\ \ u_{1,5}\ \ u_{2,5}\ ]^{\mathrm{T}} = -\left([\ \bar{A}\bar{B}\ \ \bar{B}\ ]\right)^{-1}\bar{A}^2\bar{y}_c, \tag{4.27}$$

and

$$\bar{A} = \begin{bmatrix} 1 & 0 & \alpha_1 T & \alpha_2 T \\ 0 & 1 & \beta_1 T & \beta_2 T \\ 0 & 0 & 1 & 0 \\ 0 & 0 & 0 & 1 \end{bmatrix}, \quad \bar{B} = \begin{bmatrix} \alpha_1\frac{T^2}{2} & \alpha_2\frac{T^2}{2} \\ \beta_1\frac{T^2}{2} & \beta_2\frac{T^2}{2} \\ T & 0 \\ 0 & T \end{bmatrix}, \tag{4.28}$$

will drive any $\bar{x}_0$ to 0 as long as

$$\Delta_c = -\frac{12}{5T}\psi_2, \tag{4.29}$$

where

$$\Delta_c = \tilde{\phi}(\beta_1\tilde{\nu}_1 + \beta_2\tilde{\nu}_2) - \tilde{\theta}(\alpha_1\tilde{\nu}_1 + \alpha_2\tilde{\nu}_2), \tag{4.30}$$

and

$$\psi_2 = \psi_0 + \frac{5T}{24}(\phi_0(\beta_1\nu_{1,0} + \beta_2\nu_{2,0}) - \theta_0(\alpha_1\nu_{1,0} + \alpha_2\nu_{2,0})) - \frac{1}{2}\theta_0\phi_0. \tag{4.31}$$

Note that since $u_{max} = \pm\infty$, the control in (4.25)-(4.27) will always satisfy constraints, and therefore the trajectory generated by such a control sequence is feasible.

The logic of the open-loop maneuver is the following. The control sequence in (4.25) drives $\bar{y}_0$ to 0 and ψ_0 to ψ_2. The remaining control sequences in (4.26) and (4.27) guide the base variables in a closed trajectory that travels from 0 to $\bar{y}_c$ and back to 0. The influence of this closed trajectory on ψ is reflected by ψ_3, ψ_4, ψ_5 and ψ_6,

$$\psi_3 = \psi_2 + \Delta_c\frac{T}{16} + \tilde{\theta}\tilde{\phi}\frac{1}{8} + (\alpha_1\tilde{\nu}_1 + \alpha_2\tilde{\nu}_2)(\beta_1\tilde{\nu}_1 + \beta_2\tilde{\nu}_2)\frac{T^2}{32} - \tilde{\phi}(\beta_1\tilde{\nu}_1 + \beta_2\tilde{\nu}_2)\frac{T}{8}, \tag{4.32}$$

$$\psi_4 = \psi_2 + \Delta_c \frac{5T}{24} + \frac{1}{2}\tilde{\theta}\tilde{\phi}, \tag{4.33}$$

$$\psi_5 = \psi_2 + \Delta_c \frac{17T}{48} + \tilde{\theta}\tilde{\phi}\frac{1}{8} + (\alpha_1\tilde{\nu}_1 + \alpha_2\tilde{\nu}_2)(\beta_1\tilde{\nu}_1 + \beta_2\tilde{\nu}_2)\frac{T^2}{32} + \tilde{\phi}(\beta_1\tilde{\nu}_1 + \beta_2\tilde{\nu}_2)\frac{T}{8}, \tag{4.34}$$

$$\psi_6 = \psi_2 + \Delta_c \frac{5T}{12}. \tag{4.35}$$

As can be seen, if (4.29) is satisfied, $\psi_6 = 0$, and thus $\bar{x}_0$ reaches zero in six steps.

Let $\bar{y}_c$ be chosen as

$$\begin{aligned} \tilde{\phi} &= |\psi_2|^{\frac{2}{3}}, \\ \tilde{\theta} &= -|\psi_2|^{\frac{2}{3}}, \\ \tilde{\nu}_1 &= -\tfrac{6}{5T(\alpha_1+\beta_1)}(\psi_2)^{\frac{1}{3}}, \\ \tilde{\nu}_2 &= -\tfrac{6}{5T(\alpha_2+\beta_2)}(\psi_2)^{\frac{1}{3}}. \end{aligned} \tag{4.36}$$

Then condition (4.29) is satisfied assuming that $\alpha_1 + \beta_1 \neq 0$ and $\alpha_2 + \beta_2 \neq 0$. Note that if $\alpha_1 + \beta_1 = 0$ or $\alpha_2 + \beta_2 = 0$, another $\bar{y}_c$ that satisfies (4.29) can be chosen. Also note that $\alpha_1 + \beta_1 = 0$ and $\alpha_2 + \beta_2 = 0$ will never occur at the same time since the columns of $\tilde{W}$ are linearly independent. Using (4.36) above, the control sequences in (4.26)-(4.27) become continuous functions of ψ_2, which is consequently a continuous function of $\bar{x}_0$.

Since the control sequence (4.25)-(4.27) steers the state to the origin and is continuous as a function of the initial state $\bar{x}_0$, it follows that V_N is upper bounded by the cost of this feasible control sequence, which is a continuous function of $\bar{x}_0$ and is zero at $\bar{x}_0 = 0$. Since V_N is upper and lower bounded by continuous functions of $\bar{x}_0$ which are zero at $\bar{x}_0 = 0$, V_N is continuous at $\bar{x}_0 = 0$. By Theorem 4.3, the control law is asymptotically stabilizing for all horizon lengths satisfying $N \geq 6$. $\square$

The argument of Theorem 4.4 can be extended to demonstrate the following result

under control constraints.

Corollary 4.1: For the MPC problem in (4.22)-(4.23), (4.13), let $\mathbb{X}_k = \mathbb{R}^5$ for $k = 0, 1, ..., N-1$. Then for any $u_{max} > 0$, there exists a sufficiently large horizon length $N^* \geq 6$ such that MPC generates a locally asymptotic stabilizing control to the origin when the horizon length satisfies $N \geq N^*$.

Proof: Define the following quantities,

$$\tilde{u}_{max,1} = \max\{|u_{1,0}|, |u_{1,1}|, |u_{2,0}|, |u_{2,1}|\}, \tag{4.37}$$

$$\tilde{u}_{max,2} = \max\{|u_{i,j}|,\ i = 1, 2,\ j = 2, 3, 4, 5\}, \tag{4.38}$$

and the following set

$$G(\rho) = \{\bar{x}_0 \in \mathbb{R}^5\ :\ \forall ||\bar{x}_0|| \leq \rho,\ \tilde{u}_{max,1} \leq u_{max}\}. \tag{4.39}$$

Since the base variable system is linear (defined by the matrices $\bar{A}$ and $\bar{B}$ from (4.28)) and $u_{max} > 0$, there exists a $\rho^* > 0$ such that $\forall \rho \in (0, \rho^*]$, $G(\rho) \neq \{\emptyset\}$ (i.e., there exists a ball of radius ρ^* centered at the origin where for all $\bar{x}_0$ in the ball, $\tilde{u}_{1,max} \leq u_{max}$).

Now define $N_\psi \geq 1$ as a positive integer and let $\bar{y}_c$ be chosen as

$$\begin{aligned}
\tilde{\phi} &= |\psi_2|^{\frac{2}{3}}/\sqrt{N_\psi}, \\
\tilde{\theta} &= -|\psi_2|^{\frac{2}{3}}/\sqrt{N_\psi}, \\
\tilde{\nu}_1 &= -\tfrac{6}{5T(\alpha_1+\beta_1)\sqrt{N_\psi}}(\psi_2)^{\frac{1}{3}}, \\
\tilde{\nu}_2 &= -\tfrac{6}{5T(\alpha_2+\beta_2)\sqrt{N_\psi}}(\psi_2)^{\frac{1}{3}}.
\end{aligned} \tag{4.40}$$

From the logic used in Theorem 4.4, if (4.40) holds, ψ_6 becomes

$$\psi_6 = \psi_2 - \frac{\psi_2}{N_\psi}. \tag{4.41}$$

The control sequence $\{u_{i,j},\ i = 1, 2,\ j = 2, 3, 4, 5\}$ can be repeated n times, which gives the following discrete evolution of ψ,

$$\psi_{2+4n} = \psi_2 - \frac{\psi_2}{N_\psi} n. \tag{4.42}$$

If $n = N_\psi$, ψ and the base variables reach zero in finite time. As N_ψ increases, $||\bar{y}_c||$ decreases, which consequently decreases $\tilde{u}_{max,2}$. Therefore, there exists a $N_\psi^* \geq 1$ such that for all $N_\psi \geq N_\psi^*$, $\tilde{u}_{max,2} \leq u_{max}$.

From the above it can be seen that for all $\bar{x}_0$ in a neighborhood of the origin defined by $G(\rho^*)$, the MPC problem with control constraints is feasible for any horizon lengths satisfying $N \geq 2 + 4N_\psi^* = N^*$. The control sequence for this maneuver is continuous in the initial condition $\bar{x}_0$, and therefore the cost of such a maneuver is continuous in $\bar{x}_0$ and zero at $\bar{x}_0 = 0$. The cost of this maneuver constitutes an upper bound on the value function, and hence the conclusions of this corollary follow similarly to Theorem 4.4, but only apply in a neighborhood of the origin defined by $G(\rho^*)$. □

Remark 4.4: It may be possible to increase ρ^* if the control sequence that drives $\bar{y}_0$ to 0 is allowed to take longer than two discrete-time steps. Therefore, by increasing N further, it may be possible to expand the local region of attraction $G(\rho^*)$ for the MPC law defined in (4.22)-(4.23), (4.13).

Theorem 4.4 only approaches the subject of control constraints. MPC, however, also has the ability to enforce state constraints. Though no formal proof is given in this chapter for stabilization in the presence of state constraints, simulations in Section 4.5 show that MPC can indeed generate stabilizing feedback laws when some state constraints are included.

Recall that the discrete dynamics used in the MPC formulation are only approximate. Simulation results on the full nonlinear model (2.3) (2.41), and (2.44) in Section 4.5 demonstrate successful convergence in a neighborhood of the origin where Euler angles, and thus model mismatch between the exact and approximate models, is sufficiently small.

4.4.2 Discontinuous Control Law

To illustrate that MPC generates a control law that is discontinuous in terms of state, the optimization problem (4.22)-(4.23), (4.13) is solved for various initial attitudes ranging between -0.1 and 0.1 rad and initial RW velocities of 0 rad/sec. The spacecraft and the controller in these tests have the same parameters as those in Section 4.5.

Figure 4.1 (a) shows the control action $u_{1,0}$ when $\theta = 0$ and ϕ and ψ are sampled on a unit circle of radius 0.05 rad (for a given λ, $\phi = 0.05\cos(\lambda)$ and $\psi = 0.05\sin(\lambda)$). Likewise, Figure 4.1 (b) shows the control action $u_{1,0}$ when $\phi = 0$ and θ and ψ are sampled on a unit circle of radius 0.05 rad, (for a given λ, $\theta = 0.05\cos(\lambda)$ and $\psi = 0.05\sin(\lambda)$). In both figures, the discontinuity, represented by the dashed line, occurs at $\phi = \theta = 0$.

To demonstrate the discontinuity further, Figure 4.2 (a) shows the control action $u_{1,0}$ when $\theta = 0$ and ϕ and ψ are varied across a grid of initial conditions. Figure 4.2 (b) likewise shows the control action $u_{1,0}$ when $\phi = 0$ and θ and ψ are varied across a grid. The discontinuity is present, and in addition passes through the origin. This can be reasoned from Figure 1 as well, since as the radius of the sampled unit circle decreases, the discontinuity still remains at $\phi = \theta = 0$ while ψ decreases in magnitude.

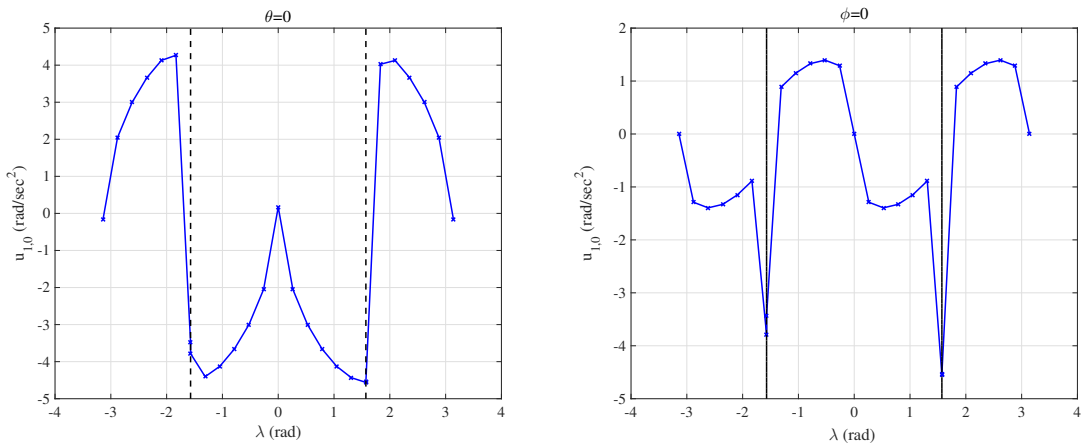

(a) (b)

Figure 4.1: Discontinuous feedback law generated by solving the MPC optimization problem for initial conditions sampled on a circle of radius 0.05 rad.

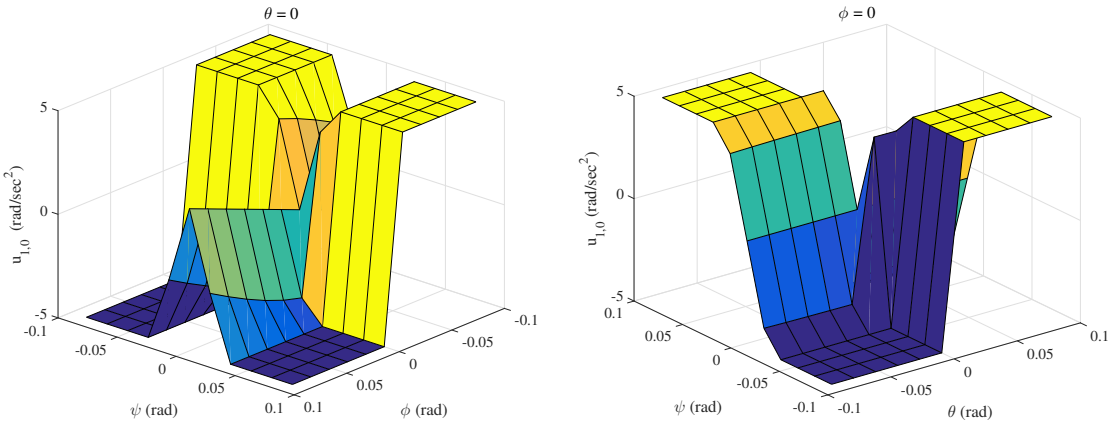

(a) (b)

Figure 4.2: Discontinuous feedback law generated by solving the MPC optimization problem for a grid of initial conditions.

4.5 Simulation Results

In this section, the MPC control problem defined in (4.22)-(4.23), (4.13) is applied to the actual nonlinear model (2.3), (2.41), and (2.44). The spacecraft bus in these simulations is assumed to have principal moments of inertia equal to 430, 1210, and

1300 kg m^2, respectively. The reaction wheels are assumed symmetric, thin, and are mounted such that the COM of the spacecraft bus and total spacecraft system coincide. The inertias of the RWs about their spin axes are $J_{ws1} = J_{ws2} = 0.043$ kg m^2. The two RWs are aligned with the minor and intermediate principal axes of the spacecraft bus, yielding

$$\bar{J} = \begin{bmatrix} 430.043 & 0 & 0 \\ 0 & 1210.043 & 0 \\ 0 & 0 & 1300 \end{bmatrix}, \quad \bar{W} = \begin{bmatrix} 0.043 & 0 \\ 0 & 0.043 \\ 0 & 0 \end{bmatrix}. \tag{4.43}$$

The model and control parameters used in all the simulations are listed in Table 4.1.

Parameter	**Units**	**Value**
u_{max}	rad/sec^2	5
T	sec	10
N	-	30
$\bar{Q}$	-	diag(1×10^5, 1×10^5, 1×10^5, 0.01, 0.01)
r_1, r_2	-	$10, 10$

Table 4.1: Simulation parameters for nonlinear MPC.

4.5.1 Beginning Simulations

For the first simulation, the initial conditions of the spacecraft are $\bar{\Theta}(0) = [\ -0.05\ \ 0.03\ \ 0.1\ ]^{\mathrm{T}}$ rad, $\bar{\omega}(0) = [\ 0\ \ 0\ \ 0\ ]^{\mathrm{T}}$ rad/sec, $\bar{\nu}(0) = [\ 0\ \ 0\ ]^{\mathrm{T}}$ rad/sec. In this simulation, only RW control constraints are enforced. The results are given in Figure 4.3. In the second simulation, the initial conditions of the spacecraft are $\bar{\Theta}(0) = [\ 0\ \ 0\ \ -0.1\ ]^{\mathrm{T}}$ rad, $\bar{\omega}(0) = [\ 0\ \ 0\ \ 0\ ]^{\mathrm{T}}$ rad/sec, $\bar{\nu}(0) = [\ 0\ \ 0\ ]^{\mathrm{T}}$ rad/sec. In this simulation, we impose an additional RW speed constraint of $||\bar{\nu}||_\infty \leq 100$ rad/sec. The results are given in Figure 4.4. Both simulations demonstrate that the MPC

formulation (4.22)-(4.23), which uses (4.13) as an approximate model for prediction, is able to stabilize the attitude of the underactuated spacecraft to the desired pointing orientation while enforcing control constraints on the exact model of the spacecraft. Moreover, the convergence rates in both simulations appear to be exponential.

Observe that in both Figures 4.3 and 4.4 the Euler angles ϕ and θ (roll and pitch) oscillate while ψ (yaw) converges to equilibrium. For problems related to nonholonomic systems, such as the underactuated spacecraft problem, a controlled drift in the underactuated axis can be induced by performing oscillatory motion in the states that are controllable. This phenomenon is related to geometric phase, which is closely connected to the controllability analysis given by Lie brackets. Thus it appears that MPC utilizes this effect in order to stabilize the underactuated spacecraft to equilibrium.

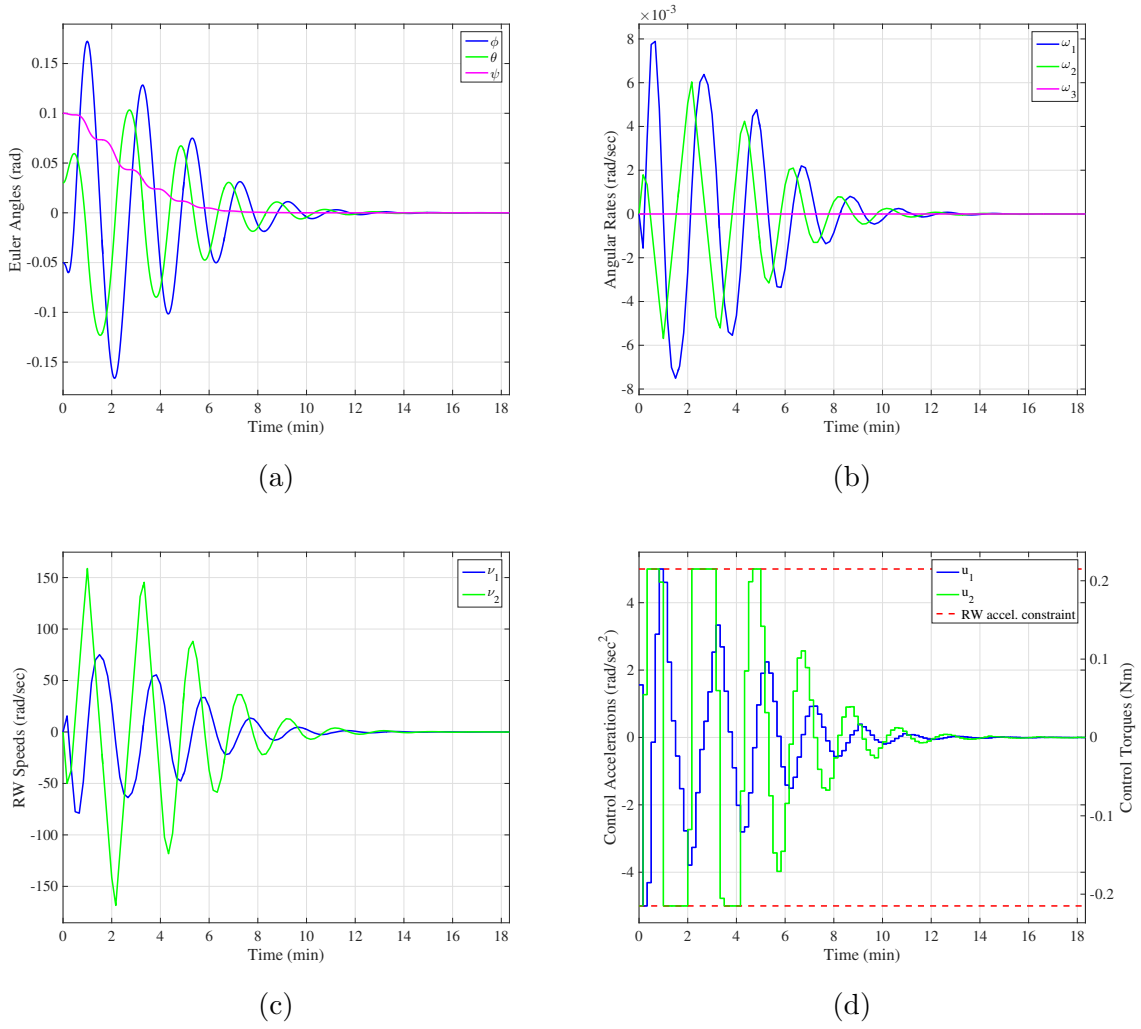

Figure 4.3: Closed-loop response of underactuated spacecraft with MPC, simulation 1. (a) Euler angles, (b) angular velocities, (c) wheel velocities, (d) wheel accelerations.

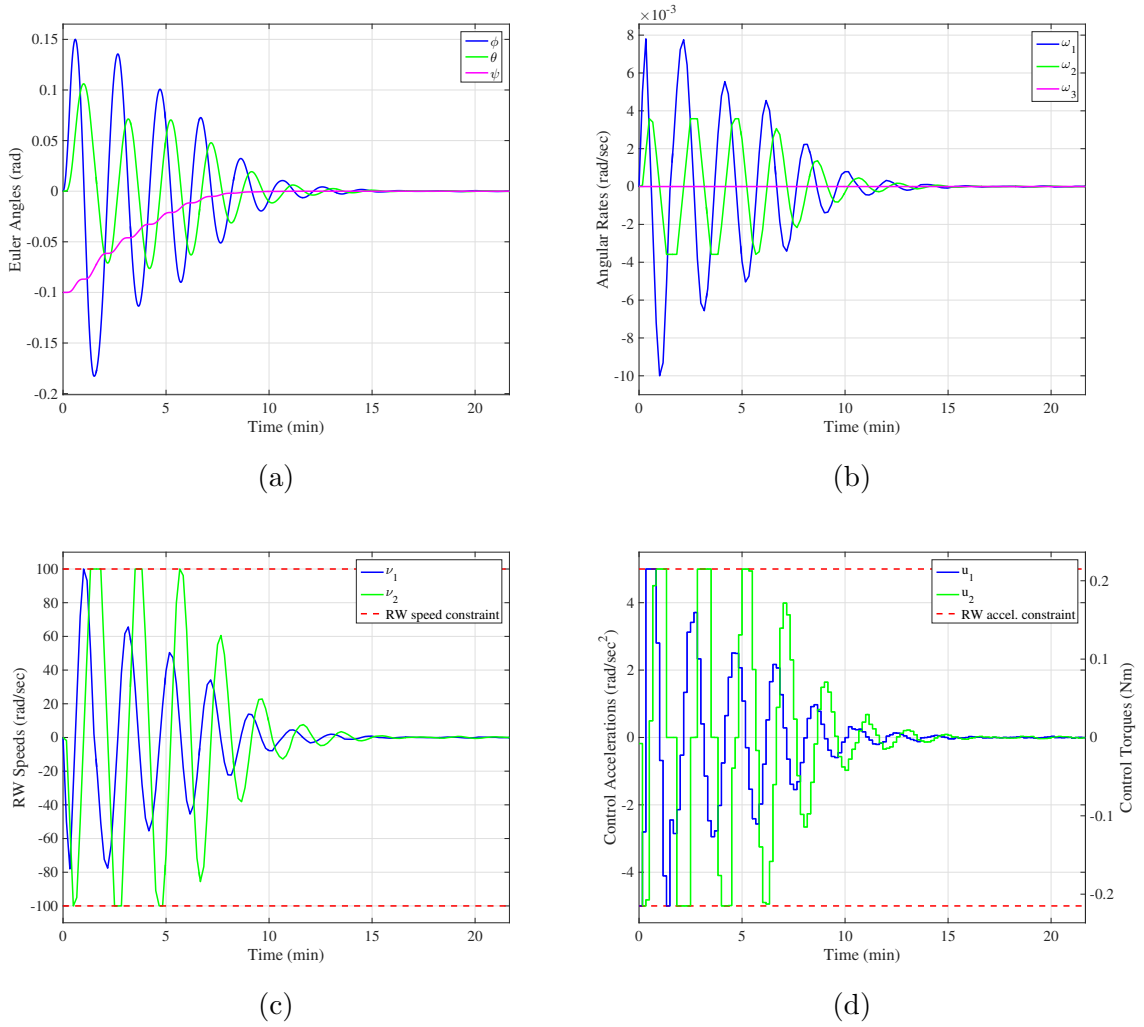

Figure 4.4: Closed-loop response of underactuated spacecraft with MPC, simulation 2. (a) Euler angles, (b) angular velocities, (c) wheel velocities, (d) wheel accelerations.

4.5.2 Simulations with Various Sampling Times

To demonstrate that the nonlinear MPC controller can handle different sampling periods, two simulations are now performed using the same initial conditions, control parameters, and constraints as the first simulation (results in Figure 4.3), but the sampling period T is changed from 10 sec to 6 sec and 40 sec, respectively. The results are shown in Figure 4.5. In both cases, the nonlinear MPC controller stabilizes the attitude while satisfying constraints. While this has not been done in simulations

shown, the design parameters in Table 1, in particular, the prediction horizon, may need to be adjusted if the sampling period changes to improve closed-loop performance.

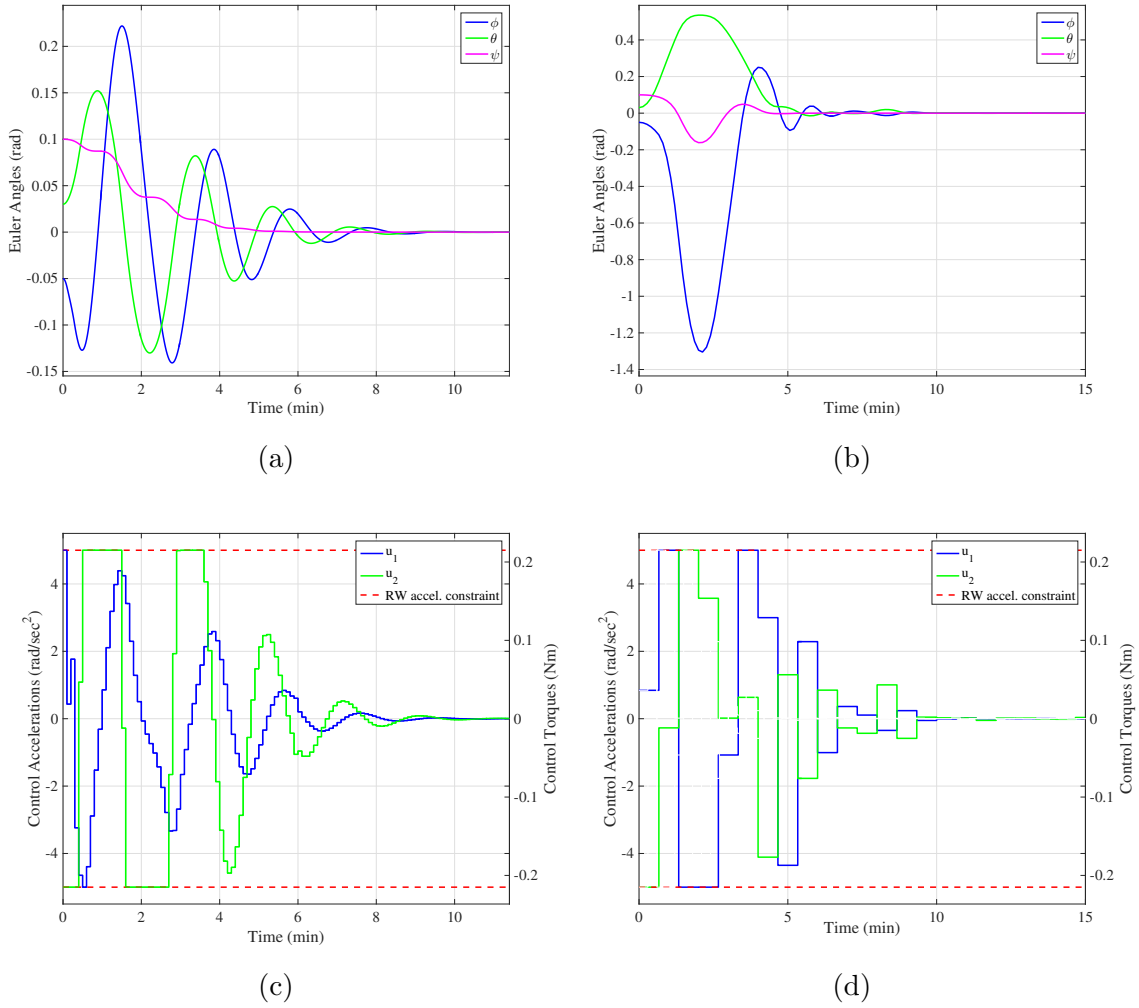

Figure 4.5: Closed-loop response of underactuated spacecraft with MPC and various sample periods. (a) Euler angles when $T = 6$ sec, (b) Euler angles when $T = 40$ sec, (c) wheel accelerations when $T = 6$ sec (d) wheel accelerations when $T = 40$ sec.

4.5.3 Large Angle Maneuver Simulations

As mentioned in the previous section, the nonlinear MPC controller is able to stabilize the attitude of the underactuated spacecraft in a neighborhood where model mismatch

is small. This neighborhood can be easily reached by external thrusters or cold gas jets, types of actuation which can be used for large maneuvers but not for precise pointing. However, it can be demonstrated that the nonlinear MPC controller can also stabilize an at-rest spacecraft with initially large Euler angles. An example is given in Figure 4.6, where the control parameters used are in Table 4.1, the initial conditions are $\bar{\Theta}(0) = [\ 0.6 \quad -0.8 \quad 1\ ]^{\mathrm{T}}$ rad, $\bar{\omega}(0) = [\ 0 \quad 0 \quad 0\ ]^{\mathrm{T}}$ rad/sec, $\bar{\nu}(0) = [\ 0 \quad 0\ ]^{\mathrm{T}}$ rad/sec and the only constraint being enforced is the control constraint. The figure demonstrates successful convergence while satisfying constraints even though the small angle assumption is clearly violated.

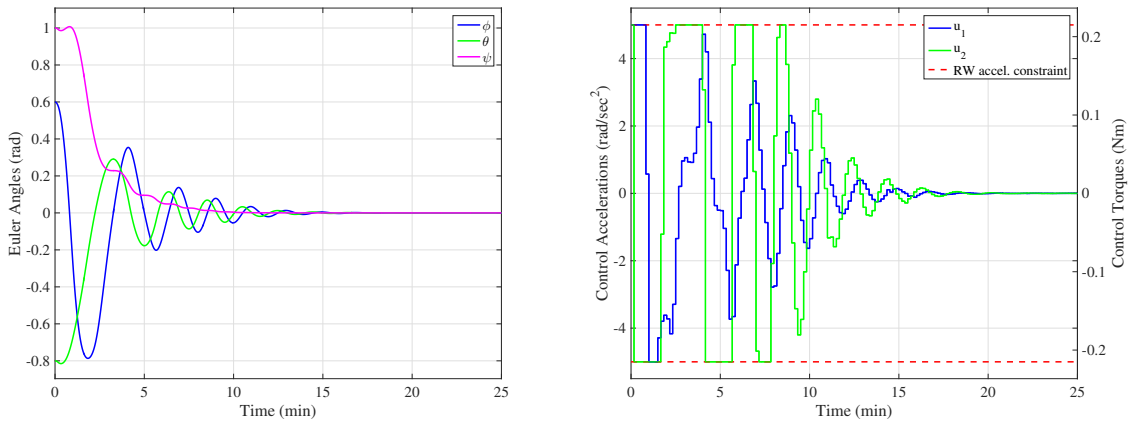

(a) (b)

Figure 4.6: Closed-loop response of underactuated spacecraft with MPC for large initial Euler angles. (a) Euler angles, (b) wheel accelerations.

To further demonstrate the range of at-rest initial conditions that the nonlinear MPC controller can stabilize, one thousand random test simulations were run with initial Euler angles belonging to the interval of $[\ -180,\ 180\ ]$ deg, initial zero angular velocity, and RW speeds initially at 0 rad/sec. Figure 4.7 gives an approximation of the region of attraction based on whether the controller was able to converge to a 0.01 rad (0.573 deg) Euler angle box and a 0.001 rad/sec angular velocity box during a given simulation time of 3000 sec. As can be seen, the region of attraction is quite

large, despite the small angle assumption being used in the controller design.

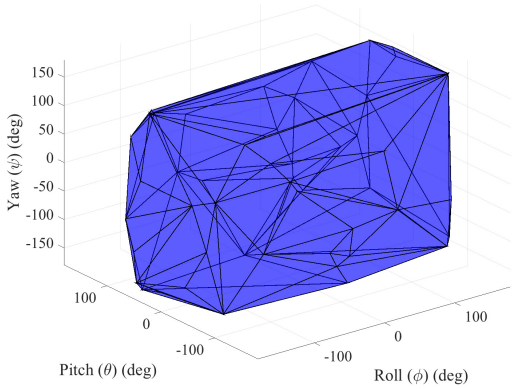

Figure 4.7: Approximation of nonlinear MPC region of attraction for at-rest maneuvers.

4.5.4 Discussion on Real-Time Applications

The MPC optimization problem in all simulations was solved using an interior-point method with MATLAB's *fmincon* function. The average and worst case computation time needed to solve the optimization problem in Section 4.5.1 using a standard computer with 2.4 GHz clock speed were 1.2 sec and 2.4 sec, respectively. Both times are less than the sample time T in these simulations, which is 10 sec (found in Table 4.1). Using custom solvers optimized for real-time implementation as a C code will clearly reduce computation time. For instance, see [98], which shows that symbolic computations and code optimization can drastically improve the computation time. Though common spaceflight hardware has processing power typically in the MHz range, the general trend has been towards growing computing power. In fact, there are now more powerful spaceflight processors available such as the 1 GHz PROTON-200k, the 1.5 GHz PROTON-400k-3X, and the 3 GHz PROTON-200k-3X [99]. Reconfigurable Field Programmable Gate Arrays (FPGAs) can also be used for spacecraft missions with large processing demands [100]. It should finally be noted that RWs are used

for nonagile maneuvers [1]. As such, the closed-loop bandwidth for actuation is in the range 0.01 Hz to 1 Hz [1], hence control solutions do not need to be computed as rapidly as for other real-time systems. Thus our application may not be dissimilar from other applications for which successful real-world implementations of nonlinear MPC have been reported [101–104]. For spacecraft with limited onboard computational ability, an explicit implementation may be used where the nonlinear MPC is precomputed offline and approximately function-fitted; the fitted function is then used online [91, 105–107]. Such an implementation is still fundamentally based on computational optimization.

Remark 4.5: Note that the underlying optimization problem is nonlinear and non-convex. Thus there are no *a priori* guarantees other than offline testing by running multiple simulations that the solver used will converge to a solution. Continuation and warm starting strategies can mitigate the risk of the solver not converging [108–110]. For some implementations, convergence is not required, only feasibility and cost decrease (this property is not analyzed for the problem in this chapter).

CHAPTER 5

Recovering Controllability By Exploiting Solar Radiation Pressure

5.1 Introduction

This chapter discusses an approach to controlling an underactuated spacecraft by including the effects of SRP torques, modeled following [43], into the spacecraft model. Our analysis shows that under appropriate assumptions, linear controllability is regained and hence spacecraft stabilization can be achieved with conventional control schemes. In particular, an LQ approach will be first applied. The LQ approach is chosen due to its robustness, its optimal control properties and its familiarity to aerospace engineers. A pole placement scheme will also be used to improve convergence time. By taking advantage of the change in the dynamics induced by SRP torques, two RWs are able to slowly correct the attitude errors over time. This method is different from any of the control techniques mentioned in the Introduction, as well as those techniques mentioned in this dissertation up to this point. Firstly, it exploits external disturbance torques, which in many control approaches are either neglected or rejected. Secondly, this method is not restricted to zero total angular momentum or the constant angular momentum assumption. Thirdly, utilizing SRP torques allows designers to use conventional and familiar feedback control schemes that are guaranteed to locally stabilize the equilibrium.

This chapter contains the following results:

- The characterization and discussion of the effects of SRP, specifically on symmetric body spacecraft;
- Sufficient conditions for zero SRP torque acting on a symmetric spacecraft;
- Results on the fixed attitude stability of an underactuated spacecraft with and without SRP;
- Necessary and sufficient conditions under which linear controllability is regained with SRP;
- Extending a novel pathway to recover linear controllability and perform control of underactuated spacecraft by taking advantage of SRP torques to a broader class of spacecraft.

After [111] was submitted for publication (which contained our preliminary findings), the press release [112] appeared, suggesting that SRP is currently being used (in an unspecified control scheme) to restore Kepler's mission controllability. The controllability analysis and results, obtained independently of [112], are thus indirectly corroborated by experimental evidence in [112].

5.2 Spacecraft Modeling

5.2.1 Spacecraft Configuration & Assumptions

The spacecraft configuration considered in this chapter consists of a rigid bus and four RWs. During the spacecraft's mission, two of the RWs fail and spin down to zero speed, leaving two operational RWs. Recall that frame $\mathcal{I}$ is aligned with the desired inertial pointing configuration. We also make the following assumptions:

Assumption 5.1 The axes of the spacecraft bus fixed frame $\mathcal{B}$ are aligned with the spacecraft bus' principal axes.

Assumption 5.2 All RWs rotors are assumed thin and identical, with the inertias about the spin axis being J_w (i.e., $J_{ws_i} = J_w$ for all i) and inertia about axes transversal axis being zero (i.e., $J_{wt_i} \approx 0$ for all i).

Assumption 5.3 The RWs are mounted such that the COM of the entire spacecraft system is the same as that of the spacecraft bus.

Assumptions 5.1-5.3 enable us to simplify the dynamics, and are common in practice.

5.2.2 Equations of Motion

We choose 3-2-1 Euler angles ψ (yaw), θ (pitch), and ϕ (roll) as our attitude representation, and assume the following:

Assumption 5.4 The maneuvers being performed involve relatively small attitude adjustments near the desired pointing orientation,

which implies that the Euler angles will avoid singularity. This assumption is reasonable considering that we are interested in using RWs for accurate pointing near the target orientation. The kinematics from Section 2.3 are

$$\dot{\bar{\Theta}} = \bar{M}(\bar{\Theta})\bar{\omega}. \tag{5.1}$$

Since only RW actuation is considered, the dynamics of the system are given in Section 2.6.2 by

$$\bar{J}\dot{\bar{\omega}} = -[\bar{\omega}]^{\times}\left(\bar{J}\bar{\omega} + \sum_{i=1}^{4} J_w \nu_i \check{w}_i\right) - \sum_{i=1}^{4} J_w \dot{\nu}_i \check{w}_i + \bar{M}_{ext}, \tag{5.2}$$

where

$$\bar{J} = \bar{J}_{\mathfrak{B}} + \sum_{i=1}^{4} \bar{J}_{\mathfrak{W}_i}. \tag{5.3}$$

If we denote the following

$$\begin{aligned} \bar{W}_{c} &= [\ \check{w}_1 \ \ \check{w}_2 \ \ \check{w}_3 \ \ \check{w}_4\ ], \\ \bar{\nu}_{c} &= [\ \nu_1 \ \ \nu_2 \ \ \nu_3 \ \ \nu_4\ ]^{\mathrm{T}}, \end{aligned} \tag{5.4}$$

then (5.2) and (5.3) become

$$\bar{J}\dot{\bar{\omega}} = -[\bar{\omega}]^{\times}\left(\bar{J}\bar{\omega} + J_{w}\bar{W}_{c}\bar{\nu}_{c}\right) - J_{w}\bar{W}_{c}\dot{\bar{\nu}}_{c} + \bar{M}_{ext}, \tag{5.5}$$

$$\bar{J} = \mathrm{diag}(J_1, J_2, J_3) + J_{w}\bar{W}_{c}\bar{W}_{c}^{\mathrm{T}}, \tag{5.6}$$

where J_1, J_2, J_3 are the spacecraft bus principal moments of inertia. We now make the following assumption:

> **Assumption 5.5** The only external moments acting upon the spacecraft are torques induced by SRP, i.e., $\vec{M}_{ext/O} = \vec{\tau}_{srp}$.

In subsequent sections, we denote $\bar{\tau}_{srp} = \vec{\tau}_{srp}\big|_{\mathcal{B}}$.

The contribution of the failed RWs to the dynamics in (5.5) vanishes once their speeds reach zero. Assuming that the failed RWs are at zero speed, the dynamics (5.5) and inertia matrix (5.6) can be rewritten to account for the contributions of only operational RWs,

$$\bar{J}\dot{\bar{\omega}} = -[\bar{\omega}]^{\times}\left(\bar{J}\bar{\omega} + J_{w}\bar{W}_{a}\bar{\nu}_{a}\right) - J_{w}\bar{W}_{a}\dot{\bar{\nu}}_{a} + \bar{M}_{ext}, \tag{5.7}$$

$$\bar{J} = \mathrm{diag}(J_1, J_2, J_3) + J_{w}\bar{W}_{a}\bar{W}_{a}^{\mathrm{T}}, \tag{5.8}$$

where

$$\bar{\nu}_{a} = [\dots \nu_{b} \dots]^{\mathrm{T}}, \quad b \in \{1, 2, 3, 4\}, \tag{5.9}$$

is the vector of all operational RWs angular rates and

$$\bar{W}_{a} = [\dots \check{w}_{b} \dots], \quad b \in \{1, 2, 3, 4\}, \tag{5.10}$$

is a matrix whose columns are the unit vectors of the spin axes of the operational RWs. For instance, if wheels 3 and 4 have failed, then $\bar{\nu}_{a} = [\ \nu_{1} \ \ \nu_{2}\ ]^{\mathrm{T}}$ and $\bar{W}_{a} = [\ \check{w}_{1} \ \ \check{w}_{2}\ ]$.

The operational RW accelerations are treated as the control inputs,

$$\dot{\bar{\nu}}_{a} = \bar{z}_{a}, \tag{5.11}$$

where

$$\bar{z}_{a} = [\dots z_{b} \dots]^{\mathrm{T}}, \quad b \in \{1, 2, 3, 4\}. \tag{5.12}$$

For instance, if wheels 1 and 2 are operational but wheels 3 and 4 have failed, $\bar{z}_{a} = [\ z_{1} \ \ z_{2}\ ]^{\mathrm{T}}$.

5.2.3 Solar Radiation Pressure Torque Model

Assume that the spacecraft is covered with ρ flat panels. The SRP torques induced by the panels are modeled based on the developments in [43]. Define

$$\alpha_{i,j} = \frac{\Phi_{sun,tot}}{c(\frac{d_{i,j}}{d_0})^2}, \tag{5.13}$$

$$\beta_{j} = \frac{4}{9} C_{diff,j}, \tag{5.14}$$

where c is the speed of light, d_0 is the nominal distance from the Sun equal to $1AU$, $\Phi_{sun,tot}$ is the solar flux at d_0, $C_{diff,j}$ is the diffusion coefficient for panel j, and $d_{i,j}$ is

the distance to a point i on panel j from the center of the Sun. The SRP at point i on panel j is given by

$$\vec{P}_{i,j} = -\alpha_{i,j}(\hat{u}_{n,j} \cdot \hat{u}_s)(\hat{u}_{n,j} + \beta_j \hat{u}_s), \tag{5.15}$$

where $\hat{u}_{n,j}$ is the normal to panel j pointing outward from the spacecraft and $\hat{u}_s$ is the unit vector representing the Sun direction. Figure 5.1 depicts the Sun direction $\hat{u}_s$ and normal vectors $\hat{u}_{n,j},\ j = 1, 2, 3$, as they apply to a cuboid spacecraft.

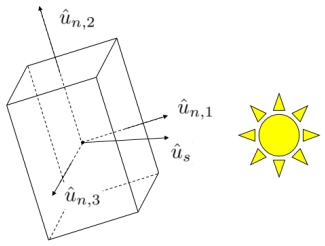

Figure 5.1: Cuboid spacecraft with physical vector description.

The distance between two points i and l on panels j and k (where j and k can represent the same panel) is very small when compared to $d_{i,j}$ and $d_{l,k}$. Therefore the difference between $\frac{d_{i,j}}{d_0}$ and $\frac{d_{l,k}}{d_0}$ becomes negligible, and $\alpha_{i,j}$ can be treated as a constant parameter, α, for all points across all panels. Thus the SRP exerted at every point along the same panel is assumed to be identical. Note that there will be a variation in SRP between panels j and k if β_j and β_k are different. The SRP exerted at each point on panel j is then

$$\vec{P}_j = -\alpha(\hat{u}_{n,j} \cdot \hat{u}_s)(\hat{u}_{n,j} + \beta_j \hat{u}_s). \tag{5.16}$$

Under the assumption that SRP acts identically across all points on the same panel, the total SRP torque about the spacecraft's COM, located at point O, due to

the jth panel, can be expressed as

$$\vec{\tau}_{j,srp} = (\vec{r}_{j/B} - \vec{r}_{O/B}) \times A_j \vec{P}_j, \tag{5.17}$$

where $\vec{r}_{j/B}$ is the vector from a reference point B to the center of the jth panel, $\vec{r}_{O/B}$ is the vector from B to the COM of the spacecraft bus, and A_j is the area of the jth panel. Since SRP is additive across all panels,

$$\vec{\tau}_{srp} = \sum_{j}^{\rho} \vec{\tau}_{j,srp} \tilde{I}_j, \tag{5.18}$$

where $\tilde{I}_j$ is an indicator function used to identify which panels are facing the Sun and are acted on by solar pressure. Assuming a regular, convex shape of the spacecraft, the indicator function is given by

$$\tilde{I}_j = \begin{cases} 1 & \text{if } (\hat{u}_{n,j} \cdot \hat{u}_s) > 0, \\ 0 & \text{otherwise.} \end{cases} \tag{5.19}$$

Observe that the total SRP torque in (5.18) is only a function of $\bar{\Theta}$. In reality SRP is a pressure based torque and hence strictly speaking also depends on spacecraft velocities due to dynamic pressure effects. These effects are very small and assumed to be negligible.

5.2.4 Linearized Model

For analysis and controller design, the equations of motion (5.1) and (5.7) are linearized. Without loss of generality, $\bar{\Theta} = 0$ is chosen as the desired attitude since $\mathcal{I}$ can be oriented to reflect desired pointing. Theorem 5.1 gives the requirement for the spacecraft to maintain $\bar{\Theta} = \bar{\omega} = 0$ in steady-state (assuming no constraints on functioning RW speeds).

Theorem 5.1: $\bar{\Theta} = \bar{\omega} = 0$ can be maintained as a (relative) equilibrium by the closed-loop system if and only if $\bar{\tau}_{srp}(0)$ is in the range of $\bar{W}_a$.

Proof: For the spacecraft bus, if $\bar{\omega}(t) = 0$ for all t, then $\dot{\bar{\Theta}}(t) = 0$ and $\dot{\bar{\omega}}(t) = 0$. If $\dot{\bar{\omega}} = 0$ then (5.7) implies

$$0 = -J_w \bar{W}_a \bar{z}_a + \bar{\tau}_{srp}(0). \tag{5.20}$$

Equation (5.20) can be satisfied if and only if $\bar{\tau}_{srp}(0)$ is in the range of $\bar{W}_a$. $\square$

Remark 5.1: Theorem 5.1 gives conditions under which $\bar{\Theta} = \bar{\omega} = 0$ can be maintained as a (relative) equilibrium for the spacecraft bus. The reaction wheels may be accelerating to compensate for SRP torque, in which case the (relative) equilibrium can be maintained until the RWs reach their saturation limits.

For three or more RWs, assuming that $\bar{W}_a$ is full rank, $\bar{\Theta} = \bar{\omega} = 0$ will always be a feasible equilibrium. With two or fewer RWs, Theorem 5.1 restricts the set of physical pointing orientations that can be maintained in steady-state with functioning RWs.

Assuming that $\bar{\tau}_{srp}(0)$ is in the range of $\bar{W}_a$, (5.1) and (5.7) are linearized about $\bar{\Theta} = \bar{\omega} = 0$, $\bar{\nu}_a = \bar{\nu}_{a,0}$, and $\bar{z}_a = \bar{z}_{a,0} = \bar{\Xi}$, where $\bar{\Xi}$ is the commanded RW accelerations to make $\bar{\Theta} = \bar{\omega} = 0$ a feasible equilibrium, i.e.,

$$\bar{\Xi} = \begin{cases} \frac{1}{J_w}(\bar{W}_a^{\mathrm{T}}\bar{W}_a)^{-1}\bar{W}_a^{\mathrm{T}}\bar{\tau}_{srp}(0) & \text{if } \operatorname{rank}(\bar{W}_a) \leq 3, \\ \text{an arbitrary } \bar{z}_a \text{ such that } J_w\bar{W}_a\bar{z}_a = \bar{\tau}_{srp}(0) & \text{otherwise.} \end{cases} \tag{5.21}$$

Assuming that there are m operational RWs and the failed RWs are at zero speed, the linearization yields the system of equations

$$\begin{bmatrix} \dot{\bar{\Theta}} \\ \dot{\bar{\omega}} \end{bmatrix} = \begin{bmatrix} 0 & I_3 \\ \bar{J}^{-1}\bar{T} & \bar{J}^{-1}J_w\left[\bar{W}_a\bar{\nu}_{a,0}\right]^{\times} \end{bmatrix} \begin{bmatrix} \bar{\Theta} \\ \bar{\omega} \end{bmatrix} + \begin{bmatrix} 0 \\ -\bar{J}^{-1}J_w\bar{W}_a \end{bmatrix} \delta\bar{z}_a, \tag{5.22}$$

where $\delta\bar{z}_a = \bar{z}_a - \bar{z}_{a,0}$ and $\bar{T}$ is the linearized matrix of $\bar{\tau}_{srp}$, i.e., $\bar{\tau}_{srp} = \bar{\tau}_{srp}(0) + \bar{T}\bar{\Theta}$.

Letting $\bar{x} = [\ \bar{\Theta}\ \ \bar{\omega}\ ]^{\mathrm{T}}$, it follows that

$$\dot{\bar{x}} = \bar{A}\bar{x} + \bar{B}\delta\bar{z}_a, \tag{5.23}$$

where

$$\bar{A} = \begin{bmatrix} 0 & I_3 \\ \bar{J}^{-1}\bar{T} & \bar{J}^{-1}J_w\left[\bar{W}_a\bar{\nu}_{a,0}\right]^{\times} \end{bmatrix}, \qquad \bar{B} = \begin{bmatrix} 0 \\ -\bar{J}^{-1}J_w\bar{W}_a \end{bmatrix}. \tag{5.24}$$

5.3 Solar Radiation Pressure Torque on a Symmetric Body Spacecraft

To provide insight into the effects of SRP, a general class of symmetric body spacecraft that have pairs of panels with the same area and diffusion coefficients (i.e., same β_j), located on the opposite ends of the spacecraft, is now considered. The panels are equal distance away from the reference point B, and the normals to the panels are parallel but opposite in direction. Denote one panel in this pair by '$p+$' and another by '$p-$'. Then,

$$\begin{gathered} \vec{r}_{p+/B} = -\vec{r}_{p-/B} = \vec{r}_p, \\ \hat{u}_{n,p+} = -\hat{u}_{n,p-} = \hat{u}_p, \\ \beta_{p+} = \beta_{p-} = \beta_p, \\ A_{p-} = A_{p+} = A_p. \end{gathered} \tag{5.25}$$

The SRP torque exerted by each individual panel, assuming they are exposed to the Sun, is

$$\begin{aligned}\vec{\tau}_{p+} &= (\vec{r}_{p+} - \vec{r}_{O/B})\times A_{p+}\vec{P}_{p+}, \\ &= \gamma_p((\vec{r}_p \times \hat{u}_p) + \beta_p(\vec{r}_p \times \hat{u}_s) - (\vec{r}_{O/B} \times \hat{u}_p) - \beta_p(\vec{r}_{O/B} \times \hat{u}_s)),\end{aligned} \tag{5.26}$$

$$\begin{aligned}\vec{\tau}_{p-} &= (\vec{r}_{p-} - \vec{r}_{O/B})\times A_{p-}\vec{P}_{p-}, \\ &= \gamma_p(-(\vec{r}_p \times \hat{u}_p) + \beta_p(\vec{r}_p \times \hat{u}_s) - (\vec{r}_{O/B} \times \hat{u}_p) + \beta_p(\vec{r}_{O/B} \times \hat{u}_s)),\end{aligned} \tag{5.27}$$

where $\gamma_p = -\alpha A_p(\hat{u}_p \cdot \hat{u}_s)$. The total SRP torque induced by the two panels is

$$\vec{\tau}_p = \vec{\tau}_{p+}\tilde{I}_{p+} + \vec{\tau}_{p-}\tilde{I}_{p-}. \tag{5.28}$$

By the assumption on directions of $\hat{u}_{p+}$ and $\hat{u}_{p-}$, $\tilde{I}_{p+}$ takes on the opposite binary value of $\tilde{I}_{p-}$ if $\gamma_p \neq 0$. If $\gamma_p = 0$, then the pair of panels does not induce any SRP torque. Knowing this, and noting that the second and third terms of (5.26) and (5.27) are the same while the first and fourth terms differ by a sign, (5.28) can be written as

$$\vec{\tau}_p = \gamma_p((-\vec{r}_{O/B} \times \hat{u}_p) + \beta_p(\vec{r}_p \times \hat{u}_s) + \text{sign}(\hat{u}_p \cdot \hat{u}_s)((\vec{r}_p \times \hat{u}_p) - \beta_p(\vec{r}_{O/B} \times \hat{u}_s))). \tag{5.29}$$

5.4 Conditions for Zero Solar Radiation Pressure Torque for All Orientations

There are cases in which the total SRP torque exerted on the spacecraft is zero for all possible orientations. Hence utilization of SRP for control is not possible. Theorem 5.2 gives a condition for which a symmetric body spacecraft covered in

pairs of symmetric panels will experience zero SRP torque, regardless of $\bar{\Theta}$.

Theorem 5.2: Let a symmetric body spacecraft be covered with ρ_s pairs of panels, having characteristics satisfying (5.25). Then the SRP torque induced on the spacecraft is zero for all $\bar{\Theta}$ if the three relations,

$$\vec{r}_i \;||\; \hat{u}_i, \quad i = 1, \ldots, \rho_s,$$

$$\vec{r}_{O/B} = 0, \tag{5.30}$$

$$\exists a \in \mathbb{R} : \sum_{i=1}^{\rho_s} \beta_i A_i \bar{r}_i \check{u}_i^{\mathrm{T}} = a I_3,$$

are all satisfied, where $\bar{r}_i = \vec{r}_i|_{\mathcal{B}}$ and $\check{u}_i = \hat{u}_i|_{\mathcal{B}}$.

Proof: The total SRP torque exerted on the symmetric spacecraft can be written using (5.29),

$$\vec{\tau}_{srp} = \sum_{i=1}^{\rho_s} \gamma_i \left((-\vec{r}_{O/B} \times \hat{u}_i) + \beta_i (\vec{r}_i \times \hat{u}_i) + \mathrm{sign}(\hat{u}_i \cdot \hat{u}_s) \left((\vec{r}_i \times \hat{u}_i) - \beta_i (\vec{r}_{O/B} \times \hat{u}_s) \right) \right). \tag{5.31}$$

If the first two conditions of (5.30) hold, (5.31) becomes

$$\vec{\tau}_{srp} = \sum_{i=1}^{\rho_s} \gamma_i \beta_i (\vec{r}_i \times \hat{u}_i). \tag{5.32}$$

Let $\check{u}_s = \hat{u}_s\big|_I$. Resolving (5.32) in $\mathcal{B}$ yields

$$\bar{\tau}_{srp} = -\alpha \left(\left(\sum_{i=1}^{\rho_s} \beta_i A_i \bar{r}_i \check{u}_i^{\mathrm{T}} \right) \mathbf{B} \check{u}_s \right) \times (\mathbf{B} \check{u}_s). \tag{5.33}$$

If the third condition of (5.30) holds, then there exists an $a \in \mathbb{R}$ such that

$$\bar{\tau}_{srp} = -a\alpha \mathbf{B} \check{u}_s \times \mathbf{B} \check{u}_s = 0. \tag{5.34}$$

Therefore regardless of orientation, the SRP will not exert any torques on the spacecraft. □

An example of when Theorem 5.2 holds is for a cuboid spacecraft where the reference point B coincides both with the COM and the center of solar radiation pressure of the spacecraft. See Section 5.7.1.

5.5 Stability of a Spacecraft

In general, the open-loop spacecraft attitude dynamics for a fixed attitude equilibrium without SRP are unstable, though the dynamics of the angular velocities can be stable depending on the axis of rotation [64]. As we discuss in this section, a fixed attitude equilibrium of an underactuated spacecraft with SRP has similar open-loop instability properties.

5.5.1 Linear Stability with Zero Solar Radiation Pressure

Consider the case of an underactuated spacecraft with two operational RWs where effects of SRP torques are zero (i.e., $\vec{\tau}_{srp} = 0$). The state matrix $\bar{A}$ in (5.24) becomes

$$\bar{A} = \begin{bmatrix} 0 & I_3 \\ 0 & \bar{J}^{-1} J_w \left[\bar{W}_a \bar{\nu}_{a,0}\right]^\times \end{bmatrix}. \tag{5.35}$$

The eigenvalues of matrix $\bar{A}$, denoted as λ, are given by

$$\lambda = 0,\ 0,\ 0,\ 0,\ \pm J_w \sqrt{(\bar{W}_a \bar{\nu}_{a,0})^{\mathrm{T}} \bar{D} (\bar{W}_a \bar{\nu}_{a,0})}, \tag{5.36}$$

where $\bar{D} = -(\mathrm{diag}(J_2 J_3,\ J_1 J_3,\ J_1 J_2))^{-1}$. The matrix $\bar{D}$ is negative definite, and, therefore, $\bar{A}$ might have one pair of purely imaginary eigenvalues, provided at least one of the RW speeds at the equilibrium is nonzero. Therefore, all eigenvalues lie on

the imaginary axis.

The requirement for stability of a linear system with eigenvalues on the imaginary axis and in the open left half plane is that each eigenvalue with zero real part must be semi-simple, i.e.,, the geometric multiplicity of the eigenvalue must be equal to its algebraic multiplicity. There is only one pair of purely imaginary eigenvalues, and so both are semi-simple. Any instability may thus be caused only by the zero eigenvalue. It can be shown that the algebraic multiplicity of the zero eigenvalue of A is four, while its geometric multiplicity is three. Thus the linearized system is open-loop unstable.

We note that the angular velocity variables are decoupled from the orientation variables for this linearized system. The state matrix for the angular velocities, denoted as $\bar{A}_\omega$, is given by

$$\bar{A}_w = \bar{J}^{-1} J_w \left[\bar{W}_a \bar{\nu}_{a,0}\right]^\times, \tag{5.37}$$

whose eigenvalues, λ_w, are

$$\lambda_w = 0, \;\; \pm J_w \sqrt{(\bar{W}_a \bar{\nu}_{a,0})^{\mathrm{T}} \bar{D} (\bar{W}_a \bar{\nu}_{a,0})}. \tag{5.38}$$

All the eigenvalues of $\bar{A}_w$ are semi-simple, and hence it can be shown that the linearized angular velocity dynamics are stable but not asymptotically stable. Due to the double integrator structure of $\bar{A}$, bounded angular velocities may cause unbounded drift in the attitude, resulting in instability.

5.5.2 Stability Analysis of Linearized Underactuated Spacecraft Dynamics with Solar Radiation Pressure Torque

We now consider the case with nonzero SRP torque (i.e., $\vec{\tau}_{srp} \neq 0$) and two functioning RWs spinning about the first and second principal axes. We analyze the stability properties of the spacecraft bus (relative) equilibrium corresponding to $\bar{\Theta} = \bar{\omega} =$

0. It is assumed that $\bar{\tau}_{srp}(0)$ is consistent with Theorem 5.1 so that the (relative) equilibrium can be maintained. Let the RW accelerations be set according to the following control law,

$$\delta\bar{z}_a = -(\bar{C}^{\mathrm{T}}\bar{C})^{-1}\bar{C}^{\mathrm{T}}\bar{J}^{-1}\bar{T}\bar{\Theta}, \tag{5.39}$$

where $\bar{C} = -(\bar{J}^{-1}J_{_w}\bar{W}_{_a})$. The feedback law in (5.39) cancels out the SRP torque components that are in the range of $\bar{W}_{_a}$. Then the dynamics matrix has the following form,

$$\bar{A} = \begin{bmatrix} 0 & I_3 \\ \bar{T}_3 & \bar{J}^{-1}J_{_w}\left[\bar{W}_{_a}\bar{\nu}_{_{a,0}}\right]^{\times} \end{bmatrix}, \tag{5.40}$$

where

$$\bar{T}_3 = \begin{bmatrix} 0 & 0 & 0 \\ 0 & 0 & 0 \\ \tilde{t}_{31} & \tilde{t}_{32} & \tilde{t}_{33} \end{bmatrix}, \tag{5.41}$$

and $\tilde{t}_{3j} \in \mathbb{R},\ j = 1, 2, 3$. Computing the eigenvalues of $\bar{A}$ yields three zero eigenvalues, a pair of complex eigenvalues, and an eigenvalue that is purely real. The zero eigenvalue has a geometric multiplicity of two and is, therefore, not semi-simple. Hence the equilibrium is unstable based on the linearized model. In addition, as apparent from (5.23), the SRP torque causes a coupling between the attitude and angular velocity dynamics which does not allow the independent analysis of the stability of angular velocity dynamics.

5.5.3 Nonlinear Stability

The analysis above is based on the linear model in (5.23). Since the linearized model has eigenvalues on the imaginary axis, the stability analysis is inconclusive as the stability/instability of an equilibrium in such a case may depend on nonlinear terms. Note that without SRP, there do exist stable equilibria where the spacecraft can

maintain directional pointing while rotating about an axis parallel to the pointing direction [64]. However, the analysis above suggests that a fixed attitude equilibrium either with or without SRP can be unstable. Intuitively, if one of the angular velocities is perturbed away from 0, a bounded drift in the Euler angles away from equilibrium can occur. This instability conclusion, supported by the linear analysis, has been verified through extensive simulations on a nonlinear model. The formal mathematical proof of instability, e.g., based on an application of Chetaev's theorem [113], is left to future work.

5.6 Regaining Linear Controllability Using Solar Radiation Pressure

5.6.1 Necessary and Sufficient Conditions for Regaining Linear Controllability

Without the effects of SRP included in (5.23), the spacecraft dynamics are linearly uncontrollable by RW accelerations if only two RWs are functioning. The following theorem gives necessary and sufficient conditions for restoring linear controllability to a spacecraft with two functioning RWs when SRP torques are included.

Theorem 5.3: Let the spacecraft have two operational RWs whose spin axes are non-parallel (i.e., rank($\bar{W}_a$)=2). The system (5.23) is linearly controllable if and only if for every eigenvalue λ of $\bar{A}$, and for any vector $\bar{\eta}_u$ in the null space of $\bar{W}_a^{\mathrm{T}}$,

$$\bar{\eta}_u^{\mathrm{T}}(\bar{J}\lambda^2 - \left[\bar{W}_a\bar{\nu}_{a,0}\right]^{\times}\lambda - \bar{T}) \neq 0. \tag{5.42}$$

Proof: The Popov-Belevitch-Hautus (PBH) test for controllability implies that (5.23)

is linearly controllable if and only if

$$\operatorname{rank}\left(\begin{bmatrix}\lambda I_6 - \bar{A} & \bar{B}\end{bmatrix}\right) = \dim(\bar{A}) \tag{5.43}$$

for every eigenvalue λ of $\bar{A}$, see [76]. By the converse, the system in (5.23) is uncontrollable if and only if there exists a nonzero vector $\bar{\eta} \in \mathbb{C}^6$ such that

$$\bar{\eta}^{\mathrm{CT}} \begin{bmatrix}\lambda I_6 - \bar{A} & \bar{B}\end{bmatrix} = 0, \tag{5.44}$$

for at least one eigenvalue, where $\bar{*}^{\mathrm{CT}}$ is the conjugate transpose of $\bar{*}$. Equation (5.44) can be reduced to two conditions,

$$\begin{aligned}\bar{\eta}^{\mathrm{CT}}(\lambda I_6 - \bar{A}) &= 0,\\ \bar{\eta}^{\mathrm{CT}}\bar{B} &= 0.\end{aligned} \tag{5.45}$$

Let $\bar{\eta} = [\ \bar{\eta}_1^{\mathrm{CT}}\ \ \bar{\eta}_2^{\mathrm{CT}}\ ]^{\mathrm{CT}}$, $\bar{\eta}_1, \bar{\eta}_2 \in \mathbb{C}^3$. Expanding the first condition of (5.45), it follows that

$$\begin{gathered}\bar{\eta}_1^{\mathrm{CT}}\lambda - \bar{\eta}_2^{\mathrm{CT}}\bar{J}^{-1}\bar{T} = 0,\\ -\bar{\eta}_1^{\mathrm{CT}} + \bar{\eta}_2^{\mathrm{CT}}(I_3 - \bar{J}^{-1}J_w\left[\bar{W}_a\bar{\nu}_{a,0}\right]^{\times}) = 0.\end{gathered} \tag{5.46}$$

Multiplying the second equation of (5.46) by λ and adding it together with the first equation of (5.46) gives

$$\bar{\eta}_2^{\mathrm{CT}}\left(I_3\lambda^2 - \bar{J}^{-1}J_w\left[\bar{W}_a\bar{\nu}_{a,0}\right]^{\times} - \bar{J}^{-1}\bar{T}\right) = 0. \tag{5.47}$$

The second condition of (5.45) can be simplified to

$$\bar{\eta}_2^{\mathrm{CT}}\bar{J}^{-1}J_w\bar{W}_a = 0. \tag{5.48}$$

Taking the conjugate transpose of (5.48), and noting that $\bar{W}_{a}^{\mathrm{CT}} = \bar{W}_{a}^{\mathrm{T}}$, $J_{w}^{\mathrm{CT}} = J_{w}$, and $(\bar{J}^{-1})^{\mathrm{CT}} = \bar{J}^{-1}$, yields

$$J_{w}\bar{W}_{a}^{\mathrm{T}}\bar{J}^{-1}\bar{\eta}_{2} = 0. \tag{5.49}$$

Let $\tilde{\eta}_{2}$ be the real part of $\bar{\eta}_{2}$. Then $\bar{J}^{-1}\tilde{\eta}_{2}$ is in null space of $\bar{W}_{a}^{\mathrm{T}}$. Denoting $\bar{\eta}_{u} = \bar{J}^{-1}\tilde{\eta}_{2}$, (5.47) can be written as

$$\bar{\eta}_{u}^{\mathrm{T}}(\bar{J}\lambda^{2} - \left[\bar{W}_{a}\bar{\nu}_{a,0}\right]^{\times}\lambda - \bar{T}) = 0. \tag{5.50}$$

Thus for (5.23) to be uncontrollable, there must exist an $\bar{\eta}_{u}$ in the null space of $\bar{W}_{a}^{\mathrm{T}}$ and an eigenvalue λ such that (5.50) holds. Reversing the arguments, it can be similarly show that if for each eigenvalue of $\bar{A}$ (5.50) cannot be satisfied with $\bar{\eta}_{u}$ in the null space of $\bar{W}_{a}^{\mathrm{T}}$, then the system is controllable. $\square$

Corollary 5.1: Theorem 5.3 can be simplified for the case when there are two operational RWs about the first two principal moments of inertia, i.e.,

$$\bar{W}_{a} = \begin{bmatrix} 1 & 0 \\ 0 & 1 \\ 0 & 0 \end{bmatrix}. \tag{5.51}$$

Let $t_{3,i},\ i = 1, 2, 3$, be the ith entry of the 3rd row of $\bar{T}$. Since $\tilde{\eta}_{u}$ is in the null of $\bar{W}_{a}^{\mathrm{T}}$, $\bar{\eta}_{u} = [\ 0 \quad 0 \quad \eta\ ]^{\mathrm{T}}$, where $\eta \in \mathbb{R}$. Equation (5.50) can be rewritten as

$$\eta\lambda^{2}\begin{bmatrix} 0 & 0 & J_{3} \end{bmatrix} - \eta\lambda\begin{bmatrix} -J_{w}\nu_{0,2} & J_{w}\nu_{0,1} & 0 \end{bmatrix} = \eta\begin{bmatrix} t_{31} & t_{32} & t_{33} \end{bmatrix}, \tag{5.52}$$

which gives the following three equations

$$J_3\lambda^2 = \tilde{t}_{33},$$

$$J_w\nu_{0,2}\lambda = \tilde{t}_{31}, \tag{5.53}$$

$$J_w\nu_{0,1}\lambda = -\tilde{t}_{32}.$$

For the system to be uncontrollable, the three equations of (5.53) must all hold for at least one eigenvalue of $\bar{A}$. By the converse, if for each eigenvalue of $\bar{A}$, one of the equations in (5.50) is not satisfied (it does not have to be the same equation for each eigenvalue), the system is controllable. □

Theorem 5.4 presented below is a consequence of Theorem 5.3 and provides a sufficient condition for an underactuated system to remain linearly uncontrollable even if SRP torques are added into the math model.

Theorem 5.4: Let the spacecraft be equipped with two operational RWs whose spin axes are not parallel. The system (5.23) is linearly uncontrollable if $\bar{\eta}_u^{\mathrm{T}}\bar{T} = 0$ for $\bar{\eta}_u$ in the null space of $\bar{W}_a^{\mathrm{T}}$.

Proof: Suppose that for $\bar{\eta}_u$ in the null space of $\bar{W}_a^{\mathrm{T}}$,

$$\bar{\eta}_u^{\mathrm{T}}\bar{T} = 0. \tag{5.54}$$

By Theorem 5.3, if there exists an eigenvalue λ of $\bar{A}$ such that

$$\bar{\eta}_u^{\mathrm{T}}(\bar{J}\lambda^2 - \left[\bar{W}_a\bar{\nu}_{a,0}\right]^{\times}\lambda - \bar{T}) = 0, \tag{5.55}$$

then the system is uncontrollable. Equation (5.54) simplifies (5.55) to

$$\bar{\eta}_u^{\mathrm{T}}(\bar{J}\lambda^2 - \left[\bar{W}_a\bar{\nu}_{a,0}\right]^{\times}\lambda) = 0. \tag{5.56}$$

If (5.54) holds then $\bar{T}$ is not full rank, which implies that $\bar{A}$ is not full rank and contains a zero eigenvalue. The eigenvalue $\lambda = 0$ satisfies (5.56), and therefore the system is uncontrollable. $\square$

Remark 5.2: The results in Theorem 5.3, Corollary 5.1, Theorem 5.4, and numerical examples suggest that the dynamics of the spacecraft with two RWs and SRP effects included are linearly controllable in a broad range of cases. Theorem 5.4 indicates that the linearized SRP torque must have nonzero projection on the uncontrolled direction for linear controllability to hold.

5.6.2 Relative Controllability

To assess the relative controllability of different spacecraft configurations, we consider the following controllability index:

$$J = \lambda_{max}\left(e^{\bar{A}^{\mathrm{T}}(t_f - t_0)}\bar{G}(t_f, t_0)^{-1}e^{\bar{A}(t_f - t_0)}\right), \tag{5.57}$$

where λ_{max} denotes the maximum eigenvalue of a matrix, t_0 is the initial time of the maneuver, t_f is the final time of the maneuver, and $\bar{G}(t_f, t_0)$ denotes the controllability gramian. The controllability index J corresponds to the maximum effort (where effort is defined as the minimum of the integral of the input squared) required to bring an initial state $\bar{x}(t_0)$ of unit norm to zero. Note that the metric is defined over a finite time interval given that the system is open-loop unstable. This metric will be used later to assess the controllability of the cuboid spacecraft.

5.7 Solar Radiation Pressure Effects on a Cuboid Spacecraft

Suppose that the spacecraft of interest is a cuboid which is a commonly used spacecraft shape. This spacecraft has a symmetric body and has dimensions L_x, L_y and L_z. Let $\hat{u}_1$ $\hat{u}_2$ and $\hat{u}_3$ be the normals to the panels covering the spacecraft sides which, due to the structure of the cuboid, are parallel to the principal axes. The reference point B is chosen as the geometric center of the cuboid spacecraft. Using the notation from Section 5.3, the parameters to obtain the SRP torque are defined as

$$\bar{r}_1 = \begin{bmatrix} \frac{L_x}{2} \\ 0 \\ 0 \end{bmatrix}, \quad \bar{r}_2 = \begin{bmatrix} 0 \\ \frac{L_y}{2} \\ 0 \end{bmatrix}, \quad \bar{r}_3 = \begin{bmatrix} 0 \\ 0 \\ \frac{L_z}{2} \end{bmatrix}, \tag{5.58}$$

$$\breve{u}_1 = \begin{bmatrix} 1 \\ 0 \\ 0 \end{bmatrix}, \quad \breve{u}_2 = \begin{bmatrix} 0 \\ 1 \\ 0 \end{bmatrix}, \quad \breve{u}_3 = \begin{bmatrix} 0 \\ 0 \\ 1 \end{bmatrix}, \tag{5.59}$$

$$A_1 = L_y L_z, \quad A_2 = L_x L_z, \quad A_3 = L_x L_y. \tag{5.60}$$

The COM of the spacecraft bus will also be offset from B, and

$$\bar{r}_{O/B} = \vec{r}_{O/B}\big|_{\mathcal{B}} = [\ l_x \ \ l_y \ \ l_z\ ]^{\mathrm{T}}. \tag{5.61}$$

This offset is of particular importance, as it influences the relative controllability of the system.

5.7.1 Conditions for Zero Solar Radiation Pressure

Based on Theorem 5.2, it may be shown that, under certain conditions, the cuboid spacecraft can experience zero SRP torque for all $\bar{\Theta}$. By the physical structure of the cuboid spacecraft, $\vec{r}_i \mid\mid \hat{u}_i,\ i = 1, 2, 3$, and so the first condition of (5.30) in Theorem 5.2 is satisfied. If B is aligned with the COM (i.e., $\vec{r}_{O/B} = 0$), the second condition of (5.30) is satisfied. Assume that the diffusion coefficient is the same for all panels ($\beta_1 = \beta_2 = \beta_3 = \beta$). Then, using the definitions in (5.58)-(5.60),

$$\sum_{i=1}^{3} \beta_i A_i \bar{r}_i \check{u}_i^{\mathrm{T}} = \frac{\beta L_x L_y L_z}{2} I_{3\times 3}, \tag{5.62}$$

which satisfies the third condition of (5.30) with $a = \frac{L_x L_y L_z}{2}$. Therefore by Theorem 5.2, if $\vec{r}_{O/B} = 0$ and all panels have the same diffusion properties, a cuboid spacecraft will experience zero SRP torque. It should be noted that if $\beta_i,\ i = 1, 2, 3$, were different, the conditions for zero SRP torque given by Theorem 5.2 may not hold and it may be possible to take advantage of SRP torques to recover linear controllability.

5.7.2 Equilibrium Analysis

Let $\vec{\tau}_{srp,x}$, $\vec{\tau}_{srp,y}$ and $\vec{\tau}_{srp,z}$ be the SRP torques exerted on the cuboid spacecraft by panels whose normals are parallel with the principal axes. Suppose that $\check{u}_s = [\, n_1 \ \ n_2 \ \ n_3 \,]^{\mathrm{T}}$ and let $\bar{\Theta} = 0$. Then the SRP torques exerted on the spacecraft, given by (5.29), resolved in $\mathcal{B}$, are

$$\vec{\tau}_{srp,x}\big|_B = \bar{\tau}_{srp,x} = \frac{A_1 \alpha n_1}{2} \begin{bmatrix} 0 \\ 2l_z + L_x \beta n_3 \\ -2l_y - L_x \beta n_2 \end{bmatrix} + \mathrm{sign}(n_1) A_1 \alpha n_1 \beta \begin{bmatrix} l_y n_3 - l_z n_2 \\ l_z n_1 - l_x n_3 \\ l_x n_2 - l_y n_1 \end{bmatrix}, \tag{5.63}$$

$$\vec{\tau}_{srp,y}\big|_B = \bar{\tau}_{srp,y} = \frac{A_2\alpha n_2}{2}\begin{bmatrix} -2l_z - L_y\beta n_3 \\ 0 \\ 2l_x + L_y\beta n_1 \end{bmatrix} + \text{sign}(n_2)A_2\alpha n_2\beta \begin{bmatrix} l_y n_3 - l_z n_2 \\ l_z n_1 - l_x n_3 \\ l_x n_2 - l_y n_1 \end{bmatrix}, \quad (5.64)$$

$$\vec{\tau}_{srp,z}\big|_B = \bar{\tau}_{srp,z} = \frac{A_3\alpha n_3}{2}\begin{bmatrix} 2l_y + L_z\beta n_2 \\ -2l_x - L_z\beta n_1 \\ 0 \end{bmatrix} + \text{sign}(n_3)A_3\alpha n_3\beta \begin{bmatrix} l_y n_3 - l_z n_2 \\ l_z n_1 - l_x n_3 \\ l_x n_2 - l_y n_1 \end{bmatrix}. \quad (5.65)$$

The conditions for $\bar{\Theta} = \bar{\omega} = 0$ to be a feasible closed-loop (relative) equilibrium are given by Theorem 5.1 and supported by (5.63)-(5.65). Suppose, for instance, $l_x = l_z = 0$ while l_y is nonzero, while the operational RWs have spin axes aligned with the first and second principal axes. If $n_1 = 0$, $n_2 = 1$, and $n_3 = 0$, then based on the above expressions, $\tau_{srp}(0) = 0$, and the spacecraft can remain at the relative equilibrium with $\bar{\Theta} = \bar{\omega} = 0$ without any RWs accelerating. If the possibility of RWs accelerating to maintain the (relative) equilibrium at $\bar{\Theta} = \bar{\omega} = 0$ is acceptable (e.g., to enable the spacecraft to obtain images while compensating for nonzero SRP with RWs), then the condition can be relaxed. In this case, as long as $n_1 = 0$ (i.e., the third principal axis is not pointed towards the Sun), the SRP torque is of the form $\tau_{srp}(0) = [\ *\quad *\quad 0\ ]^{\mathrm{T}}$ (where $*$ is an arbitrary entry) and can be compensated by the available RWs that are along the first and second principal axes.

5.7.3 Relative Controllability of the Cuboid Spacecraft

To demonstrate controllability of the cuboid spacecraft, it is assumed that the spacecraft has parameters listed in Table 5.1, the first and second RWs are operational, and $\bar{\nu}_{_{a,0}} = [\ 100\ \ 100\ ]^{\mathrm{T}}$ rad/sec . The third and fourth RWs are assumed to have

previously failed and are now at zero speed. The plot of J in (5.57) versus l_y and the time of the maneuver t_f ($t_0 = 0$) is given in Figure 5.2. The spacecraft is more controllable for larger l_y, and the control effort decreases if longer maneuver time is available. Intuitively, more SRP torque is produced when the distance between the center-of-pressure and the COM is greater. This torque can be exploited to enhance controllability.

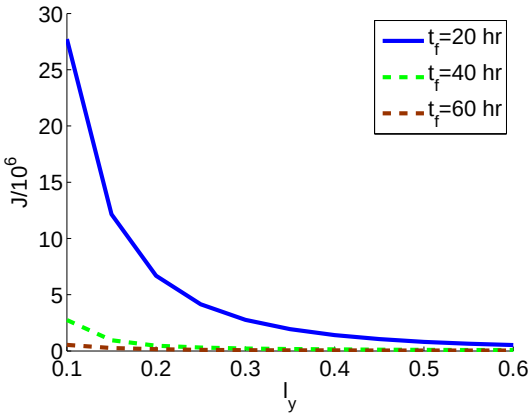

Figure 5.2: Controllability metric (scaled by 10^6) versus l_y and maneuver time, t_f.

5.8 Controller Design

Since the linearized dynamics of a spacecraft body with certain asymmetry properties are linearly controllable with the addition of SRP torques to the spacecraft model, a controller based on conventional Linear Quadratic (LQ) theory [114] can be used to stabilize the system to equilibrium. The LQ controller minimizes the cost

$$J_{LQ} = \int_0^\infty \bar{x}(\tau)^{\mathrm{T}} \bar{Q} \bar{x}(\tau) + \delta \bar{z}_a(\tau)^{\mathrm{T}} \bar{R} \delta \bar{z}_a(\tau) d\tau, \tag{5.66}$$

where $\bar{Q} = \bar{Q}^{\mathrm{T}} \geq 0$ and $\bar{R} = \bar{R}^{\mathrm{T}} > 0$ are weighting matrices. The controller has the following form,

$$\delta \bar{z}_a = \bar{K}_{LQ} \bar{x}, \tag{5.67}$$

where $\bar{K}_{LQ}$ is the LQ gain.

In the subsequent simulations, $\bar{R} = 1000 I_m$, where m is the number of operational RWs. If $m \geq 3$, $\bar{Q} = \text{diag}(10, 10, 10, 0.01, 0.01, 0.01)$ is used. If $m = 2$ and the only operational RWs spin about the first and second principal axes,
$\bar{Q} = \text{diag}(40, 10, 10, 0.04, 0.01, 0.01)$ is used to emphasize faster regulation of ϕ and ω_1 which improves the transient response.

5.9 Results

In this section, nonlinear simulations are presented where four wheels are initially operational. Two separate wheel failures occur during these simulations: one wheel fails at 5 hours and the other at 20 hours. The speed response of a failed wheel spinning down is modeled by a first order lag with a 10 min settling time. The simulations are run on the full nonlinear model of the spacecraft kinematics and dynamics, including the nonlinear model of SRP torques. All spacecraft parameters are given by Table 5.1. Nominally, $\check{u}_s = [\ 0 \quad 1 \quad 0\ ]^{\mathrm{T}}$, and simulation results are presented for two different sequences of wheel failures. Additional simulation results are then reported for the case when $\check{u}_s = [\ 0 \quad 1/\sqrt{2} \quad 1/\sqrt{2}\ ]^{\mathrm{T}}$, creating a situation where the RWs must accelerate to maintain spacecraft pointing. Finally, convergence times from different initial conditions are quantified.

Parameter	**Units**	**Value**
$\bar{J}_{\mathfrak{B}}$	kg m^2	diag(430, 1210, 1300)
J_w	kg m^2	0.043
L_x	m	2
L_y	m	2.5
L_z	m	5
l_x	m	0
l_y	m	0.1 and 0.5
l_z	m	0
$\bar{W}_c$	-	$\begin{bmatrix} 1 & 0 & 0 & 1/\sqrt{3} \\ 0 & 1 & 0 & 1/\sqrt{3} \\ 0 & 0 & 1 & 1/\sqrt{3} \end{bmatrix}$
$\bar{\Phi}_{sun}$	W/m^2	1367
$C_{diff,j}$	-	0.2
c	m/sec	299792458.0

Table 5.1: Model and control parameters for attitude control with SRP.

5.9.1 Wheel 3 Fails First

The first case considered is when RW 3 fails first, followed by RW 4. The offset of the center-of-pressure from the COM is given by $l_y = 0.5$ m and $l_x = l_z = 0$ m. The responses are shown in Figure 5.3. There is a much larger disturbance to orientation when the second wheel fails. The controller manages the first wheel failure quickly, then reconfigures and handles the second wheel failure over a longer period of time, coordinating two operational RWs in the presence of SRP.

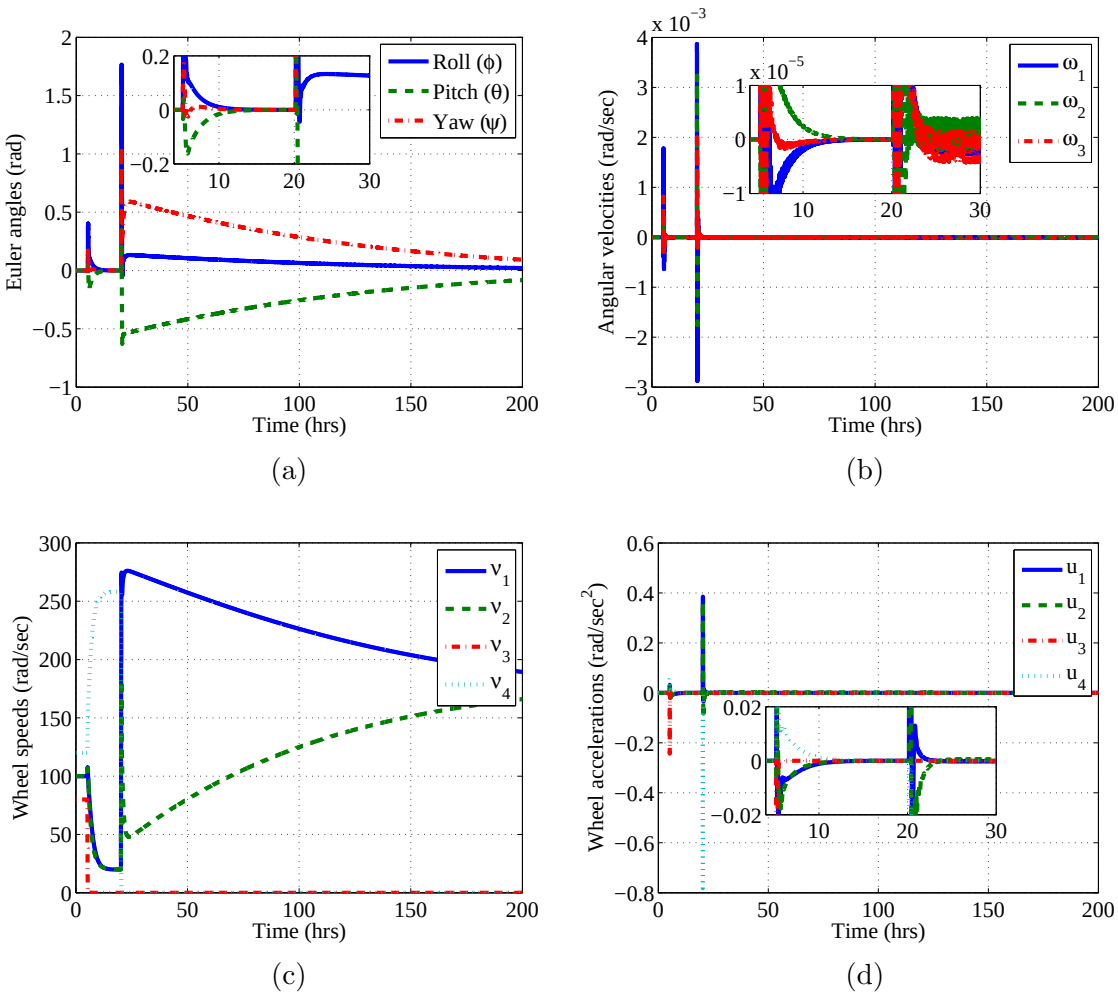

Figure 5.3: (a) Euler angles, (b) angular velocities, (c) RW speeds, and (d) RW accelerations in the nonlinear simulation when wheel 3 fails first, $l_y = 0.5$ m.

5.9.2 Wheel 4 Fails First, Reduced l_y

Now the case is considered when l_y is reduced to 0.1 m so that the spacecraft is less controllable (see Section 5.6.2). In this simulation, RW 4 fails first, followed by RW 3. The responses are shown in Figure 5.4. The controller is able to manage the failures and reduce the spacecraft orientation error over time. However, the responses are slower due to worse spacecraft controllability.

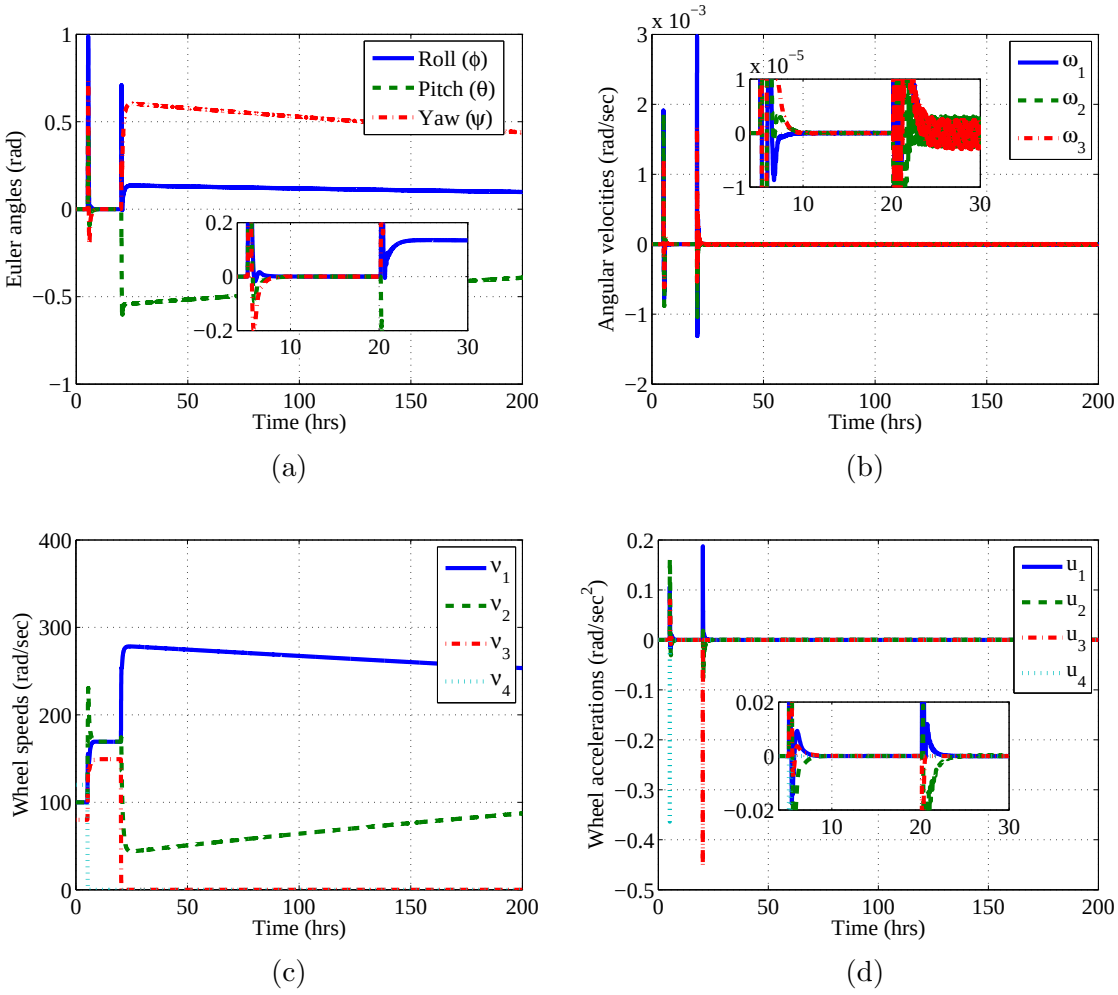

Figure 5.4: (a) Euler angles, (b) angular velocities, (c) RW speeds, and (d) RW accelerations in the nonlinear simulation when wheel 4 fails first, $l_y = 0.1$ m.

5.9.3 Wheel 4 Fails First, Skewed Pointing

In this case study, which is referred to as the skewed pointing, $l_y = 0.1$ m while $\bar{u}_s = [\ 0 \quad 1/\sqrt{2} \quad 1/\sqrt{2}\ ]^{\mathrm{T}}$. The controller is modified with an additional feed-forward term which cancels out $\bar{\tau}_{srp}(0)$. Note that the third component of $\bar{\tau}_{srp}(0)$ is zero, hence canceling the steady-state value of SRP torque by the acceleration of RWs 1 and 2 is feasible. The response is shown in Figure 5.5. Observe that the controller handles RW 3 and 4 failures and that RWs 1 and 2 continue to accelerate to be able to maintain the spacecraft orientation in steady-state with desired pointing.

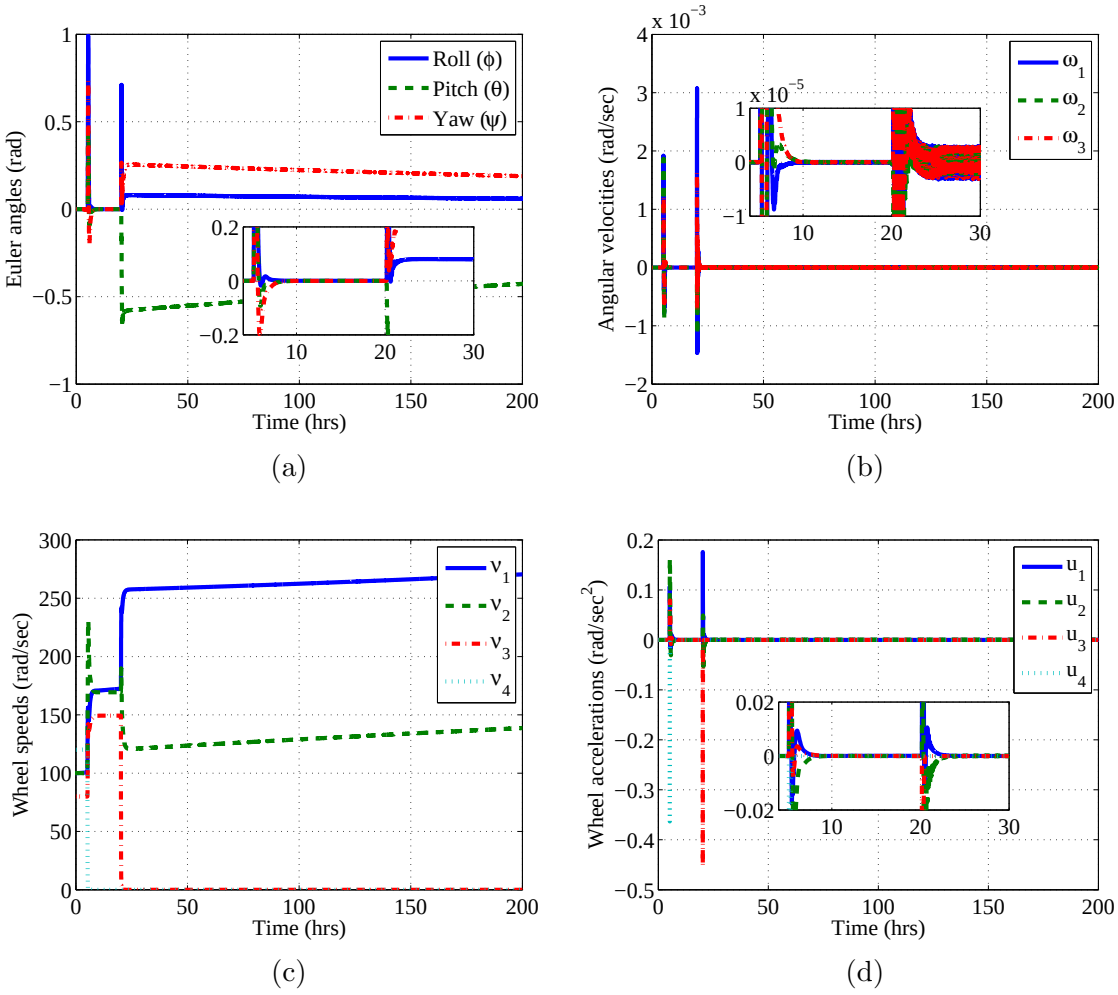

Figure 5.5: (a) Euler angles, (b) angular velocities, (c) RW speeds, and (d) RW accelerations in the nonlinear simulation when wheel 4 fails first, skewed pointing.

5.9.4 Achieving Faster Closed-loop Response Time

A faster linear controller may be designed using the pole placement method. As confirmed by simulations, more aggressive controllers, however, have smaller regions of attraction (ROA) for the nonlinear system, and are not able to always recover after the simulated sequence of wheel failures. If spacecraft thrusters (which are not as precise as reaction wheels) are employed to first reduce the attitude and angular velocity errors before the two functional RWs are used, the implementation of more aggressive controllers for RWs becomes feasible. Towards this end, a pole placement-based linear

controller was designed with the closed-loop poles of $-0.0137 \pm 0.0068i$, $-0.0208 \pm .0021i$, -0.0001, and -0.0075 (versus $-0.0012 \pm 0.0068i$, $-0.0019 \pm .0021i$, -6.4906×10^{-6}, and -0.007 for the nominal LQ controller), and Monte Carlo simulations were performed to characterize the closed-loop response from various initial conditions. For each simulation, the initial Euler angles were selected from a uniform distribution in the interval $[-2\ ,\ 2\ ]$ deg and the angular velocity was initially zero. Only two RWs (those aligned with the first two principal axes) were assumed to be functional, each initially rotating at a speed of 100 rad/sec. 1900 simulation runs were performed. The average time it took for the spacecraft orientation to enter a 0.001 deg box around the equilibrium was 35.1554 hours, with a standard deviation of 4.2532 hours. In all cases, the controller was convergent and able to bring the Euler angles to the target box. The maximum angular speed and accelerations of the wheels in these simulations were 247.5929 rad/sec and 9.7833 rad/sec^2, respectively, which are within actuator capability limits.

5.9.5 Regions of Attractions

Each controller has associated with it a unique ROA such that if the spacecraft starts within this region, the controller will stabilize the system to equilibrium. Such regions can be estimated by using scaled sublevel sets of the Lyapunov function for the linearized system, but these estimates may be quite conservative [113]. The ROA in our case cannot be easily or analytically described for an arbitrary spacecraft since the dynamics depend on the shape of spacecraft, the desired inertial pointing direction, the spin axis directions of operational RWs and the chosen control scheme. Therefore, nonlinear simulations are used to approximate the ROA for a cuboid spacecraft using the LQ and the pole placement controllers in this work. Five thousand random test simulations were run using each controller with initial Euler angles belonging to the interval of $[-60,\ 60]$ deg, initial zero angular velocity, and RW speeds initially at 100

rad/sec. The operational RWs are aligned with the first and second principal axes. The results for both controllers are shown in Figures 5.6 and 5.7, in which the red "x's" designate all the initial attitudes that the controllers can stabilize to the desired pointing equilibrium. As to be expected, the LQ controller has a larger ROA than the more aggressive pole placement controller.

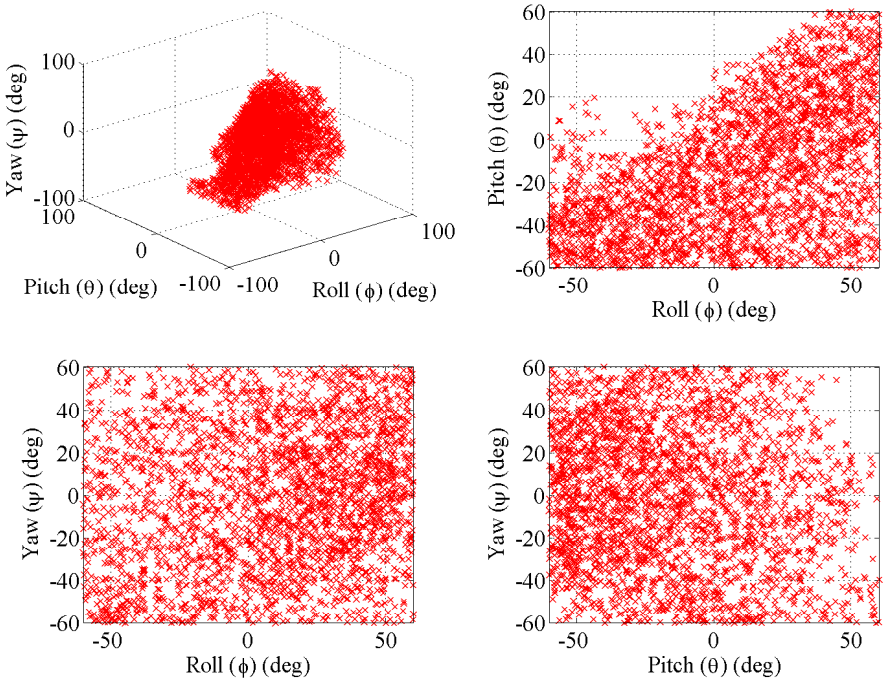

Figure 5.6: Numerical region of attraction calculation for the LQ controller.

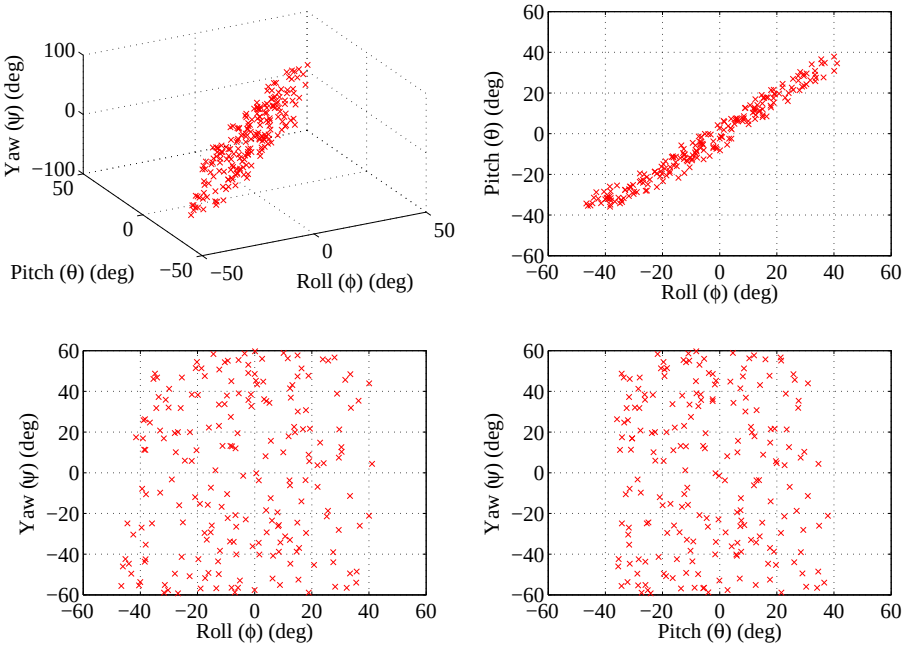

Figure 5.7: Numerical region of attraction calculation for the pole placement controller.

CHAPTER 6

Rotational and Translational Underactuated Control in a Gravity Field

In this chapter, the controllability of a spacecraft in a central gravity field equipped with only internal attitude actuators is addressed. The topic of controlling a spacecraft in a central gravity field when the translational and rotational dynamics are coupled has been discussed for dumbbell shaped [59, 60] and arbitrary shaped spacecraft [61], but in all cases the spacecraft was assumed to have actuation in the translational and rotational space, and in some cases, the spacecraft was fully actuated both in terms of translational and rotational degrees-of-freedom. The only work that has studied controllability of a spacecraft with only attitude actuators is that of Lian et. al [58], but its analysis is limited in that the translational equations are expressed in the inertial frame. In contrast to the previous literature, this chapter develops exact and approximate equations of motion that are relative to an equilibrium orbit (in a similar fashion to how the classical HCW equations are derived [62]). These new equations of motion yield controllability results that prove that controlled translational motion is possible by changing the attitude of a spacecraft.

6.1 Equations of Motion

The spacecraft under consideration in this chapter is a rigid spacecraft bus in a central gravity field equipped with either RWs or CMGs. Let this spacecraft system be denoted by $\mathfrak{T}$. In addition, we make the following assumption:

Assumption 6.1 The only force acting on the spacecraft system is gravity.

Since gravity is a conservative force, Assumption 6.1 implies that the total inertial angular momentum of the system (consisting of the spacecraft and the central body inducing the central gravity field) is conserved. Thus the attitude dynamics derived in Chapter 2 can be extended to coupled rotational and translational equations of motion with the help of an additional frame:

- A frame $\mathcal{C}$ rotating at a constant rate, associated with an equilibrium orbit of constant radius and with unit vectors $\hat{c}_x$, $\hat{c}_y$, and $\hat{c}_z$. The vector $\hat{c}_z$ is aligned with the rotation vector of the frame and is normal to the orbital plane, $\hat{c}_y$ is in the direction of the velocity vector (i.e., in-track), and $\hat{c}_x$ is given by the right hand rule $\hat{c}_x \times \hat{c}_y = \hat{c}_z$ and in the direction of the orbital radius projected onto the orbital plane.

Frame $\mathcal{C}$ can be seen as an intermediary frame between $\mathcal{I}$ and $\mathcal{B}$. In the following sections, we will let $\mathbf{C}$ and $\mathbf{D}$, respectively, be the orientation matrices of $\mathcal{C}$ relative to $\mathcal{I}$ and $\mathcal{B}$ relative to $\mathcal{C}$. Thus $\mathbf{B} = \mathbf{DC}$.

For a spacecraft modeled as a point mass, $\hat{c}_x$ is perfectly aligned with the orbital radial direction and $\mathcal{C}$ can be thought of as the traditional HCW frame [62]. These orbits, more commonly known as *great circle orbits*, have the orbit plane passing through the center of the gravitational field, see Figure 6.1 (a). For a general rigid spacecraft, such great circle orbits may not exist. In fact, if the spacecraft is asymmetric, it may have what is known as a *non-great circular orbit*, where $\hat{c}_x$ is not

aligned with the orbital radius and the orbit plane does not intersect the center of the gravitational field, see Figure 6.1 (b). There will always be for a general spacecraft at least one of these types of orbits, and conditions under which they occur is discussed in [48].

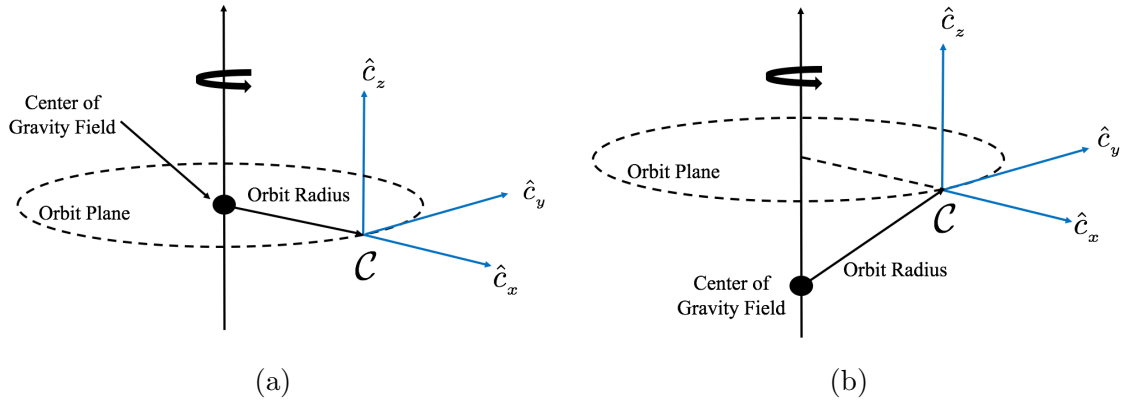

Figure 6.1: (a) Great circle orbit. (b) Non-great circle orbit.

In the following subsections, we derive a set of exact relative dynamics for controllability analysis and a set of approximate relative dynamics for simple controller analysis and design. We use the word relative as the equations of motion are written with the equilibrium orbit in mind. A summary of the equations, notations, and assumptions is given after the complete derivation.

6.1.1 Translational Equations Of Motion

6.1.1.1 Exact Translational Relative Equations

The linear momentum of the entire spacecraft system (including RWs and CMGs) COM, located at point O, relative to the center of the gravitational field, located at a point A, can be given as

$$\vec{p}_{O/A/\mathcal{I}} = m_{\mathfrak{T}} \overset{\mathcal{I}\cdot}{\vec{r}}_{O/A}. \tag{6.1}$$

The time rate of change of the linear momentum can expressed as

$$\overset{\mathcal{I}\cdot}{\vec{p}}_{O/A/\mathcal{I}} = m_{\mathfrak{T}} \overset{\mathcal{I}\cdot\cdot}{\vec{r}}_{O/A} = -\int_{\mathfrak{T}} \frac{\mu\left(\vec{r}_{O/A} + \vec{r}_{\rho/O}\right)}{\left|\vec{r}_{O/A} + \vec{r}_{\rho/O}\right|^3} dm, \tag{6.2}$$

where μ is the gravitational constant. Noting that $\mathcal{C}$ rotates at a constant rate, we can use the transport theorem to give

$$\begin{aligned} \overset{\mathcal{C}\cdot}{\vec{p}}_{O/A/\mathcal{C}} &= \overset{\mathcal{I}\cdot}{\vec{p}}_{O/A/\mathcal{C}} - 2\vec{\omega}_{\mathcal{C}/\mathcal{I}} \times \vec{p}_{O/A/\mathcal{C}} - m_{\mathfrak{T}} \vec{\omega}_{\mathcal{C}/\mathcal{I}} \times \left(\vec{\omega}_{\mathcal{C}/\mathcal{I}} \times \vec{r}_{O/A}\right). \\ &= -\int_{\mathfrak{T}} \frac{\mu\left(\vec{r}_{O/A} + \vec{r}_{\rho/O}\right)}{\left|\vec{r}_{O/A} + \vec{r}_{\rho/O}\right|^3} dm - 2\vec{\omega}_{\mathcal{C}/\mathcal{I}} \times \vec{p}_{O/A/\mathcal{C}} - m_{\mathfrak{T}} \vec{\omega}_{\mathcal{C}/\mathcal{I}} \times \left(\vec{\omega}_{\mathcal{C}/\mathcal{I}} \times \vec{r}_{O/A}\right). \end{aligned} \tag{6.3}$$

We now use the following notation

- $\bar{r} = \vec{r}_{O/A}\big|_{\mathcal{C}}$: Position vector of O relative to A expressed in $\mathcal{C}$,
- $\bar{\rho}_O = \vec{r}_{\rho/O}\big|_{\mathcal{B}}$: Position vector of an infinitesimal mass element relative to O expressed in $\mathcal{B}$,
- $\bar{p} = \vec{r}_{\mathfrak{T}/A/\mathcal{C}}\big|_{\mathcal{C}}$: Relative linear momentum vector of the spacecraft relative to point A expressed in $\mathcal{C}$,
- $\bar{\omega}_e = \vec{\omega}_{\mathcal{C}/\mathcal{I}}\big|_{\mathcal{C}}$: Angular velocity of $\mathcal{C}$ relative to $\mathcal{I}$ expressed in $\mathcal{C}$.

Resolving (6.3) in $\mathcal{C}$ and combining it with the kinematics gives the total, exact, relative translational equations of motion

$$\begin{aligned} \dot{\bar{r}} &= \tfrac{\bar{p}}{m_{\mathfrak{T}}}, \\ \dot{\bar{p}} &= -\int_{\mathfrak{T}} \frac{\mu\left(\bar{r} + \mathbf{D}^{\mathrm{T}}\bar{\rho}_O\right)}{\left|\bar{r} + \mathbf{D}^{\mathrm{T}}\bar{\rho}_O\right|^3} dm - 2\left[\bar{\omega}_e\right]^{\times} \bar{p} - m_{\mathfrak{T}} \left[\bar{\omega}_e\right]^{2\times} \bar{r}. \end{aligned} \tag{6.4}$$

6.1.1.2 Approximated Translational Relative Equations

We will now approximate the exact relative equations of motion (6.3) about an equilibrium trajectory by constructing equations in a similar fashion to how the traditional HCW dynamics are derived.

First, assume that there is a spacecraft of the same configuration as the deputy spacecraft $\mathfrak{T}$, fixed in $\mathcal{C}$, whose COM is moving in an unforced equilibrium orbit with position vector $\vec{r}_{C/A}$. We will call this spacecraft the "chief" and denote it by $\mathfrak{C}$. The objective is to determine the motion of spacecraft $\mathfrak{T}$, which we will refer to as the "deputy", relative to the chief. This is done by determining the relative linear momentum,

$$\begin{aligned} \overset{\mathcal{I}}{\vec{p}}_{\mathfrak{T}/\mathfrak{C}/\mathcal{I}} &= \overset{\mathcal{I}}{\vec{p}}_{\mathfrak{T}/A/\mathcal{I}} - \overset{\mathcal{I}}{\vec{p}}_{\mathfrak{C}/A/\mathcal{I}}, \\ &= -\int_{\mathfrak{T}} \frac{\mu\left(\vec{r}_{O/A}+\vec{r}_{\rho/O}\right)}{\left|\vec{r}_{O/A}+\vec{r}_{\rho/O}\right|^3} dm + \int_{\mathfrak{C}} \frac{\mu\left(\vec{r}_{C/A}+\vec{r}_{\rho/C}\right)}{\left|\vec{r}_{C/A}+\vec{r}_{\rho/C}\right|^3} dm. \end{aligned} \tag{6.5}$$

Using the transport theorem, (6.5) becomes

$$\begin{aligned} \overset{\mathcal{C}}{\vec{p}}_{\mathfrak{T}/\mathfrak{C}/\mathcal{C}} &= -\int_{\mathfrak{T}} \frac{\mu\left(\vec{r}_{C/A}+\vec{r}_{O/C}+\vec{r}_{\rho/O}\right)}{\left|\vec{r}_{C/A}+\vec{r}_{O/C}+\vec{r}_{\rho/O}\right|^3} dm + \int_{\mathfrak{C}} \frac{\mu\left(\vec{r}_{C/A}+\vec{r}_{\rho/C}\right)}{\left|\vec{r}_{C/A}+\vec{r}_{\rho/C}\right|^3} dm \\ &\quad -2\vec{\omega}_{\mathcal{C}/\mathcal{I}} \times \vec{p}_{O/C/\mathcal{C}} - m_{\mathfrak{T}}\vec{\omega}_{\mathcal{C}/\mathcal{I}} \times \left(\vec{\omega}_{\mathcal{C}/\mathcal{I}} \times \vec{r}_{O/C}\right). \end{aligned} \tag{6.6}$$

We now introduce the following notations:

- $R = |\vec{r}_{C/A}|$: Radius of the equilibrium orbit,
- $\bar{r}_r = \vec{r}_{O/C}\big|_{\mathcal{C}}$: Position vector of O relative to C expressed in $\mathcal{C}$,
- $\bar{r}_e = \vec{r}_{C/A}\big|_{\mathcal{C}}$: Position vector of C relative to A expressed in $\mathcal{C}$,
- $\bar{\rho}_C = \vec{r}_{\rho/O}\big|_{\mathcal{C}}$: Position of an infinitesimal mass element relative to O expressed in $\mathcal{C}$,
- $\check{r}_e = \frac{\bar{r}_e}{R}$: Unit vector in the direction of $\bar{r}_e$ expressed in $\mathcal{C}$,
- $\bar{p}_r = \vec{p}_{\mathfrak{T}/\mathfrak{C}/\mathcal{C}}\big|_{\mathcal{C}}$: Relative linear momentum of the spacecraft relative to C expressed in $\mathcal{C}$.

Resolving (6.6) in $\mathcal{C}$ gives

$$\dot{\bar{p}}_r = -\int_{\mathfrak{T}} \frac{\mu\left(\bar{r}_e+\bar{r}_r+\mathbf{D}^{\mathrm{T}}\bar{\rho}_O\right)}{\left|\bar{r}_e+\bar{r}_r+\mathbf{D}^{\mathrm{T}}\bar{\rho}_O\right|^3} dm + \int_{\mathfrak{C}} \frac{\mu\left(\bar{r}_e+\bar{\rho}_C\right)}{\left|\bar{r}_e+\bar{\rho}_C\right|^3} dm - 2\left[\bar{\omega}_e\right]^{\times}\bar{p}_r - m_{\mathfrak{T}}\left[\bar{\omega}_e\right]^{2\times}\bar{r}_r. \tag{6.7}$$

The denominators in the integral terms of (6.7) can be given as

$$\begin{aligned}
\left|\bar{r}_e+\bar{r}_r+\mathbf{D}^{\mathrm{T}}\bar{\rho}_O\right|^{-3} &= \left((\bar{r}_e+\bar{r}_r+\mathbf{D}^{\mathrm{T}}\bar{\rho}_O)^{\mathrm{T}}(\bar{r}_e+\bar{r}_r+\mathbf{D}^{\mathrm{T}}\bar{\rho}_O)\right)^{-\frac{3}{2}}, \\
&= \left(\bar{r}_e^{\mathrm{T}}\bar{r}_e + 2\bar{r}_e^{\mathrm{T}}(\bar{r}_r+\mathbf{D}^{\mathrm{T}}\bar{\rho}_O) + (\bar{r}_r+\mathbf{D}^{\mathrm{T}}\bar{\rho}_O)^{\mathrm{T}}(\bar{r}_r+\mathbf{D}r_\rho)\right)^{-\frac{3}{2}}, \\
&= R^{-3}\left(1+\tfrac{2\bar{r}_e^{\mathrm{T}}(\bar{r}_r+\mathbf{D}^{\mathrm{T}}\bar{\rho}_O)}{R^2}+\tfrac{|\bar{r}_r+\mathbf{D}^{\mathrm{T}}\bar{\rho}_O|^2}{R^2}\right)^{-\frac{3}{2}}, \\
&= R^{-3}\left(1+2\epsilon_1\cos(\kappa_1)+\epsilon_1^2\right)^{-\frac{3}{2}},
\end{aligned} \tag{6.8}$$

$$
\begin{aligned}
|\bar{r}_e + \bar{\rho}_C|^{-3} &= \left((\bar{r}_e + \bar{\rho}_C)^{\mathrm{T}}(\bar{r}_e + \bar{\rho}_C)\right)^{-\frac{3}{2}}, \\
&= \left(\bar{r}_e^{\mathrm{T}}\bar{r}_e + 2\bar{r}_e^{\mathrm{T}}\bar{\rho}_C + \bar{\rho}_C^{\mathrm{T}}r_\rho\right)^{-\frac{3}{2}}, \\
&= R^{-3}\left(1 + \tfrac{2\bar{r}_e^{\mathrm{T}}\bar{\rho}_C}{R^2} + \tfrac{|\bar{\rho}_C|^2}{R^2}\right)^{-\frac{3}{2}}, \\
&= R^{-3}\left(1 + 2\epsilon_2\cos(\kappa_2) + \epsilon_2^2\right)^{-\frac{3}{2}},
\end{aligned}
\tag{6.9}
$$

where $\epsilon_1 = \frac{|\bar{r}_r + \mathbf{D}^{\mathrm{T}}\bar{\rho}_O|}{R}$, $\epsilon_2 = \frac{|\bar{\rho}_C|}{R}$, κ_1 is the angle between $\bar{r}_e$ and $\bar{r}_r + \mathbf{D}^{\mathrm{T}}\bar{\rho}_O$, and κ_2 is the angle between $\bar{r}_e$ and $\bar{\rho}_C$. We now perform a Taylor-series expansion of (6.8) and (6.9) about $\epsilon_1 = \epsilon_2 = 0$, yielding

$$
\begin{aligned}
\left|\bar{r}_e + \bar{r}_r + \mathbf{D}^{\mathrm{T}}\bar{\rho}_O\right|^{-3} &= R^{-3}\left(1 - 3\tfrac{\bar{r}_e^{\mathrm{T}}(\bar{r}_r + D^{\mathrm{T}}\bar{\rho}_O)}{R^2} + 15\tfrac{(\bar{r}_e^{\mathrm{T}}(r + \mathbf{D}^{\mathrm{T}}\bar{\rho}_O))^2}{2R^4}\right) \\
&\quad + R^{-3}\left(-3\tfrac{|r + \mathbf{D}^{\mathrm{T}}\bar{\rho}_O|^2}{2R^2} + O(\epsilon_1^3)\right), \\
|\bar{r}_e + \bar{\rho}_C|^{-3} &= R^{-3}\left(1 - 3\tfrac{\bar{r}_e^{\mathrm{T}}\bar{\rho}_C}{R^2} + 15\tfrac{(\bar{r}_e^{\mathrm{T}}\bar{\rho}_C)^2}{2R^4} - 3\tfrac{|\bar{\rho}_C|^2}{2R^2} + O(\epsilon_2^3)\right).
\end{aligned}
\tag{6.10}
$$

Substituting (6.10) into the integral terms of (6.7) gives

$$
\begin{aligned}
-\int_{\mathfrak{T}} \frac{\mu\left(\bar{r}_e+\bar{r}_r+\mathbf{D}^{\mathrm{T}}\bar{\rho}_O\right)}{\left|\bar{r}_e+\bar{r}_r+\mathbf{D}^{\mathrm{T}}\bar{\rho}_O\right|^3}dm &= -\frac{\mu}{R^3}\int_{\mathfrak{T}}\left(\bar{r}_e+\bar{r}_r+\mathbf{D}^{\mathrm{T}}\bar{\rho}_O\right)\left(1-3\frac{\bar{r}_e^{\mathrm{T}}(\bar{r}_r+D^{\mathrm{T}}\bar{\rho}_O)}{R^2}\right)dm \\
&\quad -\frac{\mu}{R^3}\int_{\mathfrak{T}}\left(\bar{r}_e+\bar{r}_r+\mathbf{D}^{\mathrm{T}}\bar{\rho}_O\right)\left(15\frac{(\bar{r}_e^{\mathrm{T}}(\bar{r}_r+\mathbf{D}^{\mathrm{T}}\bar{\rho}_O))^2}{2R^4}\right)dm \\
&\quad +\frac{\mu}{R^3}\int_{\mathfrak{T}}\left(\bar{r}_e+\bar{r}_r+\mathbf{D}^{\mathrm{T}}\bar{\rho}_O\right)\left(3\frac{|\bar{r}_r+\mathbf{D}^{\mathrm{T}}\bar{\rho}_O|^2}{2R^2}+O(\epsilon_1^3)\right)dm, \\
&= -\frac{\mu}{R^3}\int_{\mathfrak{T}}\left(\bar{r}_e+\bar{r}_r+\mathbf{D}^{\mathrm{T}}\bar{\rho}_O\right)dm \\
&\quad -\frac{\mu}{R^3}\int_{\mathfrak{T}}\left(-3\frac{\bar{r}_e\bar{r}_e^{\mathrm{T}}\bar{r}_r}{R^2}-3\frac{\bar{r}_e\bar{r}_e^{\mathrm{T}}\mathbf{D}^{\mathrm{T}}\bar{\rho}_O}{R^2}-3\frac{\bar{r}_r\bar{r}_e^{\mathrm{T}}\bar{r}_r}{R^2}\right)dm \\
&\quad -\frac{\mu}{R^3}\int_{\mathfrak{T}}\left(-3\frac{\bar{r}_r\bar{r}_e^{\mathrm{T}}\mathbf{D}^{\mathrm{T}}\bar{\rho}_O}{R^2}-3\frac{\mathbf{D}^{\mathrm{T}}\bar{\rho}_O\bar{r}_e^{\mathrm{T}}\bar{r}_r}{R^2}-3\frac{\mathbf{D}^{\mathrm{T}}\bar{\rho}_O\bar{r}_e^{\mathrm{T}}\mathbf{D}^{\mathrm{T}}\bar{\rho}_O}{R^2}\right)dm \\
&\quad -\frac{\mu}{R^3}\int_{\mathfrak{T}}\left(15\frac{(\bar{r}_e^{\mathrm{T}}\bar{r}_r\bar{r}_r^{\mathrm{T}}\bar{r}_e+2\bar{r}_e^{\mathrm{T}}\bar{r}_r\bar{r}_e^{\mathrm{T}}\mathbf{D}^{\mathrm{T}}\bar{\rho}_O+\bar{r}_e^{\mathrm{T}}\mathbf{D}^{\mathrm{T}}\bar{\rho}_O\bar{\rho}_O^{\mathrm{T}}\mathbf{D}\bar{r}_e)}{2R^4}\bar{r}_e\right)dm \\
&\quad -\frac{\mu}{R^3}\int_{\mathfrak{T}}\left(-3\frac{\bar{r}_r^{\mathrm{T}}\bar{r}_r+2\bar{r}_r^{\mathrm{T}}\mathbf{D}^{\mathrm{T}}\bar{\rho}_O+\bar{\rho}_O^{\mathrm{T}}\bar{\rho}_O}{2R^2}\bar{r}_e+O\left(\epsilon_1^3\right)\right)dm,
\end{aligned}
\tag{6.11}
$$

$$
\begin{aligned}
-\int_{\mathfrak{C}} \frac{\mu\left(\bar{r}_e+\bar{\rho}_C\right)}{\left|\bar{r}_e+\bar{\rho}_C\right|^3} dm &= -\frac{\mu}{R^3}\int_{\mathfrak{C}} \left(\bar{r}_e+\bar{\rho}_C\right)\left(1-3\frac{\bar{r}_e^{\mathrm{T}}\bar{\rho}_C}{R^2}+15\frac{(\bar{r}_e^{\mathrm{T}}\bar{\rho}_C)^2}{2R^4}-3\frac{|\bar{\rho}_C|^2}{2R^2}+O(\epsilon_2^3)\right) dm, \\
&= -\frac{\mu}{R^3}\int_{\mathfrak{C}} \left(\bar{r}_e+\bar{\rho}_C-3\frac{\bar{r}_e\bar{r}_e^{\mathrm{T}}\bar{\rho}_C}{R^2}-3\frac{\bar{\rho}_C\bar{r}_e^{\mathrm{T}}\bar{\rho}_C}{R^2}+15\frac{\bar{r}_e^{\mathrm{T}}\bar{\rho}_C\bar{\rho}_C^{\mathrm{T}}\bar{r}_e}{2R^4}\bar{r}_e\right) dm \\
&\quad -\frac{\mu}{R^3}\int_{\mathfrak{C}} \left(-3\frac{\bar{\rho}_C^{\mathrm{T}}\bar{\rho}_C}{2R^2}\bar{r}_e+O\left(\epsilon_2^3\right)\right) dm.
\end{aligned}
\tag{6.12}
$$

We now make the following assumption:

Assumption 6.2 The inertia of the chief spacecraft, when resolved in $\mathcal{C}$, is the same as the inertia matrix of the deputy spacecraft, when resolved in $\mathcal{B}$.

Assumption 6.2 is made in order to relate (6.11) and (6.12), and as a consequence gives the following relationship

$$
-\int_{\mathfrak{T}} \left[\bar{\rho}_C\right]^{2\times} dm = -\int_{\mathfrak{T}} \left[\bar{\rho}_O\right]^{2\times} dm = \bar{J}. \tag{6.13}
$$

Recalling that

$$
\begin{aligned}
\left[\bar{\rho}_C\right]^{2\times}+I_3\bar{\rho}_C^{\mathrm{T}}\bar{\rho}_C &= \bar{\rho}_C\bar{\rho}_C^{\mathrm{T}}, \\
\left[\bar{\rho}_O\right]^{2\times}+I_3\bar{\rho}_O^{\mathrm{T}}\bar{\rho}_O &= \bar{\rho}_O\bar{\rho}_O^{\mathrm{T}}, \\
\int_{\mathfrak{T}} \bar{\rho}_C dm = \int_{\mathfrak{T}} \bar{\rho}_O dm &= 0, \\
\int_{\mathfrak{T}} \bar{\rho}_C^{\mathrm{T}}\bar{\rho}_C dm = \int_{\mathfrak{T}} \bar{\rho}_O^{\mathrm{T}}\bar{\rho}_O dm &= \frac{\mathrm{tr}\left[\bar{J}\right]}{2},
\end{aligned}
\tag{6.14}
$$

the terms within the integrals of (6.11) and (6.12) become

$$\begin{aligned}
-\int_D \frac{\mu\left(\bar{r}_e+\bar{r}_r+\mathbf{D}^{\mathrm{T}}\bar{\rho}_O\right)}{\left|\bar{r}_e+\bar{r}_r+\mathbf{D}^{\mathrm{T}}\bar{\rho}_O\right|^3}dm &= -\tfrac{\mu m_{\mathfrak{T}}}{R^3}(\bar{r}_e+\bar{r}_r)+\tfrac{3\mu m_d}{R^5}(\bar{r}_e\bar{r}_e^{\mathrm{T}})\bar{r}_r+\tfrac{3\mu m_d}{2R^5}(2\bar{r}_r\bar{r}_r^{\mathrm{T}}+\bar{r}_r^{\mathrm{T}}\bar{r}_r)\bar{r}_e \\
&\quad -\tfrac{15\mu m_{\mathfrak{T}}}{2R^7}\left(\bar{r}_e^{\mathrm{T}}\bar{r}_r\bar{r}_r^{\mathrm{T}}\bar{r}_e\right)\bar{r}_e-\tfrac{3\mu}{R^5}\mathbf{D}^{\mathrm{T}}\bar{J}\mathbf{D}\bar{r}_e+\tfrac{15\mu}{2R^7}(\bar{r}_e^{\mathrm{T}}\mathbf{D}^{\mathrm{T}}\bar{J}\mathbf{D}\bar{r}_e)\bar{r}_e \\
&\quad -\tfrac{3\mu\mathrm{tr}\left[\bar{J}\right]}{2R^5}\bar{r}_e+O(\epsilon_1^3),
\end{aligned} \tag{6.15}$$

$$-\int_D \frac{\mu\left(\bar{r}_e+\bar{\rho}_C\right)}{\left|\bar{r}_e+\bar{\rho}_C\right|^3}dm = -\tfrac{\mu m_{\mathfrak{T}}}{R^3}\bar{r}_e-\tfrac{3\mu}{R^5}\bar{J}\bar{r}_e+\tfrac{15\mu}{2R^7}(\bar{r}_e^{\mathrm{T}}\bar{J}\bar{r}_e)\bar{r}_e-\tfrac{3\mu\mathrm{tr}\left[\bar{J}\right]}{2R^5}\bar{r}_e+O(\epsilon_2^3). \tag{6.16}$$

Substituting in (6.15) and (6.16) into (6.7) and neglecting terms of third order in ϵ_1 and ϵ_2, the full, approximate translational equations of motion become

$$\begin{aligned}
\dot{\bar{r}}_r &= \tfrac{\bar{p}_r}{m}, \\
\dot{\bar{p}}_r &= \left(\tfrac{2\mu m_{\mathfrak{T}}}{R^3}I_3+\tfrac{3\mu,m_{\mathfrak{T}}}{R^3}\left[\check{r}_e\right]^{2\times}-m_{\mathfrak{T}}\left[\bar{\omega}_e\right]^{2\times}\right)\bar{r}_r-2\left[\bar{\omega}_e\right]^{\times}\bar{p}_r \\
&\quad +\tfrac{3\mu m_{\mathfrak{T}}}{2R^4}\left(2\bar{r}_r\bar{r}_r^{\mathrm{T}}+\bar{r}_r^{\mathrm{T}}\bar{r}_rI_3-5\left(\check{r}_e^{\mathrm{T}}\bar{r}_r\bar{r}_r^{\mathrm{T}}\check{r}_e\right)I_3\right)\check{r}_e \\
&\quad -\tfrac{3\mu}{2R^4}\left(2\mathbf{D}^{\mathrm{T}}\bar{J}\mathbf{D}-2\bar{J}-5\left(\check{r}_e^{\mathrm{T}}\left(\mathbf{D}^{\mathrm{T}}\bar{J}\mathbf{D}-\bar{J}\right)\check{r}_e\right)I_3\right)\check{r}_e.
\end{aligned} \tag{6.17}$$

Neglecting third-order terms is a reasonable assumption for a spacecraft in orbit around a large central body, but if the spacecraft is very large, i.e., $|\vec{r}_{\rho/O}| \sim 10$ km or $\epsilon_2 \sim 10^{-4}$, then higher-order terms must be added for accuracy [47].

The following can be said about the new approximate equations of motions (6.17):

1. If terms of second-order in ϵ_1 and ϵ_2 are neglected, then (6.17) become the traditional HCW equations if $\bar{r}_{_e} = [\ R \ \ 0 \ \ 0\ ]^{\mathrm{T}}$ and $\bar{\omega}_{_e} = [\ 0 \ \ 0 \ \ \Omega\ ]^{\mathrm{T}}$, where $n^2 = \frac{\mu}{R^3}$.

2. If the attitude is aligned with the equilibrium attitude for all time and $\bar{r}_{_e} = [\ R \ \ 0 \ \ 0\ ]^{\mathrm{T}}$ and $\bar{\omega}_{_e} = [\ 0 \ \ 0 \ \ \Omega\ ]^{\mathrm{T}}$, then (6.17) become the second-order HCW equations, whose derivation and approximate solution is given in [115].

3. If the spacecraft is completely symmetric, i.e., has an inertia matrix $\bar{J} = \alpha I_3$ for $\alpha > 0$, there is no coupling in the translational dynamics by the attitude of the spacecraft.

Remark 6.1: The dynamics (6.17) were obtained by approximating the total gravity force via a Taylor-series expansion and neglecting terms of higher than third-order in ϵ_1 and ϵ_2. Generally coupled rotational and translational equations are derived by first approximating the gravity potential function, and the total force is obtained by taking the negative gradient of the simplified potential. Both methods are given in Appendix C, with advantages and disadvantages given for both.

6.1.2 Rotational Equations of Motion

6.1.2.1 Exact Rotational Relative Equations

To derive the rotational equations of motion, it is necessary to determine the total angular momentum of the spacecraft system. Note that the angular momentum contribution due to the spacecraft rotating about the central gravity field's center at point A must also be taken into consideration. Thus we consider the total angular momentum of the spacecraft system (consisting of the spherical body inducing the central gravity field and the spacecraft itself) about point A, given as

$$\vec{H}_{_{\mathfrak{T}/A/\mathcal{I}}} = \vec{H}_{_{\mathfrak{T}/O/\mathcal{I}}} + \vec{r}_{_{O/A}} \times \vec{p}_{_{\mathfrak{T}/A/\mathcal{I}}}. \tag{6.18}$$

The total angular momentum of the spacecraft system about its COM is given by (2.25),

$$\vec{H}_{_{\mathfrak{T}/O/\mathcal{I}}} = \vec{J}_{_{\mathfrak{T}/O}}\vec{\omega}_{_{\mathcal{B}/\mathcal{I}}} + \sum_{i=1}^{N_{RW}} J_{_{ws^i}}\nu_{_i}\hat{w}_{_{ix}} + \sum_{j=1}^{N_{CMG}} \left(J_{_{gg^j}} + J_{_{rt^j}}\right)\dot{\delta}_{_j}\hat{g}_{_{jy}} + J_{_{rs^i}}\eta_{_j}\hat{g}_{_{jx}}, \tag{6.19}$$

while from the transport theorem,

$$\vec{p}_{_{\mathfrak{T}/A/\mathcal{I}}} = \vec{p}_{_{\mathfrak{T}/A/\mathcal{C}}} + \vec{\omega}_{_{\mathcal{C}/\mathcal{I}}} \times m_{_{\mathfrak{T}}}\vec{r}_{_{O/A}}. \tag{6.20}$$

We define the following notation:

- $\bar{\omega}_{_r} = \vec{\omega}_{_{\mathcal{B}/\mathcal{C}}}\big|_{_{\mathcal{B}}}$: Angular velocity of $\mathcal{B}$ relative to $\mathcal{C}$ expressed in $\mathcal{B}$
- $\bar{H}_{_{\mathfrak{T}}} = \vec{H}_{_{\mathfrak{T}/A/\mathcal{I}}}\big|_{_{\mathcal{I}}}$: Total inertial angular momentum of the system (spacecraft and central body) expressed in $\mathcal{I}$

Substituting (6.20) and (6.19) into (6.18) and resolving in $\mathcal{B}$ gives

$$\mathbf{DC}\bar{H}_{_{\mathfrak{T}}} = \bar{J}(\bar{\omega}_{_r} + \mathbf{D}\bar{\omega}_{_e}) + \mathbf{D}([\bar{r}]^{\times}\bar{p} - m_{_{\mathfrak{T}}}[\bar{r}]^{2\times}\bar{\omega}_{_e}) + \bar{h}_{_a}, \tag{6.21}$$

where

$$\bar{h}_{_a} = \sum_{i=1}^{N_{RW}} J_{_{ws^i}}\nu_{_i}\check{w}_{_i} + \sum_{j=1}^{N_{CMG}} + J_{_{rs^i}}\eta_{_j}\check{h}_{_j} \tag{6.22}$$

is the angular momentum contribution due to the actuators, and where we use again the assumption that the angular momentum contribution due to the gimbals is much smaller than that of the RWs or rotor. Note that from Assumption 6.1, $\bar{H}_{_{\mathfrak{T}}}$ is constant. Solving (6.21) for $\bar{\omega}_{_r}$ gives the relative kinematic equations

$$\begin{aligned} \dot{\mathbf{D}} &= -[\bar{\omega}_{_r}]^{\times}\mathbf{D}, \\ &= \left[\bar{J}^{-1}\left(\bar{h}_{_a} + \bar{J}\mathbf{D}\bar{\omega}_{_e} + \mathbf{D}([\bar{r}]^{\times}\bar{p} - m_{_{\mathfrak{T}}}[\bar{r}]^{2\times}\bar{\omega}_{_e}) - \mathbf{DC}\bar{H}_{_{\mathfrak{T}}}\right)\right]^{\times}\mathbf{D}. \end{aligned} \tag{6.23}$$

The control input to the system will either be reaction wheel accelerations or

gimbal rates

$$\begin{aligned} u_{_i} &= \dot{\nu}_{_i}, \quad i = 1, \ldots, N_{RW}, \\ u_{_{i+N_{RW}}} &= \dot{\delta}_{_i}, \quad i = 1, \ldots, N_{CMG}. \end{aligned} \tag{6.24}$$

6.1.2.2 Approximate Rotational Relative Equations

For the relative, approximate, rotational equations of motion, note that

$$\vec{p}_{_{\mathfrak{T}/A/\mathcal{C}}} = \vec{p}_{_{\mathfrak{T}/C/\mathcal{C}}} + \vec{p}_{_{C/A/\mathcal{C}}}. \tag{6.25}$$

The linear momentum of C relative to A in the constant rotating frame $\mathcal{C}$ is zero. Resolving (6.25) in $\mathcal{C}$ gives

$$\bar{p} = \bar{p}_{_r}. \tag{6.26}$$

Recalling that $\bar{r} = \bar{r}_{_e} + \bar{r}_{_r}$, the kinematics in (6.23) become

$$\dot{\mathbf{D}} = \left[\bar{J}^{-1}\left(\bar{h}_{_a} + \bar{J}\mathbf{D}\bar{\omega}_{_e} + \mathbf{D}([\bar{r}_{_e} + \bar{r}_{_r}]^{\times}\bar{p}_{_r} - m_{_{\mathfrak{T}}}[\bar{r}_{_e} + \bar{r}_{_r}]^{2\times}\bar{\omega}_{_e}) - \mathbf{D}\mathbf{C}\bar{H}_{_{\mathfrak{T}}}\right)\right]^{\times}\mathbf{D}. \tag{6.27}$$

For completeness, the control input, as stated in the last subsection, will be taken as either RW accelerations or gimbal rates, see (6.24).

6.1.3 Summary of Equations of Motion

As a summary, the exact relative equations of motion and the approximate equations of motion are given below, resolved in their appropriate frames. Note that the locked inertia of the spacecraft is given by

$$\bar{J} = \bar{J}_{_{\mathfrak{B}}} + \sum_{i=1}^{N_{RW}} \bar{J}_{_{\mathfrak{W}_j}} + \sum_{j=1}^{N_{CMG}} \mathbf{G}_{_j}^{\mathrm{T}}\left(\bar{J}_{_{\mathfrak{G}_j}} + \bar{J}_{_{\mathfrak{R}_j}}\right)\mathbf{G}_{_j}, \tag{6.28}$$

and the angular momentum due to the actuators is

$$\bar{h}_{a} = \sum_{i=1}^{N_{RW}} J_{ws i} \nu_{i} \check{w}_{i} + \sum_{j=1}^{N_{CMG}} + J_{rs i} \eta_{j} \check{h}_{j}. \tag{6.29}$$

Exact Relative Equations of Motion

$$\begin{aligned}
\dot{\bar{r}} &= \tfrac{\bar{p}}{m_{\mathfrak{T}}}, \\
\dot{\bar{p}} &= -\int_{\mathfrak{T}} \tfrac{\mu\left(\bar{r}+\mathbf{D}^{\mathrm{T}}\bar{\rho}_{O}\right)}{\left|\bar{r}+\mathbf{D}^{\mathrm{T}}\bar{\rho}_{O}\right|^{3}} dm - 2\left[\bar{\omega}_{e}\right]^{\times}\bar{p} - m_{\mathfrak{T}}\left[\bar{\omega}_{e}\right]^{2\times}\bar{r}, \\
\dot{\mathbf{D}} &= \left[\bar{J}^{-1}\left(\bar{h}_{a} + \bar{J}\mathbf{D}\bar{\omega}_{e} + \mathbf{D}([\bar{r}]^{\times}\bar{p} - m_{\mathfrak{T}}\left[\bar{r}\right]^{2\times}\bar{\omega}_{e}) - \mathbf{D}\mathbf{C}\bar{H}_{\mathfrak{T}}\right)\right]^{\times}\mathbf{D}, \\
u_{i} &= \dot{\nu}_{i}, \quad i = 1, \ldots, N_{RW}, \\
u_{i+N_{RW}} &= \dot{\delta}_{i}, \quad i = 1, \ldots, N_{CMG}.
\end{aligned} \tag{6.30}$$

Approximate Relative Equations of Motion

$$
\begin{aligned}
\dot{\bar{r}}_{r} &= \tfrac{\bar{p}_{r}}{m}, \\
\dot{\bar{p}}_{r} &= \left(\tfrac{2\mu m_{\mathfrak{T}}}{R^3} I_3 + \tfrac{3\mu m_{\mathfrak{T}}}{R^3} \left[\check{r}_{e}\right]^{2\times} - m_{\mathfrak{T}} \left[\bar{\omega}_{e}\right]^{2\times}\right) \bar{r}_{r} - 2 \left[\bar{\omega}_{e}\right]^{\times} \bar{p}_{r} \\
&\quad + \tfrac{3\mu m_{\mathfrak{T}}}{2R^4} \left(2\bar{r}_{r}\bar{r}_{r}^{\mathrm{T}} + \bar{r}_{r}^{\mathrm{T}}\bar{r}_{r} I_3 - 5\left(\check{r}_{e}^{\mathrm{T}}\bar{r}_{r}\bar{r}_{r}^{\mathrm{T}}\check{r}_{e}\right) I_3\right) \check{r}_{e} \\
&\quad - \tfrac{3\mu}{2R^4} \left(2\mathbf{D}^{\mathrm{T}}\bar{J}\mathbf{D} - 2\bar{J} - 5\left(\check{r}_{e}^{\mathrm{T}}\left(\mathbf{D}^{\mathrm{T}}\bar{J}\mathbf{D} - \bar{J}\right)\check{r}_{e}\right) I_3\right) \check{r}_{e}, \\
\dot{\mathbf{D}} &= \left[\bar{J}^{-1}\left(\bar{h}_{a} + \bar{J}\mathbf{D}\bar{\omega}_{e} + \mathbf{D}([\bar{r}_{e} + \bar{r}_{r}]^{\times}\bar{p}_{r} - m_{\mathfrak{T}}\left[\bar{r}_{e} + \bar{r}_{r}\right]^{2\times}\bar{\omega}_{e}) - \mathbf{D}\mathbf{C}\bar{H}_{\mathfrak{T}}\right)\right]^{\times}\mathbf{D}, \\
u_{i} &= \dot{\nu}_{i}, \quad i = 1, \ldots, N_{RW}, \\
u_{i+N_{RW}} &= \dot{\delta}_{i}, \quad i = 1, \ldots, N_{CMG}.
\end{aligned}
\tag{6.31}
$$

The following notation corresponds to all related variables:

Orientation Matrices

- $\mathbf{C}$: Orientation matrix of $\mathcal{C}$ relative to $\mathcal{I}$,
- $\mathbf{D}$: Orientation matrix of $\mathcal{B}$ relative to $\mathcal{C}$,
- $\mathbf{G}_{j}$: Orientation matrix of $\mathcal{G}_j$ relative to $\mathcal{B}$.

Rotational Vectors

- $\bar{\omega}_{e} = \vec{\omega}_{\mathcal{C}/\mathcal{I}}\big|_{\mathcal{C}}$: Angular velocity of $\mathcal{C}$ relative to $\mathcal{I}$ expressed in $\mathcal{B}$,
- $\bar{\omega}_{r} = \vec{\omega}_{\mathcal{B}/\mathcal{C}}\big|_{\mathcal{B}}$: Angular velocity of $\mathcal{B}$ relative to $\mathcal{C}$ expressed in $\mathcal{B}$,
- $\bar{H}_{\mathfrak{T}} = \vec{H}_{\mathfrak{T}/A/\mathcal{I}}\big|_{\mathcal{I}}$: Total spacecraft system angular momentum about point A expressed in $\mathcal{I}$.

Resolved Inertia Matrices

- $\bar{J} = \vec{J}_{\mathfrak{T}/O}\big|_{\mathcal{B}}$: Locked inertia matrix expressed in $\mathcal{B}$ about point O,
- $\bar{J}_{\mathfrak{B}} = \vec{J}_{\mathfrak{B}/B_c}\big|_{\mathcal{G}}$: Bus inertia matrix expressed in $\mathcal{B}$ about point B_c,
- $\bar{J}_{\mathfrak{W}_i} = \vec{J}_{\mathfrak{W}_i/W_{ic}}\big|_{\mathcal{B}}$: ith RW inertia matrix expressed in $\mathcal{B}$ about point W_{ic},
- $\bar{J}_{\mathfrak{G}_j} = \vec{J}_{\mathfrak{G}_j/G_{jc}}\big|_{\mathcal{G}_j}$: jth gimbal inertia matrix expressed in $\mathcal{G}_j$ about point G_{jc},
- $\bar{J}_{\mathfrak{R}_j} = \vec{J}_{\mathfrak{R}_j/R_{jc}}\big|_{\mathcal{G}_j}$: jth rotor inertia matrix expressed in $\mathcal{G}_j$ about point R_{jc}.

Specific Inertias

- J_{ws_i} : ith RW inertia about its spin axis,
- J_{rs_j} : jth rotor inertia about its spin axis.

Resolved Position Vectors

- $\bar{r} = \vec{r}_{O/A}\big|_{\mathcal{C}}$: Position of O relative to A expressed in $\mathcal{C}$,
- $\bar{\rho}_O = \vec{r}_{\rho/O}\big|_{\mathcal{B}}$: Position of an infinitesimal mass element relative to O expressed in $\mathcal{B}$,
- $\bar{p} = \vec{r}_{\mathfrak{T}/A/\mathcal{C}}\big|_{\mathcal{C}}$: Relative linear momentum of the spacecraft relative to A expressed in $\mathcal{C}$,
- $R = |\vec{r}_{C/A}|$: Radius of the equilibrium orbit
- $\bar{r}_r = \vec{r}_{O/C}\big|_{\mathcal{C}}$: Position of O relative to C expressed in $\mathcal{C}$,
- $\check{r}_e = \frac{\vec{r}_{C/A}}{R}\big|_{\mathcal{C}}$: Unit vector of C relative to A expressed in $\mathcal{C}$,
- $\bar{p}_r = \vec{r}_{\mathfrak{T}/C/\mathcal{C}}\big|_{\mathcal{C}}$: Relative linear momentum of the spacecraft relative to C.

Actuator Unit Vectors

- $\check{w}_i = \hat{w}_{ix}\big|_{\mathcal{B}}$: Spin axis of ith RW expressed in $\mathcal{B}$,
- $\check{h}_j = \hat{g}_{jx}\big|_{\mathcal{B}}$: Spin axis of jth rotor expressed in $\mathcal{G}_j$.

Actuator Parameters

- ν_i : ith RW rate,
- δ_j : jth gimbal angle,
- η_j : jth rotor rate.

And recall that the following assumptions were made:

Assumption 2.1 The spacecraft bus is a rigid body.

Assumption 2.2 The RW rotors are rigid.

Assumption 2.3 The RWs are symmetric about their spin axes.

Assumption 2.4 Both the gimbal and the rotor of each CMG are two separate rigid bodies.

Assumption 2.5 Both the gimbal and rotor of each CMG are symmetric about their spin axes.

Assumption 2.6 The COM of the rotor is located at the intersection of the rotor spin axis and the gimbal spin axis.

Assumption 2.7 The COM of the spacecraft system that includes the spacecraft bus, RWs, and CMGs coincides with O.

Assumption 2.9 The rotors spin at constant nonzero speeds.

Assumption 3.4.3 The speed of the rotors is much larger than that of the gimbals.

Assumption 6.1 The only force acting on the spacecraft system is gravity.

Assumption 6.2 The inertia of the chief satellite, when resolved in $\mathcal{C}$ is the same as the inertia matrix of the deputy when resolved in $\mathcal{B}$.

We also note that in all the above derivations, the equations of motion are written with respect to a nominal circular orbit, which can be either of great circle or non-great circle type; the existence and properties of which are briefly discussed in the next section.

6.2 Relative Orbits

The equations of motion (6.30) and (6.31) are general and only require that the equilibrium orbital radius and angular velocity be constant and known. However, analysis of non-great circle orbits are a challenge as currently there do not exist any closed-form solutions for such orbits, and thus numerical methods must be used [48]. This presents issues for spacecraft with only non-great circle orbits, for example, a spacecraft comprising of six point masses, two on each principal axis, for which the distances from the COM along the principal axes are not equal (i.e., when $x_1 \neq x_2, x_3 \neq x_4, x_5 \neq x_6$ in Figure 6.2) [44, 48].

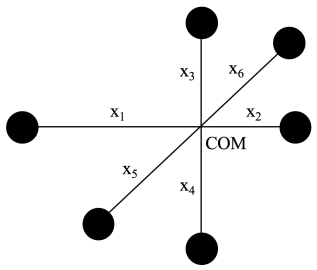

Figure 6.2: Spacecraft with no great circle equilibria.

If approximations are allowed be made to (6.30), then non-great circle orbits can be determined in the following way; consider the motion of a spacecraft in its equilibrium orbit, corresponding to $\bar{r} = \bar{r}_e$ (i.e., O coincides with C), $\bar{p} = 0$, and $\mathbf{D} = I_3$ in (6.30). The exact time rate of change of linear momentum from (6.30)

then gives the following constraint:

$$0 = -\int_{\mathfrak{T}} \frac{\mu\left(\bar{r}_{e} + \bar{\rho}_{C}\right)}{\left|\bar{r}_{e} + \bar{\rho}_{C}\right|^{3}} dm - m_{\mathfrak{T}} \left[\bar{\omega}_{e}\right]^{2\times} \bar{r}_{e}. \tag{6.32}$$

Using the second order approximation from above in (6.9), (6.32) can be explicitly written as

$$0 = -\frac{\mu m_{\mathfrak{T}}}{R^3}\bar{r}_{e} - \frac{3\mu}{R^5}\bar{J}\bar{r}_{e} + \frac{15\mu}{2R^7}(\bar{r}_{e}^{\mathrm{T}}\bar{J}\bar{r}_{e})\bar{r}_{e} - \frac{3\mu \mathrm{tr}\left[\bar{J}\right]}{2R^5}\bar{r}_{e} - m_{\mathfrak{T}}\left[\bar{\omega}_{e}\right]^{2\times}\bar{r}_{e} + O(\epsilon_2^3). \tag{6.33}$$

For non-great circle orbits, the rotation vector and the radius vector can be given, without loss of generality, as $\bar{\omega}_{e} = [\ 0\ \ 0\ \ \Omega\ ]^{\mathrm{T}}$ and $\bar{r}_{e} = [\ \sigma_1 R\ \ 0\ \ \sigma_2 R\ ]^{\mathrm{T}}$, where $\Omega > 0$, $\sigma_1 \in (0, 1]$ and $\sigma_2 = \sqrt{1-\sigma_1^2}$. Using this notation, (6.33) explicitly becomes

$$\begin{aligned}
0 &= \left(-\tfrac{\mu m_{\mathfrak{T}}}{R^3} + \tfrac{15\mu}{2R^5}(\sigma_1(\sigma_1 j_{11} + \sigma_2 j_{13}) + \sigma_2(\sigma_1 j_{13} + \sigma_2 j_{33})) - \tfrac{3\mu \mathrm{tr}\left[\bar{J}\right]}{2R^5} + m_{\mathfrak{T}}\Omega^2\right)\sigma_1 \\
&\quad -\tfrac{3\mu}{R^5}(\sigma_1 j_{11} + \sigma_2 j_{13}) + O(\epsilon_2^3), \\
0 &= -\tfrac{3\mu}{R^5}(\sigma_1 j_{12} + \sigma_2 j_{23}) + O(\epsilon_2^3), \\
0 &= \left(-\tfrac{\mu m_{\mathfrak{T}}}{R^3} + \tfrac{15\mu}{2R^5}(\sigma_1(\sigma_1 j_{11} + \sigma_2 j_{13}) + \sigma_2(\sigma_1 j_{13} + \sigma_2 j_{33})) - \tfrac{3\mu \mathrm{tr}\left[\bar{J}\right]}{2R^5}\right)\sigma_2 \\
&\quad -\tfrac{3\mu}{R^5}(\sigma_1 j_{13} + \sigma_2 j_{33}) + O(\epsilon_2^3),
\end{aligned} \tag{6.34}$$

where the locked inertia matrix is

$$\bar{J} = \begin{bmatrix} j_{11} & j_{12} & j_{13} \\ j_{12} & j_{22} & j_{23} \\ j_{13} & j_{23} & j_{33} \end{bmatrix}. \tag{6.35}$$

If terms higher than third-order in ϵ_2 are neglected, then the relations in (6.34) can be solved for a given spacecraft with inertia matrix $\bar{J}$ and a desired orbital radius $\bar{r}_{_e}$.

Now consider the case of great circle orbits, in the limiting case where $\sigma_1 = 1$. Then $\bar{r}_{_e} = [\ R\ \ 0\ \ 0\ ]^{\mathrm{T}}$ and $\bar{\omega}_{_e} = [\ 0\ \ 0\ \ \Omega\ ]^{\mathrm{T}}$, just as in HCW dynamics. The algebraic relations in (6.34) become

$$\begin{aligned} 0 &= -\tfrac{\mu m_{_{\mathfrak{T}}}}{R^3} - \tfrac{3\mu}{R^5} j_{11} + \tfrac{15\mu}{2R^5} j_{11} - \tfrac{3\mu \mathrm{tr}\left[\bar{J}\right]}{2R^5} + m_{_{\mathfrak{T}}}\Omega^2 + O(\epsilon_2^3), \\ 0 &= -\tfrac{3\mu}{R^5} j_{12} + O(\epsilon_2^3), \\ 0 &= -\tfrac{3\mu}{R^5} j_{13} + O(\epsilon_2^3). \end{aligned} \tag{6.36}$$

All three equations in (6.36) must hold if a great circle trajectory exists. If third-order terms in ϵ_2 are neglected, then the existence of such orbits imply that j_{12} and j_{13} must be zero. This is possible if the spacecraft, in its equilibrium orbit, is symmetric with respect to an axis orthogonal to the orbital plane and $\hat{c}_{_x}$ [49]. Though this result is valid up to third-order in ϵ_2, it is supported by an analysis on the exact dynamics (6.30) by [48], summarized by the following Lemma:

Lemma 6.1 [48] : For a rigid body having a plane of symmetry, there are at least four great circle relative equilibria. Furthermore, if the rigid body is symmetric with respect to two planes, there are at least eight great circle relative equilibria, and for a rigid body with three planes of symmetry, there are at least twenty-four great circle relative equilibria. □

If the assumption $j_{12} = j_{13} = 0$ holds for the spacecraft, we obtain the following relationship:

$$m_{_{\mathfrak{T}}}\Omega^2 = \frac{\mu m_{_{\mathfrak{T}}}}{R^3} + \Omega_{_\epsilon}, \tag{6.37}$$

where

$$\Omega_{\epsilon} = -\frac{9\mu}{2R^5} j_{11} + \frac{3\mu \text{tr}\left[\bar{J}\right]}{2R^5}. \tag{6.38}$$

Note that if $\Omega_{\epsilon} = 0$, then Ω is the mean motion of a point-mass satellite in a circular orbit with radius R. The results above will be useful in the analysis of local controllability of the approximate coupled equations of motion.

6.3 Small-Time Local Controllability of Coupled Dynamics

While global controllability of a rigid body in an inertial frame with just attitude actuation was discussed in [58], the subject of STLC about an equilibrium orbit was not. In the following section, we give sufficient conditions for the exact dynamics (6.30) to be STLC through the use of Lie brackets. For the approximate system (6.31), linearization is performed about the equilibrium orbit, and sufficient and necessary conditions for linear controllability are given, which in turn lead to sufficient conditions for STLC. With STLC established, control techniques can be used to locally stabilize the spacecraft's rotational and translational dynamics to its equilibrium orbit by only adjusting its attitude. Furthermore, if internal attitude actuation is used, then a spacecraft can move translationally in space without the use of propellant.

For all analysis, the following assumption is made:

> **Assumption 6.3** The spacecraft system's attitude is fully actuated by 3 RWs whose spin axes are linearly independent.

The controllability of a spacecraft equipped with CMGs is more intensive and is left for future work.

6.3.1 Local Controllability Lie Brackets for Exact Equations of Motion

The exact equations of motion (6.30) are highly nonlinear, affine in the control, and evolve on the space $\mathbb{R}^6 \times SO(3) \times \mathbb{T}^m$, where m is the number of actuators. A Lie bracket analysis can be used to determine local controllability of the exact dynamics, but since part of the dynamics evolve on $SO(3)$, the brackets must be computed differently than in Appendix A. For this section, we will use the method outlined in Appendix D.

For the controllability result we will use the following Lemma, which is an extension of the result when $\infty-$degree brackets are considered for Theorem A2 in Appendix D:

Lemma 6.2 [**2**]: Let M be a C^∞-manifold on which the system

$$\dot{x} = f(x) + \sum_{i=1}^{m} g_i(x) u_i, \tag{6.39}$$

evolves. The system (6.39) is STLC from $x_0 \in \mathsf{M}$ if $f(x_0) = 0$ and if brackets constructed with only one control vector field g_i span the tangent space of M when evaluated at x_0. $\square$ With Lemma 6.2, the following result can be stated,

Theorem 6.1: The dynamics (6.30) of a spacecraft actuated by three RWs ($m = 3$) with linearly independent spin axes are STLC from the spacecraft's equilibrium orbit of radius $\bar{r}_e$ if the matrix $\bar{P}$, given as

$$\bar{P} = \int_{\mathfrak{T}} \left(\frac{I_3}{|\bar{r}_e + \bar{\rho}_C|^3} - \frac{3(\bar{r}_e + \bar{\rho}_C)\bar{r}_e^{\mathrm{T}}}{|\bar{r}_e + \bar{\rho}_C|^5} \right) [\bar{\rho}_C]^\times \, dm, \tag{6.40}$$

is nonsingular.

Proof: For the exact equations of motion in (6.30), the drift and control vectors are

$$f = \begin{Bmatrix} \frac{\bar{p}}{m_{\mathfrak{T}}} \\ -\int_{\mathfrak{T}} \frac{\mu\left(\bar{r}+\mathbf{D}^{\mathrm{T}}\bar{\rho}_{O}\right)}{\left|\bar{r}+\mathbf{D}^{\mathrm{T}}\bar{\rho}_{O}\right|^{3}} dm - 2[\bar{\omega}_{e}]^{\times}\bar{p} - m_{\mathfrak{T}}[\bar{\omega}_{e}]^{2\times}\bar{r} \\ \left[\bar{J}^{-1}\left(\bar{h}_{a} + \bar{J}\mathbf{D}\bar{\omega}_{e} + \mathbf{D}\left([\bar{r}]^{\times}\bar{p} - m_{\mathfrak{T}}[\bar{r}]^{2\times}\bar{\omega}_{e}\right) - \mathbf{D}\mathbf{C}\bar{H}_{\mathfrak{T}}\right)\right]^{\times}\mathbf{D} \\ 0 \end{Bmatrix}, \quad g_{i} = \begin{Bmatrix} ,0 \\ 0 \\ 0 \\ e_{i} \end{Bmatrix}, \tag{6.41}$$

where e_i is the zero vector with a 1 in the ith entry (i.e., $e_i = [\ \ldots 0\ \ 1\ \ 0\ \ \ldots]^{\mathrm{T}}$) and the angular momentum due to the three RWs is given by

$$\bar{h}_{a} = \sum_{i=1}^{3} J_{w_{s}i}\nu_{i}\check{w}_{i}. \tag{6.42}$$

Using the method outlined in [8], the Lie brackets necessary for STLC, which are denoted by $L_{j,i}, \quad i,j = 1,2,3$, can be computed as

$$L_{1,i} = [f,\ g_{i}] = \begin{Bmatrix} 0 \\ 0 \\ \left[-\bar{J}^{-1}\frac{\partial \bar{h}_{a}}{\partial \nu_{i}}\right]^{\times}\mathbf{D} \\ 0 \end{Bmatrix}, \tag{6.43}$$

$$L_{2,i} = [f,\ [f,\ g_{i}]] \ = \ \begin{Bmatrix} 0 \\ -\mu\int_{\mathfrak{T}}\left(\frac{I_{3}}{\left|\bar{r}+\mathbf{D}^{\mathrm{T}}\bar{\rho}_{O}\right|^{3}} - \frac{3(\bar{r}+\mathbf{D}^{\mathrm{T}}\bar{\rho}_{O})\bar{r}^{\mathrm{T}}}{\left|\bar{r}+\mathbf{D}^{\mathrm{T}}\bar{\rho}_{O}\right|^{5}}\right)\mathbf{D}^{\mathrm{T}}\left[\bar{\rho}_{O}\right]^{\times}\bar{J}^{-1}\frac{\partial \bar{h}_{a}}{\partial \nu_{i}}dm \\ \left[\left(\bar{J}^{-1}\bar{h}_{a}\right)\times\left(\bar{J}^{-1}\frac{\partial \bar{h}_{a}}{\partial \nu_{i}}\right) + E_{1}\mathbf{D}E_{2}\right]^{\times}\mathbf{D} \\ 0 \end{Bmatrix}, \tag{6.44}$$

where

$$E_1 = \left(\bar{J}^{-1}\left[\bar{J}^{-1}\frac{\partial \bar{h}_a}{\partial \nu_i}\right]^{\times} - \left[\bar{J}^{-1}\frac{\partial \bar{h}_a}{\partial \nu_i}\right]^{\times}\bar{J}^{-1}\right), \tag{6.45}$$

$$E_2 = \left([\bar{r}]^{\times}\bar{p} - m_{\mathfrak{T}}[\bar{r}]^{2\times}\bar{\omega}_e - \mathbf{C}\bar{H}_{\mathfrak{T}}\right),$$

$$L_{3,i} = [f,\ [f,\ [f,\ g_i]]] = \left\{\begin{array}{c} \frac{\mu}{m_{\mathfrak{T}}}\int_{\mathfrak{T}}\left(\frac{I_3}{\left|\bar{r}+\mathbf{D}^{\mathrm{T}}\bar{\rho}_O\right|^3} - \frac{3(\bar{r}+\mathbf{D}^{\mathrm{T}}\bar{\rho}_O)\bar{r}^{\mathrm{T}}}{\left|\bar{r}+\mathbf{D}^{\mathrm{T}}\bar{\rho}_O\right|^5}\right)\mathbf{D}^{\mathrm{T}}\left[\bar{\rho}_O\right]^{\times}\bar{J}^{-1}\frac{\partial \bar{h}_a}{\partial \nu_i}dm \\ * \\ * \\ 0 \end{array}\right\}, \tag{6.46}$$

and where $*$ is an entry that is not of concern currently. A step-by-step computation of these brackets is given in Appendix D.

We now evaluate the Lie brackets at $\bar{r} = \bar{r}_e$, $\bar{p} = 0$, and $\mathbf{D} = I_3$. The brackets g_i span the tangent space associated with the control. The brackets $L_{1,i}$ for $i = 1, 2, 3$ will always span the tangent space of $SO(3)$ since the spin axes of the RWs are linearly independent by assumption. The Lie brackets $L_{2,i}$ and $L_{3,i}$ will span the tangent space of position and linear momentum, respectively, since by assumption, the RW spin axes span 3-dimensional space and $\bar{P}$ from (6.40) is nonsingular. Then by Lemma 6.2, the system is STLC from the equilibrium orbit. □

The integral in (6.40) can be challenging to compute exactly. By performing a Taylor-series expansion about (6.40), the following corollary to Theorem 6.1 is obtained:

Corollary 6.1: Let $\epsilon_2 << 1$. Then if

$$\frac{1}{R^5}\left(15\check{r}_e\check{r}_e^{\mathrm{T}}\left(\frac{\mathrm{tr}\left[\bar{J}\right]}{2}\left[\check{r}_e\right]^{\times} - \left[\bar{J}\check{r}_e\right]^{\times}\right) + 3\left[\bar{J}\check{r}_e\right]^{\times} - 3\bar{J}\left[\check{r}_e\right]^{\times}\right) \tag{6.47}$$

is nonsingular for a given equilibrium orbit corresponding to $\bar{r}_e$, the dynamics (6.30)

are STLC from the equilibrium orbit.

Proof: Performing a Taylor-series expansion of $\bar{P}$ in (6.40) about ϵ_2 yields

$$\bar{P} = \int_{\mathfrak{T}} \frac{1}{R^5}\left(\frac{15}{R^7}\bar{r}_e\bar{r}_e^{\mathrm{T}}\left[\bar{\rho}_C\bar{\rho}_C^{\mathrm{T}}\bar{r}_e\right]^{\times} + 3\bar{\rho}_C\bar{\rho}_C^{\mathrm{T}}\left[\bar{r}_e\right]^{\times} - 3\left[\bar{\rho}_C\bar{\rho}_C^{\mathrm{T}}\bar{r}_e\right]^{\times}\right)dm + O(\epsilon_2^3). \quad (6.48)$$

Noting that

$$\begin{aligned}\int_{\mathfrak{T}} \bar{\rho}_C\bar{\rho}_C^{\mathrm{T}}dm &= \int_{\mathfrak{T}} \left(\left[\bar{\rho}_C\right]^{2\times} + I_3\bar{\rho}_C^{\mathrm{T}}\bar{\rho}_C\right)dm, \\ &= -\bar{J} + I_3\frac{\mathrm{tr}\left[\bar{J}\right]}{2},\end{aligned} \quad (6.49)$$

$\bar{P}$ can be approximated by integrating (6.48) and neglecting terms of third-order in ϵ_2,

$$\bar{P} \approx \frac{1}{R^5}\left(15\check{r}_e\check{r}_e^{\mathrm{T}}\left(\frac{\mathrm{tr}\left[\bar{J}\right]}{2}\left[\check{r}_e\right]^{\times} - \left[\bar{J}\check{r}_e\right]^{\times}\right) + 3\left[\bar{J}\check{r}_e\right]^{\times} - 3\bar{J}\left[\check{r}_e\right]^{\times}\right). \quad (6.50)$$

The result of the corollary follows from Theorem 6.1 and Lemma 6.2. □

Note that Theorem 6.1 and Corollary 6.1 give sufficient, but not necessary conditions for (6.30) to be STLC. For several test cases, spacecraft in non-great circle orbits satisfy Theorem 6.1 and Corollary 6.1, though general claims are difficult to make. For a great circle equilibrium with a symmetric spacecraft, both Theorem 6.1 and Corollary 6.1 fail. However in the next section, the approximate system is linearized, and controllability claims can be made for great circle equilibrium orbits. This suggests that higher-order Lie brackets could yield stronger controllability conditions than the ones presented here.

6.3.2 Linear Controllability of the Translational, Approximate Relative Equations about Great Circle Equilibria

We now analyze the linear controllability properties of (6.31). Since non-great circle orbits are hard to generalize, this analysis will only be performed for spacecraft on great circle orbits. From Section 6.2, the spacecraft system requires the following assumption:

Assumption 6.4 The spacecraft inertia matrix about its COM has a least one plane of symmetry.

For the linear analysis, let the attitude be parameterized by Euler angles ϕ, θ, ψ, contained in the vector $\bar{\Theta}$. Linearizing the translational equations of (6.31) about the relative equilibrium $\bar{r}_{_r} = \bar{p}_{_r} = \bar{\Theta} = 0$ gives the following dynamics

$$\begin{aligned} \dot{\bar{r}}_{_r} &= \tfrac{\dot{\bar{p}}_r}{m_{_{\mathfrak{T}}}}, \\ \dot{\bar{p}}_{_r} &= \bar{A}_r \bar{r}_{_r} + \bar{A}_p \bar{p}_{_r} + \bar{A}_\Theta \bar{\Theta}, \end{aligned} \tag{6.51}$$

where because $\bar{r}_{_e} = [\ R \ \ 0 \ \ 0\ ]^{\mathrm{T}}$, $\bar{\omega}_{_e} = [\ 0 \ \ 0 \ \ \Omega\ ]^{\mathrm{T}}$, and by Assumption 6.4 frame $\mathcal{B}$ can be chosen such that $j_{12} = j_{13} = 0$, the matrices in (6.51) are

$$\bar{A}_r = \frac{2\mu m_{_{\mathfrak{T}}}}{R^3} I_3 + \frac{3\mu m_{_{\mathfrak{T}}}}{R^3} [\check{r}_{_e}]^{2\times} - m_{_{\mathfrak{T}}} [\bar{\omega}_{_e}]^{2\times} = \begin{bmatrix} 3m_{_{\mathfrak{T}}}\Omega^2 - 2\Omega_{_\epsilon} & 0 & 0 \\ 0 & \Omega_{_\epsilon} & 0 \\ 0 & 0 & -m_{_{\mathfrak{T}}}\Omega^2 + \Omega_{_\epsilon} \end{bmatrix}, \tag{6.52}$$

$$\bar{A}_\rho = -2\,[\bar{\omega}_{_e}]^{\times} = \begin{bmatrix} 0 & 2\Omega & 0 \\ -2\Omega & 0 & 0 \\ 0 & 0 & 0 \end{bmatrix}, \tag{6.53}$$

$$\begin{aligned}\bar{A}_{\Theta} &= -\tfrac{3\mu}{2R^4}\left(\tfrac{2}{R}\left(\bar{J}\left[\bar{r}_{_e}\right]^{\times} - \left[\bar{J}\bar{r}_{_e}\right]^{\times}\right) + \tfrac{10}{R^2}\bar{r}_{_e}^{\mathrm{T}}\bar{r}_{_e}\left[\bar{J}\bar{r}_{_e}\right]^{\times}\right), \\ &= \tfrac{3\mu}{R^4}\begin{bmatrix} 0 & 0 & 0 \\ 0 & j_{23} & (j_{11}-j_{22}) \\ 0 & (j_{33}-j_{11}) & -j_{23} \end{bmatrix}. \end{aligned} \tag{6.54}$$

Since the attitude dynamics are completely controllable by assumption, we do not linearize them. With the above linear dynamics, the following controllability statement can be made

Theorem 6.2: The approximate spacecraft dynamics (6.31) with attitude actuation by three RWs whose spin axes are linearly independent are linearly controllable about a great circle equilibrium orbit $\bar{r}_{_e}$ if and only if the spacecraft's inertia matrix satisfies one of the following requirements:

- $j_{11} \neq j_{22} \neq j_{33}$,
- $j_{22} = j_{33} \neq j_{11}$,
- $j_{23} \neq 0$ and $j_{22} = j_{11} \neq j_{33}$,
- $j_{23} \neq 0$ and $j_{33} = j_{11} \neq j_{22}$.

Proof: Recall that the PBH test for controllability [76] implies that a linear, time-invariant system $(\bar{A}, \bar{B})$ is controllable if and only if

$$\operatorname{rank}\left(\begin{bmatrix}\lambda I_6 - \bar{A} & \bar{B}\end{bmatrix}\right) = \dim(\bar{A}), \tag{6.55}$$

for every eigenvalue λ of $\bar{A}$, see [76]. By the converse, the system is uncontrollable if and only if there exists a nonzero vector $\bar{\eta} \in \mathbb{C}^6$ such that

$$\bar{\eta}^{\mathrm{CT}}\begin{bmatrix}\lambda I_6 - \bar{A} & \bar{B}\end{bmatrix} = 0, \tag{6.56}$$

for at least one eigenvalue, where $\bar{\eta}^{\mathrm{CT}}$ is the conjugate transpose of $\bar{\eta}$. Thus if there exists a left eigenvector of $\bar{A}$ such that $\bar{\eta}^{\mathrm{CT}}\bar{B} = 0$, the system is uncontrollable.

For the case of the spacecraft translational dynamics, $\bar{A}$ is given by

$$\bar{A} = \begin{bmatrix} 0 & \frac{1}{m_{\mathfrak{T}}} I_3 \\ \bar{A}_r & \bar{A}_\rho \end{bmatrix}. \tag{6.57}$$

We will now treat $\bar{\Theta}$ as the control input to the system (for reasons stated later in the proof), resulting in the control matrix

$$\bar{B} = \begin{bmatrix} 0 \\ \bar{A}_\Theta \end{bmatrix}. \tag{6.58}$$

It can be determined that all left eigenvectors of $\bar{A}$ have the form $\bar{\eta}^{\mathrm{CT}} = [\ * \ * \ * \ * \ 1 \ 0\ ]^{\mathrm{T}}$ or $\bar{\eta}^{\mathrm{CT}} = [\ * \ \ * \ \ * \ \ * \ 0 \ 1\ ]^{\mathrm{T}}$, where $*$ is an entry not of concern. The four spacecraft configurations in Theorem 6.2 are the only ones in which $\bar{\eta}^{\mathrm{CT}}\bar{B} \neq 0$ for all left eigenvectors. Thus the translational spacecraft dynamics are linearly controllable for these spacecraft configurations at equilibrium when attitude is treated as a control input. Since the attitude is completely controllable by three RWs, by dynamic extension the approximate dynamics (6.31) are linearly controllable if the spacecraft has one of the four configurations. $\square$.

With this, the following corollary can be made to Theorem 6.2:

Corollary 6.2 The approximate dynamics (6.31) with attitude actuation by three RWs whose spin axes are linearly independent are STLC from a great circle equilibrium orbit $\bar{r}_e$ if the spacecraft inertia matrix has one of the four configurations outlined in Theorem 6.2

Proof: Since the linear dynamics about the equilibrium orbit are controllable, the nonlinear approximate dynamics (6.31) are STLC, from Corollary 7.28 in [2]. $\square$

The implications of Theorem 6.2 are that if a spacecraft system satisfies one of the conditions in Theorem 6.2, then a linear controller can be designed to stabilize the translational and attitude dynamics of a spacecraft. While the maneuver may take time since gravitational effects are small, for large spacecraft, it is hypothesized that translational maneuvers can be performed in a matter of days. Since internal actuation is assumed, this means that relative translational motion of a spacecraft can be achieved with zero fuel consumption.

6.4 Simulations

To demonstrate the effect of rotational and translational coupling in a central gravity field, we present two simulations. The first simulation is for a Kepler sized spacecraft in a low-Earth, great circle orbit with an altitude of 416 km. The second simulation is for an International Space Station (ISS) sized spacecraft in the same low-Earth, great circle orbit. Both spacecraft are modeled as constant density cuboids, and thus satisfy the requirement for great circle orbits. All simulations are run on the approximate nonlinear dynamics in (6.31). The spacecraft parameters, equilibrium orbits, and initial conditions are given in Tables 6.1-6.2.

In both simulations, the spacecraft parameters and equilibrium orbits are chosen such that the spacecraft system is linearly controllable. We also make the following assumption:

Assumption 6.5 The spacecraft's attitude is instantaneously manipulatable.

Assumption 6.5 allows us to treat the attitude as the control input to the spacecraft system. In order to make this assumption reasonable, we linearize the coupled rotational and translational dynamics using (6.51) and discretize the dynamics using a sampling period of 500 sec. With this large sampling period, there is clearly sufficient time for the spacecraft to stabilize to the desired attitude necessary for translational

control. Since both spacecraft systems in both simulations are linearly controllable, an LQ controller is applied to each. The weighting matrices used to construct these controllers are included in Tables 6.1-6.2.

The Kepler sized spacecraft simulation is shown in Figure 6.3 and the ISS sized spacecraft simulation is shown in Figure 6.4. In Figure 6.3, the Kepler sized spacecraft initially begins with an offset in the in-track direction (i.e., the y-direction in frame $\mathcal{C}$) by 10 m with zero relative linear momentum, see Table 6.1 for initial conditions. In contrast, Figure 6.3 shows the ISS sized spacecraft's trajectory when it is initially offset in the in-track direction by 100 m with zero relative linear momentum, see Table 6.2 for initial conditions. In both cases, a linear controller is able to stabilize the translational spacecraft dynamics to the equilibrium orbit by just adjusting the spacecraft's attitude. It is worth noting that the attitude maneuvers in Figures 6.3 (b) and 6.4 (b) are approximately of the same magnitude, however, the ISS sized spacecraft exploits its large mass and inertia matrix to move farther in less time than the Kepler sized spacecraft.

Parameter	**Value**
Mass $m_{\bar{\mathfrak{s}}}$	1052 kg
Inertia $\bar{J}$	diag(0.0039, 0.0026, 0.0026) kg km^2
Equilibrium Orbit $\bar{r}_e$	$[\ 6787\ \ 0\ \ 0]^{\mathrm{T}}$ km
Orbit Angular Rate $\bar{\omega}_e$	$[\ 0\ \ 0\ \ 0.0011\ ]^{\mathrm{T}}$ rad sec^{-1}
Initial Position $\bar{r}_r(0)$	$[\ 0\ \ 0.01\ \ 0\ ]^{\mathrm{T}}$ km
Initial Linear Momentum $\bar{p}_r(0)$	$[\ 0\ \ 0\ \ 0\ ]^{\mathrm{T}}$ km sec^{-1}
LQ weight on Position and Linear Momentum for $\bar{Q}$	I_6
LQ weight on attitude $\bar{R}$	$(1 \times 10^{-4})I_3$

Table 6.1: Simulation parameters for Kepler sized spacecraft.

Parameter	**Value**
Mass $m_{\bar{\mathfrak{s}}}$	419455 kg
Inertia $\bar{J}$	diag(195.18, 425.47, 592.69) kg km^2
Equilibrium Orbit $\bar{r}_e$	$[\ 6787\ \ 0\ \ 0]^{\mathrm{T}}$ km
Orbit Angular Rate $\bar{\omega}_e$	$[\ 0\ \ 0\ \ 0.0011\ ]^{\mathrm{T}}$ rad sec^{-1}
Initial Position $\bar{r}_r(0)$	$[\ 0\ \ 0.1\ \ 0\ ]^{\mathrm{T}}$ km
Initial Linear Momentum $\bar{p}_r(0)$	$[\ 0\ \ 0\ \ 0\ ]^{\mathrm{T}}$ km sec^{-1}
LQ weight on Position and Linear Momentum for $\bar{Q}$	diag(1, 1×10^7, 1, 1, 1, 1)
LQ weight on attitude $\bar{R}$	$(5 \times 10^3)I_3$

Table 6.2: Simulation parameters for ISS sized spacecraft.

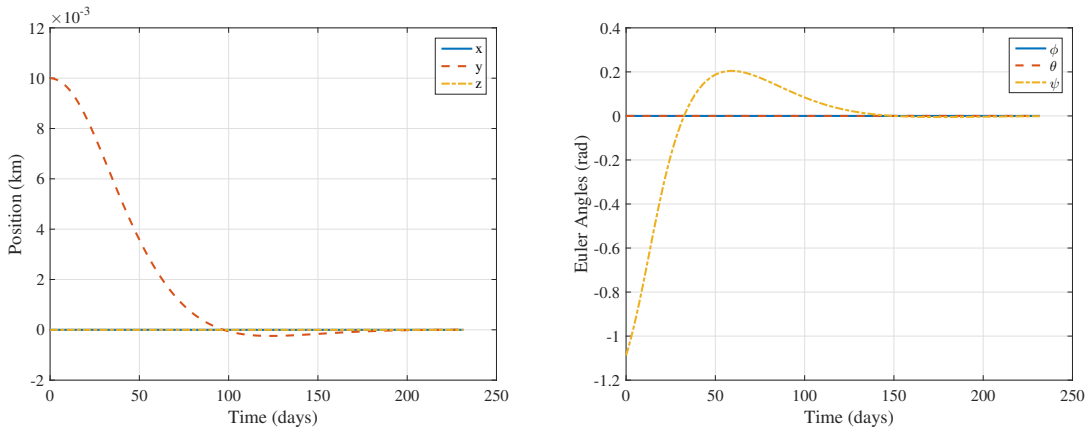

(a) (b)

Figure 6.3: Simulation 1, Kepler sized spacecraft. (a) Relative position, (b) attitude.

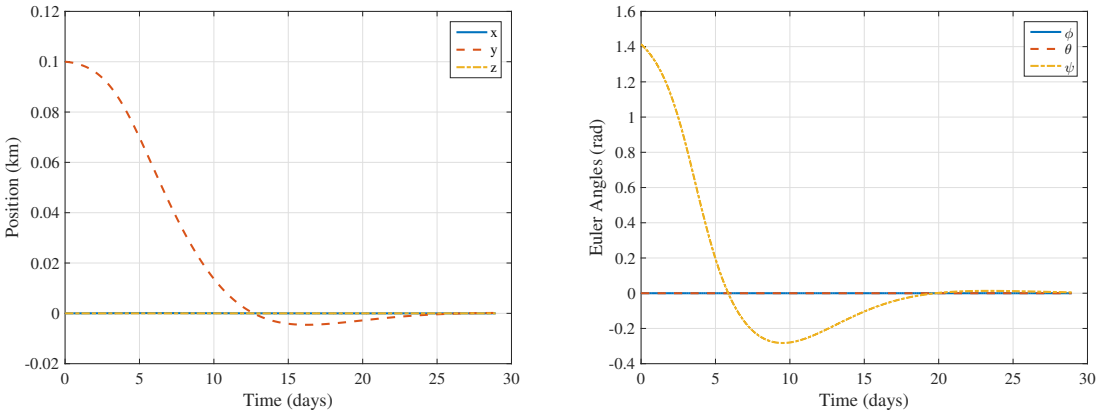

(a) (b)

Figure 6.4: Simulation 2, ISS sized spacecraft. (a) Relative position, (b) attitude.

CHAPTER 7

Conclusions and Future Work

7.0.1 Conclusions

This dissertation presented various advances in control of underactuated spacecraft. The following two problems were treated:

- The attitude (orientation) control of a spacecraft when equipped with either two pairs of thrusters, or two reaction wheels (RWs), or two control moment gyros (CMGs);
- The orbit and attitude control of a spacecraft when equipped with only RWs or CMGs.

The overall results contribute to the goal of extending spacecraft operational life during failure modes as well as enhancing the capability of spacecraft which are underactuated by design. The specific contributions are summarized as follows:

Underactuated Attitude Control Using Geometric Switching Feedback Control

We presented various switching feedback laws to locally control the attitude of an underactuated spacecraft with two pairs of thrusters, or two RWs, or two CMGs to an inertial pointing configuration. The feedback laws exploited the decomposition of the system states into base variables that are directly controllable and fiber variables that

are not directly controllable. By stabilizing the base variables to periodic motions, a change in the fiber variables can be induced, which is regulated by changing parameters at discrete time instants. All the switching schemes were shown to stabilize an underactuated spacecraft to the desired pointing configuration in simulation.

In the case of RW actuation, the switching scheme stabilized the attitude when the component of the total, inertial angular momentum vector along the uncontrollable axis is zero. If this was not the case, controlled oscillations in a neighborhood around the desired pointing configuration were achieved with a modified switching scheme. Additional analysis results of the spacecraft response properties have been presented to characterize trajectory limits as the excitation frequency of the base variables increases.

Attitude Underactuated Control Using Model Predictive Control

We presented the application of nonlinear Model Predictive Control (MPC) to stabilize the attitude of an underactuated spacecraft with two RWs and zero angular momentum. It was shown that MPC based on an approximate model was able to generate a feedback law that was discontinuous in terms of state and locally stabilized the system to the desired pointing equilibrium. Simulations on the full nonlinear model demonstrated successful inertial pointing maneuvers with fast exponential convergence rates and with constraints being satisfied.

Recovering Controllability By Exploiting Solar Radiation Pressure

We uncovered an unconventional pathway to recover linear controllability through incorporating Solar Radiation Pressure (SRP) torques into the spacecraft attitude model. For certain fixed inertial pointing directions and realistic spacecraft configurations, linear controllability is recovered and spacecraft control becomes feasible with conventional Linear Quadratic (LQ) and pole placement techniques. While the ma-

neuvers take time, the approach presented is not restricted to the assumption of zero angular momentum; in fact, due to the presence of solar radiation pressure torques, the total angular momentum may not be zero and is not conserved. The results open up the possibility of applying a variety of conventional control techniques to the underactuated spacecraft control problem.

Rotational and Translational Underactuated Control in a Gravity Field

We developed two sets of novel, coupled translational and rotational equations that described the motion of a spacecraft, equipped with only internal moment actuators, about an equilibrium orbit in a central gravity field. One set of equations exactly described the motion of the spacecraft. Using these equations, sufficient conditions for small-time local controllability (STLC) about the equilibrium orbit were given which depend on the inertia of the spacecraft and the equilibrium orbit. The second set of equations are an approximation which extend the traditional Hill-Clohessy-Wiltshire (HCW) relative equations of motion. For these equations, linear controllability of certain spacecraft configurations was proven. The fact that linear controllability is restored opens the door to constructing conventional controllers that can move the spacecraft translationally by only changing its orientation.

7.0.2 Future Work

While this dissertation has made strides toward advancing underactuated spacecraft control capabilities, there are still many directions to be explored. Below are several research topics that are of interest in the future.

Attitude Control of an Underactuated Spacecraft with CMGs

The work in Chapter 3 only presented preliminary results of a switching controller for the case of two skewed CMGs with zero total angular momentum. The next step

would be performing a more comprehensive study of the case of two skewed CMGs and developing a similar controller for the case of two CMGs whose gimbal axes are aligned with zero total angular momentum. Extensions to the nonzero angular momentum case would follow, as well as a similar limiting analysis when the frequency of the gimbal angle motions becomes large.

The application of MPC to control a spacecraft with two CMGs also appears promising. A nonlinear MPC may be utilized to exploit the nonlinear dynamics for controllability, and its development would be similar to the case of RWs. However, the difficultly lies in the singular configurations of the CMGs. While it is desired to avoid these configurations, trajectories that contain singular configurations may yield benefits in terms of cost.

From a pure controllability analysis standpoint, there remains the open question of whether a spacecraft system, equipped with two CMGs that have parallel gimbal axes, under the zero total angular momentum assumption, is STLC from at-rest equilibria. This problem is challenging in that sufficient conditions given by Lie brackets [2, 93] cannot be used (this is because to show controllability with CMGs, bad brackets must be constructed). Approaching the question of local controllability from another standpoint, in particular optimal control, may lead to some insights.

Underactuated Spacecraft Attitude Control with Magnetorquers

The only class of broadly used attitude actuators not investigated in this dissertation were magnetorquers. While weak in comparison to thruster pairs, RWs, and CMGs, there are several advantages to magnetic actuation. Magnetorquers have similar advantages to RWs and CMGs in that they do not require fuel. In addition, torques are generated due to the interaction of magnetic fields, and thus these actuators are not restricted by the law of angular momentum conservation. The difficulty with magnetorquers is that the uncontrollable axis varies with time. The work in this

dissertation concerning CMGs addressed the varying uncontrollable axis by utilizing $SO(3)$-based attitude representation. This approach also appears promising for the case of magnetorquers.

Control of Underactuated Spacecraft by Exploiting External Forces

It was demonstrated that the addition of SRP allowed the attitude dynamics of an underactuated spacecraft to be linearly controllable in some cases. It stands to reason that the addition of other perturbation forces could lead to the restoration of linear controllability as well. Perturbation forces such as air drag, gravity gradient torques, and residual magnetic moment could be exploited for control purposes when a spacecraft is in low Earth orbit, where SRP is not a major factor. Constructing control laws of this kind may also change the practice that disturbances should be rejected, and instead shift the line of thinking to exploiting these disturbances for control.

The inclusion of external forces would not be limited to just attitude underacted control. The perturbations listed above are also known to have an effect on a spacecraft's translational motion. Including air drag and magnetic moment in the mathematical model of coupled rotational and translational equations could lead to additional results when considering the controllability of a spacecraft in orbit equipped with only attitude actuators.

Control of Underactuated Spacecraft in a Gravity Field

In Chapter 6, STLC conditions about an equilibrium orbit were given for spacecraft equipped with RWs. However the equations of motion were derived for CMGs as well. CMG singularity is always an issue when trying to prove any local controllability result, so the next extension would be to construct brackets where this would not be an issue. Other avenues of research would involve looking at global controllability as

well as including a higher fidelity gravity model in the analysis, e.g. J2 perturbations.

In addition to the control analysis, control schemes could be developed to utilize this coupling effect to stabilize both the translational and rotational equations of motion. While it was shown that in some instances linear controllability is regained, a nonlinear controller could potentially exploit the gravity terms and possibly yield faster stabilization of the dynamics. Potential control schemes along these lines could be based on nonlinear MPC and on the geometric switching laws discussed in this dissertation.

APPENDIX A

Lie Brackets and Controllability

Let a general system for $\bar{x} \in \mathbb{R}^n$ that is affine in the control be given by

$$\dot{\bar{x}} = f_0(\bar{x}) + \sum_{i=1}^{m} f_i(\bar{x}) u_i, \tag{A.1}$$

where m is the number of control inputs, $u_i,\ i = 1, ..., m$ are the specific control inputs that are piecewise continuous (note $\bar{u} = [\ u_1\ \ u_2\ \ ...\ \ u_m\ ]^{\mathrm{T}}$), f_0 is the drift vector field, which is continuous (C^∞) in the state, and $f_i,\ i = 1, ..., m$, are the control vector fields which are continuous in the state. By studying the vector fields of (A.1) as well as the vector fields generated by Lie brackets, certain controllability properties of (A.1) can be obtained.

To begin, a Lie bracket of system (A.1) is a bilinear, skew-symmetric map that takes any two vector fields, $f_j(\bar{x})$ and $f_k(\bar{x})$, $j, k \in \{0, 1, ...m\}$ and generates a third vector field on $\mathbb{R}^n$ in the following way [2, 7],

$$[\ f_j,\ \ f_k\ ] = \frac{\partial f_k(\bar{x})}{\partial \bar{x}} f_j(\bar{x}) - \frac{\partial f_j(\bar{x})}{\partial \bar{x}} f_k(\bar{x}). \tag{A.2}$$

Let B denote any arbitrary Lie bracket of system (A.1). Define the operator $|B|_a$ as the number of times the vector field f_a appears in the bracket, for any $a \in \{0, 1, ..., m\}$. A bracket B is bad if $|B|_0$ is odd and $|B|_a$ is even $\forall a \in 1, 2, ..., m$. Otherwise the

bracket B is good. Lastly, define the χ-degree operator of bracket B as follows [2]

$$\deg_1(B) = \frac{1}{\chi}|B|_0 + \sum_{i=1}^{m} |B|_i, \tag{A.3}$$

where $\chi \in [1, \infty]$. In particular, the $1-$degree operator of bracket B is

$$\deg_1(B) = \sum_{i=0}^{m} |B|_i. \tag{A.4}$$

The 1-degree operator is hence the total number of vector fields of (A.1) used to generate Lie bracket B.

The following theorems summarize accessibility and controllability results found in [2,93] and specialize them to the case of the system (A.1). Refer to [2,93] for more general definitions.

Theorem A1: Let $(\bar{x}^*, \bar{u}^*)$ be an equilibrium of (A.1). Define D_∞ as the set of all vector fields in (A.1) and all vector fields constructed from Lie brackets. The system (A.1) is *accessible from* $(\bar{x}^*, \bar{u}^*)$ if and only if the D_∞ spans $\mathbb{R}^n$ when the vector fields are evaluated at $(\bar{x}^*, \bar{u}^*)$. This is known as the Lie Algebra Rank Condition. □

Theorem A2: Let $(\bar{x}^*, \bar{u}^*)$ be an equilibrium of (A.1). Define D_∞ as the set of all vector fields in (A.1) and all vector fields constructed from Lie brackets. In addition, let $\hat{D} \subset D_\infty$ and p be the largest 1-degree of all vector fields in $\hat{D}$ generated by Lie brackets. The system (A.1) is *STLC from* $(\bar{x}^*, \bar{u}^*)$ if there exists a $\hat{D}$ such that:

i. $\hat{D}$ satisfies the Lie Algebra Rank Condition when evaluated at $(\bar{x}^*, \bar{u}^*)$.

ii. All bad brackets in D_∞ of χ-degree less than p when evaluated at $(\bar{x}^*, \bar{u}^*)$ are linear combinations of good brackets in $\hat{D}$ of lower order, when evaluated at $(\bar{x}^*, \bar{u}^*)$.

□

Note that Theorem A1 is sufficient and necessary while Theorem A2 is only sufficient.

The dynamics of (4.4) are now analyzed with the help of these two theorems.

Theorem A3: The dynamics in (4.4) are STLC from any equilibria.

Proof: The drift vector field and the control vector fields of (4.7) are

$$f_0 = \begin{bmatrix} (\alpha_1\nu_1 + \alpha_2\nu_2) + (\beta_1\nu_1 + \beta_2\nu_2)\sin(\phi)\tan(\theta), \\ (\beta_1\nu_1 + \beta_2\nu_2)\cos(\phi) \\ (\beta_1\nu_1 + \beta_2\nu_2)\sin(\phi)\sec(\theta) \\ 0 \\ 0 \end{bmatrix}, \tag{A.5}$$

$$f_1 = [\ 0 \quad 0 \quad 0 \quad 1 \quad 0\ ]^{\mathrm{T}},$$

$$f_2 = [\ 0 \quad 0 \quad 0 \quad 0 \quad 1\ ]^{\mathrm{T}}.$$

Using (A.2), three Lie brackets are generated

$$B_1 = [\ f_1, \quad f_0\ ] = \begin{bmatrix} \alpha_1 + \beta_1\sin(\phi)\tan(\theta) \\ \beta_1\cos(\phi) \\ \beta_1\sin(\phi)\sec(\theta) \\ 0 \\ 0 \end{bmatrix}, \tag{A.6}$$

$$B_2 = [\ f_2, \quad f_0\ ] = \begin{bmatrix} \alpha_2 + \beta_2\sin(\phi)\tan(\theta) \\ \beta_2\cos(\phi) \\ \beta_2\sin(\phi)\sec(\theta) \\ 0 \\ 0 \end{bmatrix}, \tag{A.7}$$

$$B_3 = [\ B_1,\ \ B_2\ ] = \begin{bmatrix} \cos(\phi)\sin(\theta)\sec(\theta)(\alpha_1\beta_2 - \alpha_2\beta_1) \\ -\sin(\phi)(\alpha_1\beta_2 - \alpha_2\beta_1) \\ \cos(\phi)\sec(\theta)(\alpha_1\beta_2 - \alpha_2\beta_1) \\ 0 \\ 0 \end{bmatrix}. \tag{A.8}$$

Let $\hat{D} = \{f_1,\ f_2,\ B_1,\ B_2,\ B_3\}$. Note that $\hat{D}$ spans $\mathbb{R}^5$ when evaluated at any equilibrium, which implies D_∞ spans $\mathbb{R}^5$ when evaluated at any equilibrium. By Theorem A1, the system is accessible from all equilibria.

It now is necessary to determine if the system is STLC from all equilibria. Note that in $\hat{D}$, B_3 is constructed by using the drift vector f_0 twice and the control vectors f_1 and f_2 each once. Thus the bracket is good and has a 1-degree of 4, the largest of any other brackets in $\hat{D}$. The only bad brackets that can be constructed with a 1-degree less than 4 in D_∞ are $[\ f_1\ ,\ B_1\ ]$ and $[\ f_2,\ B_2\ ]$ (in the construction of each of these brackets, f_0 is used once and either f_1 or f_2 is used twice, and hence the brackets are bad). These brackets are zero and thus are linear combinations of those brackets of 1-degree of 2 or less. By Theorem A2, the system is STLC from any equilibrium. □

APPENDIX B

Open-Loop Control Law for Approximate Attitude Dynamics

Let $\bar{x}_0 = [\ \phi_0\ \ \theta_0\ \ \psi_0\ \ 0\ \ 0\ ]^{\mathrm{T}}$ be any equilibrium of (4.13) and $\bar{x}^* = [\ \phi^*\ \ \theta^*\ \ \psi^*\ \ \nu_1^*\ \ \nu_2^*\ ]^{\mathrm{T}}$ be the desired state. Furthermore define $\bar{y}_0 = [\ \phi_0\ \ \ \theta_0\ \ \ 0\ \ \ 0\ ]^{\mathrm{T}}$ as the initial base variable vector, $\bar{y}^* = [\ \phi^*\ \ \ \theta^*\ \ \ \nu_1^*\ \ \ \nu_2^*\ ]^{\mathrm{T}}$ as the desired base variable vector, and $\bar{y}_c = [\ \tilde{\phi}\ \ \tilde{\theta}\ \ \tilde{\nu}_1\ \ \tilde{\nu}_2\ ]^{\mathrm{T}}$ as an arbitrary base variable vector. Then the control sequence

$$[\ u_{1,0}\ \ u_{2,0}\ \ u_{1,1}\ \ u_{2,1}\ ]^{\mathrm{T}} = \left([\ \bar{A}\bar{B}\ \ \ \bar{B}\ ]\right)^{-1}(\bar{y}^* - \bar{A}^2\bar{y}_0), \tag{B.1}$$

$$[\ u_{1,2}\ \ u_{2,2}\ \ u_{1,3}\ \ u_{2,3}\ ]^{\mathrm{T}} = \left([\ \bar{A}\bar{B}\ \ \ \bar{B}\ ]\right)^{-1}(\bar{y}_c - \bar{A}^2\bar{y}^*), \tag{B.2}$$

$$[\ u_{1,4}\ \ u_{2,4}\ \ u_{1,5}\ \ u_{2,5}\ ]^{\mathrm{T}} = \left([\ \bar{A}\bar{B}\ \ \ \bar{B}\ ]\right)^{-1}(\bar{y}^* - \bar{A}^2\bar{y}_c), \tag{B.3}$$

where

$$\bar{A} = \begin{bmatrix} 1 & 0 & \alpha_1 T & \alpha_2 T \\ 0 & 1 & \beta_1 T & \beta_2 T \\ 0 & 0 & 1 & 0 \\ 0 & 0 & 0 & 1 \end{bmatrix}, \quad \bar{B} = \begin{bmatrix} \alpha_1 \frac{T^2}{2} & \alpha_2 \frac{T^2}{2} \\ \beta_1 \frac{T^2}{2} & \beta_2 \frac{T^2}{2} \\ T & 0 \\ 0 & T \end{bmatrix}, \tag{B.4}$$

will guide any $\bar{x}_0$ to $\bar{x}^*$ as long as

$$\psi_2 + \frac{5T}{12}\Delta_c = \psi^*, \tag{B.5}$$

where

$$\Delta_c = (\tilde{\phi} - \phi^*)(\beta_1(\tilde{\nu}_1 - \nu_1^*) + \beta_2(\tilde{\nu}_2 - \nu_2^*)) - (\tilde{\theta} - \theta^*)(\alpha_1(\tilde{\nu}_1 - \nu_1^*) + \alpha_2(\tilde{\nu}_2 - \nu_2^*)), \tag{B.6}$$

and

$$\psi_2 = \psi_0 + \frac{5T}{24}((\phi^* - \phi_0)(\beta_1\nu_1^* + \beta_2\nu_2^*) - (\theta^* - \theta_0)(\alpha_1\nu_1^* + \alpha_2\nu_2^*)) + \frac{1}{2}(\theta^* - \theta_0)(\phi^* + \phi_0). \tag{B.7}$$

Note that (B.7) is the drift in the uncontrollable angle ψ due to the control input (B.1). If (B.5) is satisfied, $\bar{x} = \bar{x}^*$ in six steps. Now, let

$$\begin{aligned} \tilde{\phi} &= \phi^* + \sqrt{|\psi^* - \psi_2|}, \\ \tilde{\theta} &= \theta^* - \sqrt{|\psi^* - \psi_2|}, \\ \tilde{\nu}_1 &= \tfrac{6}{5T(\alpha_1+\beta_1)}\text{sign}(\psi^* - \psi_2)\sqrt{|\psi^* - \psi_2|} + \nu_1^*, \\ \tilde{\nu}_2 &= \tfrac{6}{5T(\alpha_2+\beta_2)}\text{sign}(\psi^* - \psi_2)\sqrt{|\psi^* - \psi_2|} + \nu_2^*. \end{aligned} \tag{B.8}$$

It can be seen that (4.29) is satisfied, assuming that $\alpha_1 + \beta_2 \neq 0$ and $\alpha_2 + \beta_2 \neq 0$ (this will not occur if the two RWs are not parallel). If either $\alpha_1 + \beta_2 \neq 0$ or $\alpha_2 + \beta_2 \neq 0$, then other choices for $\bar{y}_c$ do exist. Also note that this maneuver is possible for all sample times $T > 0$, and only relies on the maneuvering being performed in six steps.

APPENDIX C

Approximations in Rotational and Translational Coupling in a Central Gravity Field

Traditionally, rotational and translational equations are derived by approximating the gravity potential function via a Taylor-series expansion, integrating over the spacecraft body, and using that approximation to derive the total gravitational force. Less often is the gravitational force approximated by a Taylor-series and then integrated over the body to yield the total force. In this appendix, we will use both methods to derive the translational equations for a rigid body in a central gravity field up to similar order in the Taylor-series. Then both techniques will be compared. While the derivations here are for a central gravity field, the work can be extended to include J2 and higher-order gravitational perturbations [44, 64].

C.1 Approximation at the Gravitational Potential Level

The gravitational potential of an infinitesimal mass element dm in a rigid spacecraft $\mathfrak{T}$ is

$$dV = -\frac{\mu}{|\vec{r}_{O/A} + \vec{r}_{\rho/O}|} dm, \tag{C.1}$$

where $\vec{r}_{O/A}$ is the physical vector from the center of the gravity field at A to the COM of the spacecraft at O and $\vec{r}_{\rho/O}$ is the physical vector from the COM of the spacecraft to an infinitesimal mass element. We observe that the denominator of the potential in (C.1) can be written as

$$\begin{aligned} |\vec{r}_{O/A} + \vec{r}_{\rho/O}|^{-1} &= \left(\left(\vec{r}_{O/A} + \vec{r}_{\rho/O}\right) \cdot \left(\vec{r}_{O/A} + \vec{r}_{\rho/O}\right)\right)^{-\frac{1}{2}}, \\ &= \left(\vec{r}_{O/A} \cdot \vec{r}_{O/A} + 2\vec{r}_{O/A} \cdot \vec{r}_{\rho/O} + \vec{r}_{\rho/O} \cdot \vec{r}_{\rho/O}\right)^{-\frac{1}{2}}, \\ &= R^{-1} \left(1 + 2\epsilon \cos(\kappa) + \epsilon^2\right)^{-\frac{1}{2}}, \\ &= E_{dV}(\epsilon), \end{aligned} \tag{C.2}$$

where $R = |\vec{r}_{O/A}|$, $\epsilon = \frac{|\vec{r}_{\rho/O}|}{R}$ and κ is the angle between $\vec{r}_{O/A}$ and $\vec{r}_{\rho/O}$. Expanding (C.2) by a Taylor-series about $\epsilon = 0$ gives

$$|\vec{r}_{O/A} + \vec{r}_{\rho/O}|^{-1} = E_{dV_0} + E_{dV_1} + E_{dV_2} + O(\epsilon^3), \tag{C.3}$$

where

$$
\begin{aligned}
E_{dV_0} &= E_{dV}(0) &&= R^{-1}, \\
E_{dV_1} &= \left.\frac{\partial E_{dV}}{\partial \epsilon}\right|_{\epsilon=0} \epsilon &&= \left.-\frac{1}{2R}\left(1+2\epsilon\cos(\kappa)+\epsilon^2\right)^{-\frac{3}{2}}\left(2\cos(\kappa)+2\epsilon\right)\right|_{\epsilon=0} \epsilon \\
&&&= -R^{-1}\cos(\kappa), \\
&&&= -\frac{\vec{r}_{O/A}\cdot\vec{r}_{\rho/O}}{R^3}, \\
E_{dV_2} &= \left.\frac{1}{2}\frac{\partial^2 E_{dV}}{\partial \epsilon^2}\right|_{\epsilon=0} \epsilon^2 &&= \left.\frac{3}{8R}\left(1+2\epsilon\cos(\kappa)+\epsilon^2\right)^{-\frac{5}{2}}\left(2\cos(\kappa)+2\epsilon\right)^2\right|_{\epsilon=0} \epsilon^2 \\
&&&\quad \left.-\frac{1}{2R}\left(1+2\epsilon\cos(\kappa)+\epsilon^2\right)^{-\frac{3}{2}}\right|_{\epsilon=0} \epsilon^2, \\
&&&= \left(\frac{3}{2R}\cos(\kappa)^2-\frac{1}{R}\right)\epsilon^2, \\
&&&= \frac{3\left(\vec{r}_{O/A}\cdot\vec{r}_{\rho/O}\right)^2}{2R^5}-\frac{\vec{r}_{\rho/O}\cdot\vec{r}_{\rho/O}}{2R^3}.
\end{aligned}
\tag{C.4}
$$

Integrating (C.3) over the entire body gives the approximate potential of the spacecraft in a central gravity field

$$
V = \mu\left(V_0+V_1+V_2+O(\epsilon^3)\right), \tag{C.5}
$$

where

$$
\begin{aligned}
V_0 &= \int_{\mathfrak{T}} E_{dV_0} dm &&= -\int_{\mathfrak{T}} \tfrac{\mu}{R} dm, \\
&&&= -\tfrac{m_{\mathfrak{T}}\mu}{R}, \\
V_1 &= \int_{\mathfrak{T}} E_{dV_1} dm &&= \int_{\mathfrak{T}} \tfrac{\mu \vec{r}_{O/A}\cdot\vec{r}_{\rho/O}}{R^3} dm \\
&&&= 0, \\
V_2 &= \int_{\mathfrak{T}} E_{dV_2} dm &&= \int_{\mathfrak{T}} \mu \left(\tfrac{\vec{r}_{\rho/O}\cdot\vec{r}_{\rho/O}}{2R^3} - \tfrac{3\left(\vec{r}_{O/A}\cdot\vec{r}_{\rho/O}\right)^2}{2R^5} \right) dm, \\
&&&= \int_{\mathfrak{T}} \mu \left(\tfrac{\vec{r}_{\rho/O}\cdot\vec{r}_{\rho/O}}{2R^3} - \tfrac{3\left(\vec{r}\,'_{O/A}\left(\vec{r}_{\rho/O}\vec{r}\,'_{\rho/O}\right)\vec{r}_{O/A}\right)}{2R^5} \right) dm, \\
&&&= \tfrac{\mu \mathrm{tr}\left[\vec{J}_{\mathfrak{T}/O}\right]}{4R^3} - \int_{\mathfrak{T}} \tfrac{3\mu}{2R^5} \vec{r}\,'_{O/A} \left(I_3 \vec{r}_{\rho/O}\cdot\vec{r}_{\rho/O} + \left[\vec{r}_{\rho/O}\right]^{2\times} \right) \vec{r}_{O/A} dm, \\
&&&= -\tfrac{\mu \mathrm{tr}\left[\vec{J}_{\mathfrak{T}/O}\right]}{2R^3} + \tfrac{3\mu}{2R^3} \hat{r}' \vec{J}_{\mathfrak{T}/O} \hat{r},
\end{aligned}
\tag{C.6}
$$

where $\hat{r} = \frac{\vec{r}_{O/A}}{R}$ and $\hat{r}'$ is the dual of $\hat{r}$ [63]. The approximate gravitational force on the spacecraft's COM is then given by taking the negative gradient of the potential function (C.5),

$$F_V = F_{V_0} + F_{V_1} + F_{V_2} + O(\epsilon^3), \tag{C.7}$$

where

$$\begin{aligned} F_{V0} &= -\nabla V_0 = -\tfrac{m_{\mathfrak{T}\mu}}{R^3}, \\ F_{V1} &= -\nabla V_1 = 0, \\ F_{V2} &= -\nabla V_2 = -\tfrac{3\mu \mathrm{tr}\left[\bar{J}_{\mathfrak{T}/O}\right]}{2R^4}\hat{r} + \tfrac{15\mu}{2R^4}\left(\hat{r}'\vec{J}_{\mathfrak{T}/O}\hat{r}\right)\hat{r} - \tfrac{3\mu}{R^4}\vec{J}_{\mathfrak{T}/O}\hat{r}. \end{aligned} \tag{C.8}$$

C.2 Approximation at the Force Level

Consider now the gravitational force acting on an infinitesimal mass element of the spacecraft,

$$d\vec{f} = -\frac{\mu}{\left|\vec{r}_{O/A} + \vec{r}_{\rho/A}\right|^3}\left(\vec{r}_{O/A} + \vec{r}_{\rho/O}\right). \tag{C.9}$$

Similarly, as before, the denominator of (C.9) can be written as

$$\begin{aligned} |\vec{r}_{O/A} + \vec{r}_{\rho/O}|^{-3} &= \left(\left(\vec{r}_{O/A} + \vec{r}_{\rho/O}\right)\cdot\left(\vec{r}_{O/A} + \vec{r}_{\rho/O}\right)\right)^{-\frac{3}{2}}, \\ &= \left(\vec{r}_{O/A}\cdot\vec{r}_{O/A} + 2\vec{r}_{O/A}\cdot\vec{r}_{\rho/O} + \vec{r}_{\rho/O}\cdot\vec{r}_{\rho/O}\right)^{-\frac{3}{2}}, \\ &= R^{-3}\left(1 + 2\epsilon\cos(\kappa) + \epsilon^2\right)^{-\frac{3}{2}}, \\ &= E_{df}(\epsilon). \end{aligned} \tag{C.10}$$

Performing a Taylor-series expansion of (C.10) about $\epsilon = 0$ gives

$$|\vec{r}_{O/A} + \vec{r}_{\rho/O}|^{-3} = E_{df_0} + E_{df_1} + E_{df_2}, \tag{C.11}$$

where

$$
\begin{aligned}
E_{df_0} &= E_f(0) &&= R^{-3}, \\
E_{df_1} &= \left.\frac{\partial E_f}{\partial \epsilon}\right|_{\epsilon=0} \epsilon &&= \left.-\tfrac{3}{2R^3}\left(1+2\epsilon\cos(\kappa)+\epsilon^2\right)^{-\frac{5}{2}}\left(2\cos(\kappa)+2\epsilon\right)\right|_{\epsilon=0}\epsilon, \\
&&&= -3R^{-3}\cos(\kappa), \\
&&&= -\tfrac{3\vec{r}_{O/A}\cdot\vec{r}_{\rho/O}}{R^5},
\end{aligned}
\tag{C.12}
$$

$$
\begin{aligned}
E_{df_2} &= \left.\tfrac{1}{2}\tfrac{\partial^2 E_{dV}}{\partial \epsilon^2}\right|_{\epsilon=0}\epsilon^2 &&= \left.\tfrac{15}{8R^3}\left(1+2\epsilon\cos(\kappa)+\epsilon^2\right)^{-\frac{7}{2}}\left(2\cos(\kappa)+2\epsilon\right)^2\right|_{\epsilon=0}\epsilon^2 \\
&&&\quad \left.-\tfrac{3}{2R^3}\left(1+2\epsilon\cos(\kappa)+\epsilon^2\right)^{-\frac{5}{2}}\right|_{\epsilon=0}\epsilon^2, \\
&&&= \left(\tfrac{15}{2R^3}\cos(\kappa)^2-\tfrac{3}{R^3}\right)\epsilon^2, \\
&&&= \tfrac{15\left(\vec{r}_{O/A}\cdot\vec{r}_{\rho/O}\right)^2}{2R^7}-\tfrac{3\vec{r}_{\rho/O}\cdot\vec{r}_{\rho/O}}{2R^5}.
\end{aligned}
\tag{C.13}
$$

The total force due to gravity on the spacecraft's COM is determined by integrating (C.11) over the body,

$$
F_f = F_{f_0} + F_{f_1} + F_{f_2}, \tag{C.14}
$$

where

$$
\begin{aligned}
F_{f_0} &= -\int_{\mathfrak{T}} \mu(df_0)(\vec{r}_{O/A}+\vec{r}_{\rho/O})dm &&= -\int_{\mathfrak{T}} \tfrac{\mu}{R^3}dm, \\
&&&= -\tfrac{m_{\mathfrak{T}}\mu}{R^3},
\end{aligned}
\tag{C.15}
$$

$$
\begin{aligned}
F_{f_1} &= -\int_{\mathfrak{T}} \mu(df_0)(\vec{r}_{O/A} + \vec{r}_{\rho/O}) &= \int_{\mathfrak{T}} \frac{3\mu \vec{r}_{O/A} \cdot \vec{r}_{\rho/O}}{R^5}(\vec{r}_{O/A} + \vec{r}_{\rho/O})dm, \\
&&= \int_{\mathfrak{T}} \frac{3\mu}{R^5}\left(\vec{r}_{\rho/O}\vec{r}\,'_{\rho/O}\right)\vec{r}_{O/A}dm, \\
&&= \int_{\mathfrak{T}} \frac{3\mu}{R^5}\left(I_3\vec{r}_{\rho/O} \cdot \vec{r}_{\rho/O} + \left[\vec{r}_{\rho/O}\right]^{2\times}\right)\vec{r}_{O/A}dm, \\
&&= \frac{3\mu \mathrm{tr}\left[\vec{J}_{\mathfrak{T}/O}\right]}{2R^4}\hat{r} - \frac{3\mu}{R^4}\vec{J}_{\mathfrak{T}/O}\hat{r},
\end{aligned}
\tag{C.16}
$$

$$
\begin{aligned}
F_{f_2} &= -\int_{\mathfrak{T}} \mu(df_2)(\vec{r}_{O/A}+\vec{r}_{\rho/O})dm &&= -\mu\int_{\mathfrak{T}}\left(\frac{15\left(\vec{r}_{O/A}\cdot\vec{r}_{\rho/O}\right)^2}{2R^7}-\frac{3\vec{r}_{\rho/O}\cdot\vec{r}_{\rho/O}}{2R^5}\right)\vec{r}_{O/A}dm \\
&&&\quad -\mu\int_{\mathfrak{T}}\left(\frac{15\left(\vec{r}_{O/A}\cdot\vec{r}_{\rho/O}\right)^2}{2R^7}-\frac{3\vec{r}_{\rho/O}\cdot\vec{r}_{\rho/O}}{2R^5}\right)\vec{r}_{\rho/O}dm, \\
&&&= -\mu\int_{\mathfrak{T}}\left(\frac{15\left(\vec{r}\,'_{O/A}\left(\vec{r}_{\rho/O}\vec{r}\,'_{\rho/O}\right)\vec{r}_{O/A}\right)}{2R^7}\right)\vec{r}_{O/A}dm \\
&&&\quad +\mu\int_{\mathfrak{T}}\frac{3\vec{r}_{\rho/O}\cdot\vec{r}_{\rho/O}}{2R^5}\vec{r}_{O/A}dm+O(\epsilon^3), \\
&&&= -\int_{\mathfrak{T}}\frac{15\mu}{2R^7}\vec{r}\,'_{O/A}\left(I_3\vec{r}_{\rho/O}\cdot\vec{r}_{\rho/O}\right)\vec{r}_{O/A}dm \\
&&&\quad -\int_{\mathfrak{T}}\frac{15\mu}{2R^7}\left(\left[\vec{r}_{\rho/O}\right]^{2\times}\right)\vec{r}_{O/A}dm \\
&&&\quad +\frac{3\mu\mathrm{tr}\left[\vec{J}_{\mathfrak{T}/O}\right]}{4R^4}\hat{r}+O(\epsilon^3), \\
&&&= -\frac{3\mu\mathrm{tr}\left[\vec{J}_{\mathfrak{T}/O}\right]}{R^4}\hat{r}+\frac{15\mu}{2R^4}\left(\hat{r}'\vec{J}_{\mathfrak{T}/O}\hat{r}\right)\hat{r}+O(\epsilon^3).
\end{aligned}
\tag{C.17}
$$

C.3 Comparisons of Approximations

Comparing F_V from (C.7), (C.8) and F_f from (C.14)-(C.17), we see that

$$
F_V = F_f = -\frac{m_{\mathfrak{T}}\mu}{R^2}\hat{r}-\frac{3\mu}{R^4}\vec{J}_{\mathfrak{T}/O}\hat{r}-\frac{3\mu\mathrm{tr}\left[\vec{J}_{\mathfrak{T}/O}\right]}{2R^4}\hat{r}+\frac{15\mu}{2R^4}(\hat{r}'\vec{J}_{\mathfrak{T}/O}\hat{r})\hat{r}+O(\epsilon^3). \tag{C.18}
$$

Though both approximations yield the same result, each method has its advantages.

If the approximation is performed at the potential level, all terms of order n in ϵ

will be collected together when the Taylor-series is performed up to order n. This is useful when it is necessary to obtain all gravitational perturbations of a certain order in ϵ.

If the approximation is performed at the force level, then a Taylor-series of order n will yield all terms up to order n in ϵ as well as some terms, but not all, of order $n+1$ in ϵ. Thus, the force level approximation provides more information on the total gravitational force than the potential function when using the same order Taylor-series expansion.

APPENDIX D

Computation of Lie Brackets for the Control of an Underactuated Spacecraft in a Central Gravity Field Problem

D.1 Lie Bracket Computation

In this appendix, we compute the Lie brackets for the coupled rotational and translational dynamics using the following method from [8]; Let X and Y be two vector fields on a smooth manifold N, which itself is an embedded submanifold of M. Denote $\tilde{X}$ and $\tilde{Y}$ as C^∞ extensions to M of the vector fields of X and Y. Then $[X,\ Y]$ is the restriction of $[\tilde{X},\ \tilde{Y}]$ to N. For the particular case that $\mathsf{M} = \mathbb{R}^n$, for every $x \in \mathsf{N} \subseteq \mathsf{M}$, the Lie bracket can be computed as follows:

$$[X,\ Y](x) = \left.\frac{d}{dt}\right|_{t=0} \left\{\tilde{Y}(x + tX(x)) - \tilde{X}(x + tY(x))\right\}. \tag{D.1}$$

For the coupled rotational and translational system, we can see that the drift

vector f and the control vectors g_i for the exact system are

$$f = \left\{ \begin{array}{c} \frac{\bar{p}}{m_{\mathfrak{T}}} \\ -\int_{\mathfrak{T}} \frac{\mu\left(\bar{r}+\mathbf{D}^{\mathrm{T}}\bar{\rho}_O\right)}{\left|\bar{r}+\mathbf{D}^{\mathrm{T}}\bar{\rho}_O\right|^3} dm - 2[\bar{\omega}_e]^{\times}\bar{p} - m_{\mathfrak{T}}[\bar{\omega}_e]^{2\times}\bar{r} \\ \left[\bar{J}^{-1}\left(\bar{h}_a + \bar{J}\mathbf{D}\bar{\omega}_e + \mathbf{D}\left([\bar{r}]^{\times}\bar{p} - m_{\mathfrak{T}}[\bar{r}]^{2\times}\bar{\omega}_e\right) - \mathbf{D}\mathbf{C}\bar{H}_{\mathfrak{T}}\right)\right]^{\times}\mathbf{D} \\ 0 \end{array} \right\}, \quad g_i = \left\{ \begin{array}{c} 0 \\ 0 \\ 0 \\ e_i \end{array} \right\}, \tag{D.2}$$

where e_i is the zero vector with a 1 in the ith entry (i.e., $e_i = [\ \ldots 0\ \ 1\ \ 0\ \ \ldots]^{\mathrm{T}}$) and

$$\bar{h}_a = \sum_{i=1}^{N_{RW}} J_{ws_i}\nu_i\check{w}_i + \sum_{j=1}^{N_{CMG}} + J_{rs_i}\eta_j\check{h}_j. \tag{D.3}$$

The complete coupled spacecraft system evolves on an embedded manifold of $\mathbb{R}^{15+N_{RW}+N_{CMG}}$ (6 states for the position and velocity variables, 9 for the orientation matrix on $SO(3)$, and $N_{RW} + N_{CMG}$ for the control inputs), and thus by letting $x \in \mathbb{R}^3 \times \mathbb{R}^3 \times SO(3) \times \mathbb{R}^m$, we can use the above method to compute Lie brackets. In order to facilitate either RW or CMG control inputs, we define variables Υ_i such that

$$\begin{aligned} \Upsilon_i &= \nu_i, \quad i = 1, \ldots, N_{RW}, \\ \Upsilon_{i+N_{RW}} &= \delta_i, \quad i = 1, \ldots, N_{CMG}, \\ \bar{\Upsilon} &= [\ \Upsilon_1\ \ \Upsilon_2\ \ \ldots\ \ \Upsilon_{N_{RW}+N_{CMG}}\ ]^{\mathrm{T}}. \end{aligned} \tag{D.4}$$

We also make the following assumption on CMG inertias from Chapter 3,

> **Assumption 3.4.2** The inertia of the spacecraft bus is much larger than that of the CMGs,

which allows us to not consider the variation in $\bar{J}$ due to $\bar{\Upsilon}$.

The following pages outline a step-by-step calculation of all the necessary Lie

brackets using the procedure below:

Step 1 Compute $x + tX(x)$ and $x = x + tY(x)$.

Step 2 Compute $\tilde{Y}(x + tX(x))$ and $\tilde{X}(x + tY(x))$.

Step 3 Take the time derivative of both $\tilde{X}$ and $\tilde{Y}$, evaluated at $t = 0$.

Step 4 Use the two quantities to compute the bracket.

Occasionally, we will use the following shorthand for Lie brackets such that notation is not overwhelming:

$$L_{X,Y} = [X,\ Y]\,. \tag{D.5}$$

In the case that the Lie bracket is constructed using n drift vector fields and one control vector field, the following notation will be used:

$$L_{f^n,g_i} = [f,\ [f,\ [\ldots,\ [f,\ g_i]]]]\,. \tag{D.6}$$

D.2 Computation of Brackets of 1-degree of 2

There are only two 1-degree of 2 brackets that can be constructed; $[f,\ g_i]$ and $[g_i,\ g_j]$. The bracket $[f,\ g_i]$ is of particular importance as it will affect the tangent space of $SO(3)$.

D.2.1 Computation of Brackets of 1-degree of $[f,\ g_i]$

D.2.1.1 Step 1

$$x + tf(x) = \begin{Bmatrix} \bar{r} + t\frac{\bar{p}}{m_{\mathfrak{T}}} \\ \bar{p} + t\left(-\int_{\mathfrak{T}} \frac{\mu\left(\bar{r}+\mathbf{D}^{\mathrm{T}}\bar{\rho}_O\right)}{\left|\bar{r}+\mathbf{D}^{\mathrm{T}}\bar{\rho}_O\right|^3} dm - 2[\bar{\omega}_e]^{\times}\bar{p} - m_{\mathfrak{T}}[\bar{\omega}_e]^{2\times}\bar{r} \right) \\ \mathbf{D} + t\left[\bar{J}^{-1}\left(\bar{h}_a + \bar{J}\mathbf{D}\bar{\omega}_e + \mathbf{D}\left([\bar{r}]^{\times}\bar{p} - m_{\mathfrak{T}}[\bar{r}]^{2\times}\bar{\omega}_e\right) - \mathbf{D}\mathbf{C}\bar{H}_{\mathfrak{T}}\right)\right]^{\times}\mathbf{D} \\ \bar{\Upsilon} \end{Bmatrix}, \tag{D.7}$$

$$x + tg_i(x) = \begin{Bmatrix} \bar{r} \\ \bar{p} \\ \mathbf{D} \\ \bar{\Upsilon} + te_i \end{Bmatrix}. \tag{D.8}$$

D.2.1.2 Step 2

$$\tilde{f}(x+tg_i(x)) = \begin{Bmatrix} \frac{\bar{p}}{m_{\mathfrak{T}}} \\ -\int_{\mathfrak{T}} \frac{\mu\left(\bar{r}+\mathbf{D}^{\mathrm{T}}\bar{\rho}_O\right)}{\left|\bar{r}+\mathbf{D}^{\mathrm{T}}\bar{\rho}_O\right|^3} dm - 2[\bar{\omega}_e]^{\times}\bar{p} - m_{\mathfrak{T}}[\bar{\omega}_e]^{2\times}\bar{r} \\ \left[\bar{J}^{-1}\left(\bar{h}_a(\bar{\Upsilon} + te_i) + \bar{J}\mathbf{D}\bar{\omega}_e + \mathbf{D}\left([\bar{r}]^{\times}\bar{p} - m_{\mathfrak{T}}[\bar{r}]^{2\times}\bar{\omega}_e\right) - \mathbf{D}\mathbf{C}\bar{H}_{\mathfrak{T}}\right)\right]^{\times}\mathbf{D} \\ 0 \end{Bmatrix}, \tag{D.9}$$

$$\tilde{g}_i(x + tf(x)) = \begin{Bmatrix} 0 \\ 0 \\ 0 \\ e_i \end{Bmatrix}. \tag{D.10}$$

D.2.1.3 Step 3

$$\left.\frac{d}{dt}\right|_{t=0} \tilde{f}(x + tg_i(x)) = \begin{Bmatrix} 0 \\ 0 \\ \left[\bar{J}^{-1}\frac{\partial \bar{h}_a}{\partial \Upsilon_i}\right]^{\times} \mathbf{D} \\ 0 \end{Bmatrix}, \tag{D.11}$$

$$\left.\frac{d}{dt}\right|_{t=0} \tilde{g}_i(x + tf(x)) = 0. \tag{D.12}$$

D.2.1.4 Step 4

$$L_{f,g_i} = [f,\ g_i] = \begin{Bmatrix} 0 \\ 0 \\ \left[-\bar{J}^{-1}\frac{\partial \bar{h}_a}{\partial \Upsilon_i}\right]^{\times} \mathbf{D} \\ 0 \end{Bmatrix}. \tag{D.13}$$

D.2.2 Computation of L_{g_i,g_j}

D.2.2.1 Step 1

$$x + tg_i(x) = \begin{Bmatrix} \bar{r} \\ \bar{p} \\ \mathbf{D} \\ \bar{\Upsilon} + te_i \end{Bmatrix}. \tag{D.14}$$

D.2.2.2 Step 2

$$\tilde{g_j}(x + tg_i) = \begin{Bmatrix} 0 \\ 0 \\ 0 \\ e_j \end{Bmatrix}. \tag{D.15}$$

D.2.2.3 Step 3

$$\left.\frac{d}{dt}\right|_{t=0} \tilde{g}_i(x + t g_j(x)) = 0. \tag{D.16}$$

D.2.2.4 Step 4

$$L_{g_j, g_i} = 0. \tag{D.17}$$

D.3 Brackets of 1-degree of 3

The following are the only 1-degree of 3 brackets that can be constructed:

$$[f,\ L_{f,g_i}],\quad [g_i,\ L_{f,g_i}],\quad [g_j,\ L_{f,g_i}]. \tag{D.18}$$

Note that the only bad bracket in this set is $[g_i,\ L_{f,g_i}]$. Of particular concern is the bracket $L_{f^2,g_i} = [f,\ L_{f,g_i}] = [f,\ [f,\ g_i]]$ since this will affect the linear momentum tangent space.

D.3.1 Computation of $L_{g_j,L_{f,g_i}}$

D.3.1.1 Step 1

$$x + tg_i(x) = \begin{Bmatrix} \bar{r} \\ \bar{p} \\ \mathbf{D} \\ \bar{\Upsilon} + te_i \end{Bmatrix}, \tag{D.19}$$

$$x + tL_{f,g_j} = \begin{Bmatrix} \bar{r} \\ \bar{p} \\ \left(I_3 - t\left[\bar{J}^{-1}\frac{\partial \bar{h}_a}{\partial \Upsilon_i}\right]^{\times}\right)\mathbf{D} \\ \bar{\Upsilon} \end{Bmatrix}. \tag{D.20}$$

D.3.1.2 Step 2

$$\tilde{L}_{f,g_i}(x + tg_j(x)) = \begin{Bmatrix} 0 \\ 0 \\ -\left[\bar{J}^{-1}\frac{\partial \bar{h}_a}{\partial \Upsilon_i}(\bar{\Upsilon} + e_j t)\right]^{\times} D \\ 0 \end{Bmatrix}, \tag{D.21}$$

$$\tilde{g}_j(x + L_{f,g_i} t) = \left\{ \begin{array}{c} 0 \\ 0 \\ 0 \\ e_j \end{array} \right\}. \tag{D.22}$$

D.3.1.3 Step 3

$$\left. \frac{d}{dt} \right|_{t=0} \tilde{L}_{f,g_i} = \left\{ \begin{array}{c} 0 \\ 0 \\ -\left[\bar{J}^{-1} \frac{\partial^2 h}{\partial \Upsilon_i \partial \Upsilon_j} \right]^{\times} D \\ 0 \end{array} \right\}, \tag{D.23}$$

$$\left. \frac{d}{dt} \right|_{t=0} \tilde{g}_j(x + L_{f,g_i}) = 0. \tag{D.24}$$

D.3.1.4 Step 4

$$L_{g_j, L_{f,g_i}} = \left\{ \begin{array}{c} 0 \\ 0 \\ -\left[\bar{J}^{-1} \frac{\partial^2 h}{\partial \Upsilon_i \partial \Upsilon_j} \right]^{\times} D \\ 0 \end{array} \right\}. \tag{D.25}$$

D.3.2 Computation of L_{f^2,g_i}

D.3.2.1 Step 1

$$x + t L_{f,g_i} = \left\{ \begin{array}{c} \bar{r} \\ \bar{p} \\ \\ \left(I_3 - t \left[\bar{J}^{-1} \frac{\partial \bar{h}_a}{\partial \Upsilon_i} \right]^{\times} \right) \mathbf{D} \\ \bar{\Upsilon} \end{array} \right\}, \tag{D.26}$$

$$x+tf(x)=\left\{\begin{array}{c}\bar{r}+t\frac{\bar{p}}{m_{\mathfrak{T}}}\\ \bar{p}+t\left(-\int\limits_{\mathfrak{T}}\frac{\mu\left(\bar{r}+\mathbf{D}^{\mathrm{T}}\bar{\rho}_{O}\right)}{\left|\bar{r}+\mathbf{D}^{\mathrm{T}}\bar{\rho}_{O}\right|^{3}}dm-2[\bar{\omega}_{e}]^{\times}\bar{p}-m_{\mathfrak{T}}[\bar{\omega}_{e}]^{2\times}\bar{r}\right)\\ \left(I_{3}+t\left[\bar{J}^{-1}\left(\bar{h}_{a}+\bar{J}\mathbf{D}\bar{\omega}_{e}+\mathbf{D}\left([\bar{r}]^{\times}\bar{p}-m_{\mathfrak{T}}[\bar{r}]^{2\times}\bar{\omega}_{e}\right)-\mathbf{D}\mathbf{C}\bar{H}_{\mathfrak{T}}\right)\right]^{\times}\right)\mathbf{D}\\ \bar{\Upsilon}\end{array}\right\}. \tag{D.27}$$

D.3.2.2 Step 2

$$\begin{aligned}\tilde{L}_{f,g_i}(x+tf(x)) &= \left\{\begin{array}{c}0\\0\\-\left[\bar{J}^{-1}\frac{\partial\bar{h}_{a}}{\partial\bar{\Upsilon}_{i}}\right]^{\times}\left(I_{3}+t\left[\bar{J}^{-1}\left(\bar{h}_{a}+\bar{J}\mathbf{D}\bar{\omega}_{e}\right)\right]^{\times}\right)\mathbf{D}\\0\end{array}\right\}\\ &+\left\{\begin{array}{c}0\\0\\-\left[\bar{J}^{-1}\frac{\partial\bar{h}_{a}}{\partial\bar{\Upsilon}_{i}}\right]^{\times}\left(t\left[\bar{J}^{-1}\left(\mathbf{D}\left([\bar{r}]^{\times}\bar{p}-m_{\mathfrak{T}}[\bar{r}]^{2\times}\bar{\omega}_{e}\right)\right)\right]^{\times}\right)\mathbf{D}\\0\end{array}\right\}\\ &+\left\{\begin{array}{c}0\\0\\-\left[\bar{J}^{-1}\frac{\partial\bar{h}_{a}}{\partial\bar{\Upsilon}_{i}}\right]^{\times}\left(-t\left[\bar{J}^{-1}\left(\mathbf{D}\mathbf{C}\bar{H}_{\mathfrak{T}}\right)\right]^{\times}\right)\mathbf{D}\\0\end{array}\right\},\end{aligned} \tag{D.28}$$

$$\tilde{f}(x+tL_{f,g_i})=\left\{\begin{array}{c}\frac{\bar{p}}{m_{\mathfrak{T}}}\\ \int\limits_{\mathfrak{T}}A_{1}A_{2}dm-2[\bar{\omega}_{e}]^{\times}\bar{p}-m_{\mathfrak{T}}[\bar{\omega}_{e}]^{2\times}\bar{r}\\ A_{3}\\0\end{array}\right\}, \tag{D.29}$$

where

$$
\begin{aligned}
A_1 &= -\mu\left(\bar{r}+\mathbf{D}^{\mathrm{T}}\left(I_3-t\left[\bar{J}^{-1}\frac{\partial\bar{h}_a}{\partial\Upsilon_i}\right]^{\times}\right)^{\mathrm{T}}\bar{\rho}_O\right),\\
A_2 &= \left(\bar{r}^{\mathrm{T}}\bar{r}+\bar{\rho}_O^{\mathrm{T}}\bar{\rho}_O+2\bar{r}^{\mathrm{T}}\mathbf{D}^{\mathrm{T}}\left(I_3-t\left[\bar{J}^{-1}\frac{\partial\bar{h}_a}{\partial\Upsilon_i}\right]^{\times}\right)^{\mathrm{T}}\bar{\rho}_O\right)^{-\frac{3}{2}},\\
A_3 &= \left[\bar{J}^{-1}\left(\bar{h}_a+\bar{J}\left(I_3-t\left[\bar{J}^{-1}\frac{\partial\bar{h}_a}{\partial\Upsilon_i}\right]^{\times}\right)\mathbf{D}\bar{\omega}_e\right)\right]^{\times}\left(I_3-t\left[\bar{J}^{-1}\frac{\partial\bar{h}_a}{\partial\Upsilon_i}\right]^{\times}\right)\mathbf{D}\\
&\quad+\left[\bar{J}^{-1}\left(I_3-t\left[\bar{J}^{-1}\frac{\partial\bar{h}_a}{\partial\Upsilon_i}\right]^{\times}\right)\mathbf{D}\left([\bar{r}]^{\times}\bar{p}-m_{\mathfrak{T}}[\bar{r}]^{2\times}\bar{\omega}_e\right)\right]^{\times}\left(I_3-t\left[\bar{J}^{-1}\frac{\partial\bar{h}_a}{\partial\Upsilon_i}\right]^{\times}\right)\mathbf{D}\\
&\quad+\left[\bar{J}^{-1}\left(I_3-t\left[\bar{J}^{-1}\frac{\partial\bar{h}_a}{\partial\Upsilon_i}\right]^{\times}\right)\left(-\mathbf{D}\mathbf{C}\bar{H}_{\mathfrak{T}}\right)\right]^{\times}\left(I_3-t\left[\bar{J}^{-1}\frac{\partial\bar{h}_a}{\partial\Upsilon_i}\right]^{\times}\right)\mathbf{D}.
\end{aligned}
\tag{D.30}
$$

D.3.2.3 Step 3

Note that

$$
\left.\frac{d}{dt}\right|_{t=0}A_1=-\mu\left(\mathbf{D}^{\mathrm{T}}\left[\bar{J}^{-1}\frac{\partial\bar{h}_a}{\partial\Upsilon_i}\right]^{\times}\bar{\rho}_O\right),
\tag{D.31}
$$

$$
\left.\frac{d}{dt}\right|_{t=0}A_2=-3|\bar{r}+\mathbf{D}^{\mathrm{T}}\bar{\rho}_O|^{-5}\bar{r}^{\mathrm{T}}\mathbf{D}^{\mathrm{T}}\left[\bar{J}^{-1}\frac{\partial\bar{h}_a}{\partial\Upsilon_i}\right]^{\times}\bar{\rho}_O,
\tag{D.32}
$$

$$
\begin{aligned}
A_4 = \frac{d}{dt}\Big|_{t=0} A_3 \;\; &= \;\; -\left[\bar{J}^{-1}\bar{h}_a\right]^{\times}\left[\bar{J}^{-1}\frac{\partial \bar{h}_a}{\partial \Upsilon_i}\right]^{\times}\mathbf{D} - [D\bar{\omega}_e]^{\times}\left[\bar{J}^{-1}\frac{\partial \bar{h}_a}{\partial \Upsilon_i}\right]^{\times}\mathbf{D} \\
&\quad -\left[\bar{J}^{-1}\mathbf{D}\left([\bar{r}]^{\times}\bar{p} - m_{\mathfrak{T}}[\bar{r}]^{2\times}\bar{\omega}_e - \mathbf{C}\bar{H}_{\mathfrak{T}}\right)\right]^{\times}\left[\bar{J}^{-1}\frac{\partial \bar{h}_a}{\partial \Upsilon_i}\right]^{\times}\mathbf{D} \\
&\quad -\left[\bar{J}^{-1}\left[\bar{J}^{-1}\frac{\partial \bar{h}_a}{\partial \Upsilon_i}\right]^{\times}\mathbf{D}\left([\bar{r}]^{\times}\bar{p} - m_{\mathfrak{T}}[\bar{r}]^{2\times}\bar{\omega}_e - \mathbf{C}\bar{H}_{\mathfrak{T}}\right)\right]^{\times}\mathbf{D} \\
&\quad -\left[\left[\bar{J}^{-1}\frac{\partial \bar{h}_a}{\partial \Upsilon_i}\right]^{\times}\mathbf{D}\bar{\omega}_e\right]^{\times}\mathbf{D}, \\
&= \;\; -\left[\bar{J}^{-1}\bar{h}_a\right]^{\times}\left[\bar{J}^{-1}\frac{\partial \bar{h}_a}{\partial \Upsilon_i}\right]^{\times}\mathbf{D} - \left[\bar{J}^{-1}\frac{\partial \bar{h}_a}{\partial \Upsilon_i}\right]^{\times}[\mathbf{D}\bar{\omega}_e]^{\times}\mathbf{D} \\
&\quad -\left[\bar{J}^{-1}\mathbf{D}\left([\bar{r}]^{\times}\bar{p} - m_{\mathfrak{T}}[\bar{r}]^{2\times}\bar{\omega}_e - \mathbf{C}\bar{H}_{\mathfrak{T}}\right)\right]^{\times}\left[\bar{J}^{-1}\frac{\partial \bar{h}_a}{\partial \Upsilon_i}\right]^{\times}\mathbf{D} \\
&\quad -\left[\bar{J}^{-1}\left[\bar{J}^{-1}\frac{\partial \bar{h}_a}{\partial \Upsilon_i}\right]^{\times}\mathbf{D}\left([\bar{r}]^{\times}\bar{p} - m_{\mathfrak{T}}[\bar{r}]^{2\times}\bar{\omega}_e - \mathbf{C}\bar{H}_{\mathfrak{T}}\right)\right]^{\times}\mathbf{D}.
\end{aligned}
\tag{D.33}
$$

Therefore

$$
\begin{aligned}
\left(\left(\tfrac{d}{dt}A_1\right)A_2 + A_1\left(\tfrac{d}{dt}A_2\right)\right)\Big|_{t=0} \;\; &= \;\; -\frac{\mu\left(\mathbf{D}^{\mathrm{T}}\left[\bar{J}^{-1}\frac{\partial \bar{h}_a}{\partial \Upsilon_i}\right]^{\times}\bar{\rho}_O\right)}{\left|\bar{r}+\mathbf{D}^{\mathrm{T}}\bar{\rho}_O\right|^3} \\
&\quad +\frac{3\mu\left(\bar{r}+\mathbf{D}^{\mathrm{T}}\bar{\rho}_O\right)\bar{r}^{\mathrm{T}}\mathbf{D}^{\mathrm{T}}\left[\bar{J}^{-1}\frac{\partial \bar{h}_a}{\partial \Upsilon_i}\right]^{\times}\bar{\rho}_O}{\left|\bar{r}+\mathbf{D}^{\mathrm{T}}\bar{\rho}_O\right|^5}, \\
&= \;\; \mu\left(\frac{I_3}{\left|\bar{r}+\mathbf{D}^{\mathrm{T}}\bar{\rho}_O\right|^3} - \frac{3(\bar{r}+\mathbf{D}^{\mathrm{T}}\bar{\rho}_O)\bar{r}^{\mathrm{T}}}{\left|\bar{r}-\mathbf{D}^{\mathrm{T}}\bar{\rho}_O\right|^5}\right)\mathbf{D}^{\mathrm{T}}\left[\bar{\rho}_O\right]^{\times}\bar{J}^{-1}\frac{\partial \bar{h}_a}{\partial \Upsilon_i},
\end{aligned}
\tag{D.34}
$$

which gives

$$\left.\frac{d}{dt}\right|_{t=0}\tilde{f}(x+tL_{f,g_i}) = \left\{\begin{array}{c} 0 \\ \mu\int\limits_{\mathfrak{T}}\left(\frac{I_3}{\left|\bar{r}+\mathbf{D}^{\mathrm{T}}\bar{\rho}_O\right|^3}-\frac{3(\bar{r}+\mathbf{D}^{\mathrm{T}}\bar{\rho}_O)\bar{r}^{\mathrm{T}}}{\left|\bar{r}-\mathbf{D}^{\mathrm{T}}\bar{\rho}_O\right|^5}\right)\mathbf{D}^{\mathrm{T}}\left[\bar{\rho}_O\right]^{\times}\bar{J}^{-1}\frac{\partial\bar{h}_a}{\partial\Upsilon_i}dm \\ A_4 \\ 0 \end{array}\right\}, \tag{D.35}$$

$$\begin{aligned}\left.\frac{d}{dt}\right|_{t=0}\tilde{L}_{f,g_i}(x+tf(x)) &= \left\{\begin{array}{c} 0 \\ 0 \\ -\left[\bar{J}^{-1}\frac{\partial\bar{h}_a}{\partial\Upsilon_i}\right]^{\times}\left[\bar{J}^{-1}\left(\bar{h}_a+\bar{J}\mathbf{D}\bar{\omega}_e\right)\right]^{\times}\mathbf{D} \\ 0 \end{array}\right\} \\ &+\left\{\begin{array}{c} 0 \\ 0 \\ -\left[\bar{J}^{-1}\frac{\partial\bar{h}_a}{\partial\Upsilon_i}\right]^{\times}\left[\bar{J}^{-1}\left(\mathbf{D}\left([\bar{r}]^{\times}\bar{p}-m_{\mathfrak{T}}[\bar{r}]^{2\times}\bar{\omega}_e\right)\right)\right]^{\times}\mathbf{D} \\ 0 \end{array}\right\} \\ &+\left\{\begin{array}{c} 0 \\ 0 \\ -\left[\bar{J}^{-1}\frac{\partial\bar{h}_a}{\partial\Upsilon_i}\right]^{\times}\left[\bar{J}^{-1}\left(-\mathbf{D}\mathbf{C}\bar{H}_{\mathfrak{T}}\right)\right]^{\times}\mathbf{D} \\ 0 \end{array}\right\}.\end{aligned} \tag{D.36}$$

D.3.2.4 Step 4

$$L_{f^2,g_i} = \left\{ \begin{array}{c} 0 \\ -\mu \int\limits_{\mathfrak{T}} \left(\frac{I_3}{\left|\bar{r}+\mathbf{D}^{\mathrm{T}}\bar{\rho}_O\right|^3} - \frac{3(\bar{r}+\mathbf{D}^{\mathrm{T}}\bar{\rho}_O)\bar{r}^{\mathrm{T}}}{\left|\bar{r}-\mathbf{D}^{\mathrm{T}}\bar{\rho}_O\right|^5} \right) \mathbf{D}^{\mathrm{T}} \left[\bar{\rho}_O\right]^{\times} \bar{J}^{-1} \frac{\partial \bar{h}_a}{\partial \Upsilon_i} dm \\ \left[\left(\bar{J}^{-1}\bar{h}_a\right) \times \left(\bar{J}^{-1} \frac{\partial \bar{h}_a}{\partial \Upsilon_i} \right) + E_1 \mathbf{D} E_2 \right]^{\times} \mathbf{D} \\ 0 \end{array} \right\}, \tag{D.37}$$

where

$$\begin{aligned} E_1 &= \left(\bar{J}^{-1} \left[\bar{J}^{-1} \frac{\partial \bar{h}_a}{\partial \Upsilon_i} \right]^{\times} - \left[\bar{J}^{-1} \frac{\partial \bar{h}_a}{\partial \Upsilon_i} \right]^{\times} \bar{J}^{-1} \right), \\ E_2 &= \left([\bar{r}]^{\times} \bar{p} - m_{\mathfrak{T}} [\bar{r}]^{2\times} \bar{\omega}_e - \mathbf{C} \bar{H}_{\mathfrak{T}} \right). \end{aligned} \tag{D.38}$$

D.4 Brackets of 1-degree of 4

None of the brackets of 1-degree of 4 will be bad. However, there are two brackets that are of concern. The first is $L_{f^3,g_i} = [f,\ [f,\ [f,\ g_i]]]$, which will affect the position tangent space. The second is $[[f,\ g_i],\ [f,\ g_j]]$, which in the absence of full controllability in the attitude dynamics, will result in a third control direction for RWs.

D.4.1 Computation of L_{f^3,g_i}

To be brief, let $*$ denote an entry that is not of concern

D.4.1.1 Step 1

$$x + tL_{f^2,g_i} = \left\{ \begin{array}{c} \bar{r} \\ \bar{p} + t\left(-\mu \int_{\mathfrak{T}} \left(\frac{I_3}{\left|\bar{r}+\mathbf{D}^{\mathrm{T}}\bar{\rho}_O\right|^3} - \frac{3(\bar{r}+\mathbf{D}^{\mathrm{T}}\bar{\rho}_O)\bar{r}^{\mathrm{T}}}{\left|\bar{r}+\mathbf{D}^{\mathrm{T}}\bar{\rho}_O\right|^5} \right) \mathbf{D}^{\mathrm{T}} \left[\bar{\rho}_O\right]^{\times} \bar{J}^{-1} \frac{\partial \bar{h}_a}{\partial \Upsilon_i} \right) dm \\ \left(I_3 + t\left[\left(\bar{J}^{-1}\bar{h}_a\right) \times \left(\bar{J}^{-1} \frac{\partial \bar{h}_a}{\partial \Upsilon_i} \right) + E_1 \mathbf{D} E_2 \right]^{\times} \right) \mathbf{D} \\ \bar{\Upsilon} \end{array} \right\}, \tag{D.39}$$

$$x + tf(x) = \left\{ \begin{array}{c} \bar{r} + t\frac{\bar{p}}{m_{\mathfrak{T}}} \\ \bar{p} + t\left(-\int_{\mathfrak{T}} \frac{\mu\left(\bar{r}+\mathbf{D}^{\mathrm{T}}\bar{\rho}_O\right)}{\left|\bar{r}+\mathbf{D}^{\mathrm{T}}\bar{\rho}_O\right|^3} dm - 2[\bar{\omega}_e]^{\times}\bar{p} - m_{\mathfrak{T}}[\bar{\omega}_e]^{2\times}\bar{r} \right) \\ \left(I_3 + t\left[\bar{J}^{-1}\left(\bar{h}_a + \bar{J}\mathbf{D}\bar{\omega}_e + \mathbf{D}\left([\bar{r}]^{\times}\bar{p} - m_{\mathfrak{T}}[\bar{r}]^{2\times}\bar{\omega}_e \right) - \mathbf{D}\mathbf{C}\bar{H}_{\mathfrak{T}} \right) \right]^{\times} \right) \mathbf{D} \\ \bar{\Upsilon} \end{array} \right\}. \tag{D.40}$$

D.4.1.2 Step 2 & 3

$$\left.\frac{d}{dt}\right|_{t=0} \tilde{L}_{f^2,g_i}(x+f(x)t) = \begin{Bmatrix} 0 \\ * \\ * \\ 0 \end{Bmatrix}, \tag{D.41}$$

$$\left.\frac{d}{dt}\right|_{t=0} \tilde{f}(x+L_{f^2,g_i}) = \begin{Bmatrix} -\frac{\mu}{m_{\mathfrak{T}}} \int\limits_{\mathfrak{T}} \left(\frac{I_3}{\left|\bar{r}+\mathbf{D}^{\mathrm{T}}\bar{\rho}_O\right|^3} - \frac{3(\bar{r}+\mathbf{D}^{\mathrm{T}}\bar{\rho}_O)\bar{r}^{\mathrm{T}}}{\left|\bar{r}-\mathbf{D}^{\mathrm{T}}\bar{\rho}_O\right|^5} \right) \mathbf{D}^{\mathrm{T}} \left[\bar{\rho}_O\right]^{\times} \bar{J}^{-1} \frac{\partial \bar{h}_a}{\partial \Upsilon_i} dm \\ * \\ * \\ 0 \end{Bmatrix}. \tag{D.42}$$

D.4.1.3 Step 4

$$L_{f^3,g_i} = \begin{Bmatrix} \frac{\mu}{m_{\mathfrak{T}}} \int\limits_{\mathfrak{T}} \left(\frac{I_3}{\left|\bar{r}+\mathbf{D}^{\mathrm{T}}\bar{\rho}_O\right|^3} - \frac{3(\bar{r}+\mathbf{D}^{\mathrm{T}}\bar{\rho}_O)\bar{r}^{\mathrm{T}}}{\left|\bar{r}-\mathbf{D}^{\mathrm{T}}\bar{\rho}_O\right|^5} \right) \mathbf{D}^{\mathrm{T}} \left[\bar{\rho}_O\right]^{\times} \bar{J}^{-1} \frac{\partial \bar{h}_a}{\partial \Upsilon_i} dm \\ * \\ * \\ 0 \end{Bmatrix}. \tag{D.43}$$

D.4.2 Computation of $[[f,\ g_i],\ [f,\ g_j]]$

D.4.2.1 Step 1

$$x + tL_{f,g_i} = \begin{Bmatrix} \bar{r} \\ \bar{p} \\ \\ \left(I_3 - t\left[\bar{J}^{-1}\frac{\partial \bar{h}_a}{\partial \Upsilon_i}\right]^{\times}\right)\mathbf{D} \\ \bar{\Upsilon} \end{Bmatrix}. \tag{D.44}$$

D.4.2.2 Step 2

$$\tilde{L}_{f,g_j}(x + tL_{f,g_i}) = \begin{Bmatrix} 0 \\ 0 \\ -\left[\bar{J}^{-1}\frac{\partial \bar{h}_a}{\partial \Upsilon_j}\right]^{\times}\left(I_3 - t\left[\bar{J}^{-1}\frac{\partial \bar{h}_a}{\partial \Upsilon_i}\right]^{\times}\right)\mathbf{D} \\ 0 \end{Bmatrix}. \tag{D.45}$$

D.4.2.3 Step 3

$$\left.\frac{d}{dt}\right|_{t=0} \tilde{L}_{f,g_j}(x + tL_{f,g_i}) = \begin{Bmatrix} 0 \\ 0 \\ \left[\bar{J}^{-1}\frac{\partial \bar{h}_a}{\partial \Upsilon_j}\right]^{\times}\left[\bar{J}^{-1}\frac{\partial \bar{h}_a}{\partial \Upsilon_i}\right]^{\times}\mathbf{D} \\ 0 \end{Bmatrix}. \tag{D.46}$$

D.4.2.4 Step 4

$$[[f,\ g_i],\ [f,\ g_j]] = \begin{bmatrix} 0 \\ 0 \\ \left[\det\left[\bar{J}^{-1}\right]\bar{J}\left(\frac{\partial \bar{h}_a}{\partial \Upsilon_j} \times \frac{\partial \bar{h}_a}{\partial \Upsilon_i}\right)\right]^{\times}\mathbf{D} \\ 0 \end{bmatrix}. \tag{D.47}$$

BIBLIOGRAPHY

[1] Leve, F., Hamilton, B., and Peck, M., *Spacecraft Momentum Control Systems*, Springer, 2015.

[2] Bullo, F. and Lewis, A. D., *Geometric Control of Mechanical Systems*, Springer, 2000.

[3] Moos, H., "Overview of the Far Ultraviolet Spectroscopic Explorer Mission," *The Astrophysical Journal Letters*, Vol. 538, No. 1, 2000, pp. L1–L6.

[4] Cowen, R., "The Wheels Come Off Kepler," http://www.nature.com/news/the-wheels-come-off-kepler-1.13032, May 2013, [Online; accessed 18-October-2013].

[5] de Selding, P., "Japan's Asteroid Sample-Return Mission Has Problems," http://www.space.com/1642-japan-asteroid-sample-return-mission-problems.html, October 2014, [Online; accessed 27-February-2015].

[6] Crouch, P. E., "Spacecraft Attitude Control and Stabilization: Applications of Geometric Control Theory To Rigid Body Models," *Automatic Control, IEEE Transactions on*, Vol. 29, No. 4, 1984, pp. 321–331.

[7] Krishnan, H., McClamroch, N. H., and Reyhanoglu, M., "Attitude Stabilization of a Rigid Spacecraft Using Two Momentum Wheel Actuators," *Journal of Guidance, Control, and Dynamics*, Vol. 18, No. 2, 1995, pp. 256–263.

[8] Bhat, S. P. and Tiwari, P. K., "Controllability of Spacecraft Attitude using Control Moment Gyroscopes," *Automatic Control, IEEE Transactions on*, Vol. 54, No. 3, 2009, pp. 585–590.

[9] Bhat, S. P. and Paranjape, A. A., "Small-Time Local Controllability and Stabilizability of Spacecraft Attitude Dynamics under CMG Actuation," *SIAM Journal on Control and Optimization*, Vol. 52, No. 2, 2014, pp. 797–820.

[10] Gui, H., Jin, L., and Xu, S., "Small-Time Local Controllability of Spacecraft Attitude Using Control Moment Gyros," *Automatica*, Vol. 53, 2015, pp. 141–148.

[11] Bayadi, R., Banavar, R. N., and Maschke, B. M., "Small-time Local Controllability of the Orientation of a Spacecraft Actuated by CMGs," *IFAC World Congress, Proceedings of the 18th International Federation of Automatic Control*, 2011, pp. 13828–13833.

[12] Byrnes, C. I. and Isidori, A., "On the Attitude Stabilization of Rigid Spacecraft," *Automatica*, Vol. 27, No. 1, 1991, pp. 87–95.

[13] Krishnan, H., Reyhanoglu, M., and McClamroch, H., "Attitude Stabilization of a Rigid Spacecraft Using Two Control Torques: A Nonlinear Control Approach Based on the Spacecraft Attitude Dynamics," *Automatica*, Vol. 30, No. 6, 1994, pp. 1023–1027.

[14] Jin, L. and Xu, S., "Underactuated Spacecraft Angular Velocity Stabilization and Three-Axis Attitude Stabilization Using Two Single Gimbal Control Moment Gyros," *Acta Mechanica Sinica*, Vol. 26, No. 2, 2010, pp. 279–288.

[15] Brockett, R., "Asymptotic Stability and Feedback Stabilization," *Differential Geometric Control Theory*, 1983, pp. 181–191.

[16] Zabczyk, J., "Some Comments on Stability," *Applied Mathematics and Optimization*, 1989, pp. 1–9.

[17] Gurvits, L. and Li, Z., "Smooth Time-Periodic Feedback Solutions for Nonholonomic Motion Planning," *Nonholonomic Motion Planning*, Springer, 1993, pp. 53–108.

[18] Walsh, G. C., Montgomery, R., and Sastry, S. S., "Orientation Control of the Dynamic Satellite," *American Control, Proceedings of the IEEE Conference on*, Vol. 1, IEEE, 1994, pp. 138–142.

[19] Ge, X.-S., Chen, L.-Q., and Liu, Y.-z., "Attitude Control of Underactuated Spacecraft Through Flywheels Motion Using Genetic Algorithm with Wavelet Approximation," *Intelligent Control and Automation, Fifth World Congress on*, Vol. 6, IEEE, 2004, pp. 5466–5470.

[20] Horri, N. M. and Hodgart, S., "Attitude Stabilization of an Underactuated Satellite Using Two Wheels," *Aerospace, Proceedings of the IEEE Conference on*, Vol. 6, IEEE, 2003, pp. 6_2629–6_2635.

[21] Horri, N. M., Palmer, P., and Hodgart, S., "Practical Implementation of Attitude-Control Algorithms for an Underactuated Satellite," *Journal of Guidance, Control, and Dynamics*, Vol. 35, No. 1, 2012, pp. 40–45.

[22] Gui, H., Jin, L., and Xu, S., "Attitude Maneuver Control of a Two-Wheeled Spacecraft with Bounded Wheel Speeds," *Acta Astronautica*, Vol. 88, 2013, pp. 98–107.

[23] Urakubo, T., Tsuchiya, K., and Tsujita, K., "Attitude Control of a Spacecraft with Two Reaction Wheels," *Journal of Vibration and Control*, Vol. 10, No. 9, 2004, pp. 1291–1311.

[24] Sordalen, O., Egeland, O., and De Wit, C. C., "Attitude Stabilization with a Nonholonomic Constraint," *Decision and Control, Proceedings of the 31st IEEE Conference on*, IEEE, 1992, pp. 1610–1611.

[25] Morin, P., Samson, C., Pomet, J.-B., and Jiang, Z.-P., "Time-Varying Feedback Stabilization of the Attitude of a Rigid Spacecraft with Two Controls," *Systems & Control Letters*, Vol. 25, No. 5, 1995, pp. 375–385.

[26] Morin, P. and Samson, C., "Time-Varying Exponential Stabilization of the Attitude of a Rigid Spacecraft with Two Controls," *Decision and Control, Proceedings of the 34th IEEE Conference on*, Vol. 4, IEEE, 1995, pp. 3988–3993.

[27] Li, S. and Tian, Y.-P., "Exponential Stabilization of the Attitude of a Rigid Spacecraft with Two Controls," *American Control, Proceedings of the IEEE Conference on*, Vol. 1, IEEE, 2002, pp. 797–802.

[28] Godhavn, J.-M. and Egeland, O., "Attitude Control of an Underactuated Satellite," *Decision and Control, Proceedings of the 34th IEEE Conference on*, Vol. 4, 1995, pp. 3986–3987.

[29] Liu, W., *Averaging Theorems for Highly Oscillatory Differential Equations and the Approximation of General Paths by Admissible Trajectories for Nonholonomic Systems*, PhD Dissertation, Rutgers Univ., 1992.

[30] Leonard, N. E. and Krishnaprasad, P., "Averaging For Attitude Control and Motion Planning," *Decision and Control, Proceedings of the 32nd IEEE Conference on*, IEEE, 1993, pp. 3098–3104.

[31] Leonard, N. E. and Krishnaprasad, P. S., "Motion Control of Drift-Free, Left-Invariant Systems on Lie Groups," *Automatic Control, IEEE Transactions on*, Vol. 40, No. 9, 1995, pp. 1539–1554.

[32] Yamada, K., Yoshikawa, S., and Yamaguchi, I., "Feedback Attitude Control of a Spacecraft by Two Reaction Wheels: 98-c-02," *International Symposium on Space Technology and Science, Proceedings of the*, Vol. 21, AGNE SHOFU PUBLISHING INC., 1998, pp. 550–555.

[33] Kasai, S., Kojima, H., and Satoh, M., "Spacecraft Attitude Maneuver Using Two Single-Gimbal Control Moment Gyros," *Acta Astronautica*, Vol. 84, 2013, pp. 88–98.

[34] Han, C. and Pechev, A. N., "Underactuated Satellite Attitude Control with Two Parallel CMGs," *Control and Automation, Proceedings of the IEEE International Conference on*, IEEE, 2007, pp. 666–670.

[35] Gui, H., Jin, L., and Xu, S., "Local Controllability and Stabilization of Spacecraft Attitude by Two Single-Gimbal Control Moment Gyros," *Chinese Journal of Aeronautics*, Vol. 26, No. 5, 2013, pp. 1218–1226.

[36] Gui, H., Jin, L., Xu, S., and Hu, Q., "Attitude Stabilization of a Spacecraft by Two Skew Single-Gimbal Control Moment Gyros," *Guidance, Navigation, and Control, Proceedings of the AIAA Conference on*, 2013.

[37] Boyer, F. and Alamir, M., "Further Results on the Controllability of a Two-Wheeled Satellite," *Journal of Guidance, Control, and Dynamics*, Vol. 30, No. 2, 2007, pp. 611–619.

[38] Kim, S. and Kim, Y., "Spin-Axis Stabilization of a Rigid Spacecraft using Two Reaction Wheels," *Journal of Guidance, Control, and Dynamics*, Vol. 24, No. 5, 2001, pp. 1046–1049.

[39] Katsuyama, Y., Sekiguchi, K., and Sampei, M., "Spacecraft Attitude Control by 2 Wheels with Initial Angular Momentum," *SICE Annual Conference, Proceedings of the*, IEEE, 2013, pp. 1890–1895.

[40] Kwon, S., Shimomura, T., and Okubo, H., "Pointing Control of Spacecraft Using Two SGCMGs via LPV Control Theory," *Acta Astronautica*, Vol. 68, No. 7, 2011, pp. 1168–1175.

[41] Grüne, L. and Pannek, J., *Nonlinear Model Predictive Control; Theory and Algorithms*, Springer, 2010.

[42] Meadows, E. S., Henson, M. A., Eaton, J. W., and Rawlings, J. B., "Receding Horizon Control and Discontinuous State Feedback Stabilization," *International Journal of Control*, Vol. 62, No. 5, 1995, pp. 1217–1229.

[43] Linares, R., Jah, M. K., Crassidis, J. L., Leve, F. A., and Kelecy, T., "Astrometric and Photometric Data Fusion for Inactive Space Object Mass and Area Estimation," *Acta Astronautica*, Vol. 99, 2014, pp. 1–15.

[44] Beleckij, V. V., *Motion of an Artificial Satellite about its Center of Mass*, Israel Program for Scientific Translations, 1966.

[45] Sarychev, V., "Effect of Earth's Oblateness on the Rotational Motion of an Artificial Earth Satellite," *ARS Journal*, Vol. 32, No. 5, 1962, pp. 834–838.

[46] Moran, J. P., "Effects of Plane Librations on the Orbital Motion of a Dumbbell Satellite," *ARS Journal*, Vol. 31, No. 8, 1961, pp. 1089–1096.

[47] Sincarsin, G. and Hughes, P., "Gravitational Orbit-Attitude Coupling for Very Large Spacecraft," *Celestial Mechanics*, Vol. 31, No. 2, 1983, pp. 143–161.

[48] Wang, L.-S., Maddocks, J. H., and Krishnaprasad, P. S., "Steady Rigid-Body Motions in a Central Gravitational Field," Tech. rep., DTIC Document, 1991.

[49] Beck, J. A. and Hall, C. D., "Relative Equilibria of a Rigid Satellite in a Circular Keplerian Orbit," *Journal of the Astronautical Sciences*, Vol. 46, No. 3, 1998, pp. 215–247.

[50] Scheeres, D., "Relative Equilibria for General Gravity Fields in the Sphere-Restricted Full 2-Body Problem," *Celestial Mechanics and Dynamical Astronomy*, Vol. 94, No. 3, 2006, pp. 317–349.

[51] Misra, G. and Sanyal, A., "Analysis of Orbit-Attitude Coupling of Spacecraft Near Small Bodies," *Guidance, Navigation, and Control, Proceeding of the AIAA Conference on*, 2015, pp. 2015–1777.

[52] Bellerose, J. and Scheeres, D. J., "Energy and Stability in the Full Two Body Problem," *Celestial Mechanics and Dynamical Astronomy*, Vol. 100, No. 1, 2008, pp. 63–91.

[53] Scheeres, D. J., "Stability in the Full Two-Body Problem," *Modern Celestial Mechanics: From Theory to Applications*, Springer, 2002, pp. 155–169.

[54] Wang, Y., Xu, S., and Zhu, M., "Stability of Relative Equilibria of the Full Spacecraft Dynamics Around an Asteroid with Orbit–Attitude Coupling," *Advances in Space Research*, Vol. 53, No. 7, 2014, pp. 1092–1107.

[55] Wang, Y. and Xu, S., "Relative Equilibria of Full Dynamics of a Rigid Body with Gravitational Orbit-Attitude Coupling in a Uniformly Rotating Second Degree and Order Gravity Field," *Astrophysics and Space Science*, Vol. 354, No. 2, 2014, pp. 339–353.

[56] Scheeres, D. J., *Orbital Motion in Strongly Perturbed Environments*, Springer, 2012.

[57] Wang, Y. and Xu, S., "On the Nonlinear Stability of Relative Equilibria of the Full Spacecraft Dynamics Around an Asteroid," *Nonlinear Dynamics*, Vol. 78, No. 1, 2014, pp. 1–13.

[58] Lian, K.-Y., Wang, L.-S., and Fu, L.-C., "Controllability of Spacecraft Systems in a Central Gravitational Field," *Automatic Control, IEEE Transactions on*, Vol. 39, No. 12, 1994, pp. 2426–2441.

[59] Sanyal, A. K., Shen, J., and McClamroch, N. H., "Dynamics and Control of an Elastic Dumbbell Spacecraft in a Central Gravitational Field," *Decision and Control, Proceedings of the 42nd IEEE Conference on*, Vol. 3, IEEE, 2003, pp. 2798–2803.

[60] Sanyal, A. K., Shen, J., and McClamroch, N. H., "Control of a Dumbbell Spacecraft Using Attitude and Shape Control Inputs Only," *American Control, Proceeding of the IEEE Conference on*, Vol. 2, IEEE, 2004, pp. 1014–1018.

[61] Wang, Y. and Xu, S., "Stabilizing the Coupled Orbit–Attitude Dynamics of a Rigid Body in a J 2 Gravity Field using Hamiltonian Structure," *Acta Astronautica*, Vol. 113, 2015, pp. 180–203.

[62] De Ruiter, A., Damaren, C., and Forbes, J., *Spacecraft Dynamics and Control*, Wiley, 2012.

[63] Bernstein, D., *Geometry, Kinematics, Statics, and Dynamics*, University of Michigan, 2014.

[64] Hughes, P., *Spacecraft Attitude Dynamics*, Dover, 2004.

[65] Karami, M. A. and Sassani, F., "Spacecraft Momentum Dumping Using Fewer Than Three External Control Torques," *Journal of Guidance, Control, and Dynamics*, Vol. 32, No. 1, 2009, pp. 242–247.

[66] Ratan, S. and Rogers, K., "Directed Momentum Management for Rotating Spacecraft," *Guidance, Navigation, and Control, Proceedings of the AIAA Conference and Exhibit on*, 2002.

[67] Chen, X., Steyn, W. H., Hodgart, S., and Hashida, Y., "Optimal Combined Reaction-Wheel Momentum Management for Earth-Pointing Satellites," *Journal of Guidance, Control, and Dynamics*, Vol. 22, No. 4, 1999, pp. 543–550.

[68] Hablani, H. B., "Pole-Placement Technique for Magnetic Momentum Removal of Earth-Pointing Spacecraft," *Journal of Guidance, Control, and Dynamics*, Vol. 20, No. 2, 1997, pp. 268–275.

[69] Lebsock, K., "Magnetic Desaturation of a Momentum Bias System," *Journal of Guidance, Control, and Dynamics*, Vol. 6, No. 6, 1983, pp. 477–483.

[70] Chen, X., Sun, H., and Zhang, J., "Reaction-Wheel Momentum Dumping by Hybrid Control of Magnetorquers and Thrusters," *Guidance, Navigation, and Control, Proceedings of the AIAA Conference on*, 2010, p. 7901.

[71] Leve, F. A., "Evaluation of Steering Algorithm Optimality for Single-Gimbal Control Moment Gyroscopes," *Control Systems Technology, IEEE Transactions on*, Vol. 22, No. 3, 2014, pp. 1130–1134.

[72] Wertz, J. R., *Spacecraft Attitude Determination and Control*, Vol. 73, Springer Science & Business Media, 2002.

[73] Schalkowski, S. and Harris, M., "Spacecraft Mass Expulsion Torques," NASA SP-8034, 1969.

[74] Kolmanovsky, I. and McClamroch, N. H., "Hybrid Feedback Laws for a Class of Cascade Nonlinear Control Systems," *Automatic Control, IEEE Transactions on*, Vol. 41, No. 9, 1996, pp. 1271–1282.

[75] Rui, C., Kolmanovsky, I., and McClamroch, N. H., "Hybrid Control for Stabilization of a Class of Cascade Nonlinear Systems," *American Control, Proceedings of the IEEE Conference on*, Vol. 5, IEEE, 1997, pp. 2800–2804.

[76] Chen, C., *Linear System Theory and Design*, Oxford University Press, 1984.

[77] Kolmanovsky, I. and McClamroch, N., "Controllability and Motion Planning for Noncatastatic Nonholonomic Control Systems," *Mathematical and Computer Modeling*, Vol. 24, No. 1, 1996, pp. 31–42.

[78] Coleman, M., "Background on Big O Notation," http://www.maths.manchester.ac.uk/~mdc/MATH31022/Present/Background/Background%20big%20O%20notation.pdf, [Online; accessed 15-October-2015].

[79] Bhat, S. P., "Controllability of Nonlinear Time-varying Systems: Applications to Spacecraft Attitude Control Using Magnetic Actuation," *Automatic Control, IEEE Transactions on*, Vol. 50, No. 11, 2005, pp. 1725–1735.

[80] Crassidis, J. L., Markley, F. L., Anthony, T. C., and Andrews, S. F., "Nonlinear Predictive Control of Spacecraft," *Journal of Guidance, Control, and Dynamics*, Vol. 20, No. 6, 1997, pp. 1096–1103.

[81] Wen, J. T., Seereeram, S., and Bayard, D. S., "Nonlinear Predictive Control Applied to Spacecraft Attitude Control," *American Control, Proceedings of the IEEE Conference on*, Vol. 3, IEEE, 1997, pp. 1899–1903.

[82] Hegrenas, O., Gravdahl, J. T., and Tøndel, P., "Attitude Control by Means of Explicit Model Predictive Control, Via Multi-Parametric Quadratic Programming," *American Control, Proceedings of the IEEE Conference on*, IEEE, 2005, pp. 901–906.

[83] Gupta, R., Kalabic, U. V., Di Cairano, S., Bloch, A. M., and Kolmanovsky, I. V., "Constrained Spacecraft Attitude Control on SO (3) Using Fast Nonlinear Model Predictive Control," *American Control, Proceedings of the IEEE Conference on*, IEEE, 2015, pp. 2980–2986.

[84] Kim, J. and Crassidis, J. L., "Spacecraft Attitude Control Using Approximate Receding-Horizon Model-Error Control Synthesis," *Journal of Guidance, Control, and Dynamics*, Vol. 29, No. 5, 2006, pp. 1023–1031.

[85] Myung, H.-S. and Bang, H., "Nonlinear Predictive Attitude Control of Spacecraft Under External Disturbances," *Journal of Spacecraft and Rockets*, Vol. 40, No. 5, 2003, pp. 696–699.

[86] Ikeda, Y., Nakajima, T., and Chida, Y., "Attitude Control of Spacecraft by NMPC with Consideration of Singularity Avoidance of CMG," *Decision and Control, Proceedings of IEEE 51st Annual Conference on*, IEEE, 2012, pp. 1733–1739.

[87] Cao, Y. and Chen, W.-H., "Automatic Differentiation Based Nonlinear Model Predictive Control of Satellites Using Magneto-Torquers," *Industrial Electronics and Applications, Proceeding of the 4th IEEE Conference on*, IEEE, 2009, pp. 913–918.

[88] Silani, E. and Lovera, M., "Magnetic Spacecraft Attitude Control: A Survey and Some New Results," *Control Engineering Practice*, Vol. 13, No. 3, 2005, pp. 357–371.

[89] Guiggiani, A., Kolmanovsky, I., Patrinos, P., and Bemporad, A., "Fixed-Point Constrained Model Predictive Control of Spacecraft Attitude," *American Control, Proceedings of the IEEE Conference on*, IEEE, 2015, pp. 2317–2322.

[90] De Oliveira Kothare, S. L. and Morari, M., "Contractive Model Predictive Control for Constrained Nonlinear Systems," *Automatic Control, IEEE Transactions on*, Vol. 45, No. 6, 2000, pp. 1053–1071.

[91] Bemporad, A., Morari, M., Dua, V., and Pistikopoulos, E. N., "The Explicit Linear Quadratic Regulator for Constrained Systems," *Automatica*, Vol. 38, No. 1, 2002, pp. 3–20.

[92] Bloch, A. M., Reyhanoglu, M., and McClamroch, N. H., "Control and Stabilization of Nonholonomic Dynamic Systems," *Automatic Control, IEEE Transactions on*, Vol. 37, No. 11, 1992, pp. 1746–1757.

[93] Sussmann, H. J., "A General Theorem on Local Controllability," *SIAM Journal on Control and Optimization*, Vol. 25, No. 1, 1987, pp. 158–194.

[94] Jakubczyk, B. and Sontag, E. D., "Controllability of Nonlinear Discrete-Time Systems: a Lie-Algebraic Approach," *SIAM Journal on Control and Optimization*, Vol. 28, No. 1, 1990, pp. 1–33.

[95] Albertini, F. and Sontag, E. D., "Further Results on Controllability Properties of Discrete-Time Nonlinear Systems," *Dynamics and Control*, Vol. 4, No. 3, 1994, pp. 235–253.

[96] Lin, W. and Byrnes, C. I., "Design of Discrete-Time Nonlinear Control Systems via Smooth Feedback," *Automatic Control, IEEE Transactions on*, Vol. 39, No. 11, 1994, pp. 2340–2346.

[97] Goodwin, G., Seron, M., and De Doná, J., *Constrained Control and Estimation; An Optimisation Approach*, Springer-Verlag, 2005.

[98] Walker, K., Samadi, B., Huang, M., Gerhard, J., Butts, K., and Kolmanovsky, I., "Design Environment for Nonlinear Model Predictive Control," Tech. rep., SAE Technical Paper, 2016.

[99] N/A, "Aerospace Technology," http://www.ati-space.com/ATI.files/11$_$index.files/utyuu$_$aboute.htm, 2016, [retrieved 16-October-2014].

[100] Pingree, P. J., "Advancing NASA's On-Board Processing Capabilities with Reconfigurable FPGA Technologies: Opportunities & Implications," *Parallel & Distributed Processing, Workshops and Phd Forum of the 2010 IEEE International Symposium on*, IEEE, 2010, pp. 1–1.

[101] N/A, "Boiler Optimization Systems," http://www02.abb.com, 2011, [retrieved 10-March-2016].

[102] N/A, "Basell Optimizes Ethylene Plant with Honeywell MPC and RTO," https://www.honeywellprocess.com, 2017, [retrieved 10-March-2016].

[103] Diehl, M., Uslu, I., Findeisen, R., Schwarzkopf, S., Allgöwer, F., Bock, H. G., Bürner, T., Gilles, E. D., Kienle, A., Schlöder, J. P., et al., "Real-Time Optimization for Large Scale Processes: Nonlinear Model Predictive Control of a High Purity Distillation Column," *Online Optimization of Large Scale Systems*, Springer, 2001, pp. 363–383.

[104] Diehl, M., Bock, H. G., Schlöder, J. P., Findeisen, R., Nagy, Z., and Allgöwer, F., "Real-Time Optimization and Nonlinear Model Predictive Control of Processes Governed by Differential-Algebraic Equations," *Journal of Process Control*, Vol. 12, No. 4, 2002, pp. 577–585.

[105] Seron, M. M., De Dona, J. A., and Goodwin, G. C., "Global Analytical Model Predictive Control with Input Constraints," *Decision and Control, Proceedings of the 39th IEEE Conference on*, Vol. 1, IEEE, 2000, pp. 154–159.

[106] TøNdel, P., Johansen, T. A., and Bemporad, A., "An Algorithm for Multi-Parametric Quadratic Programming and Explicit MPC Solutions," *Automatica*, Vol. 39, No. 3, 2003, pp. 489–497.

[107] Grieder, P., Borrelli, F., Torrisi, F., and Morari, M., "Computation of the Constrained Infinite Time Linear Quadratic Regulator," *Automatica*, Vol. 40, No. 4, 2004, pp. 701–708.

[108] Dinh, Q. T., Savorgnan, C., and Diehl, M., "Adjoint-Based Predictor-Corrector Sequential Convex Programming for Parametric Nonlinear Optimization," *SIAM Journal on Optimization*, Vol. 22, No. 4, 2012, pp. 1258–1284.

[109] Zavala, V. M., Laird, C. D., and Biegler, L. T., "A Fast Moving Horizon Estimation Algorithm Based on Nonlinear Programming Sensitivity," *Journal of Process Control*, Vol. 18, No. 9, 2008, pp. 876–884.

[110] Kungurtsev, V. and Diehl, M., "SQP Methods for Parametric Nonlinear Optimization," 2013.

[111] Flynn, M., Leve, F., Petersen, C., and Kolmanovsky, I., "Linear Control of Underactuated Spacecraft with Two Reaction Wheels Made Feasible by Solar Radiation Pressure," *American Control, Proceedings of the IEEE Conference on*, IEEE, 2015, pp. 3193–3198.

[112] Howell, E., "Kelper K2 Finds First Exoplanet, A Super-Earth, While Surfing Sun's Pressure Wave For Control," http://www.universetoday.com/117462/, December 2014, [Online; accessed 27-Feburary-2015].

[113] Khalil, H., *Nonlinear Systems*, Prentice Hall, 3rd ed., 2002.

[114] Anderson, B. and Moore, J., *Optimal Control: Linear Quadratic Control Methods*, Prentice Hall, 1990.

[115] Stringer, M. T., Newman, B., Lovell, T. A., and Omran, A., "Analysis of a New Nonlinear Solution of Relative Orbital Motion," *Space Flight Dynamics, Proceedings of the 23rd International Symposium on*, Jet Propulsion Laboratory, 2012.